

NETHERLANDS  
PUBLICATIONS ON GEODESY

GEODETIC

COMMISSION  
NEW SERIES  
NUMBER 36

REFRACTION OF TRANSATMOSPHERIC SIGNALS  
IN GEODESY

PROCEEDINGS OF THE SYMPOSIUM

THE HAGUE, THE NETHERLANDS, MAY 19 - 22, 1992

edited by

J.C. DE MUNCK  
T.A.TH. SPOELSTRA

1992

NEDERLANDSE COMMISSIE VOOR GEODESIE, THIJSSEWEG 11, 2629 JA DELFT, THE NETHERLANDS  
TEL. (31)-15-782819, FAX (31)-15-782348

PRINTED BY W.D. MEINEMA B.V., DELFT, THE NETHERLANDS

ISBN 90 6132 243 X

## CONTENTS

<b>PREFACE .....</b>	vii
<b>ACKNOWLEDGMENTS .....</b>	viii
<b>COMMITTEES AND SUPPORTING ORGANIZATIONS .....</b>	ix
<b>1. KEYNOTE ADDRESS</b>	
F.K. Brunner <i>Refraction, Refractive Index and Dispersion: Some Relevant History</i> .....	3
<b>2. TROPOSPHERE</b>	
G. Elgered <i>Refraction in the Troposphere</i> (invited) .....	13
K. Kaniuth, H. Tremel <i>Analysis of Spatial and Temporal Correlations of Meteorological Parameters Associated with Tropospheric Delay Modelling</i> .....	21
J.L. Davis, G. Elgered, A.E. Niell, I.I. Shapiro <i>Horizontal Gradients in the "Wet" Atmospheric Propagation Delay</i> .....	25
J.C. De Munck <i>The Influence of Horizontal Tropospheric Gradients Derived by Assuming Spherical, but Sloping Layers</i> .....	29
J.Y. Huang, Y.P. Wang <i>Depolarization Effects of the Rainy Medium in Millimeter Wave Propagation</i> .....	33
T.A. Akhundov, A.A. Stotskii <i>Zenith Angle Dependence of Path Length through the Troposphere</i> .....	37
<b>3. GEODETIC VLBI</b>	
R.N. Treuhhaft <i>Tropospheric and Charged Particle Propagation Errors in Very Long Baseline Interferometry</i> (invited) .....	45
D.N. Matsakis, T.M. Eubanks <i>Analysis of NAVNET Geodetic VLBI Post-Fit Delay Residuals</i> .....	55
E. Sardón, A. Rius, N. Zarraoa <i>Ionospheric Calibration of VLBI Data Using GPS Observations</i> .....	59
T.A. Akhundov, V.N. Alexeev, G.B. Baykov, A.A. Stotskii <i>Tools for Troposphere Correction for VLBI Network "Quasar"</i> .....	63
H. Schuh <i>Influence of Measurement Errors of the Meteorological Data Used for Tropospheric Models in VLBI</i> .....	65

#### **4. IONOSPHERE**

T.A.Th. Spoelstra <i>The Ionosphere as a Refractive Medium</i> . . . . .	69
P.F.J. Van Velthoven <i>Climatology of Phase Errors due to Ionospheric Acoustic-Gravity Waves Observed by the Westerbork Radio Synthesis Telescope</i> . . . . .	77
E.L. Afraimovich, O.N. Boitman, V.N. Zvezdin, N.P. Minko, S.V. Fridman <i>The Physical Composition of the Oscillation Spectrum of Total Electron Content in the Ionosphere</i> . . . . .	81
P.F.J. Van Velthoven <i>Evaluation of Total Electron Content from Signals of Polar Orbiting Satellites</i> . . . . .	83
Huang Tianxi, He Jin, Liu Xuanmou <i>Modelling of the Ionosphere over North and South China for a Sunspot Cycle</i> . . . . .	87
Y. Yan <i>The Refraction of Electromagnetic Waves for a Magnetoplasma Slab</i> . . . . .	88
S.M. Golynski, V.D. Gusev <i>Deviation of Ray Trajectories in Refractive Media under the Influence of Random Inhomogeneities</i> . . . . .	91

#### **5. GPS AND OTHER SATELLITE SYSTEMS**

R.B. Langley <i>The Effect of the Ionosphere and Troposphere on Satellite Positioning Systems</i> (invited) .	97
L. Bányai, K. Kovács <i>The GPS Technique and Ionospheric Research in the GGRI</i> . . . . .	99
V.V. Vodjannikov, O.G. Gontarev, B.V. Troitsky <i>Refraction of Transitionospheric L Band Signals</i> . . . . .	103
J.-G. Leclerc, A. el A. el Alaoui <i>A Three Dimensional Representation of Tropospheric Refractivity with Application to GPS</i> . . . . .	105
E.L. Afraimovich, Yu.I. Vakulin, N.M. Minko <i>Response of the Ionosphere to a Very Strong Magnetic Storm of April 9-11, 1990 and Estimating the Error of a GPS-type Navigation System</i> . . . . .	109
A.H. Dodson, G. Elgered, P.O.J. Jarlemark, P.J. Shardlow <i>Wet Path Delay Effects on Precise GPS Height Determination</i> . . . . .	111

#### **6. SATELLITE LASER RANGING**

P.L. Bender <i>Atmospheric Refraction and Satellite Laser Ranging</i> (invited) . . . . .	117
--	-----

#### **7. GEODETIC IMAGING, REMOTE SENSING, INSTRUMENTATION**

B. Bürki, M. Cocard, A. Geiger, R. Gyger, H.-G. Kahle <i>Development of a Portable Dual Frequency Microwave Water Vapor Radiometer for Geodetic Applications</i> . . . . .	129
E.L. Afraimovich, V.N. Zvezdin, N.P. Minko, A.I. Terekhov, S.V. Fridman <i>The "TIR"-Project - Transitionospheric Radio Probing with Satellites Signals</i> . . . . .	135

Yang Yi-Pei, T.A.Th. Spoelstra	
<i>Limitations in Data Quality Imposed by the Ionosphere</i>	137
L. Wanninger	
<i>Monitoring Total Ionospheric Electron Content and Ionospheric Irregularities with GPS</i>	141
Xu Peiyuan	
<i>Water Vapor Radiometer for Chinese VLBI and GPS Geodesy</i>	147
N. Jakowski, H.-D. Bettac, A. Jungstand	
<i>Ionospheric Corrections for Radar Altimetry and Geodetic Positioning Techniques</i>	151
<b>8. MODELS, THEORY, CORRECTION TECHNIQUES</b>	
T.A. Herring	
<i>Modelling Atmospheric Delays in the Analysis of Space Geodetic Data</i> (invited)	157
Dai Kailiang, Ma Jianming	
<i>Comparison of Total Electron Content Predicted by IRI with the Data Observed in China</i>	165
K. Becek	
<i>A Simulation Study of the Refraction Effect</i>	168
A.I. Terekhov, M. Yu. Udobov	
<i>Correction for Ionospheric Refraction Distortions on the Basis of a Tomographic Processing of Signals from Navigation Satellites NNSS</i>	169
V.E. Kunitsyn	
<i>Compensation for Ionospheric Errors in Geodetic Measurements with the Help of Radiotomography Data</i>	171
M. Cocard, V. Eckert, A. Geiger, B. Bürki	
<i>Three-Dimensional Modelling of Atmospheric Parameters for Automatic Path Delay Corrections</i>	175
A.A. Stotskii	
<i>Path Length Fluctuations through the Earth Troposphere: Turbulent Model and Data of Observations</i>	179
W.J. Han, Y.J. Zheng, X.D. Wu, W.L. Zhang	
<i>A New Method to Predict Tropospheric Range Error</i>	183
R. Leitinger, P. Pesec	
<i>Ionospheric Corrections for the Land Based Altimetry Campaign</i>	187
A. Geiger, M. Cocard	
<i>Collocational Methods in Atmospheric Ray Tracing</i>	191
Huang Tianxi, Liu Xuanmou, Zhang Wenping	
<i>Trans-Ionospheric Propagation Prediction of Short Wave Radio Propagation on the Wuhan-Rome Path</i>	196
<b>AUTHOR INDEX</b>	197



## **PREFACE**

It is with great pleasure that the Netherlands Geodetic Commission presents the proceedings of the "Symposium on Refraction of Transatmospheric Signals in Geodesy".

Already in 1878 when the famous geodesist Heinrich Bruns formulated his grand view of the determination of the figure of the earth, he identified atmospheric refraction as main obstacle in its realisation. Despite of the enormous technological progress, the use of active microwave sensors, the introduction of modern space techniques and a much better understanding of the geometry and physics of the atmosphere, refraction is still a major limitation, although on a much higher level of precision than at Bruns' time. Hence still better atmospheric sensors and models need to be developed. But we also know that what is ones noise is the others signal. In recent years due to the enormous progress in computer modelling and due to an abundance of recorded measurements through the atmosphere it becomes feasible to determine the physical structure of atmosphere by inverse methods.

With this duality in mind T.A.Th. Spoelstra took the initiative to bring together scientists concerned with these subjects and in particular the members of the IAG Special Study Group 4.93 on "wave propagation in refractive media". After consultation with F.K. Brunner and a few others it was decided to organize this symposium. We are glad to notice that a large number of outstanding scientists followed the invitation.

The Netherlands Geodetic Commission thanks Mr. Spoelstra and all members of the organizing committees for the preparations and all advices owing to which we hope and expect the symposium will become a success.

The Netherlands Geodetic Commission is grateful for the support provided by the Department of Geodesy of Delft University of Technology, the International Association of Geodesy, the Nederlandse Vereniging voor Geodesie, the Royal Netherlands Academy of Arts and Sciences (KNAW) and the Survey Department of Rijkswaterstaat.

R. Rummel,  
Chairman of the Netherlands Geodetic Commission

## **ACKNOWLEDGMENTS**

We are indebted to the members of the Scientific Organizing Committee and many other individuals who made their contributions to the success we expect from this symposium. Most prominently in this regard is Mrs. H.W.M. Verhoog-Krouwel of the Netherlands Geodetic Commission, whose many efforts in the process of the preparation of this proceedings were outstanding.

We also thank the Netherlands Geodetic Commission, the International Association of Geodesy, the Survey Department of Rijkswaterstaat, Department of Geodesy of Delft University of Technology, the Nederlandse Vereniging voor Geodesie, and the Royal Netherlands Academy of Arts and Sciences (KNAW) for their valuable and highly appreciated material and immaterial contributions and supports of several kinds. Their support smoothed the organization and realization of this symposium significantly.

The Local Organizing Committee

## **COMMITTEES AND SUPPORTING ORGANIZATIONS**

### **Scientific Organizing Committee**

G. Beutler	(Switzerland)
C. Boucher	(France)
F.K. Brunner	(Chairman, Australia)
G. Elgered	(Sweden)
I. Fejes	(Hungary)
H.C. van de Hulst	(The Netherlands)
R. Leitinger	(Austria)
T.A.Th. Spoelstra	(Vice-Chairman, The Netherlands)
A.A. Stotskii	(Russia)
R.N. Treuhaft	(U.S.A.)

### **Local Organizing Committee**

F.J.J. Brouwer	(Treasurer)
G. Cornet	(Member)
J.C. De Munck	(Secretary)
F.H. Schröder	(Executive Secretary)
T.A.Th. Spoelstra	(Chairman)

### **Supporting Organizations**

Department of Geodesy of Delft University of Technology  
International Association of Geodesy  
Nederlandse Vereniging voor Geodesie  
Netherlands Geodetic Committee  
Royal Netherlands Academy of Arts and Sciences (KNAW)  
Survey Department of Rijkswaterstaat



---

## **1. KEYNOTE ADDRESS**



## REFRACTION, REFRACTIVE INDEX AND DISPERSION: SOME RELEVANT HISTORY

F.K. BRUNNER

School of Surveying, University of New South Wales  
Sydney, NSW, 2033, Australia

**ABSTRACT.** This paper reviews the history of the original contributions to the development of the refraction law, the refraction integrals and the refractive index formulae. The fundamental work of the Dutch scientists Snellius, Huygens and Lorentz are highlighted in relation to refraction effects. The use of dispersion for the determination of the refraction effect is discussed briefly. The utility of the refraction effect as a remote sensing tool is addressed.

### 1. INTRODUCTION

In astronomy and geodesy we use measurements of electromagnetic signals which propagate through the Earth's envelope. It has been recognized that the major limitation to further improvements of the accuracy of these space measurements is the effect of the propagation medium. The term space measurements encompasses satellite microwave ranging and its rate of change, satellite laser ranging, very long baseline interferometry, baseline measurements using GPS, satellite-to-satellite ranging, satellite altimetry, astrometry, astronomical seeing and imaging. The propagation medium consists of two different regions, the ionosphere and the (electrically) neutral atmosphere. The propagation effects in these two regions depend on the frequencies of the electromagnetic waves. Therefore, microwaves behave differently to light waves in the two regions.

State-of-the-art reviews and contributed papers of this symposium will establish the current accuracy requirements for the calculation of trans-atmospheric refraction effects, show achievements, and draw the "battle lines" for future work. For this key note address, I thought it appropriate to highlight some relevant historical developments. This will also permit me to remind you of the great Dutch contributions which are still of fundamental importance to our research field. Naturally a historical note about such a rich topic involving refraction, optics and electromagnetic wave propagation requires focus.

371 years ago, but only about 30 km from here, Willebrord Snell discovered the law of refraction. A review of this fundamental discovery and subsequent developments seems an appropriate starting point. Fermat's principle follows. The introduction of the concept of a refractive index ( $n$ ) is also of great interest to us. The derivation of general formulae for  $n$  shall be sketched next. The most successful instrumental solutions for the determination of the propagation effects use the wavelength dependence of  $n$ , i.e. dispersion. Thus the

history of the dispersion formulae will be outlined including some remarks about precursors of electromagnetic waves propagating through a dispersive medium.

This selection of topics is personal. Time limitations have required the exclusion of other highly interesting topics, such as the history of geometrical optics or atmospheric turbulence effects on wave propagation. Nevertheless, I hope that these few historical excursions show the intense struggles of our famous ancestors to develop general physical theories capable of explaining refraction effects.

In the last section of this paper I will address the utility of the refraction effects as a remote sensing technique for the determination of atmospheric parameters. This is a complimentary feature of the refraction effect which is – at least in my opinion – not sufficiently appreciated by those who consider atmospheric refraction as a nuisance only.

## 2. EARLY HISTORY OF REFRACTION

Some atmospheric refraction effects – such as the flattened shape of the solar and lunar disks near the horizon and the twinkling of stars – were known in ancient times. Claudius Ptolemy (130 A.D.) knew also of the fundamental refraction effect, i.e. celestial bodies are seen slightly above their true positions. He also measured the angles of incidence of light ( $\Theta_i$ ) in air and refraction ( $\Theta_r$ ) in water. However, the ancient Greek did not find the law which could explain their refraction measurements.

It was not until 1621 that Snell discovered the long hidden "law of refraction" connecting the two angles  $\Theta_i$  and  $\Theta_r$ :

$$\sin \Theta_i = K \sin \Theta_r \quad (1)$$

where  $K$  is some constant. According to Snell,  $K$  was a number which was characteristic of the medium.

Willebrord Snel van Royen (1580 – 1626) was a famous professor at the University of Leiden. (Note, in English it has become custom to spell Snel as Snell rather than Snellius). He invented also the point resection method and was the first person who measured by triangulation a meridian chain (between Alkmaar and Bergen op Zoom, about 130 km long) in order to determine the radius of the earth. Snell's life and geodetic achievements were beautifully documented by Haasbroek (1968). His contemporaries were Brahe and Kepler whom he knew personally. In 1587 Tycho Brahe was the first to make quantitative measurements of the magnitude of astronomical refraction for which he devised an ingenious method. Kepler published a theory of astronomical refraction in 1604, when the correct refraction law was still unknown. The first to make use of Snell's law for developing a theory of astronomical refraction was Cassini in 1656. Like Brahe and Kepler he considered the earth's atmosphere to be a spherical shell with constant density, so that all the refraction occurred only at the upper limit of the atmosphere. Many famous scientists (e.g. Newton, Bessel, Bouquer, Bradley) were attracted by astronomical refraction to develop new theories, see Mahan (1962).

Let us return to Snell's law. He died before it was published, and his results were uncovered in 1632. René Descartes was the first to publish the formulation of the refraction law in terms of sines in 1637. A charge of plagiarism was made. In Descartes' derivation  $K$  is interpreted as the ratio of velocities,  $K = v_r/v_i$ . Since  $K > 1$  when light enters a denser medium, Descartes concluded that the velocity in it must be greater in that medium. Descartes used bouncing balls as his model for light propagation.

Pierre de Fermat (1601 – 1665) took exception to Descartes' model. In 1657 he rederived the law of refraction from his own "principle of least time", i.e. the "flight time" of light between any two points is a minimum. The justification for his principle was that "nature is essentially lazy" (Stavroudis, 1972). Fermat was firmly committed to a finite velocity of light, which was measured for the first time by Olaf Römer in 1675 from the observations of the eclipses of Jupiter's satellites. Fermat arrived at exactly the opposite result of Descartes

$$K = v_i/v_r \quad (2)$$

which asserts that light must travel more slowly in a denser medium.

Whilst Snell discovered a law, Fermat formulated a theoretical principle. For example, this principle allows us to calculate that the speed of light in water is less than in air from the measurement of refraction angles. A brilliant prediction which is not possible from Snell's law. Hence, a theoretical principle allows us to predict new things (Feynman et al., 1963).

Two physical theories of light were created during the seventeenth century. Huygens formulated the geometrical wave theory of light, and Newton formulated a mechanical theory of propagation of particles. Christiaan Huygens (1629 – 1695) was a famous Dutch scientist who lived in Den Haag. Huygens' wave theory is in agreement with Snell's law and the constant K agrees with Fermat's conclusion. Newton's theory appeared to explain the phenomenon colour with greater elegance, but Newton supported Descartes' postulate of a faster velocity of light in a denser medium.

### 3. REFRACTIVE INDEX

We can interpret the constant K as the relative refractive index of the two media. However, it is of greater advantage to introduce an absolute refractive index n for any medium

$$n = c/v \quad (3)$$

where c is the velocity of light in vacuum and v is the speed of light in the medium. K is then the ratio of the appropriate two n values. In the optical sense, any medium can now be characterised by the refractive index  $n(x,y,z)$  which is a function of position (x,y,z).

Fermat's principle can now be formulated in terms of the optical distance between two points A and B which is defined by the line integral

$$\int_A^B ds n(x,y,z) \quad (4)$$

taken over any path connecting A and B. Substituting (3) into (4) reminds us of the original time relationship. Fermat's principle states that the actual path selected by light makes the value of the integral (4) least. The physically correct formulation (Born and Wolf, 1980) says that the first variation of the integral (4), in the sense of the calculus of variations, must be zero. The actual path selected is called a ray. The design of many optical instruments is based on this principle.

Fermat's principle and also the mathematical theory of geometrical optics as formulated by Hamilton in 1832 introducing the characteristic function of an optical system, says nothing about the nature of light. Quite unconnected to optics, the studies of electricity and magnetism gave meaningful results during the nineteenth century. James Clark Maxwell (1831 – 1879) brilliantly summarized all knowledge on the subject in one single set of differential equations in 1873. He showed that an electromagnetic field could propagate as a transverse wave. He derived the speed of this wave in terms of electric and magnetic properties of the medium. Light was proposed to be an electromagnetic wave. The experimental verification of long electromagnetic waves was achieved by Hertz in 1888.

Using the Maxwell equations the refractive index  $n$  is obtained as

$$n = \sqrt{\epsilon \mu} \quad (5)$$

where  $\epsilon$  is the dielectric permittivity and  $\mu$  is the magnetic permeability of the medium. Equation (5) is called Maxwell's formula. The dependence of  $n$  (through  $\epsilon$  and  $\mu$ ) on the wavelength of the electromagnetic wave, called dispersion, will be discussed shortly.

Let us introduce the wave number  $k_0$

$$k_0 = 2\pi/\lambda_0 \quad (6)$$

where  $\lambda_0$  is the wavelength in vacuum. Under certain simplifying assumptions, the Maxwell equations can be reduced to the so-called Helmholtz wave equation

$$\nabla^2 U + k_0^2 n^2 U = 0 \quad (7)$$

where  $\nabla$  is the del operator and  $U$  is the complex amplitude of the wave. Using an original suggestion by Debye, Sommerfeld and Runge showed in 1911 that the equations of geometrical optics can be obtained from (7) in the limit by letting  $\lambda_0$  approach zero (Born and Wolf, 1980). The main result is the so-called eikonal equation of geometrical optics

$$(\nabla \Phi)^2 = n^2 \quad (8)$$

where  $\Phi$  is the optical path length, a scalar function of position.

Refraction corrections are often related to the "refraction integrals", which are based on results from geometrical optics. The optical path length is given as

$$\Phi = \int_{\text{path}} ds n \quad (9)$$

and the refraction angle  $\delta$  (the difference between apparent and true position of a target) by

$$\delta = \int_{\text{path}} \frac{ds}{l} \left( \frac{s}{l} \nabla_T (\log n) \right) \quad (10)$$

where  $\nabla_T$  is the transverse gradient to the path, and  $s$  is the length of the path counted from the source to the observer, and  $l$  is the total path length.

In order to evaluate the refraction integrals (9) and (10), the values of  $n$  must be known. In 1880 Lorentz and independently Lorenz were able to show

a relationship between  $n$  and the density ( $\rho$ ) of the medium. The derivation is based on the assumption that the electric dipole moment of a molecule under the influence of a field is proportional to the effective field. This leads to the Lorentz-Lorenz equation

$$\frac{n^2 - 1}{n^2 + 2} = R \frac{\rho}{W} \quad (11)$$

where  $W$  is the molecular weight, and  $R$  is the molar refractivity of the medium. It can be shown that the refractive index of a mixture of gases is the sum of the appropriate contributions of molar refractivities. Hendrik Anton Lorentz (1853 – 1928) was a professor at the University of Leiden who made many important contributions to physics.

#### 4. DISPERSION

Newton began his famous experiments on dispersion at the age of 23 in 1665. He concluded that white light was composed of a mixture of independent colours, where every colour corresponds to a specific vibration of the aether caused by the propagating light corpuscles.

Lorentz was able to explain dispersion using his electron theory of matter. In this theory the medium is considered to consist of electrically charged electrons and atomic nuclei moving in a vacuum. If a non-polar molecule is subjected to an electric field, the electrons and nuclei are displaced by the so-called Lorentz force, generating a dipole moment. The resulting differential equation for the motion of an electron can be solved. Let us introduce the resonance (or absorption) frequency of the medium  $\omega_0$ . For the simplified situation of no collision between the atoms, the refractive index can be expressed as (Born and Wolf, 1980)

$$\frac{n^2 - 1}{n^2 + 2} = \frac{e^2 N}{12 \pi^2 \epsilon_0 m (\omega_0^2 - \omega^2)} \quad (12)$$

where  $N$  is the number of molecules per unit volume,  $\epsilon_0$  is the dielectric permittivity in vacuum,  $e$  is the charge and  $m$  the mass of the electron, and  $\omega$  is the frequency of the field. For a medium with several different absorption frequencies, the summation of the appropriate terms of the right-hand-side of (12) is applicable. The frequency dependence of  $n$  determines the mode of dispersion: normal or anomalous dispersion.

If the electrons are not bound to a nucleus (i.e. free electrons) then  $n$  may be expressed by the equation

$$n^2 - 1 = \frac{e^2 N}{4\pi^2 m \epsilon_0 \omega^2} \quad (13)$$

This equation is useful in explaining refraction of radio waves by the ionosphere assuming isotropic conditions.

Hertzsprung (1912) is credited for the original idea to use angle measurements at different colours for the calculation of the refraction effect. According to the information available to me, Näbauer (1924) was the first to propose and investigate the theory of the "dispersion method", independently of Hertzsprung's

work. For the following argument let us assume that the refractive index can be expressed as the product of two terms

$$n(x,y,z) - 1 = a(\omega) A(x,y,z) \quad (14)$$

where  $a(\omega)$  depends on the frequency  $\omega$  of radiation [see (12)], and  $A(x,y,z)$  depends on the density distribution of the propagation medium [see (11)]. If, for example, the optical path length (9) is measured twice at two different frequencies then the resulting two equations can be used to eliminate the "atmospheric integral" of the  $A(x,y,z)$  term along the optical path. This permits the calculation of the vacuum distance. Thus the effect of the refractive medium has been eliminated. Similarly, the vertical refraction effect can be eliminated. This method has been applied successfully to eliminate atmospheric propagation effects for the case that the dispersion effect of the radiation frequencies is large enough to be measurable, e.g. ionospheric propagation effect on microwaves. However, it should be noted that even the dispersion method is not rigorous, as different frequencies will, of course, have different paths according to Fermat's principle. Therefore the elimination of the "atmospheric integral" is only approximately possible, see Gu and Brunner (1990).

Another at least theoretical solution of the refraction problem would be the use of the precursor phenomenon, which occurs when a limited wavetrain or a wave packet propagates through a dispersive medium. Precursors were predicted by Sommerfeld (1914), who showed that the very front of a signal propagates with the velocity  $c$  in any dispersive medium. The dispersion electrons are originally at rest when the signal reaches them. Dispersion is due to the induced periodic oscillation of the electrons. Thus, to begin with, the medium is optically void like vacuum. Immediately behind the wavefront a disturbance arrives which is termed a precursor. The first precursor arrives with zero amplitude which increases afterwards steadily. The low amplitude of the precursor may be explained by the withdrawal of energy from the incident wave to build up the oscillation of the electrons. The previous conclusion that precursors have not sufficient energy to be measurable in geodetic applications appears to be still valid (Brunner, 1979).

## 5. UTILITY OF REFRACTION EFFECTS

We now leave the historical development of the foundations of refraction studies. As the following state-of-the-art reports will establish, much progress was made in the accurate modelling of the refraction effects on astrometric and geodetic measurements during the past three decades. Nevertheless, the atmospheric refraction effect still remains the most significant accuracy limitation; see Mueller and Zerbini (1989). The instrumental measurement noise of most systems is significantly better than our current capability to correct for the atmospheric propagation effects. No doubt, improvement of this situation is very important especially for geodetic space measurements in order to provide the most accurate information for crustal motion and sea level changes.

It is worthwhile to remember here that what is a severe accuracy limitation (nuisance) for geodetic and astrometric measurements, is a very useful signal for remote sensing applications. The use of the refraction effect for remote sensing of atmospheric parameters has become feasible since recent significant improvements of the precision of the measurement systems. The refraction integrals (9) and (10) show that the line averages of atmospheric density and density gradients can be calculated if the refraction effect is known. Subsequently

atmospheric density can be expressed as a function of pressure, temperature and humidity. For ionospheric conditions the total electron content of a slant path is obtained. A few examples should be given here to highlight this exciting field of remote sensing: (i) The application of tomography to ionospheric studies. (ii) The use of occultation measurements for studying the atmospheric envelope of planets including the earth using space crafts and natural celestial radiation sources. (iii) Careful measurements of the effects of atmospheric turbulence on the propagation of transatmospheric signals, e.g. star light, can be used to calculate atmospheric parameters, e.g. wind speed at various heights above the earth's surface. (iv) Images of the setting sun can be used to infer the detailed structure of the temperature field close to the ground.

With the impressive recent advances in modelling the transatmospheric propagation effects, with the promising new remote sensing applications already available, and with the prospect for further new ideas, the next years in the field of refraction studies should be exciting and productive.

#### ACKNOWLEDGEMENTS

This paper was written whilst I was on leave at the Geodetic Institute, Universität der Bundeswehr, Munich with Prof. Walter Welsch as my host. This leave was supported by the Deutsche Forschungsgesellschaft (DFG).

#### REFERENCES

- Born, M., Wolf, E. (1980) Principles of Optics, 6th ed., Pergamon  
Brunner, F.K. (1979) On Precursors of Electromagnetic Wave Propagation.  
Refractional Influences in Astronomy and Geophysics, in eds. E. Tengström,  
G. Teleki, Reidel Publ., p. 357  
Feynman, R.P., Leighton, R.B., Sands, H. (1963) The Feynman Lectures on  
Physics. Addison Wesley Publ.  
Gu, M., Brunner, F.K. (1990) Manuscripta Geodaetica, 15, 357  
Haasbroek, N.D. (1968) Gemma Frisius, Tycho Brahe and Snellius and their  
Triangulations. Publ. Geodetic Commission Netherlands, Delft  
Hertzsprung, E. (1912) Astron. Nachr. 192, 308  
Mahan, A.I. (1962) Applied Optics, 1, 497  
Mueller, I.I., Zerbini, S., (eds.) (1989) The Interdisciplinary Role of Space  
Geodesy, Lecture Notes in Earth Sciences, Springer Verlag, Volume 22  
Nähbauer, M. (1924) Strahlenablenkung und Farbenzerstreuung genügend steiler  
Sichten durch die Luft. Abh. Bayer. Akad. Wissensch. Vol. 30, Part 1  
Sommerfeld, A. (1914) Ann. Phys. 44, 177  
Stavroudis, O.N. (1972) The Optics of Rays, Wavefronts, and Caustics.  
Academic Press



## **2. TROPOSPHERE**



## REFRACTION IN THE TROPOSPHERE

G. ELGERED

Department of Radio and Space Science

Onsala Space Observatory

Chalmers University of Technology

S-439 00 Onsala, Sweden

tel +46 30060650, fax +46 30062621, e-mail geo@oden.oso.chalmers.se

**ABSTRACT.** The atmospheric refraction introduces uncertainties in the time of arrival of transatmospheric signals due to bending and retardation along the propagation path. Geodetic applications include both optical and radio signals and due to differences in refractivity these are affected slightly different by the neutral atmosphere. We will discuss the temporal and spatial variations of the fundamental atmospheric quantities pressure, temperature, water vapor, and liquid water. Results obtained using different instruments and methods to estimate these and related quantities are presented.

### 1. INTRODUCTION

The path distortions which radio signals undergo when traversing the atmosphere of the earth are important for many applications in areas such as space geodesy using radio positioning systems, radar altimetry from satellites, radio propagation experiments and radio astronomy. This refraction introduces uncertainties in the time of arrival of the signal due to bending and retardation along the propagation path. The path is determined from the knowledge of the index of refraction in the atmosphere using Fermat's Principle. Ray-tracing techniques can been used to study variations in the length and the bending of the path (*Freehafer*, 1951).

The index of refraction  $n$  is conveniently expressed in terms of the refractivity  $N$  defined as

$$N = 10^6 (n - 1) \quad (1)$$

An often used expression for  $N$  has the following form:

$$N = k_1 \frac{p_d}{T} Z_d^{-1} + k_2 \frac{e}{T} Z_w^{-1} + k_3 \frac{e}{T^2} Z_w^{-1} \quad (2)$$

where  $p_d$  is the partial pressure of the dry constituents of air,  $e$  is the partial pressure of water vapor (*i.e.*, the total pressure  $P = p_d + e$ ),  $T$  is the absolute temperature, and  $Z_d^{-1}$  and  $Z_w^{-1}$  are the inverse compressibility factors for dry air and water vapor, respectively (corrections for the departure of air from an ideal gas (*Owens*, 1967)). The

parameters  $k_1$ ,  $k_2$ , and  $k_3$  can be obtained from laboratory measurements (*Boudouris*, 1963). The first two terms are important at optical frequencies whereas the third term is responsible for most of the variations in the radio range. Detailed discussions on the value of the refractivity are given by *Owens* (1967) for optical frequencies and by *Hill et al.*, (1982) and *Hill* (1988) for radio frequencies. In this presentation we will first give theoretical background for the radio path delays and their dependence on the atmospheric variables. Thereafter, we will present measured variations in pressure, temperature, humidity, and liquid water and discuss their site dependence.

## 2. PATH DELAY DUE TO ATMOSPHERIC GASES

In the radio range it is convenient to express the path delay in two terms. One term can be derived using the assumption of hydrostatic equilibrium in the atmosphere. Only during extreme conditions deviations from hydrostatic equilibrium may cause errors of several mm in the zenith delay (*Hauser*, 1989). This term, which we call the hydrostatic delay, is proportional to the total pressure at the ground  $P_0$ . (*Davis et al.*, 1985):

$$\Delta L_h = (2.2768 \pm 0.0005 \text{ (mm/mbar)}) \frac{P_0}{f(\Phi, H)} \quad (3)$$

where

$$f(\Phi, H) = (1 - 0.00266 \cos 2\Phi - 0.00028H) \quad (4)$$

is used to model the variation of the acceleration due to gravity (*Saastamoinen*, 1972),  $\Phi$  is the latitude, and  $H$  is the height in km of the station above the ellipsoid. The hydrostatic path delay in the zenith direction will consequently be determined with high accuracy from the total pressure at the ground and an effective value of the acceleration due to gravity in the atmosphere above the site. Its elevation dependence can be defined by a “mapping-function” which is often defined to also include the small but significant effect of the geometric delay.

The left-over terms of the refractivity are integrated in order to obtain an expression for the wet path delay  $\Delta L_w$  which is then defined as:

$$\Delta L_w = (0.382 \pm 0.004) K^2 \text{ mbar}^{-1} \int_S \frac{e}{T^2} Z_w^{-1} ds \quad (5)$$

Equations (3)–(5) summarizes the radio path delay caused by the gases in the neutral atmosphere. Additionally, we note that the mapping function used to model the elevation dependence of the hydrostatic path delay is mainly sensitive to variations in the temperature profile of the atmosphere.

## 3. PATH DELAY DUE TO LIQUID WATER

Liquid water in the atmosphere is known as clouds and rain. Let us first study the case when clouds have drop sizes much smaller than the wavelength of the radio signal. The following expression has been obtained for the non-dispersive delay due to clouds, for a water temperature of 283 K (*Liebe et al.*, 1989):

$$\Delta L_c = 0.15 \rho_c h_c \quad (6)$$

where the delay  $\Delta L_c$  is in cm, the liquid water density  $\rho_c$  is in  $\text{g m}^{-3}$ , and the path length  $h_c$  through the cloud is in km. The dispersive component of the delay due to liquid water droplets is at least ten times smaller than the non-dispersive component for frequencies below 30 GHz.

Upper bounds of  $1 \text{ g m}^{-3}$  liquid water density and of 5 km for the cloud height give a value of the zenith delay due to clouds of 0.75 cm. Therefore, the delay due to clouds can, in general, be neglected or modeled if the integrated amount of liquid water is known. A microwave radiometer used to estimate the wet delay is usually designed so that the integrated amount of liquid water is estimated simultaneously with the wet delay.

In order to estimate the delay due to rain one should have knowledge about the drop-size distribution as well as the shape and orientation of the drops along the propagation path. A model presented by *Uzunoglu et al.* (1977) indicates that the expected delay due to rain along a ground path for a signal at 11 GHz is approximately 0.6 cm per km path length within the rain cell for the extreme rainfall rate of 100 mm/h. Hence the delay caused by rain can most of the time be ignored.

#### 4. PRESSURE VARIATIONS

The radio path delay in the zenith direction is proportional to the ground pressure according to (3). A change of 1 mbar in the ground pressure corresponds to a change in the path delay of approximately 0.23 cm. Figure 1 shows ground pressure measurements at seven sites at different latitudes. The RMS variations over a 12 hour period ranges from 1 to 5 mbar, which corresponds to path delay variations from 0.2 to 1.1 cm in the zenith direction. The well known meteorological effect of larger variations in the pressure at high latitudes (*Handbook of Geophysics and the Space Environment*, 1985) is clearly seen in Figure 1.

#### 5. TEMPERATURE VARIATIONS

The temperature variations in the atmosphere are mainly in the vertical profile. Temperature profiles are acquired with radiosondes launched at hundreds of sites over the globe. Normally two launches per day are made at 0 and 12 universal time. During the last one to two decades the use of ground-based as well as satellite-based remote sensing instruments for estimation of the temperature of the atmosphere has increased (see e.g. *Hogg et al.*, (1983); *Westwater et al.*, (1984); and *Smith*, (1991)).

As mentioned above the temperature profile is important in order to derive an appropriate mapping function for a given site. Quantities such as the lapse rate (the temperature gradient with height) and the tropopause height can be used in order to derive both site and seasonal dependent mapping functions. Average values of temperature profiles as a function of latitude and time of year have been presented by *Kochanski* (1955) and *Crutcher* (1969). A simple example of seasonal variation is given in Figure 2. The monthly means of the temperature profiles measured at Göteborg-Landvetter Airport in Sweden for January and July 1985 show significant

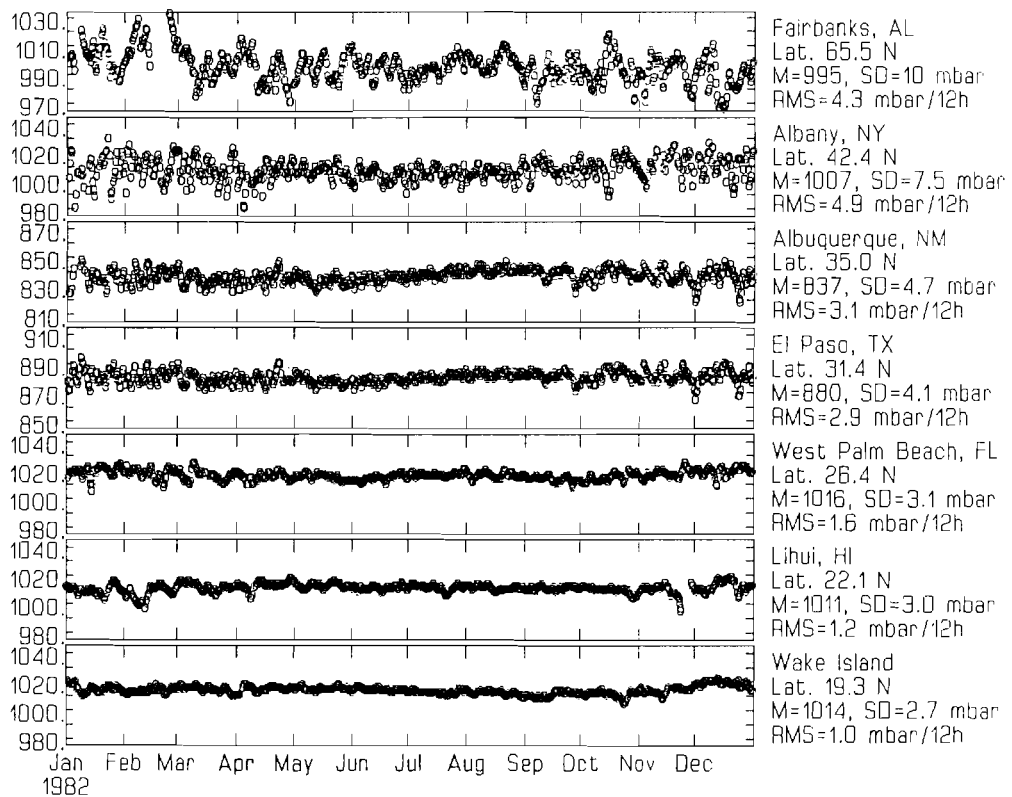


Figure 1. Variations in the ground pressure. The site name and latitude, the mean value (M), the standard deviation (SD), and the RMS of the change over a 12-hour period are given to the left of the plot for each site.

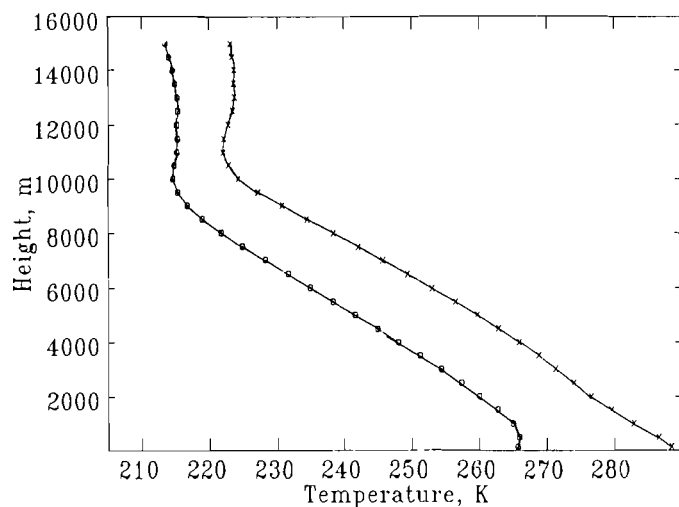


Figure 2. Mean temperature profiles at Göteborg-Landvetter Airport for January (o) and July (x), 1985.

differences. The tropopause height decreases and the lapse rate is close to zero in the first kilometer due to frequent temperature inversions close to the ground during the winter. The site dependence of mapping functions have been discussed by, *e.g.*, *Davis et al.* (1985) and *Ifadis* (1986).

## 6. HUMIDITY AND CLOUDS

Since the humidity and temperature are highly correlated the large scale variations depend on the latitude. In terms of average zenith values over the year, the wet delay range from only a couple of mm around the poles to 40 cm or more in the equatorial region. In the temperate regions a lot of variations is caused by moving low pressures. An example of variations caused by a moving low pressure with its associated warm and cold fronts is seen in Figure 3. It shows the equivalent zenith wet delay measured with radiosondes every 12 hours at Göteborg–Landvetter Airport and estimated from microwave radiometer data taken at the Onsala Space Observatory (distance 37 km from the airport). The warm front reaches the area around lunch on October 12. The gap in the radiometer data together with the increase in the amount of liquid water indicate that it was raining for several hours thereafter. Rain is also falling just before noon on October 13 when the following cold front passes the area. We conclude that the passage of a weather front can cause changes in the wet delay of several cm in an hour. Statistics of weather front passes and changes in the wet delay show that most of the large variations in the wet delay in the temperate climate of Sweden coincide with moving weather fronts (*Elgered et al.*, 1990).

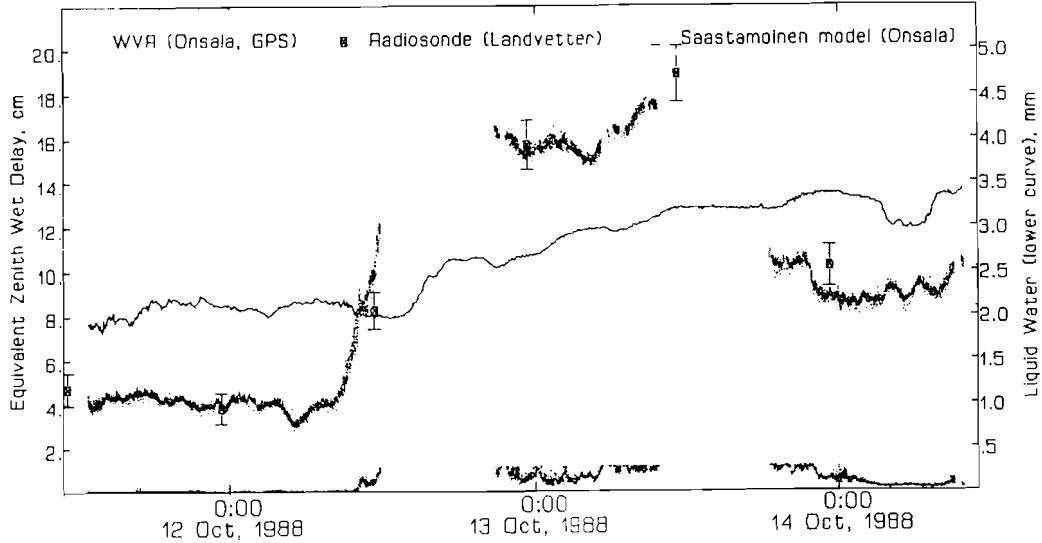


Figure 3. Measurements of the wet delay (upper curve of dots, left scale) and liquid water content (lower curve of dots, right scale) using a microwave radiometer. The gaps in these data are caused by rain. Radiometer data implying a liquid water content of more than 0.3 mm are ignored. The points with the vertical error bar show radiosonde measurements of the wet delay and the solid line shows the wet delay estimated using ground measurements of temperature and humidity (*Saastamoinen*, 1972).

A weather front passage can also cause horizontal gradients in the wet delay. This is shown in Figure 4. The wet delay changes from about 8 to 15 cm in a couple of hours. During the passage of the warm front a clear signature is seen in the  $270^\circ$  long azimuth scans carried out with the radiometer. The wind at the ground was 7 m/s SW at 9 UT. This direction agrees rather well with the maximum value in the azimuth scan. Passages of weather fronts have also been seen in Raman Lidar data (*Melfi et al.*, 1989).

Variations in the humidity are also caused by small scale phenomena such as thunder-storms and cloud formations. Microwave radiometer measurements during thunder storm conditions have been reported for many sites, *e.g.*, by *Westwater and Guiraud*, (1980), *Ware et al.*, (1985), and *Elgered et al.*, (1990). Excess values of the humidity in and around clouds have been measured using airborne sensors (*Radke and Hobbs*, 1991). Another example is variations in the height of an inversion which due to the strong correlation between temperature and humidity can cause significant (periodic) variations in the wet delay (*Decker et al.*, 1981).

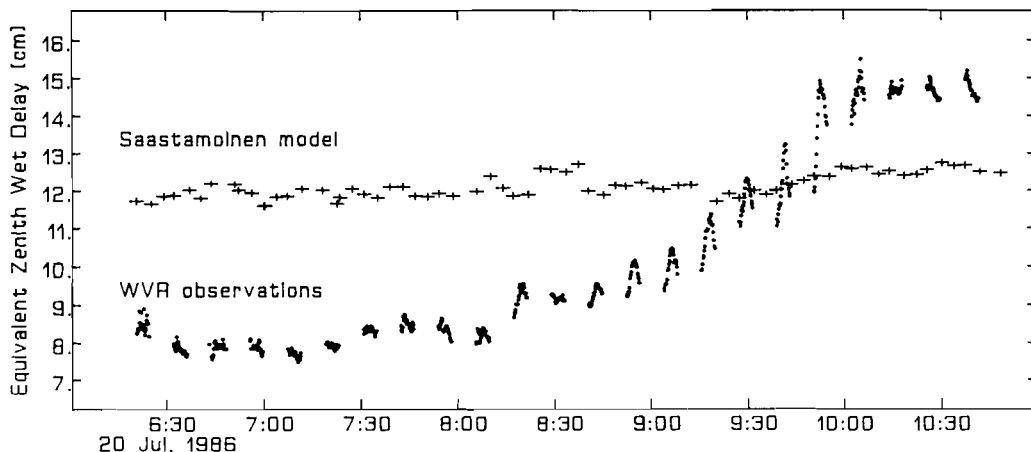


Figure 4. Microwave radiometer measurements of the wet delay during a warm front passage. Each group of data consists of an azimuth scan at a constant elevation of  $30^\circ$ . The scans start in the east moves over the south and west making one observation every  $10^\circ$  and end in the north. Note the total lack of correlation between the delay obtained from the ground-based model (*Saastamoinen*, 1972) and the delay estimates from the radiometer.

## REFERENCES

- Boudouris, G., (1963) *J. Res. Natl. Bur. Stand.*, **67D**, 631  
 Crutcher, H.L., (1969) in *Climate of the Free Atmosphere*, ed. D.F. Rex, Elsevier, Amsterdam, p 45  
 Davis, J.L., Herring, T.A., Shapiro, I.I., Rogers, A.E.E., Elgered, G. (1985) *Radio Sci.*, **20**, 1593  
 Decker, M.T., Einaudi, F., and Finnigan, J.J. (1981) *J. of Appl. Meteorol.*, **20**, 1231  
 Elgered, G., Johansson, J.M., and Rönnäng, B.O. (1990) *Res. Rept. No. 165*, Onsala Space Obs., Chalmers Univ. of Tech., Göteborg

- Freehafer, J.D. (1951) in *Propagation of Short Radio Waves*, **13**, ed. D.E. Kerr, McGraw-Hill, New York, p. 41
- Handbook of Geophysics and the Space Environment* (1985) ed. A.S. Jursa, p. 15-48
- Hauser, J.P. (1989) *J. of Geophys. Res.*, **94**, 10182
- Hill, R.J., Lawrence, R.S., Priestley, J.T. (1982) *Radio Sci.*, **17**, 1251
- Hill, R.J. (1988) *IEEE Trans. Ant. and Propagat.*, **AP-36**, 423
- Hogg, D.C., Decker, M.T., Guiraud, F.O., Earnshaw, K.B., Merritt, D.A., Moran, K.P., Sweezy, W.B., Strauch, R.G., Westwater, E.R. and Little, C.G. (1983) *J. of Climate and Appl. Meteorol.*, **22**, 807
- Ifadis, I. (1986) *Technical Report No. 38L*, School of Electrical and Computer Engineering, Chalmers Univ. of Tech., Göteborg
- Kochanski, A. (1955) *J. of Meteorology*, **12**, 95
- Liebe, H.J., Manabe, T., and Hufford, G.A. (1989) *IEEE Trans. Ant. and Propagat.*, **AP-37**, 1617
- Melfi, S.H., White, D., and Ferrare, R. (1989) *J. of Appl. Meteorology*, **28**, 789
- Owens, J.C. (1967) *Appl. Opt.*, **6**, 51
- Radke, L.F., and P.V. Hobbs (1991) *J. Atmos. Sci.*, **48**,
- Saastamoinen, J. (1972) in *The Use of Artificial Satellites for Geodesy, Geophys. Monogr. Ser.*, **15**, ed. S.W. Henriksen *et al.*, American Geophysical Union, Washington, D.C., p. 247
- Smith, W.L. (1991) *Q. J. R. Meteorol. Soc.*, **117**, 267
- Uzunoglu, N.K., Evans, B.G. Holt, A.R. (1977) *Proc. IEE*, **124**, 417
- Ware, R.H., Rocken, C., Goad, C.C., and Snider, J.B. (1985) *IEEE Trans. on Geosci. and Remote Sens.*, **GE-23**, 467
- Westwater, E.R., and Guiraud, F.O. (1980) *Radio Sci.*, **15**, 947
- Westwater, E.R., Sweezy, W.B., McMillin, L.M., and Dean, C. (1984) *J. of Climate and Appl. Meteorol.*, **23**, 689



# ANALYSIS OF SPATIAL AND TEMPORAL CORRELATIONS OF METEOROLOGICAL PARAMETERS ASSOCIATED WITH TROPOSPHERIC DELAY MODELLING

K. KANIUTH, H. TREMEL  
Deutsches Geodätisches Forschungsinstitut (DGFI), Abt. I  
Marstallplatz 8  
D-8000 München 22, Germany

**ABSTRACT.** A data set resulting from 14,501 radio sonde flights performed by a network of 63 European aerological stations during a one year period is analysed. In particular, the spatial and temporal correlation of the precipitable water vapour, being a measure of the wet component of the tropospheric path delay, is investigated. In addition, the dependence of the height of the tropopause on surface temperature and site location is studied.

## 1. INTRODUCTION

The uncertainty associated with estimating the delay due to the refractivity of the troposphere poses significant limitations when applying Global Positioning System (GPS) or other microwave system measurements for highly accurate geodetic positioning. Whereas the hydrostatic part of the tropospheric path delay can be modelled rather well the so called wet component is difficult to predict because of the irregular distribution of water vapour in the atmosphere. None of the models presently used for estimating the effect based on surface meteorological measurements only can ultimately achieve the required accuracy. Therefore, several investigations in particular aiming at improving the modelling of the wet path delay were performed, and new approaches were proposed (Askne and Nordius 1987, Hendy and Brunner 1990). When processing GPS networks it is common practice to solve for additional parameters accounting for insufficiently modelled tropospheric refraction. For properly constraining these parameters by introducing appropriately chosen variance/covariance functions also the knowledge about the temporal and spatial variations of relevant meteorological parameters might be helpful. By analysing radio sonde data this paper tries to contribute to this topic.

## 2. DATA ANALYSIS

We had at our disposal a data set resulting from 14,501 radio sonde flights performed by a network of 63 European aerological stations between August 1988 and July 1989 (Figure 1). Very few of these stations performed radio sonde launches on a 6 hours

schedule, most of them only every 12 hours at midnight and noon UT. Among others the following meteorological parameters resulted from the radio sonde flights:

- Height of the Tropopause (HTP)
- Integrated Precipitable Water Vapour (PWV).

The HTP data is analysed because some of the well known models for estimating the wet path delay in closed form assume this parameter to be defined a priorily. We try to verify the dependence of HTP on the surface temperature and possibly on the site location. PWV is related to the wet path delay  $\Delta L_W$  at zenith by the expression (Hogg et al. 1981)

$$\Delta L_W [\text{cm}] = 6.277 \text{ PWV} [\text{g/cm}^2] \quad (1)$$

Although this relation depends slightly on season and site location PWV is assumed to be a reliable measure of  $\Delta L_W$ . For describing the spatial and temporal correlation of PWV we are using Pearson's linear correlation coefficient  $r$  as well as Spearman's rank order correlation coefficient  $r_s$ :

$$r = \frac{\sum_i (x_i - \bar{x})(y_i - \bar{y})}{\sqrt{\sum_i (x_i - \bar{x})^2} \sqrt{\sum_i (y_i - \bar{y})^2}}, \quad r_s = \frac{\sum_i (R_i - \bar{R})(S_i - \bar{S})}{\sqrt{\sum_i (R_i - \bar{R})^2} \sqrt{\sum_i (S_i - \bar{S})^2}} \quad (2)$$

with  $x_i, y_i$  being the pairs of PWV quantities under analysis and  $R_i, S_i$  being the ranks of  $x_i$  and  $y_i$  respectively;  $\bar{x}, \bar{y}, \bar{R}$  and  $\bar{S}$  stand for the mean values. In presenting the results we do not distinguish between these two measures of correlation because for none of the analysed data series any significant difference occurred.

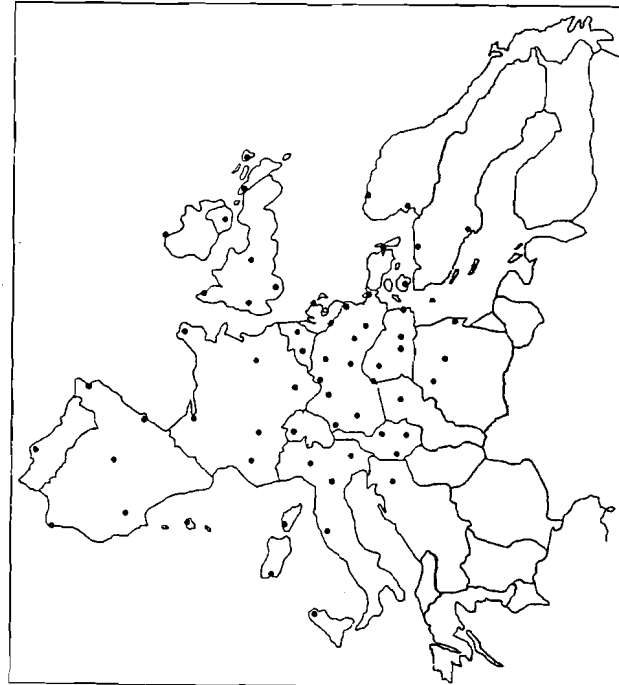


Figure 1. Location of the aerological stations included in the analysis

### 3. RESULTS

Although analysed also separately we cannot display individual results for the data series of any particular site; instead the results presented refer either to the complete data set or to certain station arrays. The temperature dependence of HTP turned out to be significant for all stations. When analysing the total data set also a latitude dependence showed up, and HTP can be described by the relation

$$HTP [km] = (10.226 \pm 0.020) + (0.078 \pm 0.001)T_S [^{\circ}C] + (0.094 \pm 0.016)\cos\varphi \quad (3)$$

with  $T_S$  = surface temperature and  $\varphi$  = site latitude.

The temporal correlation of PWV has also been analysed for each of the 63 aero-logical stations separately. In case of the majority of sites the number of samples was sufficient to show an individual correlation function. Significant differences occurred only between sites presumably belonging to different climatic areas. Therefore, Figure 2 presents the temporal correlation of PWV for 6 regional station arrays: SCAN = Southern Scandinavia, BRIT = British Islands, CENT = Central Europe, WEST = Western Europe, IBER = Iberian Peninsula, IMED = Italian Mediterranean.

With regard to the spatial correlation of PWV isotropy has been assumed. Figure 3 shows the correlation as function of the spherical distance on the Earth's surface. We have also analysed whether or not the correlation of PWV depends on the amount of PWV itself rather than on distance (Figure 2).

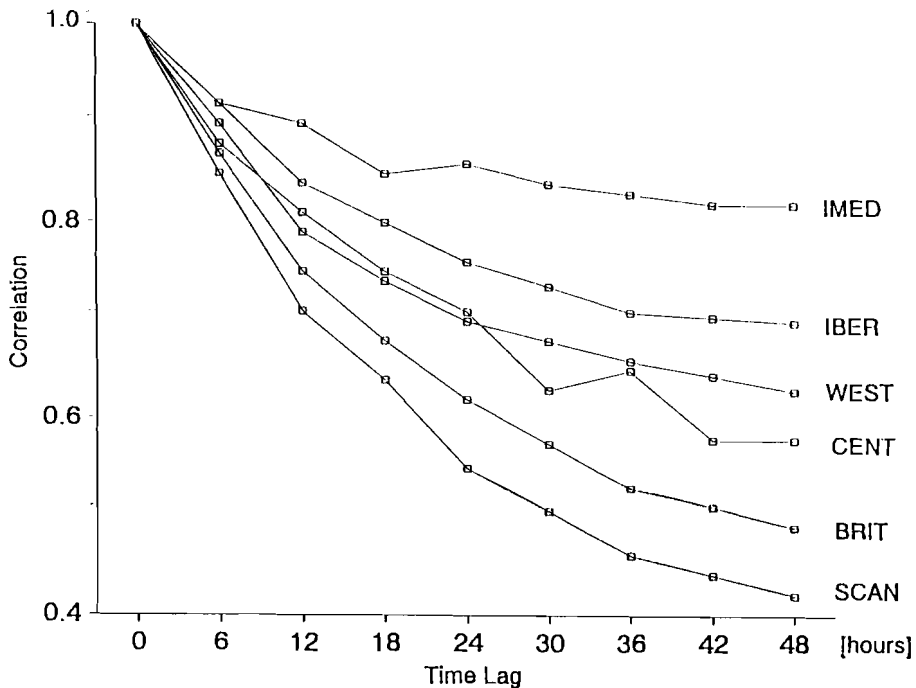


Figure 2. Correlation of PWV as function of time lag

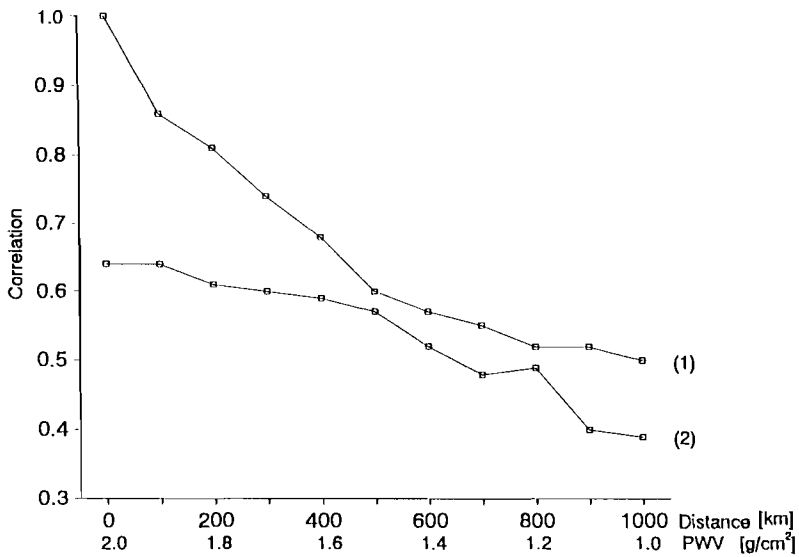


Figure 3. Correlation of PWV as function of distance (1) and of  $|PWV|$  (2).

#### 4. CONCLUSION

As to the temporal distribution and spacing the data set was rather inhomogenous. Moreover, due to a possible wind drift of the balloons the derived Precipitable Water Vapour (PWV) values do not necessarily reflect the true vertical wet path delay. Nevertheless, it seems that the obtained results allow the following conclusions:

- The Height of the Tropopause (HTP) can be described as a linear function of surface temperature and shows also a slight latitude dependence; equation (3) is recommended for application in the area covered by the analysed data set.
- There is a remarkable correlation of PWV over distances of up to several hundred kilometers; in addition, there is an indication for a slight correlation increase with the amount of PWV itself increasing.
- The temporal correlations of PWV significantly differ between the various regions analysed; by far the highest correlations resulted for the Italian Mediterranean area.
- The application of covariance functions describing the spatial and temporal correlations of PWV to GPS network adjustments should be considered.

#### ACKNOWLEDGEMENT

The radio sonde data set has been made available by the Deutscher Wetterdienst, Wetteramt München.

#### REFERENCES

- Askne, J., Nordius, H. (1987) *Radio Sc.* **22** (3), p. 379  
 Hendy, M.R., Brunner, F.K. (1990) *Aust. J. Geod. Phot. Surv.* **53**, p. 53  
 Hogg, D.C., Guiraud, F. O., Decker, M.T., (1981) *Astron. Astrophys.* **95**, p. 304

# HORIZONTAL GRADIENTS IN THE "WET" ATMOSPHERIC PROPAGATION DELAY

J.L. DAVIS,<sup>1</sup> G. ELGERED,<sup>2</sup> A.E. NIELL,<sup>3</sup> I.I. SHAPIRO<sup>1</sup>

<sup>1</sup>Harvard-Smithsonian Center for Astrophysics,  
60 Garden St., Cambridge, Massachusetts 02138, USA

<sup>2</sup>Onsala Space Observatory, S-439 00 Onsala, Sweden

<sup>3</sup>Haystack Observatory, Westford, Massachusetts 01886, USA

**ABSTRACT.** We have used water vapor radiometer data to investigate the local spatial and temporal variation of the "wet" atmospheric propagation delay near Onsala Space Observatory, Sweden. The data were obtained at this location from a wide range of azimuths and from elevation angles greater than 25°. In analyzing the data, we used a six-parameter model which has proven adequate (RMS zenith wet delay residual  $\sim 1$  mm) for up to 30 minutes of data. Our estimated gradient and gradient-rate vectors have preferred directions, possibly indicating a prevailing structure in the three-dimensional temperature and humidity fields related to the air-land-sea interaction. These estimated gradients are larger, by 1–2 orders of magnitude, than gradients determined by others from averaging over long ( $\sim 100$ -km) horizontal distances.

## 1. INTRODUCTION

To account for atmospheric propagation effects in the analysis of space-geodetic data, we are investigating the estimation of the wet delay using water vapor radiometer (WVR) data [Resch, 1984; Elgered et al., 1991]. If this method proves sufficiently accurate, its use could improve the accuracy with which site positions (especially the vertical coordinate) are determined with VLBI and GPS. A potential strength of this method is its sensitivity to spatial, i.e., horizontal, variations in the propagation delay. For example, Dixon and Kornreich Wolf [1990] noted that radiometrically determined values for the wet delay exhibited a systematic but time-variable difference when the WVR was consecutively pointed in diametrically opposite azimuths. The maximum size of the difference, referenced to an elevation of 30°, was  $\sim 20$  mm.

This paper describes our investigation of horizontal variations of the wet delay and the statistical characterization of those variations for the Onsala, Sweden, VLBI site.

## 2. MATHEMATICAL MODEL

The model for the WVR data we have adopted is

$$\begin{aligned} \Delta \tilde{L}^z(\epsilon, \phi, \Delta t) = & \Delta L^z + \cot \epsilon \\ & \times \left[ \Xi_n \cos \phi + \Xi_e \sin \phi + \dot{\Xi}_n \Delta t \cos \phi + \dot{\Xi}_e \Delta t \sin \phi \right] + V_L \Delta t \quad (1) \end{aligned}$$

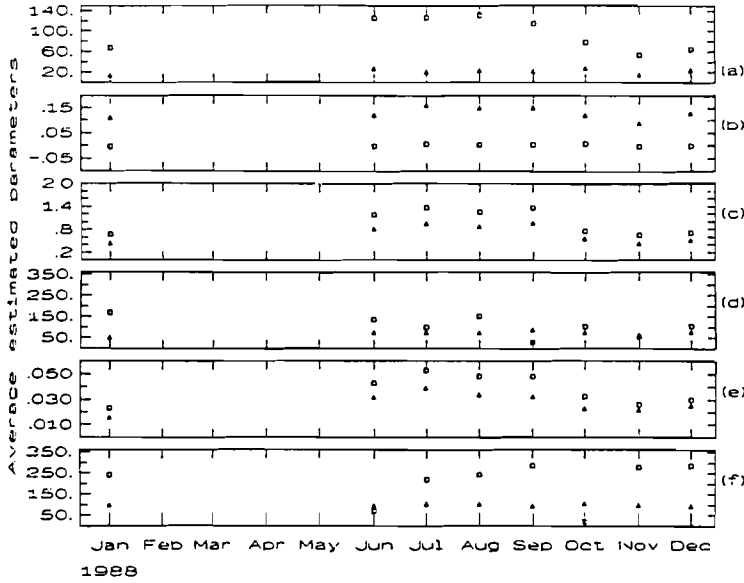


Figure 1. Squares: monthly averages for 1988 for the six parameters of the model (1). Triangles: WRMS residual about the mean. See text for estimation procedure. (a) Zenith delay, mm. (b) Zenith delay rate,  $\text{mm min}^{-1}$ . (c) Zenith delay gradient, mm. (d) Azimuth of the zenith delay gradient, degrees. (e) Zenith delay gradient rate,  $\text{mm min}^{-1}$ . (f) Azimuth of the zenith delay gradient rate, degrees.

where  $\Delta\tilde{L}^z(\epsilon, \phi, \Delta t)$  is the equivalent zenith wet delay obtained from WVR observations at time  $\Delta t$ , relative to some reference epoch, in the direction of elevation angle  $\epsilon$  and azimuth  $\phi$ . The parameters to be estimated from the WVR data are  $\Delta L^z$ , the zenith wet delay at time  $\Delta t = 0$ , the north (n) and east (e) components of the wet delay gradient  $\tilde{\Xi}$  and gradient rate  $\dot{\tilde{\Xi}}$ , and the zenith delay rate  $V_L$ . The rationale for (1) is given in Davis et al. [1992].

### 3. STATISTICAL CHARACTERIZATION OF PARAMETERS

In order to obtain a better understanding of the gradients in the vicinity of the Onsala site, we undertook a large-scale analysis of WVR data. For this study, we chose to use all Onsala WVR data from 1988, the first year in which the WVR was often performing the azimuth scans described above. Unfortunately, no data were available for February through May, when the WVR was undergoing maintenance and some upgrading, or participating in other observations. Furthermore, no data were used if the WVR brightness temperatures indicated a columnar zenith liquid water content of 0.3 mm or greater, i.e., during precipitation or heavy cloud cover.

The gradient analysis code operated by grouping together all the WVR data within a user-defined time period (30 minutes for this study). The WVR-determined equivalent zenith delay data in this period were then used to estimate the six parameters of (1). The program then searched for the first WVR observation that followed the group of data used for this solution, and the process continued. In this manner, we obtained

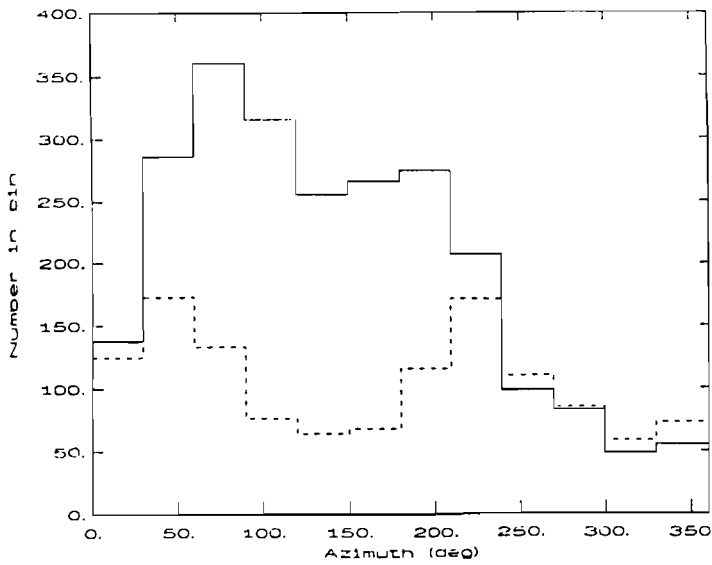


Figure 2. Histogram of azimuths ( $0^\circ$  north,  $90^\circ$  east) for estimated gradient (solid) and gradient-rate (dashed) parameters. The bin width is  $30^\circ$ , and only estimates with standard deviations of less than  $10^\circ$  are considered.

independent estimates of the six parameters approximately every 30 minutes. Some 30-minute spans did not contain enough data to obtain a solution, due, for example, to outages caused by high liquid content.

The monthly averages for the estimated parameters are indicated by the squares in Figure 1a-f. The weighted root-mean-square (WRMS) variations about the average for each month are plotted as triangles. The gradient and gradient-rate parameters are presented as magnitude and direction instead of orthogonal components.

The delay gradient parameters cannot be used to determine uniquely the height profile for the gradient of the wet refractive index. Davis et al. [1992] assumed an exponential profile for the gradient and inferred an average surface gradient for the refractive index of  $0.25\text{--}1.00 \text{ N km}^{-1}$ . Blanchiere-Ciarletti et al. [1989] determined refractivity gradients of up to  $4 \text{ N km}^{-1}$  using an airplane-mounted sensor. On the other hand, temperature gradients determined by Gardner [1977] imply surface N-gradients of  $\sim 0.01 \text{ N km}^{-1}$ , and temperature gradients determined by Elgered et al. [1990] imply surface N-gradients of  $\sim 0.1 \text{ N km}^{-1}$ . These latter two studies used data from sites separated by  $\sim 100 \text{ km}$ . Thus, it appears that local gradients may be several orders of magnitude greater than gradients averaged over 100-km scales.

Figure 2 shows a histogram of gradient directions (solid line). The bin width is  $30^\circ$ , and only direction estimates with standard deviations of  $10^\circ$  or less are counted. The nonuniformity of the distribution of gradient directions is clearly apparent from this plot. Figure 2 also includes the histogram of the gradient-rate estimates (dashed line). Fewer gradient-rate estimates meet our restriction of  $\sigma < 10^\circ$  (1259 out of 5815 total) than did gradients (2383). The distribution of gradient-rate azimuths is less peaked than that for the gradient azimuths, but two smaller peaks, in the bins for  $30^\circ\text{--}60^\circ$  and  $210^\circ\text{--}240^\circ$ , are visible. These bins are separated by  $180^\circ$ , indicating gradient rate vectors of opposite sign but in the same direction.

#### 4. CONCLUSIONS

We have used water vapor radiometer data to investigate the local spatial and temporal variation of the wet propagation delay. Assuming a simple exponential profile for the wet refractivity gradient, we found that the estimated gradient parameters imply surface wet-refractivity horizontal gradients of order  $0.1\text{--}1 \text{ N km}^{-1}$ , on average. These gradients are larger, by 1–2 orders of magnitude, than gradients determined by others for averaging over long ( $\sim 100\text{-km}$ ) distances. This result implies that for applications sensitive to local gradients, such as propagation-delay models for radio-interferometric geodetic studies, the use of meteorological data from widely spread stations may be inadequate. The gradient model presented here is inadequate for times longer than about 30 minutes, even if no gradients are present, because of the complicated stochastic-like temporal behavior of the wet atmosphere. When gradients are present, they can change magnitude by  $\sim 50\%$  over 10–15 minutes. Nevertheless, our ability to fit the radiometer data implies that on time scales  $< 30$  min and for elevation angles  $> 25^\circ$ , the local structure of the wet atmosphere can be described with a simple model. The estimated gradient and gradient-rate vectors have preferred directions, which indicates a prevailing structure in the three-dimensional temperature and humidity fields, possibly related to the air-land-sea interaction.

#### ACKNOWLEDGEMENTS

This work was supported by National Aeronautics and Space Administration grant NAG5-538 and contract NAS5-30543. The research using water vapor radiometry at the Onsala Space Observatory is supported by the Swedish Natural Science Research Council (which also provided visiting scientist funds for J.L.D.), the Hasselblad Foundation, and the European Space Agency.

#### REFERENCES

- Blanchetiere-Ciarletti, V., Lavergnat, J., Sylvain, M., Weill, A. (1989) *Radio Sci.* **24**, 705  
Davis, J.L., Elgered, G., Niell, A.E., Kuehn, C.E. (1992) in press  
Dixon, T.H., Kornreich Wolf, S. (1990) *Geophys. Res. Lett.* **17**, 203  
Elgered, G., Johansson, J.M., Rönnäng, B.O. (1990) *Res. Rep.* **165**, Chalmers University of Technology, Göteborg, Sweden, 400 pp.  
Elgered, G., Davis, J.L., Herring, T.A., Shapiro, I.I. (1991) *J. Geophys. Res.* **96**, 6541  
Gardner, C.S. (1977) *Appl. Opt.* **16**, 2427  
Resch, G.M. (1984) in *Geodetic Refraction*, ed. F.K. Brunner, Springer-Verlag, New York, p. 53

# THE INFLUENCE OF HORIZONTAL TROPOSPHERIC GRADIENTS DERIVED BY ASSUMING SPHERICAL, BUT SLOPING LAYERS

J.C. DE MUNCK

Mathematical and Physical Geodesy, Delft Univ. of Technol.,  
Stadhouderslaan 64, 2517 JA DEN HAAG

**ABSTRACT.** The influence of horizontal troposphere gradients on radio satellite baseline measurement is derived by assuming the dry and the wet tropospheric components to be spherically layered, but each tilted with respect to the horizon. Their slopes are related to the gradient of respectively the barometric pressure and the total water vapour content.

The sensitivity of the height difference to the tropospheric effects is considered in particular.

## 1. INTRODUCTION

The influence of the troposphere on radio satellite baseline measurements will be treated assuming a sloping dry (hydrostatic) and a sloping wet component, both components being spherically layered.

Being merely theoretical models, the slopes of the dry and the wet components are related to respectively the gradient of the barometric pressure and the gradient of the water vapour content of the atmosphere.

Results are discussed for double difference measurements, in particular with examples for GPS satellites. For more details see [De Munck 1991].

## 2. TROPOSPHERIC CORRECTION

The distance between a satellite and a terrestrial point is calculated by multiplying the measured travelling time by the free space light velocity, and adding the (negative) tropospheric correction  $C$  and other corrections.

For a horizontally layered troposphere the correction  $C$  depends on the zenith angle  $z$ ; the relation is often expressed as:

$$C = p(z) C_0 \quad (1)$$

where  $p(z)$  is called the mapping function, depending on the vertical velocity profile, and where  $C_0$  is the tropospheric correction in zenith direction.

In our calculations we choose for the mapping function the Chao model [H. Schuh, 1986.], for the dry component and, for want of something better, also for the wet component.

### 3. SLOPE OF THE TROPOSPHERE

For a concentrically layered spherical troposphere whose normal  $T$  in the neighbourhood of the baseline has a very small zenith angle  $\varepsilon$  and a bearing  $\psi_T$  (Figure 1), the slope mapping function becomes:

$$p' = p(z - \varepsilon \cos \beta) \quad (2)$$

where:  $\beta = \psi_s - \psi_T$  is the angle between the vertical planes through the line  $A_1S$  and the atmospheric normal  $T$  (see Figure 1) and where  $-180^\circ \leq \beta \leq 180^\circ$  and  $0 \leq \varepsilon \ll 1 \text{ rad}$

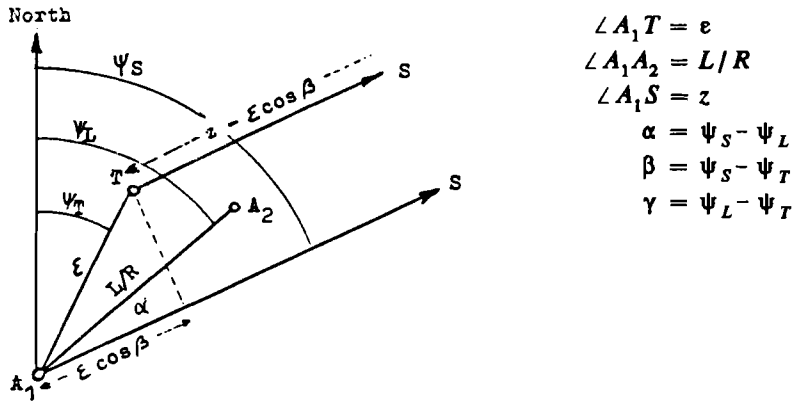


Figure 1. The directions of the slope.

Applying (2) on (1) the correction  $C'$  to a measured (pseudo) distance in a sloping ('') troposphere is found as:

$$C' = p[z - \varepsilon \cos \beta] \times C_0 \quad (3)$$

Strictly speaking, in equation (3), the correction should be taken perpendicular to the layers and not vertical, but the difference is very small.

#### 3.1 THE SLOPING DRY TROPOSPHERIC COMPONENT

For the dry (hydrostatic) component of the troposphere the slope angle  $\varepsilon_d$  is closely related to the horizontal gradient of the barometric pressure: The difference in atmospheric pressure  $\Delta P$  at two points in the horizontal plane is caused by an air column of a height  $\Delta h$ . The theory of the hydrostatic balance of the atmospheric air as an ideal gas yields:

$$\frac{\Delta P}{P} = \frac{\Delta h}{H_d} \quad (4)$$

where  $P$  is the atmospheric pressure, and  $H_d \cong 8000 \text{ m}$  the atmospheric scale height.

N.B. In our paper we will use the sub indices  $d$  and  $w$  for the dry (the hydrostatic) and the wet component, and  $s$  for values near the surface.

For the "dry" slope angle one finds  $\varepsilon_d = - \Delta h / \Delta l_d$ , or with (4):

$$\varepsilon_d = - \frac{H_d}{P} \frac{dP}{dl_d} \quad (5)$$

where  $l_d$  is a horizontal distance in the direction of gradient  $P$ .

### 3.2 SLOPING WET COMPONENT

The wet component will assumed to be structured as (sloping) concentric layers of constant water vapour pressure.

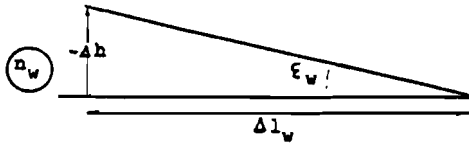


Figure 2. The humidity slope

We will express the slope of these layers as a function of the relative differential vertical humidity correction,  $\Delta C_{0w} / C_{0w}$ , which is identical to the relative differential water vapour content.

Figure 2 yields:

$$\Delta C_{0w} = \Delta \int_0^h N_w 10^{-6} dh = -N_{ws} 10^{-6} \varepsilon_w \Delta l_w \quad (6)$$

where  $N_w$  the wet component of the refractivity,  $N_{ws}$ , (surface value)  $\cong 4.5 \cdot e_s$  for moderate surface temperature, if  $e_s$  is the vapour pressure near the surface in mbar, and  $\Delta l_w$  a horizontal distance along the humidity gradient.

Now the wet slope can be expressed as a function of surface water vapour pressure  $e_s$  and the relative vertical wet correction,  $\Delta C_{0w} / C_{0w}$ :

$$-\varepsilon_w = \frac{10^6}{4.5e_s} \frac{C_{0w}}{\Delta l_w} \frac{\Delta C_{0w}}{C_{0w}} \quad (7)$$

### 4. TROPOSPHERIC IMPACT ON HEIGHT DIFFERENCES

Using the above relations, we calculated the sensitivity for tropospheric effects of the height difference  $h$  (and the other components) of a baseline, measured with the method of double differences [De Munck, 1991].

A double difference measurement  $m^{ab}$  is here the differenced difference of the measured distances  $m$  from the two end points 2 and 1 of the baseline to two satellites  $b$  and  $a$ :

$$m^{ab} \triangleq (m_2^b - m_2^a) - (m_1^b - m_1^a) \quad (8)$$

Introducing the dry and the wet "tropospheric parameters"  $D_{d,w}^i$  for profiles and  $E_{d,w}^i$  for gradients, with  $i = a$  or  $b$ , we found equation (10).

$$D_d^i \triangleq \frac{dp_d^i}{dz^i} \frac{dz^i}{dl}, \quad E_d^i \triangleq p_d^i \frac{dp}{Pdl_d}, \quad D_w^i \triangleq \frac{dp_w^i}{dz^i} \frac{dz^i}{dl}, \quad E_w^i \triangleq p_w^i \frac{dC_{0w}}{C_{0w} dl_w} \quad (9)$$

$$\left. \begin{aligned}
& m^{ab} + LC_{0d} \left\{ D_d^b \cos \alpha^b - D_d^a \cos \alpha^a + (E_d^b - E_d^a) \cos \gamma_d \right\} + \\
& + LC_{0w} \left\{ D_w^b \cos \alpha^b - D_w^a \cos \alpha^a + (E_w^b - E_w^a) \cos \gamma_w \right\} + \\
& + h (\cos z^b - \cos z^a) + L(\cos \alpha^b \sin z^b - \cos \alpha^a \sin z^a)
\end{aligned} \right\} \quad (10)$$

where  $\alpha^i$  is the bearing of the satellite relative to the baseline, and  $\gamma$  the bearing of the baseline relative to the slope. See Figure 1.

Differentiation yields the sensitivity of  $h$  for measuring errors:

$$\frac{\partial h}{\partial m^{ab}} = \frac{-1}{\cos z^b - \cos z^a} \quad (11)$$

Apparently the zenith angles have to differ as much as possible.

Similarly the sensitivity of  $h$  can be found for the tropospheric parameters. The most important, and often the only significant one, is the sensitivity for the humidity gradient, in particular if the gradient is in the direction of the baseline ( $\cos \gamma_w \rightarrow 0$ ). This sensitivity is given by:

$$\frac{\partial h}{\partial E_w^b} - \frac{\partial h}{\partial E_w^a} = \frac{LC_{0w} \cos \gamma_w}{\cos z^b - \cos z^a} \quad (12)$$

For  $z^a = 45^\circ$ ,  $z^b = 75^\circ$ , a vertical humidity correction  $\Delta C_{0w} = -0.1$  m, and an, according to [Muller 1989] very high, uncertainty of 10% in the relative vertical wet correction over 100 km, i.e.  $\Delta C_{0w} / C_{0w} = 10^{-6}$  m<sup>-1</sup>, one finds an uncertainty in the height difference in mm:

$$|\delta h_{E_w}| = |54 \cos \gamma_w| \quad (13)$$

In a humid tropical climate this uncertainty might be 3 times as large.

Because this uncertainty appears to be independent of satellite bearings, it can not be eliminated by using more satellites, in contrast with most of the other tropospheric errors which, in addition, are much smaller.

## 5. CONCLUSIONS

For double difference baseline measurement the most important tropospheric effect is the gradient of the total water vapour content, causing an error of up to a few cm in height difference over 100 km in a moderate climate.

Studies of the total water vapour content of the atmosphere that may lead to a higher accuracy for terrestrial baselines and for relative positioning with radio satellites can be recommended, for instance: theoretical meteorological studies, experiments with microwave radiometers, also from satellites, and comparison between laser- and microwave satellite ranges. In the latter case, however, one can not detect systematic influences of clouds.,

A baseline slope can only be determined with satellites at zenith angles sufficiently different from each other.

## REFERENCES

- Muller, F (1989) (K.N.M.I. at De Bilt) Personal communication.
- De Munck, J.C. (1991) Publ. 91. 3 Mathematical & Physical Geodesy Group, Delft.
- Schuh, H. (1987) Publ. C no. 328 Deutsche Geodätische Commission, Munich.

# DEPOLARIZATION EFFECTS OF THE RAINY MEDIUM IN MILLIMETER WAVE PROPAGATION

J.Y. HUANG, Y.P. WANG  
Xidian University, Box 274, 710071  
Xi'an, P.R. China

**ABSTRACT.** When working frequencies of radio waves through the atmosphere go beyond 10GHz, the rain will induce serious attenuation and give rise to the effect of depolarization as well. In this paper we give the results in dealing with depolarization by rain for millimeter waves involving coherent and incoherent scattering. They show that the longer the pathlength, the higher the frequencies and the stronger the rain rate, the more depolarization caused by incoherent the scattering must be taken into account.

## 1. INTRODUCTION

When high precision is required for radio systems using transatmospheric propagation of millimetre waves, effects of rain induced attenuation and crosspolarization are inevitable because of the nonspherical shape of raindrops. In order to clarify these effects, we have to investigate properties of millimetre wave propagation.

In general, in a random medium the field can be divided into a coherent part  $\langle \phi \rangle$  and an incoherent (fluctuating) part  $\phi_f$ , namely,  $\phi = \langle \phi \rangle + \phi_f$ . When  $\langle \phi_f \rangle = 0$ , we have an intensity relation such that

$$\langle |\phi|^2 \rangle = |\langle \phi \rangle|^2 + \langle |\phi_f|^2 \rangle \quad (1)$$

where  $|\langle \phi \rangle|^2$  is the coherent intensity and  $\langle |\phi_f|^2 \rangle$  is the incoherent intensity. There are coherent and incoherent depolarization discriminations (XPD's) corresponding to the coherent and incoherent intensities in equation (1) respectively. XPD is a measure of the depolarization effect which means that an increase of XPD, results in a smaller depolarization effect. Since measurements can not distinguish coherent XPD from incoherent XPD, in addition to the calculation of coherent XPD we have to solve the Foldy-Twersky integral equation (Ishimaru, 1978) for the total intensity which combines both.

The rain induced effects depend strongly on climatological conditions, hence the millimeter wave propagation has also the property of locality. In the following calculations, the main local precipitation conditions (for Xi'an) are:

(1) the average canting angle  $\theta_0$  and its standard deviation  $\sigma$  of raindrops in different rain rates (R):

$$\begin{aligned} \theta_0 &= 6^\circ, & \sigma &= 20.4^\circ && \text{when } R > 40 \text{ mm/h} \\ \theta_0 &= 7.2^\circ, & \sigma &= 33^\circ && \text{when } R \leq 40 \text{ mm/h} \end{aligned}$$

(2) the rain rates of yearly cumulative percentage probabilities

p (%)	1.	0.5	0.2	0.1	0.05	0.02	0.01	0.005	..
R (mm/h)	1.7	2.7	4.4	5.7	8.9	11.9	17.4	25.9	..

## 2. COHERENT XPD'S

Coherent XPD's are calculated according to the following definition (Huang, et al., 1991)

$$\text{XPD} = 10 \log (\text{copolar coherent power}/\text{crosspolar coherent power}) \quad (2)$$

Figures 1 and 2 show the calculated XPD's of horizontal polarization for two frequencies. The curves show that in a random medium with precipitation, longer pathlength and stronger rain rate will result in less XPD's. This is due to the effect of multiple scattering which reduces the copolar and coherent part in the total power transmitted.

## 3. TOTAL XPD'S

Total XPD's have been calculated by means of the solution of the Foldy-Twersky integral equation for the correlation function when  $\bar{r}_a = \bar{r}_b$ , as

$$\langle \bar{E}^a \bar{E}^{a*} \rangle = \langle \bar{E}^a \rangle \langle \bar{E}^{a*} \rangle + \iiint \bar{\bar{G}}_s^a \cdot \langle \bar{E}^s \bar{E}^{s*} \rangle \cdot \bar{\bar{G}}_s^{a*} d\bar{r}_s \quad (3)$$

where  $\bar{E}^a$  and  $\bar{E}^s$  are fields at the observing point  $\bar{r}_a$  and the scattering point  $\bar{r}_s$ , respectively. The notations  $\cdot$  and  $\langle \cdot \rangle$  denote the complex conjugate and the expectation value, respectively.  $\bar{\bar{G}}_s^a$  is a transformation dyadic Green's function which transforms the scattering field at  $\bar{r}_s$  to the observing point  $\bar{r}_a$ .

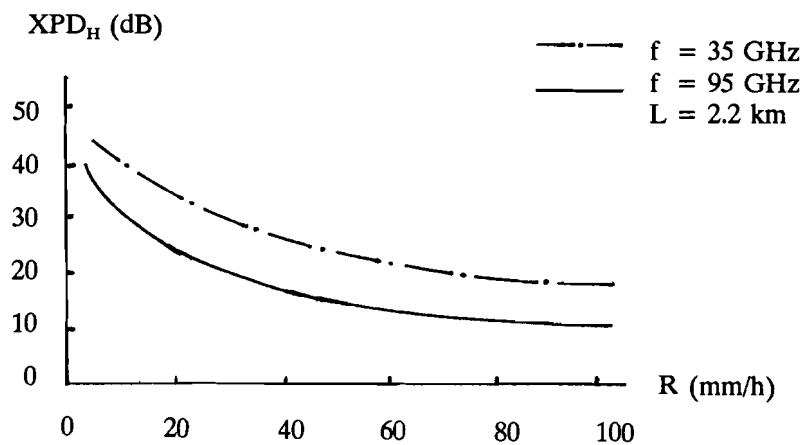


Figure 1. Coherent XPD versus rain rate with specific path

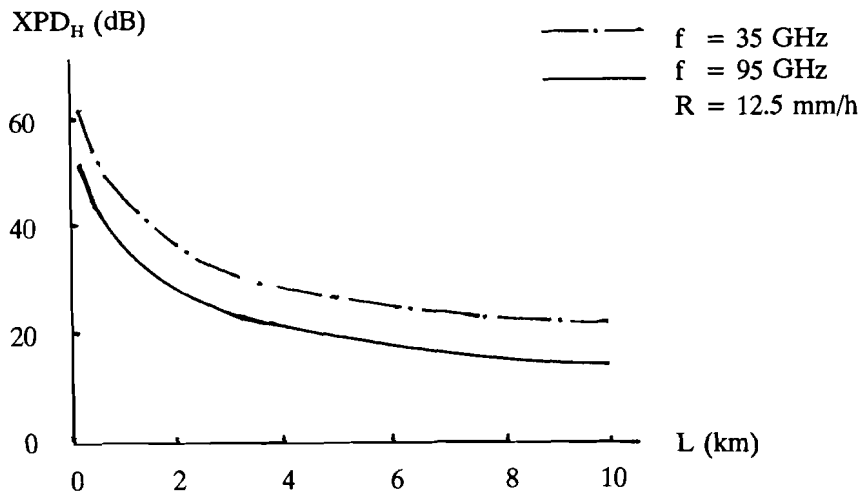


Figure 2. Coherent XPD versus pathlength with specific rain rate

Obviously, equation (3) is a matrix equation. According to the definition

$$\text{XPD} = 10 \log (\text{copolar power}/\text{crosspolar power}) \quad (4)$$

the XPD's of the total transmitting power have been calculated based on the above mentioned local precipitation conditions and other derived parameters (not presented here). Results for horizontal polarization are shown in figures 3 and 4, in which those of coherent fields are also drawn for comparison. The lower of XPD's of the total power means that the crosspolar power becomes higher with pathlength or rain rate.

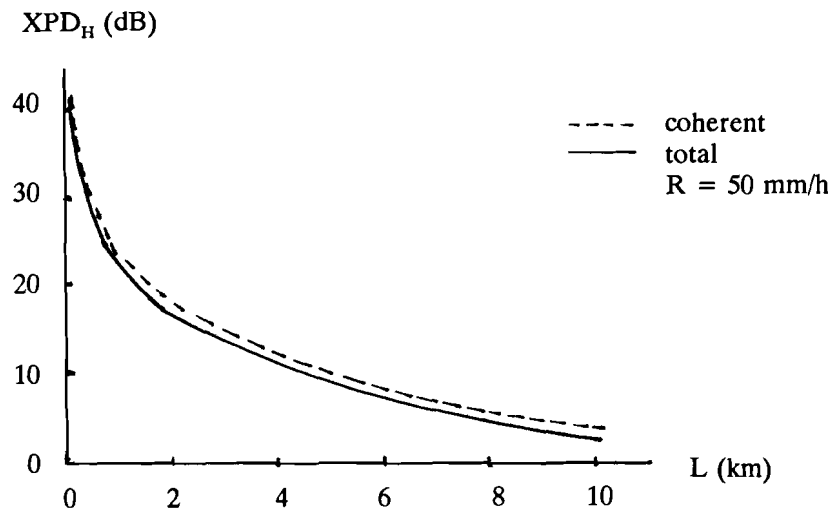


Figure 3. Horizontal XPD versus pathlength with specific rain rate

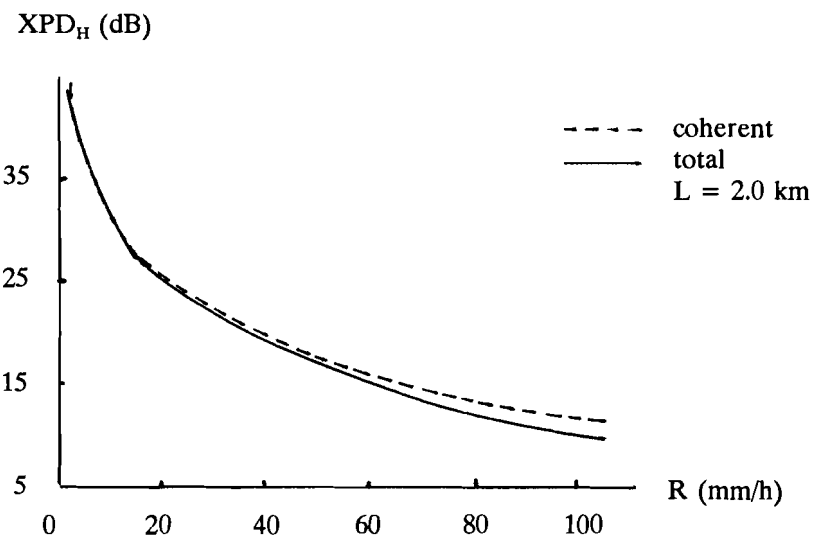


Figure 4. Horizontal XPD versus pathlength with specific rain rate

#### 4. POSTSCRIPT

All the results derived above for a ground link can easily be transformed to slant path conditions by means of the method already well-known (CCIR, 1989).

#### REFERENCES

- CCIR (1989), Recommendations and Reports
- Huang, J.Y., et al. (1991), *J. Wuhan University* 4 (in Chinese)
- Ishimaru, A. (1978), *Wave Propagation and Scattering in Random media*, Academic Press., New York, vol. 2
- Ishimaru, A., et al. (1984), *Radio Sci.* 19, 5, 1356 - 1366

## ZENITH ANGLE DEPENDENCE OF PATH LENGTH THROUGH THE TROPOSPHERE

T.A. AKHUNDOV, A.A. STOTSKII  
Institute of Applied Astronomy,  
197042, St. Petersburg, Russia

### 1. INTRODUCTION

The main contribution to the excess path length through the terrestrial troposphere is its "dry" component. For the direction to the zenith it may be easily obtained by measuring the surface value of the air pressure. But for other applications, for example for VLBI, it is necessary to know path length through the troposphere in inclined directions with the zenith angle  $z$ .

So it is necessary to know the angular function  $B(z)$ :

$$B(z) = \frac{\int N(l) dl}{\int N(h) dh} \quad (1)$$

where  $h$  is an altitude,  $N(l) = [n(l) - 1] 10^{-6}$  the distribution of the refractivity along the ray with zenith angle  $z$  and  $N(h)$  its vertical distribution.

Here we do not consider the wet term of the excess path length, which can better be measured by using a water vapour radiometer (WVR) method.

In this contribution we consider different models of  $B(z)$  and give an estimate of errors due to random fluctuations in the refractive index.

### 2. MODELS OF ANGULAR FUNCTION $B(z)$

Assuming that the refractive index of the troposphere is a function of the height but not of the horizontal distance, the angular function for rectilinear paths is

$$B(z) = \left\{ \int N(h) dh \right\}^{-1} \int \frac{N(h) dh}{\left\{ 1 - \frac{R^2}{(R+h)^2} \sin^2 z \right\}^{1/2}} \quad (2)$$

where  $R$  is the radius of the Earth.

If the zenith angle is large it is necessary to take in account the lengthening of the path due to refractive bending. In this case

$$B(z) = \frac{\int \frac{N(h) dh}{\left\{1 - \frac{R^2}{(R+h)^2} \left[\frac{n(o)}{n(h)}\right]^2 \sin^2 z\right\}^{1/2}}}{\int N(h) dh} \quad (3)$$

Let us find out to what results these formulas lead with different kinds of distributions  $N(h)$ . Let us consider three models:

Homogeneous media:

$$N(h) = N_0, \quad 0 < h < h_u \quad (4)$$

Exponential function (Bean and Dutton, 1966):

$$N(h) = N_0 \exp\left(-\frac{h}{H}\right) \quad (5)$$

Two-Quartic profile (Hopfield, 1969):

$$N(h) = \frac{N_0(h_m - h)^4}{h_m^4} \quad 0 < h < h_m. \quad (6)$$

Where  $h_m = a + bT_0 = 40.082 + 0.14898T_0$  (km),  $a$  and  $b$  empiric coefficients, and  $N_0$  and  $T_0$  refractivity and temperature at the surface of the earth.

The model functions  $B(z)$  calculated by using these profiles were compared with the experimental functions  $B(z)$ , which were calculated on the basis of measured profiles for pressure and temperature. 10 radiosonde profiles were used with a large range of surface level temperature values.

Figure 1 shows the r.m.s. values of differences between each of the models and the experimental functions  $B(z)$ . For clarity the differences are given in units of length obtained for a mean value for the path length in the direction towards zenith being equal to 231 cm. From the results of these calculations one can conclude that the model based on two-quartic profile accounting for refractive bending is the best. This model has the additional advantage that it depends on surface temperature. This enables us to make the model more precise during observations. Furthermore, this model may be adopted to real climate conditions of the observing site by a proper choice of the empirical coefficients of the model, for example from data of a radiosonde survey.

It is evident that calculations according the formula (3) are not convenient because of need of numerical integration. Black (1978) gave a simple approximation for calculation  $B(z)$  with Hopfield's profile, but in this case the refractive bending was not taken in account.

For simplification of expression (3) with Hopfield's profile we used a Taylor series expansion to approximate  $B(z)$ :

$$B(z) = [1 - F \sin^2 z]^{-1/2}, \quad (7)$$

where  $F = c + d T_0$ ,  $c$  and  $d$  constant coefficients.

The value of the coefficient  $F$  obtained by a least squares fit when comparing (7) with (3) for different  $z$  and profile parameters is:

$$F = 0.999234 - 0.15 \times 10^{-5} T_0 \quad (8)$$

Another way to get a value of  $F$  is to compare (7) with  $B(z)$  calculated on the basis of the experimental pressure and temperature profiles. For the profiles used in this work we obtained:

$$F = 0.998139 - 0.12 \times 10^{-5} T_0 \quad (9)$$

The function (7) with (9) approximates the real function  $B(z)$  even better than a precise expression (3) (fig.1), as in this case local meteorological parameters are taken into account.

Thus, the knowledge of the mean pressure and temperature profiles improves the precision of the determination of the function  $F(z)$  considerably and consequently also the dry term of excess path length through the troposphere along the line of sight.

### 3. FLUCTUATIONS OF THE REFRACTIVE INDEX

Let us estimate the errors which are inserted into  $B(z)$  by the fluctuations of the refractive index in horizontal direction. It is convenient to introduce, as a measure of these errors, a structure function  $D_L(-z,z)$  of the difference between the path lengths along the rays directed at the angles  $z$  from the vertical.

To construct this structure function we used a turbulence model for the structure function  $D_1(\rho)$  for parallel paths through the troposphere spaced at distance  $\rho$  (Stotskii, 1992):

$$D_1(\rho) = \begin{cases} C_1^2 \rho^{5/3} & \rho < L_1 = 2.2 \text{ km} \\ C_L^2 \rho^{2/3} & L_1 < \rho < L_2 = 2400 \text{ km} \\ C_s^2 & \rho > L_2 \end{cases} \quad (10)$$

As in our case both spatial domains:  $\rho < L_1$  and  $\rho > L_1$  are relevant, the angular structure function consists of two terms:

$$D_L(-z,z) = 2.91 B(z) \int_0^{h_v} C_n^2(h) (2\rho(h,z))^{5/3} dh + 2B^2(z) \int_{h_v}^{h_m} C_n(h) (2\rho(h,z))^{2/3} dh, \quad (11)$$

where  $h_v = 0.5 L_1 \operatorname{ctg} z$  is the altitude where  $\rho = L_1$ .

In order to obtain the quantitative estimates, let us assume that the structure coefficient  $C_n$  decreases with altitude according the law of the Two-Quartic profile. It can be done for the case of large  $z$  when two-dimensional turbulence prevails. That is why in the dependence  $C_n(h)$  it is sufficient to take into account a regular component of  $N(h)$  only.

Now let us introduce the structure function  $D_L(z)$  which represents the difference between the path length in direction  $z$  and the path length in zenith direction multiplied by  $B(z)$ . The structure function  $D_L(z)$  may be obtained from  $D_L(-z,z)$  if we change in (11)  $2\rho(h,z)$  to  $\rho(h,z)$ . Thus we finally have:

$$\begin{aligned}
D_L(z) = & 2.91 B(z) C_n^2(0) \int_0^{h_v} \frac{(h_m - h)^8}{h_m^8} \rho^{5/3}(h, z) dh + \\
& + 2B^2(z) C_n^2(0) \int_{h_v}^{h_m} \frac{(h_m - h)^4}{h_m^4} \rho^{2/3}(h, z) \int_{h_v}^h \frac{(h_m - h')^4}{h_m^4} dh' dh,
\end{aligned} \tag{12}$$

where

$$\rho(h, z) = [(R + h)^2 \operatorname{ctg}^2 z + 2h(R + h)]^{1/4} - (R + h) \operatorname{ctg} z \tag{13}$$

Taking the typical value of  $C_n(0) = 0.015 \times 10^{-2} \text{ cm}^{-4}$  we shall get the function  $D_L(z)$  as shown in Fig.2 (continuous line). Dotted lines show the behaviour of this function for limited three-dimensional ( $\rho < L_1$ ) and two-dimensional ( $\rho > L_1$ ) cases of turbulence.

The structure function  $D_L(z)$  indicates the maximum deviation of the excess path length along the ray with zenith angle  $z$  from the excess path length in zenith by using the function  $B(z)$ , i.e. the error which results from the assumptions for the spherical-layer troposphere.

#### 4. CONCLUSION

The errors in the determination of the excess path length in directions deviating from the zenith direction on the basis of the measured zenith value include two components:

1) The errors of the model of  $B(z)$ . The use of a quite perfect model such as (3)+(6) or its approximation in form (7) enables us to obtain a quite acceptable precision in the regions of small and medium zenith angles, but when  $z$  is large the effects of this kind of errors are substantial.

2) The errors connected with fluctuations of troposphere refractivity in horizontal direction. These errors may be of primary importance in the region of medium zenith angles.

Thus the more precise determination of the dry component of inclined path length in a large domain of zenith angles is hardly possible on the basis of using a straightforward angular function. The knowledge of a real inclined profile of refractive index is necessary, for example, by means of radiometric measurements of the temperature distribution along the inclined path.

An additional improvement of the model of the angular function  $B(z)$  may be effective only for the region of directions which are close to the horizon.

#### REFERENCES

- Bean, B.R. and Dutton, E.J. (1966) Radio Meteorology, NBS Monogr.
- Black, H.D. (1978) J.Geophys.Res. **83**, B4, p.1875
- Hopfield, H.S. (1969) J.Geophys.Res. **74**, 15, p.4487
- Stotskii, A.A. (1992), in this issue.

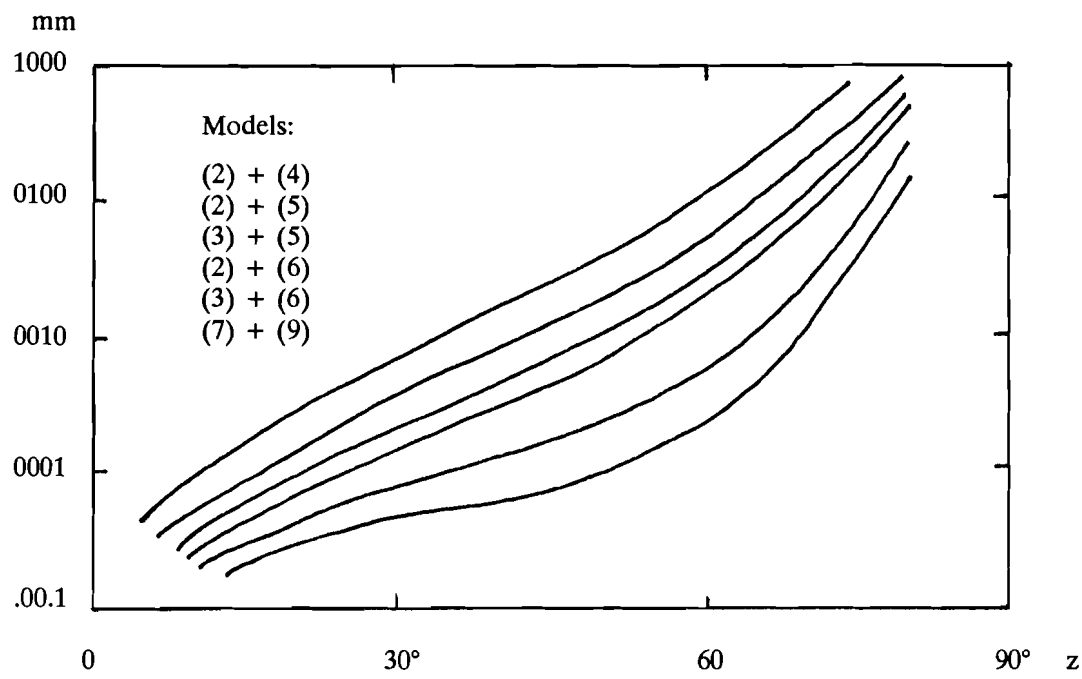


Figure 1. R.m.s. differences between the each of the models of  $B(z)$  and the experimental functions  $B(z)$ , displayed according the numbers of the formulas in the left upper corner.

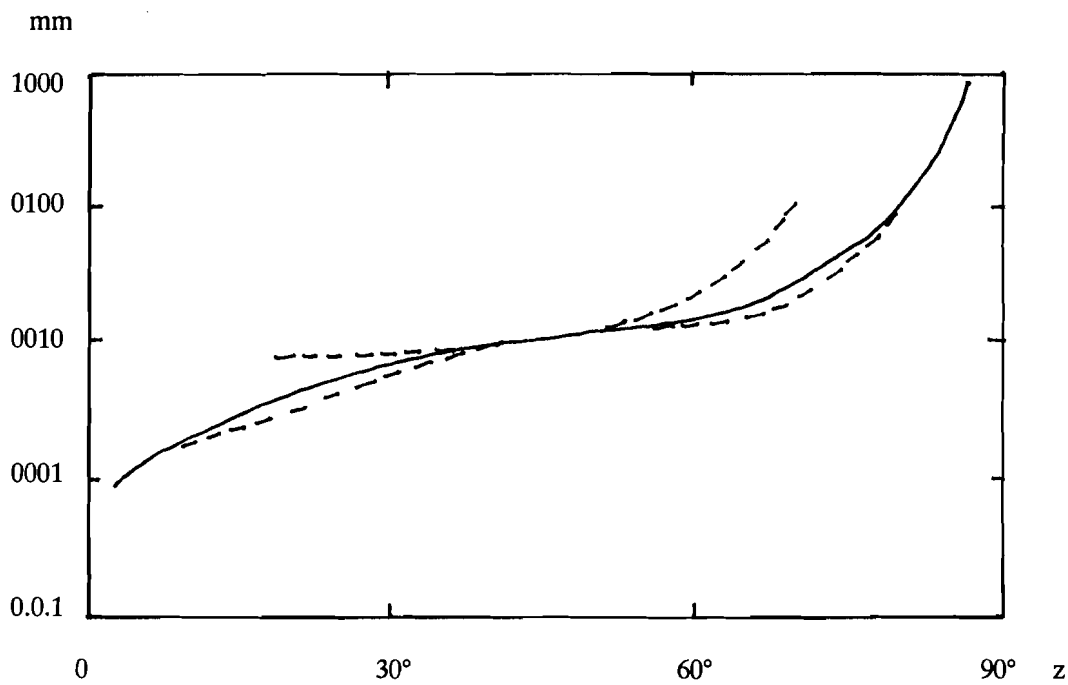


Figure 2. Angular structure function  $D_L(z)$  of path length through the troposphere.



### **3. GEODETIC VLBI**



# TROPOSPHERIC AND CHARGED PARTICLE PROPAGATION ERRORS IN VERY LONG BASELINE INTERFEROMETRY

R. N. TREUHAFT  
Jet Propulsion Laboratory  
California Institute of Technology  
4800 Oak Grove Drive  
Pasadena, California 91109 USA

**ABSTRACT.** This review talk on propagation errors in Very Long Baseline Interferometry (VLBI) will mainly be concerned with neutral atmospheric effects due to tropospheric propagation. There will also be some discussion of charged particle propagation as it affects VLBI observations close to the sun. After a brief description of the static troposphere, stochastic effects will be discussed, with an emphasis on methods for optimal estimation. It will be shown that a variety of estimation approaches produce the same error, which is a characteristic 7-10 mm error on a 10000 km baseline length measurement. Water vapor radiometry (WVR) and Global Positioning System (GPS) measurements will be discussed as methods for calibration, in order to reduce the error below that attainable with estimation techniques. Dual frequency ( $\approx$ 2300 MHz and  $\approx$ 8400 MHz) calibration of charged particle effects for rays passing within a few degrees of the sun will also be discussed.

## 1. INTRODUCTION

The purpose of this paper is to show why and at what level atmospheric propagation delays limit the accuracy of geodetic and astrometric parameters estimated in VLBI. In section 2, the magnitude and geometric signature of the tropospheric delay will be discussed, as well as how the tropospheric delay errors induce vertical errors in the VLBI station coordinates. Because mapping functions are used to estimate zenith delay parameters from line-of-sight measurements in VLBI, their evolving complexity will also be discussed. In section 3, a description of the stochastic nature of the tropospheric delay will be followed by a discussion of various approaches to statistical estimation of tropospheric effects from the VLBI data. The ultimate limitation of statistical approaches will be shown to induce  $\approx$ 7-10 mm for the error in the measured length of a 10600-km baseline. This baseline (Deep Space Network California-Australia) is chosen because it is the longest regularly-measured VLBI baseline, and therefore has the largest projection of local station vertical components into the baseline length. Tropospheric errors calculated for this baseline length will exceed those calculated for shorter baselines, with similar station climates. Given the limitations of stochastic estimation techniques, the utility of WVR and GPS delay calibrations for correcting VLBI water vapor delays will be assessed. Because dual frequency calibration can remove ionospheric charged particle delays to better than the 1-picosecond (0.3 mm)

level, they will not be treated in this paper. However, the effects of charged particles in the solar plasma will be discussed in section 4, for observations within a few degrees of the sun. Observations close to the sun are being employed in order to determine parameters in relativistic gravitation theories, and the charged particle error is a dominant one for those measurements.

## 2. STATIC TROPOSPHERIC EFFECTS IN VLBI

In this section, a discussion of the magnitude and geometric signature of the tropospheric delay will be followed by a discussion of mapping functions used in VLBI.

### 2.1 The Magnitude and Geometric Signature of Tropospheric Delays

The single-station tropospheric delay  $\tau_t$  can be expressed as an integral, along the line of sight, of the refractivity  $\chi(\vec{l})$  (index of refraction - 1) at the position  $\vec{l}$  over the speed of light  $c$ :

$$\tau_t = \frac{1}{c} \int_{trop} dl \chi(\vec{l}) \quad (1)$$

The integral in eq. (1) is taken to be along the path of the electromagnetic ray through the troposphere over the station. The delay  $\tau_t$  is due to a dry and wet component of the troposphere. Average dry (wet) tropospheric delays can be found by the product of the average dry (wet) refractivities and the corresponding average heights. The resulting dry (wet) delays are about 230 cm (10 cm) for typical VLBI observing sites (Bean and Dutton 1966).

The tropospheric delay of eq. (1) can cause shifts in the VLBI geometric delay which, as a function of elevation angle, look similar to those caused by station location shifts. In the VLBI analysis, unmodelled tropospheric delays may therefore prompt erroneous shifting of station location coordinates to compensate for atmospheric effects. In order to see how this happens, consider the VLBI geometric delay  $\tau_g$ :

$$\tau_g = \frac{\vec{B} \cdot \hat{k}}{c} \quad (2)$$

where  $\vec{B}$  is the baseline vector pointing from station 1 to station 2, and  $\hat{k}$  is a unit vector in the direction of wave propagation from the radio source. Note that the VLBI geometric delay is positive if the wavefront arrives at station 2 after it arrives at station 1. From eq. (2), it can be shown that an unmodelled shift in station 2's vertical (horizontal) coordinate  $\Delta V$  ( $\Delta H$ ) will cause changes in the VLBI geometric delay  $\Delta\tau_V$  ( $\Delta\tau_H$ ) as follows:

$$c\Delta\tau_V = -\Delta V \sin \theta_{el} \quad (3)$$

$$c\Delta\tau_H = -\Delta H \cos \theta_{el} \cos \phi \quad (4)$$

where  $\theta_{el}$  is the elevation angle and  $\phi$  is the difference between the azimuth angle of the horizontal shift and that of the source propagation direction. In eqs. (3) and (4),

the vertical direction is assumed to be positive pointing upward, and the horizontal direction is assumed to be positive pointing along the projection of the radio source direction on the plane perpendicular to the local vertical.

In order to show in what manner unmodelled tropospheric delays resemble eqs. (3) and (4), rewrite eq. (1) for a uniform troposphere and an approximately flat Earth as

$$\begin{aligned}\tau_t &= \frac{1}{c \sin \theta_{el}} \int_{trop} dz \chi(z) \\ &= \frac{1}{\sin \theta_{el}} \tau_z\end{aligned}\quad (5)$$

where  $z$  is altitude above the station and eq. (5) can be regarded as defining the zenith tropospheric delay  $\tau_z$ . The unmodelled or residual tropospheric delay  $\Delta\tau_t$  can be expressed as

$$\Delta\tau_t = \frac{1}{\sin \theta_{el}} \Delta\tau_z \quad (6)$$

Figure 1 below shows the delay, as a function of elevation angle, induced by a) an unmodelled station vertical shift of 2 cm and a bias of 3 cm, and b) an unmodelled zenith delay of 1 cm. Biases in VLBI can arise from clock epoch offsets, and biases of the order of 3 cm or more are usual.

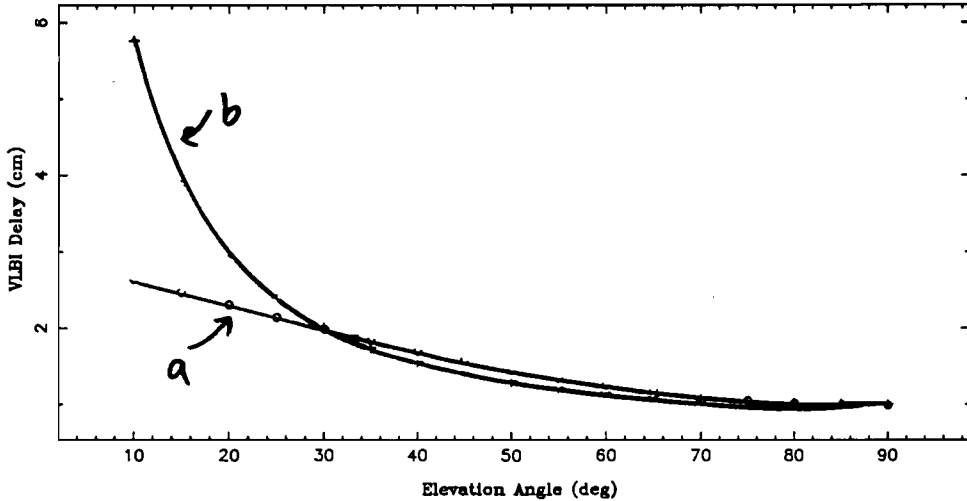


Figure 1. The unmodelled, VLBI geometric delay, as a function of elevation angle, due to a) a simultaneous shift in single-station vertical coordinate by 2 cm and a clock shift of 3 cm, and b) a shift of the zenith troposphere by 1 cm.

From the figure, it is clear that the signatures of the combined vertical and clock shifts are similar to the zenith tropospheric shift. Only below 20° do the curves get appreciably different. Thus, static zenith tropospheric errors propagate into local station vertical coordinates, but the two effects can be separated if a wide range of elevation angles is observed.

Examination of eqs. (4) and (6) suggests that horizontal station shifts and zenith tropospheric shifts have different delay signatures from scan to scan. This is because

the delays induced by horizontal shifts depend on the azimuth of the radio source observed, while those induced by vertical shifts do not. Note that for a very restricted set of source azimuth angles, horizontal shifts can also have similar delay signatures to those from unmodelled zenith tropospheric delays. One key difference between intercontinental VLBI and GPS tropospheric effects lies in the fact that intercontinental VLBI experiments cannot cover a wide range of azimuths, because each telescope must point in a limited region of mutual visibility. In GPS experiments, the azimuth range depends on the available satellites. It can be much more symmetric about any horizontal shift than a VLBI azimuth range, and can therefore substantially decouple horizontal station coordinate shifts from zenith tropospheric shifts.

## 2.2 The Tropospheric Mapping Function

The mapping function is an expression which gives the line of sight tropospheric delay in terms of the zenith delay. The concept of a mapping function is useful because, to an accuracy of 1-2 cm line-of-sight (Treuhhaft and Lanyi 1987), the troposphere can be considered to be uniform. In eq. (6), the term  $1/\sin \theta_{el}$  is the mapping function which gives the line of sight delay in terms of the zenith delay, for a flat Earth. For a curved Earth with radius  $R$  and tropospheric height  $h$ , a correction term of the order of

$$\frac{h}{R \tan^2 \theta_{el} \sin \theta_{el}} \quad (7)$$

must be subtracted from the flat-Earth mapping function in order to take into account the fact that the curved-Earth tropospheric path length is shorter than that corresponding to a flat-Earth. The complete derivation of the mapping functions used in VLBI is discussed below.

The two mapping functions used most often in VLBI are the CfA mapping function (Davis et al. 1985, Davis et al. 1991) and the Lanyi mapping function (Lanyi 1984). Viewed from a broad perspective, these two mapping functions achieve the same goal with two different practical approaches. Both mapping functions are based on a ray trace calculation. As the name implies, this calculation traces an electromagnetic ray through the atmosphere to determine how the phase retardation of the wave due to the refractive medium depends on elevation. The ray trace calculation assumes an atmosphere in hydrostatic equilibrium, and a temperature profile. From these two assumptions, the pressure and temperature needed to calculate refractivity along a ray path (Bean and Dutton 1966) are derived. The refractivities along the ray path are then integrated as in eq. (1). While Lanyi uses an analytic approach, Davis et al. adjust parameters in a phenomenological continued fraction expression to achieve agreement with ray tracing. The only significant difference in physical assumptions in the initial formulations of the two mapping functions was that Lanyi allowed for a constant temperature up to an inversion height, while Davis et al. assumed that the temperature decreased steadily from the Earth's surface up to the tropopause. These two mapping functions represent an enormous improvement over previous expressions such as the Marini (Marini 1972) or the Chao (Chao 1974) mapping functions. Differences between the newer mapping functions based on ray tracing and the older ones can be as large as 10 cm below 10° elevation.

Because the mapping function is determined by the pressure and temperature along the path of the incoming wave, any unmodelled thermodynamic effects can change the

mapping function. Davis et al. (1991) consider the possibility of unmodelled mapping function effects, noting that the observed scatter in the baseline lengths from a set of experiments was greater than that expected based on stochastic models. For example, mismodelling the inversion layer, as Davis et al. note, can produce few-mm errors in extracted baseline coordinates. As will be seen below, this is also the error level associated with fluctuations in the wet component of the troposphere.

### 3. STOCHASTIC TROPOSPHERIC EFFECTS IN VLBI

Although the wet component of the tropospheric delay is smaller in magnitude than the dry, it is much more highly variable. For example, typical VLBI sites may experience a 1-cm rms zenith delay standard deviation per day. In this section, the propagation of the wet fluctuation delays into baseline components will be discussed, followed by a description of the role of water vapor radiometry and GPS calibration techniques in VLBI.

#### 3.1 Minimizing Stochastic Effects by Estimation

A statistical development of the time behavior of the wet tropospheric delay, based on Kolmogorov turbulence, is given by Treuhhaft and Lanyi (1987). The two basic assumptions of that development are that 1) spatial irregularities in the wet tropospheric refractivity are described by Kolmogorov turbulence, and 2) these spatial irregularities are transported by the wind across a site. Most VLBI analyses include some form of stochastic estimation to minimize the effects of the wet fluctuations. The three approaches most generally taken are 1) frequent estimation of a constant or linearly time varying zenith troposphere parameter (Sovers et al. 1988), 2) Kalman filtering (Herring et al. 1990), or 3) observable covariance matrix formulation (Treuhhaft and Lowe 1991). The description of fluctuations in Treuhhaft and Lanyi (1987) gives a way to evaluate the effect of tropospheric fluctuations on VLBI parameter estimates for any given parameter estimation strategy. Linear estimation strategies can be thought of as mapping a set of VLBI delays into a set of VLBI parameters as follows:

$$P_i = \sum_{j=1}^N b_{ij} \tau_j \quad (8)$$

where  $P_i$  is the  $i^{th}$  parameter, for example baseline length, the  $b_{ij}$  coefficients are determined from the particular parameter estimation strategy (e.g. Hamilton 1964),  $N$  is the number of observations, and  $\tau_j$  is the  $j^{th}$  VLBI delay. If *a priori* parameter information is available, then it must be included in the  $\tau_j$  sum in eq. (8) with a coefficient of unity for the relevant parameter and zero for all others. Assuming no significant *a priori* information for parameters is used, the covariance between  $P_i$  and some other parameter estimate  $P_j$ ,  $cov(P_i, P_j)$ , due to tropospheric fluctuations, is given by:

$$cov(P_i, P_j) = \sum_{k=1}^N \sum_{l=1}^N b_{ik} b_{jl} cov(\tau_k, \tau_l) \quad (9)$$

where the delay covariance  $cov(\tau_k, \tau_l)$  is due only to the tropospheric fluctuations.

In order to investigate the fundamental limitations of estimation techniques, the model of Treuhhaft and Lanyi (1987) was assumed to describe the correct statistics, i.e. the observable covariance matrix of the above reference was assumed to be equal to  $cov(\tau_k, \tau_l)$  in eq. (9). Various estimation approaches were then tried, and the standard deviation of the baseline length parameter on a typical Deep Space Network (DSN) California-Australia baseline (10600 km) was calculated for each approach. For the calculations using eq. (9), the tropospheric fluctuations were assumed to take place in Australia only, and they were described by a structure constant  $C$  of  $1.2 \times 10^{-7} m^{-1/3}$ , a wet tropospheric height of 2 km, and a wind speed of 8 m/sec, blowing toward the east.

The performance of the three estimation strategies mentioned above is summarized below. Frequent, independent zenith delay estimation (every 1/2 hour) and constrained zenith delay estimation (approximating a Kalman filter) yielded about the same length standard deviation of about 8 mm. Using the observable covariance formulation, with the same fluctuation parameters used to generate the  $b$  values as were used to generate  $cov(\tau_k, \tau_l)$  yielded a 3-mm standard deviation. As expected, a minimum variance parameter estimate is obtained when data analysis equations are generated with the observed covariance matrix. However, this 3-mm standard deviation is an underestimate of the typical length standard deviation obtainable with the observable covariance formulation, because the exact parameters (structure constant, height, and wind velocity) which determine the covariance matrix are not known in the VLBI analysis. In order to evaluate the effect of the lack of knowledge of one of these parameters, the direction of the wind was systematically changed in the analysis, while the direction in the assumed  $cov(\tau_k, \tau_l)$  was held fixed. The results are plotted in figure 2 below.

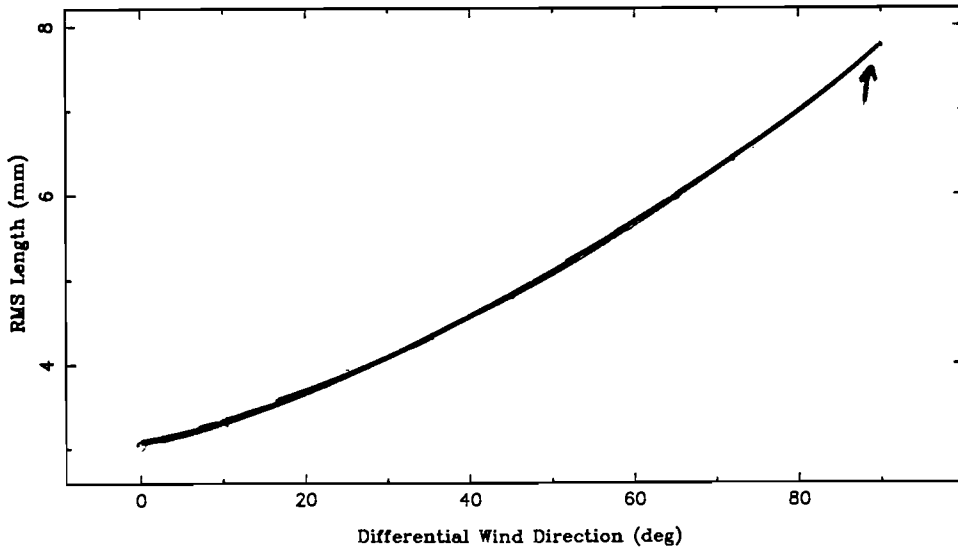


Figure 2. The California-Australia baseline length standard deviation, due to wet tropospheric fluctuations, as a function of the assumed direction of the wind, relative to the actual direction. The arrow shows the performance of a random walk Kalman filter, which was approximated by frequent, constrained zenith delay estimates.

From Figure 2, it can be seen that differences between the covariance matrix used to generate the analysis  $b$  parameters and that which the data actually obey will induce up to 8-mm rather than the optimal 3-mm standard deviations, with an average around 6 mm. Using frequent constrained zenith delay estimates, which approximates a random walk Kalman filter, the standard deviation indicated by the arrow is obtained. The random walk Kalman filter has no spatial information, and it mismodels the stochastic Kolmogorov behavior described by the covariance matrix approach (Herring et al. 1990). The general conclusion of this study is that, while using the observable covariance matrix approach would result in a substantial improvement over other approaches if the exact statistical nature of the tropospheric fluctuations were known, in practice they are not known and the covariance matrix approach may therefore represent only a slight improvement over the other techniques. It should be noted that uncertainties in other parameters such as wind speed, tropospheric height, and structure constant  $C$  will also degrade the apparent benefit of the covariance matrix approach over the other approaches mentioned. In order to include a range of possible tropospheric activity at both stations, an error of about 7-10 mm should be assigned for the tropospheric contribution to the 10600-km baseline length using any of the above stochastic estimation techniques for the tropospheric delay. Using the observable covariance matrix approach, with more exact stochastic model inputs than are typically practical, could improve this error by a factor of two.

### *3.2 Calibrating Stochastic Effects*

Given the above limitations to stochastic estimation techniques and the desire to achieve mm-level accuracy, calibration techniques which measure and remove the water vapor signature have been considered. Water vapor radiometry (Resch et al. 1984) has received more attention than any other technique over the last decade. But it has been shown that application of water vapor radiometer (WVR) calibration at Onsala produces only marginal improvement in baseline repeatability (Elgered et al. 1991). Errors in the currently-practiced technique of water vapor radiometry are of the order of 5-10 mm (Elgered et al. 1991, Wilcox 1991). Many of the errors associated with water vapor radiometry result because power, rather than phase or delay, is measured. The electromagnetic delay must be inferred from the power received by the radiometer, and this involves many model assumptions, most importantly the thermodynamics along the line of sight. It is possible that the technique of water vapor radiometry is fundamentally limited at the few-mm level, and, given errors associated with stochastic estimation, WVR accuracies should ideally be at the mm level or below. Fundamental changes in the way water vapor radiometry is done will probably be required before the technique shows much promise for improving upon stochastic estimation methods.

One possible alternative to WVR calibration is to use the delays from multiple GPS satellites to calibrate the troposphere. If satellite orbits and station locations could be sufficiently determined, and if charged particle effects could be removed at the picosecond level by dual frequency techniques, then residual GPS delays could possibly be associated with water vapor fluctuations along their lines of sight. A model must be assumed to infer the water vapor delay along VLBI lines of sight from those of the GPS lines of sight. Using a stochastic model such as the one mentioned above, the GPS delays can be schematically introduced into the VLBI analysis as follows:

$$\tau_{VLBI_i} = \tau_V(\hat{s}_i) + \tau_t(\hat{s}_i) \quad (10)$$

$$\tau_{GPS_j} = \tau_G(\hat{s}_j) + \tau_t(\hat{s}_j) \quad (11)$$

where  $\tau_{VLBI_i}$  is the  $i^{th}$  VLBI delay,  $\tau_V(\hat{s}_i)$  is the VLBI delay along a unit vector pointing in the direction  $\hat{s}_i$  due to everything but the troposphere, and  $\tau_t(\hat{s}_i)$  is the tropospheric delay in the same direction. The expressions for the  $j^{th}$  GPS delay in eq. (11) are similar, and it assumed that  $cov(\hat{s}_i, \hat{s}_j)$  is given by a modelled troposphere covariance, as in eq. (9). The degree to which a full constellation of GPS satellites can separate tropospheric effects from geodetic and astrometric signatures in  $\tau_{VLBI_i}$  is currently under investigation in JPL's Telecommunications and Data Acquisition Advanced Systems Program.

#### 4. CHARGED PARTICLE EFFECTS IN VLBI

Propagation effects through the charged particles in the Earth's ionosphere are calibrated to much better than 1 mm by dual frequency calibration at  $S$  and  $X$  bands. However, attempts to use current VLBI capabilities to measure the  $\gamma$  parameter of relativistic gravitation theories (Lowe 1990; Robertson et al. 1991) rely on observations close to the sun. Within a few degrees of the sun, the electron columnar content is about 3 orders of magnitude greater than that of the Earth's ionosphere (Tyler et al. 1977). The steady-state radial gradient in the solar plasma electron density and the fluctuations of that density (Woo and Armstrong 1979) are the principal obstacles to achieving the submilliarcsecond accuracies necessary to produce a 1 part in  $10^4$   $\gamma$  measurement. Lowe (1992) has shown that the steady-state effect causes errors of the order of  $10^{-5}$  in  $\gamma$  ( $\approx 3\text{psec}$ ), and that the fluctuation effect can be reduced to a similar level if rapid sampling (faster than 10 samples per second) strategies can be employed. Rapid sampling has the effect of "freezing" the solar plasma fluctuations for time intervals over which they cause only small phase fluctuations.

#### ACKNOWLEDGMENTS

O. J. Sovers installed and debugged much of the troposphere covariance code, which greatly facilitated the production of Figure 2. This work represents one phase of research carried out at the Jet Propulsion Laboratory, California Institute of Technology, under contract with the National Aeronautics and Space Administration.

#### REFERENCES

- Bean, B. R., Dutton, E. J. (1966) *Radio Meteorology NBS Monograph No. 92*, U.S. Government Printing Office
- Chao, C. C. (1974) *NASA-JPL Tech. Rep. TR-32-1587*, 61
- Davis, J. L., Herring, T. A., Shapiro, I. I., Rogers, A. E. E., Elgered, G. (1985) *Radio Sci.* **20**, 1593
- Davis, J. L., Herring, T. A., Shapiro, I. I. (1991) *J. Geophys. Res.* **96**, 643
- Elgered, G., Davis, J. L., Herring, T. A., and Shapiro, I. I. (1990) *J. Geophys. Res.* **96**, 6541
- Hamilton, W. C. (1964) *Statistics in Physical Science* Ronald Press, New York

- Herring, T. A., Davis, J. L., Shapiro, I. I. (1990) *J. Geophys. Res.* **95**, 12,561
- Lanyi, G. E. (1984) *IAG COSPAR* **2**, 184
- Lowe, S. T., Edwards, C. D., Estabrook, F. B., Hellings, R. W., Treuhaft, R. N. (1990)  
*Improving the Accuracy of the Gamma Parameter of Relativistic Gravity Theories with VLBI, Proposal to JPL Director's Discretionary Fund*
- Lowe, S. T. (1992), private communication
- Marini, J. W. (1972) *Radio Sci.* **7**, 223
- Resch, G. M., Hogg, D. E., Napier, P. J. (1984) *Radio Sci.* **19**, 411
- Robertson, D. S., Carter, W. E., and Dillinger, W. H. (1991) *Nat.* **349**, 768
- Sovers, O. J., Edwards, C. D., Lanyi, G. E., Liewer, K. M., Treuhaft, R. N. (1988) *Astron. J.* **95**, 1647
- Treuhaft, R. N., Lanyi, G. E. (1987) *Radio Sci.* **22** 251
- Treuhaft, R. N., Lowe, S. T. (1991) *Astron. J.* **102**, 1879
- Tyler, G. L., Brenkle, J. P., Komarek, T. A., Zygelbaum, A. I. (1977) *J. Geophys. Res.* **82**, 4335
- Wilcox, J. Z. (1991) *The Standard Deviation of WVR Gain Estimated From Tip Curves Due to Wet Troposphere Fluctuations* JPL Interoffice Memorandum 335.6-91-032
- Woo, R. and Armstrong, J. W. (1979) *J. Geophys. Res.* **84** 7288



## ANALYSIS OF NAVNET GEODETIC VLBI POST-FIT DELAY RESIDUALS

D.N. MATSAKIS, T.M. EUBANKS  
U.S. Naval Observatory,  
Washington, DC 20392, U.S.A.

**ABSTRACT.** Residuals from solutions using geodetic data from Very Long Baseline Interferometry (VLBI) have been used in a study of the delay and delay rate error introduced from errors in the modelling of the tropospheric propagation delay and delay rate. These residuals were subdivided into classes based on integration time, the signal to noise ratio, and the elevation angles at the two stations involved in the observation. This subdivision of residuals makes it possible to separate effects due to tropospheric propagation from other causes of VLBI residual errors. The delay rate residuals are found to depend strongly both on the total air mass of the observation and the integration time. The integration time effect seems to be also of tropospheric origin, and can be used to determine the power law of high frequency variations in the tropospheric propagation delay. Except for a strange enhancement in the delay rate residual scatter for the baselines to the Hawaii station with integration times on the order of 200 seconds, most of our findings are consistent with the theoretical models of Treuhart and Lanyi (1987). The cause of the excess Kauai delay rate scatter must be regarded as unknown, but may be due to instrumental error.

### 1. INTRODUCTION.

As part of its participation in the National Earth Orientation Service (NEOS), the U.S. Naval Observatory has developed a program in Very Long Baseline Interferometry (VLBI) to monitor changes in the Earth's rotation on a regular basis. The Navy VLBI Network (NAVNET) measures the orientation of the Earth in space from Mark III VLBI observations acquired with telescopes in Alaska, Hawaii, Florida, and West Virginia; other radio telescopes also participate on an occasional basis. The NAVNET data are used to estimate UT1, Polar Motion, and Nutation for inclusion in the International Earth Rotation Service (IERS) combined solutions. The data analyzed below were taken, correlated, and reduced using standard procedures and the GSFC CALC/SOLVE package. The very last step in the process involves use of the SOLVE package to remove nuisance instrumental parameters and to extract information on the Earth orientation parameters and/or antenna positions. The data analyzed below are the residuals to such solutions, using only the 4 core antennas.

Roughly 30,000 data points are used in this analysis. The overall weighted rms residual scatter in this solution was about 46 picoseconds (ps) for the delay data and 100 femtoseconds/second (fs/s) for the delay rate data. The binned rms statistics reported herein are unweighted rms scatters; the unweighted rms scatter from the entire solution is about 60 picoseconds for the delay and 130 femtoseconds/second for the rate data.

### 3. THE BINNING ANALYSIS

As shown in the figures, the delay residuals seem to follow the theoretical value computed from the correlator-determined signal-to-noise-ratio, which depends upon the receiver noise as well as the intra-scan atmospheric noise. The linear relation fails at the lowest values; the variance can be approximated as 35 ps squared plus the theoretical value. Figure 2 shows that there is no excess noise at low elevations; the tendency for the scatter to be too small at the largest formal error values is probably caused by manual "trimming" of the points with the largest residuals in the data-editing process.

Figures 3-4 show that, in contrast to the delays, the delay fringe rate scatter does not depend upon the signal to noise ratio or the theoretical noise; it does depend strongly upon the number of air masses.

Since any unmodelled error active on a time scale less than the scan length would increase the computed theoretical scatter, the excess variance is sensitive only to fluctuations variable on time scales longer than a few minutes. The dependence of only the fringe rate excess variance on the total atmospheric column density indicates that atmospheric fluctuations significantly contribute to the fringe rate error budget, but have little effect on the delay errors.

### 4. RESIDUAL CLOSURE

Most modellable noise sources, including the atmosphere, are antenna-based; the signed sum of their values for all baselines connecting any three antennas is zero. The most significant source of baseline-based noise is contributed from the system noise of the antenna receivers. From the analysis of the residuals it would be expected that the atmosphere-limited fringe rate residuals would show closure whereas the snr-limited delay residuals would not. This is shown to be the case in Table 1, and further supports the conclusion of the previous section.

### 5. THE POWER-LAW DEPENDENCE OF HIGH FREQUENCY DELAY FLUCTUATIONS

It is possible to use the variation of residual scatter with integration time to estimate the spectral index of the power law. Our estimate for the rate (2.71) agrees well with that of Treuhart and Lanyi (1987), and indicates that the rate noise is dominated by the highest frequencies available. In contrast, the atmospheric contribution to the delay is found to be small and dominated by the longest frequencies.

### 6. CONCLUSION

We have found that the NAVNET precision in delay is limited by non-antenna based error sources, while the delay rate residuals can be used to extract information about the tropospheric irregularities.

Table 1. Closure Relations for 4 NAVNET Triangles

The baseline-dependent variance was taken to be the variance of the appropriate algebraic sum of the three associated baseline residuals. The variance of the antenna-based residuals was taken as the difference between the sum of the three individual baseline variances and the baseline-dependent variance. This procedure is not guaranteed to give a realistic answer, particularly if one or the other noise source dominates. In one case this variance was a very small negative number, hence its rms was undefined.

Baseline Triangle	Delay RMS (ns)		Fringe Rate RMS (ps/s)	
	BL-based	Ant-based	BL-based	Ant-based
GB, Rich, Kauai	.11	.34	.10	.16
GC, Rich, Kauai	.12	undefined	.11	.14
GC, GB, Rich	.075	.026	.069	.12
GC, GB, Kauai	.10	.025	.086	.16

## REFERENCES

Treuhart, R.N. and Lanyi, G.E., The effect of the dynamic wet troposphere on radio interferometric measurements, Radio Science, 22, 251-265, 1987

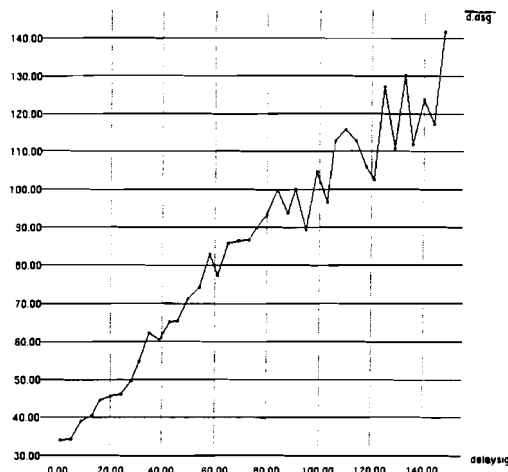


Figure 1. RMS of Delay Residuals (picosec) as function of Theoretical (Receiver) Prediction

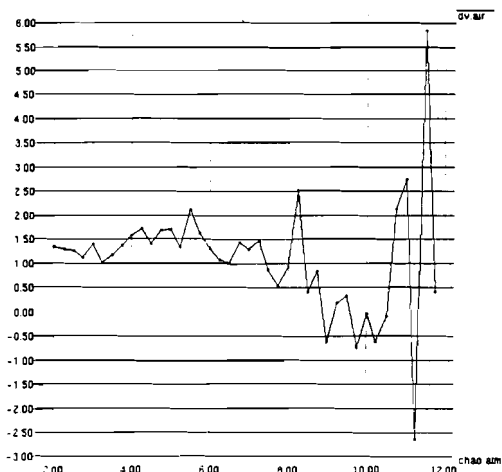
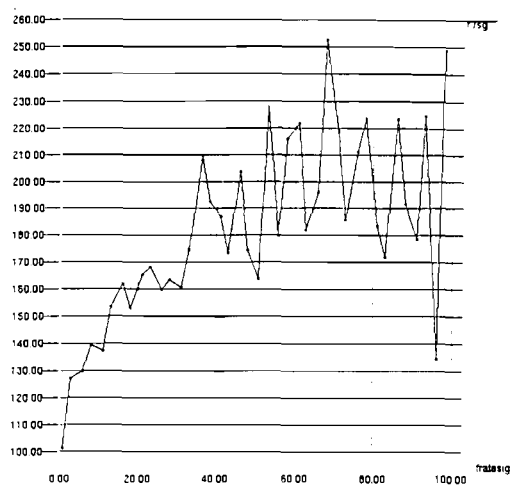
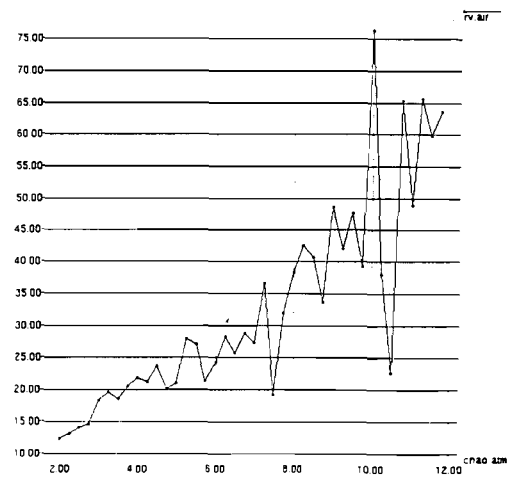


Figure 2. Variance of Delay Residuals ( $p1\text{cosec}^2$ ) after subtraction of theoretical predictions, as a function of number of air masses.



**Figure 3.** RMS of Fringe Rate Residuals (fsec/s) as a function of Theoretical (Receiver) Prediction.



**Figure 4.** Variance of Fringe Rate Residuals (fs/s squared) after subtraction of theoretical predictions, as a function of number of air masses

# IONOSPHERIC CALIBRATION OF VLBI DATA USING GPS OBSERVATIONS

E. SARDÓN, A. RIUS, N. ZARRAOA  
Instituto de Astronomía y Geodesia (CSIC-UCM)  
Facultad de Ciencias Matemáticas  
28040 Madrid, Spain

**ABSTRACT.** VLBI and GPS high precision geodesy is currently performed using dual frequency band observations of quasars or satellites, in order to reduce the ionospheric effects. Single frequency observations could be a necessity due to a lack of equipment or instrumental deficiencies. This paper addresses the problem of mapping the ionospheric total electron content (TEC) using GPS data, and its application to the calibration of single frequency VLBI experiments. Dual frequency GPS observations have been made at the VLBI sites in Madrid, Wettzell and Onsala, concurrently with S/X Mark III geodetic VLBI experiments. Then the X-Band VLBI data, calibrated with the ionospheric model derived from the GPS data, have been analyzed to produce geodetic estimates. The comparison of these estimates with those obtained with the standard analysis procedure indicates no significative change in the estimates with a small degradation in the precision.

## 1. INTRODUCTION

The time travel of the signals from the quasars and from the GPS satellites is modified by the presence of the ionosphere: a signal experiences a delay  $d_{ion}$  (in m) which, for our purposes, could be modeled with enough accuracy as (see Sovers and Fanslow, 1987 for details):

$$d_{ion} = \alpha_f \cdot I \quad (1)$$

where  $I$  is the number of electrons per unit area or TEC along the direction of observation (in  $m^{-2}$ ),  $\alpha_f = 40.3/f^2$  (in  $m^3$ ) and  $f$  is the frequency of the signal (in Hz). The dispersive character of the ionospheric delay allows the calibration of this effect by the use of two frequencies.

For each  $station_j$  and for each  $satellite^i$ , we could form the following equation (see Blewitt, 1989 for details):

$$L_{kj}^i = p_j^i - \alpha_{f_k} \cdot I_j^i - \lambda_k \cdot b_{kj}^i \quad (2)$$

where  $L_{kj}^i$ ,  $k=1,2$ , is the carrier phase, in range units, corresponding to the frequency  $f_k$ ,  $p_j^i$  consists of the nondispersive terms of the phase delay,  $I_j^i$  is the TEC in the direction  $satellite^i - receiver_j$ ,  $\lambda_k$  is the carrier wavelength at frequency  $f_k$ , and  $b_{kj}^i$  are the initialization constants for  $satellite^i - receiver_j$  at frequency  $f_k$ .

Terms taking into account multipath, phase center offsets and noise are not considered. In our process we have used the pseudorange observations only to detect the cycle slips and to estimate the phase ambiguities. These ambiguities have been subtracted from the observed phases, so (2) is converted in a system with two equations and two unknowns. But there can be a remaining part, not estimated, in the initialization constants containing the uncalibrated biases of the phase delay produced in the satellite and in the receiver, systematic errors, etc. Then, for each time  $t$  we will have :

$$I_j^i(t) = \bar{I}_j^i(t) + k^i + k_j \quad (3)$$

where  $\bar{I}_j^i$  is the true TEC in the direction of observation,  $k^i$  is a constant term for the *satellite*<sup>i</sup> and  $k_j$  a constant term for the *receiver*<sub>j</sub>.

## 2. ESTIMATION OF THE IONOSPHERIC DELAY

If we collect data at different epochs  $t$ , we will have a set of equations (3), with a number of unknowns greater than the number of equations. But the TEC  $\bar{I}_j^i$  can be factored as

$$\bar{I}_j^i(t) = S(e_j^i) \cdot F(\vec{d}_j^i, t) \quad (4)$$

where  $e_j^i$  is the elevation of the *satellite*<sup>i</sup> seen from the *receiver*<sub>j</sub>,  $\vec{d}_j^i$  is the geocentric direction of the intersection of the signal path with a mean ionospheric layer (S in figure 1b), the slant function S maps the TEC into the  $\vec{d}_j^i$  direction (see Sovers and Fanselow, 1987) and  $F$  is a function describing the TEC in the direction  $\vec{d}_j^i$  at time  $t$ .

Notice that for satellites with elevations higher than 10 degrees, at each time  $t$ , the observable region of the ionosphere as seen from the center of the earth is a cone of angle 11 degrees. Because of this, we expect that, at least, the spatial linear approximation of  $F$  is required around the zenith direction:

$$\bar{I}_j^i(t) = S(e_j^i) \cdot [F(\vec{d}_{zenith_j}, t) + DF(\vec{d}_{zenith_j}, t) \cdot (\vec{d}_j^i - \vec{d}_{zenith_j})] \quad (5)$$

where  $\vec{d}_{zenith_j}$  is the direction of the zenith in the *station*<sub>j</sub> and  $DF$  is the spatial differential of  $F$ .

The main agent causing the ion production in the ionosphere is the solar radiation, in such a way that we can expect a roughly symmetric distribution around the Sun direction. So, we consider the geocentric reference system defined in figure 1a, with axis z towards the solar center and the equation (5) is rewritten as (see figure 1b)

$$\bar{I}_j^i(t) = S(e_j^i) \cdot [A_j(t) + B_j(t) \cdot da + C_j(t) \cdot db] \quad (6)$$

where  $da = a_j^i - a_{zenith_j}$ ,  $db = b_j^i - b_{zenith_j}$  and  $A_j(t)$ ,  $B_j(t)$  and  $C_j(t)$  represent the coefficients of the local linear approximation to the global function  $F$ .  $A_j(t)$  is the TEC at zenith of *station*<sub>j</sub>.

The parameters to be solved are the constants  $k^i$ ,  $k_j$  (one of them is set arbitrarily to zero), and at each *station*<sub>j</sub> and for each time  $t$  the values  $A_j(t)$ ,  $B_j(t)$  and  $C_j(t)$ . We have considered  $A$ ,  $B$  and  $C$  to be random walk stochastic processes and solved them, along with the constants, using a Kalman filter software (Sardón et al., 1991).

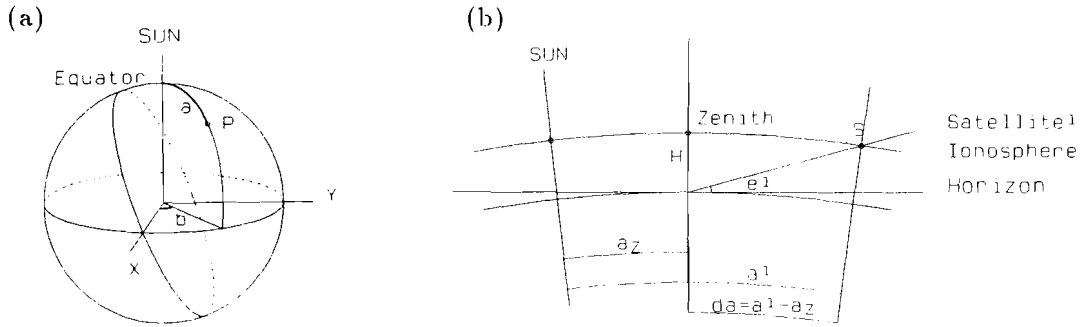


Figure 1. Coordinates  $a$  and  $b$  of the point  $P$  in the chosen reference system (a) and local ionosphere around the zenith  $Z$  of the  $station_j$  (b)

### 3. APPLICATION TO THE VLBI DATA

With this procedure we have analyzed GPS data collected at Madrid (Spain), Wettzell (Germany), Onsala (Sweden), Goldstone (California) and Tidbinbilla (Australia) during the NASA Crustal Dynamic Project VLBI experiment EUROPE2 -90 (5 and 6 September 1990). All the receivers were ROGUE, except a TI-4100 used at Onsala. The reason for including Goldstone and Tidbinbilla, in this case, is to facilitate the estimation of the satellite constants. Figure 2 shows the zenith TEC estimate in this way at Madrid, Wettzell and Onsala.

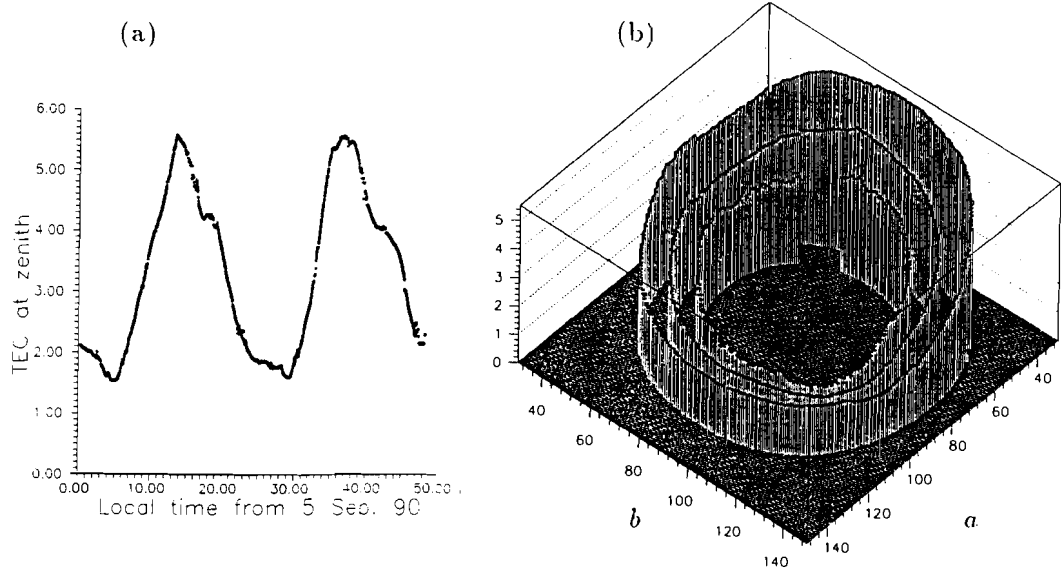


Figure 2. Zenith TEC in  $10^{17} e/m^2$  at Madrid as a function of time in hours (a) and the same quantity at Madrid (outer), Wettzell (medium) and Onsala (inner) as a function of  $a$  and  $b$  in degrees (b).

The computation of predicted ionospheric delays in other directions, at other frequencies and other times is made using (6) (with a time interpolation for the computation of the coefficients A, B and C) and (1).

We have analyzed the S/X Mark III VLBI data collected at Wettzell, Madrid and Onsala during the EUROPE2 experiment. In one solution, we have used the standard calibration for the ionosphere (using S and X Band data). In a second solution, we have used X-Band data supplemented with the ionosphere information obtained as described above (the ionospheric delay for each baseline is computed differencing the delays for both stations). Table 1 shows the difference in the baseline lengths ( $\Delta b$ ) between the VLBI points obtained with both solutions and the corresponding formal errors ( $\sigma_{S/X}$  and  $\sigma_{X/GPS}$ ).

TABLE 1.

Baseline	$\Delta b$ (mm)	$\sigma_{S/X}$ (mm)	$\sigma_{X/GPS}$ (mm)
Mad-Ons (2205 km)	4	15	20
Mad-Wet (1655 km)	0	10	14
Ons-Wet (920 km)	-3	9	11

The main conclusion is that the length estimates change within their formal errors and that those corresponding to the solution with GPS data are slightly larger than those for the standard VLBI solution, due probably to our present limitations in modeling the ionosphere at low elevations.

#### ACKNOWLEDGMENTS

The GPS data from Wettzell was gathered and provided by Dr. S. Starker, H. Nau and T. Julg from the DLR Institut fur Hochfrequenztechnik (Germany). The data from Onsala was provided by Dr. Miranda Chin at USA National Geodetic Survey. The data from the Deep Space Network Stations (Madrid, Goldstone, Tidbinbilla) was provided by Tom Lockhart from JPL. This research has been funded by the Spanish CICYT under contract PB88-0021.

#### REFERENCES

- Blewitt, G. (1989) "Carrier Phase Ambiguity Resolution for the Global Positioning System Applied to Geodetic Baselines up to 2000 km", *Journal of Geophysical Research*, vol 94, no. B8.
- Sardón, E., Rius,A., Zaraoa, N. (1991) "Kalman Analysis of Geodetic VLBI Experiments", *Proceedings of the VIII Working Meeting on European VLBI for Geodesy and Astrometry* Dwingeloo. (in press).
- Sovers, O. J., Fanselow, J. L. "Observation Model and Parameter Partials for the JPL VLBI Parameter Estimation Software MASTERFIT-1987", *JPL Publication 83-39, Rev.3* 1987.

## TOOLS OF TROPOSPHERE CORRECTION FOR VLBI NETWORK "QUASAR"

T.A. AKHUNDOV, V.N. ALEXEEV, G.B. BAYKOV, A.A. STOTSKII  
Institute of Applied Astronomy,  
197042, St. Petersburg, Russia

In 1988 the USSR Academy of Sciences made a decision to built VLBI network "Quasar". The first three stations of this network (near St. Petersburg, in the Northern parts of the Caucasus and near Lake Baikal) and the Centre of Operations in St. Petersburg are under construction at the present time. The radio telescopes at the stations have a diameter of 32 m in diameter and are designed to operate in the cm wave-length band (Finkelstain et al., 1990).

Each station will be equipped with a special system to measure the excess path length through the troposphere during the observations.

The system consists of three subsystems:

1) Automatic meteorological station. The values of meteorological parameters are used to calculate the dry component of excess path length and to correct coefficients in algorithm to determine the wet component considering the local weather conditions (Johansson et al., 1987).

This station is also used to display the general weather situation for the observing station in the Network.

To avoid the dependence on local conditions the sensors for the ambient temperature, humidity and wind velocity and direction may be placed at distance to 200 m from radio telescope.

The temperature sensor is of a platinum resistance type. The thermometer has an internal calibration system with a reference stable resistor.

The barometer is of a crystal oscillator type. It is located in the host device

TABLE 1  
Performance specification of meteorological station

Measured parameter	Range	Accuracy
Temperature (C)	-50 - +50	0.25
Pressure (mba)	600 - 1090	0.5
Humidity (%)	30 - 100	5
Mean wind velocity (v) for 10 min (m/s)	1.5 - 40	0.5 + 0.05v
Max. wind velocity (v) for 10 min (m/s)	8 - 55	0.5 + 0.05v
Wind direction (degree)	0 - 360	10
Rain	Yes / No	
Precipitations (P) during 10 min or 1 hour (mm)	0 - 150	0.2 + 0.05P

2) Dual frequency water vapor radiometer. The frequency pair is chosen according to Wu (1979). The radiometer with two antennas will be situated directly on the radio telescope reflector. The radiometer is of a Dicke type with two reference loads - hot and cold. There are two ferrite switches: (antenna/load) and (hot load/cold load). The radiometer cases are stabilized in temperature. The loads have an additional high precision temperature stabilization.

TABLE 2  
Performance specification of radiometers

Frequencies (GHz)	20.3 / 31.4
Antennas: type	horn-reflector
diameter (mm)	700 / 500
Noise temperature of input amplifier (K)	380 / 520
Bandwidth (MHz)	1000
Temperature of reference loads	
hot (K)	298
cold (K)	228
Inter. time (s)	1
Sensitivity (K, int.time 1 s)	0.05 / 0.1

3) Control and signal processing subsystem. This subsystem realizes following functions:

- remote control of the radiometer and meteorological station
- processing the data
- communication with the central computer
- status display

The subsystem is based on DVK-3 computer. Communication with the meteorological station, radiometer and central computer is performed by using interface of an RS 232 type.

At present the prototype of the system is being tested and calibrated. The calibration is performed by using external cooled load and data of radio sondes.

## REFERENCES

- Finkelstein, A.M et al. (1990) in Inertial Coordinate System on the Sky, eds. J.V. Lieske and V.K. Abalakin, p. 293  
 Johansson, J.M., Elgered, G., Davis, J.L. (1987) Research Report No 152, Onsala Space Obs.  
 Wu, S.C.(1979) IEEE Trans. AP-27, 2, p. 233

# INFLUENCE OF MEASUREMENT ERRORS OF THE METEOROLOGICAL DATA USED FOR TROPOSPHERIC MODELS IN VLBI

H. SCHUH  
German Aerospace Research Establishment (DLR),  
Linder Höhe, D-5000 Köln 90, Germany

**ABSTRACT.** Until now surface temperatures, pressures and relative humidities are entered into tropospheric path delay models used for VLBI data analysis. Both, the dry and the wet component of the tropospheric correction can be treated separately and it can be split up into the zenith path delay and a correction due to the elevation of the observed radio source. Measurement errors of the meteorological data, however are completely neglected.

The error propagation law was applied to the Marini model for the zenith path delay and to the CFA.2 model as one of the most commonly used mapping functions in order to estimate the dependence of the tropospheric path delay at the elevation of observation on measurement errors of the input parameters ( $T_0$ ,  $p_0$ ,  $e_0$ ). From the results of our investigation the required accuracies of the meteorological measurements can be estimated if a certain error of the tropospheric path delay correction at different elevation angles shall not be exceeded. For instance, to get an error contribution of less than 5 mm from each input parameter at an elevation of  $10^\circ$ , the pressure  $p_0$  has to be measured to better than 0.5 mbar and the water vapor pressure  $e_0$  to better than 0.1 mbar. Errors of the temperature  $T_0$  affect the total error much less. Additionally, the results allow to calculate more realistic a priori sigmas of the delay and delay rate observables than at present even if the accuracies of the meteorological data are only roughly known. This will improve the stochastical model of the VLBI least squares fit whatever strategy for the correction of the propagation delay is chosen, i.e. whether direct measurement of the wet delay are applied or whether the wet delay is estimated from the VLBI data.



## **4. IONOSPHERE**



# THE IONOSPHERE AS A REFRACTIVE MEDIUM

T.A.TH. SPOELSTRA

Netherlands Foundation for Research in Astronomy,  
Postbus 2, 7990 AA Dwingeloo, The Netherlands

**ABSTRACT.** In geodetic applications ionospheric refraction is primarily a calibration problem, which is especially complicated by variations in the magneto-ionic properties of the medium at various spatial and temporal scales. Ionospheric sounding techniques may provide calibration data, but they are in general not able to determine the electron distribution along and perpendicular to the line of sight. Climatological knowledge of ionospheric irregularities provides useful information to estimate forecast accuracies based on models and to enable improved scheduling of observations. Methods to reconstruct the ionospheric electron density distribution from measured data may improve the calibration quality.

## 1. INTRODUCTION

The problem with the ionosphere is not that it is a refractive medium for electromagnetic waves, but that the distribution of the charged particles and the structure geomagnetic field which in a combination cause this refraction are far from simple. Here "simple" means for the distribution of charged particles "uniform and spherically symmetric" and for the geomagnetic field "a dipole field". In particular these structural characteristics imply the need for sophisticated calibration techniques in passive and active frequency use, and for ionosphere models for possible applications in corrections as well as predictions. Especially irregularities at different spatial and temporal scales, as e.g. acoustic-gravity waves and magnetic storms, distort attempts to apply corrections and develop predictions.

The main contribution to the refraction comes from electrons because they are more mobile than the heavier ions. For geodetic applications the geomagnetic field plays only a secondary role.

By means of different sounding techniques several aspects of the ionosphere can be investigated which may be used to calibrate geodetic data. However, at present there is no technique available by which the integrated electron content along the line of sight, the electron distribution along and perpendicular to the line of sight and the structure of the geomagnetic field can be studied simultaneously. Incoherent scatter radar provides the nearest approach to this aim. This implies that at present we are not able to determine at the time and direction of our observation/transmission the spatial and temporal characteristics of the ionosphere, although partial information is available.

For geodesy the main problem of the ionosphere as a refractive medium is that its influence has to be removed from the observed data as much as possible by any reasonable calibration method to achieve the required accuracy of the geodetic results. A by-product is that the calibration information mimics the conditions in the ionosphere and can therefore be used for aeronomic research.

## 2. REFRACTION PROBLEM IN THE CALIBRATION

Geodetic observations need to be calibrated in order to derive meaningful results. The tolerances one derives for the corrected data (and from those also for the correction parameters) depend strongly on the distribution of the remaining errors as a function of spatial coordinate, time and frequency used. An instructive way to consider this seems to be thinking of the Fourier-transform of the data in the time domain to a "map" as an operation, which for each map position produces the real component of the weighted sum of all measured vectors in the time domain. The input vectors for this summation consist of two pairs: noise and signal vectors affected by imperfections. The latter may be considered as the proper signal vectors plus error vectors, defined by the signal vectors and the fractional errors in complex amplitude.

For the same reason the resulting map may be considered as the sum of three maps:

- 1) the ideal, noise-free map;
- 2) the noise map;
- 3) the error map.

Of the two unwanted components the noise map has a predefined rms amplitude determined by integration time and system noise. Thus, our main concern is the error map which involves also the propagation errors, and which can be considered as a component of the sky-brightness-distribution times the beam reception pattern, convolved with an unknown complex function. This is of course only a first order consideration, because if the errors in amplitude and phase are dependent on the position of the source/transmitter with respect to the line of sight, so will the unknown convolving function.

Calibration of the data means then that this unknown convolving function should be made as small as possible. The aim is to make it smaller than the noise. Tolerances for calibration are properly reached when this has been achieved. When this can not be done, this function must be made as small as possible with respect to the antenna pattern.

For the refraction problem, the aim is to make the contribution of the propagation errors to this unknown convolving function smaller than all other factors in this function.

## 3. HOW TO DETERMINE THE ERROR MAP ?

In the calibration process our primary goal is to determine the error map as accurate as possible. Since the aim of our research is geodesy, this goal is properly reached by two possible methods:

- "self-calibration": we use this term for any calibration method which works exclusively on the data themselves while the presumably known characteristics of the problem, of the instrument used and of the radio source/transmitter are taken into account in the calibration algorithm. In radio astronomy this method is widely used. In this method in principle no knowledge of the propagation medium is needed. A limitation of this method is that it provides only relative positional accuracy.
- absolute calibration: we use this term for any calibration method which accounts for the characteristics of the propagation medium: i.e. magneto-ionic characteristics of the ionosphere. The correction factors used to calculate the error map are basically part of an algorithm to reconstruct the distribution of the charged particles in the ionosphere and the geomagnetic field.

The error map or reconstruction algorithm has to deal with variations in the magneto-ionic medium at a variety of time scales and spatial scales. A basic limitation is that practically every calibration technique uses in some way a model assumption about the medium, even if one uses measured values for ionospheric parameters, e.g. the total electron content TEC from the critical frequency of the F2 layer,  $f_{0F2}$ . In some cases uncertainties and ambiguities can be removed as in e.g. Faraday rotation measurements of a polarized signal of a discrete source, if done at more than three wavelengths (this is necessary to remove ambiguities in the number of rotations of the polarization angle): in this case both the strength of the geomagnetic field along the line of sight and the electron content along the line of sight can be determined unambiguously. However, in practice quasi-geostationary satellites used for this purpose transmit a suitable signal only at one frequency, e.g. 136 MHz. Thus multi-frequency Faraday rotation measurements are not possible in geodetic applications. But even if this method can be used one should be aware of the fact that due to the characteristics of the medium the geometrical ray path from the radio source/transmitter to the receiver is different for each frequency used.

#### 4. IONOSPHERIC IRREGULARITIES

The magneto-ionic characteristics of the ionosphere vary at different time scales. To first approximation the refractive index is mainly determined by the electron density. Therefore, the measurements are more sensitive for variations of the ionospheric electron content than for variations in the geomagnetic field. Although during high geomagnetic activity in many cases the electron distribution is disturbed, the relation between geomagnetic activity and distortions of the ionospheric electron density is still marginally understood.

The ionospheric electron density shows variations at a time scale of 24 hours (the daily variations) and irregularities superimposed on this diurnal variation. Several classes of ionospheric irregularities are interpreted in terms of acoustic-gravity waves travelling through the ionosphere. Large scale travelling ionospheric disturbances, LSTIDs, have horizontal phase speeds of 300-1000 m/s, periods ranging from 30 minutes to 3 hours, and horizontal wavelengths exceeding 1000 km. They propagate equatorward from the polar regions. Medium scale travelling ionospheric irregularities, MSTIDs, have horizontal phase speeds of 100 - 300 m/s, periods from about 10 minutes to about 1 hour and horizontal wavelengths of several hundreds of km. They occur more frequently than LSTIDs. LSTIDs and MSTIDs are gravity waves.

Small scale travelling ionospheric disturbances, SSTIDs, have periods of several minutes and wavelengths of tens of kilometers. They are associated with the acoustic branch of the spectrum of acoustic-gravity waves. As to their origin equally little is known as for the MSTIDs.

An illustration of the effects of ionospheric irregularities on trans-ionospheric radio signals is Figure 1 which gives an amplitude and phase plot of an observation with the Dutch Westerbork Synthesis Radio Telescope, WSRT. The refraction effects are clearly seen in the interferometer phase. The fluctuations in phase have different time scales: [a] a large scale slowly varying component is caused by the slowly varying component of TEC (Spoelstra, 1983); [b] before about 16.30 UT manifestations of medium scale travelling ionospheric disturbances, MSTIDs, are seen; [c] after about 19.00 UT the observation is affected by ionospheric scintillation.

Among the many unknowns related with these TIDs are their origin and their propagation characteristics through the ionosphere. Possible generating sources for gravity waves are the solar terminator (Beer, 1978), the aurorae (Evans, 1977), jetstreams and instabilities in wind

fields (Bertin et al., 1975, 1978), orographic excitation, or instability of tidal waves in the upper atmosphere (Gavrilov et al., 1981; Kelder and Spoelstra, 1987).

The travelling ionospheric disturbances, TIDs, may imply variations in the ionospheric electron density of several percent of the TEC.

In the calibration procedure the horizontal and vertical gradients in the electron density distribution in addition to the TEC have to be taken into account in the refraction correction (Spoelstra, 1987). Thus any reconstruction algorithm has to implement these in the calculation of the error map. The appearance of manifestations of TIDs in measurements imply that to the gradients inherent to the regular structure of the ionosphere gradients due to these wavelike patterns have to be added. A similar approach should be made in the reduction of data affected by ionospheric scintillation.

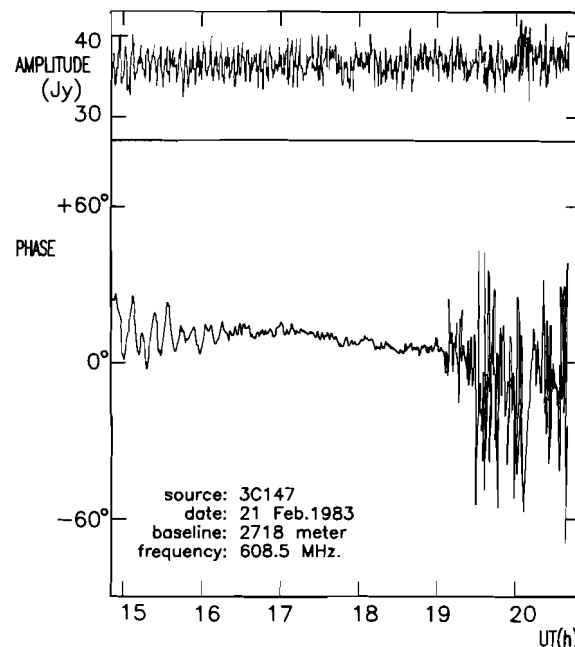


Figure 1. Ionospheric effects observed with the Westerbork Synthesis Radio Telescope, WSRT, at 2.7 km baseline. The ionospheric effects are only seen in interferometer phase. This registration shows slowly varying waves during the first 1.5 hours (medium scale TIDs) and rapid variations (scintillation) during the last 2.5 hours, both added to an even more slowly varying background (which is due to the daily variation of the electron content).

In addition to variations at time scales of a daily variations of ionospheric parameters, one has to consider the dependence of the electron density distribution as a function of season and phase in the solar cycle. The dependence of the total electron density on solar activity and season is well-known (e.g. Giraud and Petit, 1978, p.71). Less is known about the climatology of ionospheric irregularities.

## 5. MODELS

Models use the partial information of the spatial and temporal characteristics of the ionosphere combined with theoretical knowledge. But at present they are not able to provide better results than monthly median values for e.g. foF2, thus with a typical accuracy of about 30%. TEC values based on measured quantities reflecting ionospheric parameters, as obtained from ionosonde observations, have accuracies of typically 15%. This is supported by a recent evaluation by Brown et al.(1991) of six frequently used ionospheric models, i.e. the Bent model, the Fully Analytic Ionospheric Model, the Ionospheric Conductivity and Electron Density model, the Penn State model and the Hybrid model [for references see Brown et al.(1991)]. They showed that none of the models is able to predict the median TEC values within the natural variability of the measured data. Even when models do very well at predicting foF2, the uncertainties in the profile still cause serious errors in predicting TEC. The mean deviations are about  $2 \times 10^{16} \text{ m}^2$  for the solar minimum year and more than  $10 \times 10^{16} \text{ m}^2$  for the solar maximum year.

The short term ionospheric variations complicate the processing of single and dual frequency observations for each technique used and imply a significant reduction of the achievable positional accuracy. They imply often range errors of a several mm. Single frequency observations can at times easily become useless for precise geodetic positioning under conditions of intense ionospheric activity. Models do not yet account for ionospheric irregularities, so that when these irregularities occur, the reliability of the models is reduced.

Since also a critical energy budget evaluation of different excitation mechanisms for ionospheric irregularities and a critical confrontation of the different kinds of observations with existing proposals/models is not available with sufficient completeness, at present models cannot even be developed to take into account these irregularities. In addition, the physical understanding of the relevant aspects of the solar-terrestrial relationship need to be improved for a sound basis for these models.

Part of the questions about the solar-terrestrial relationship may be alleviated experimentally by an adequate climatology of ionospheric irregularities (see Section 6).

One may try to make a careful choice of ionospheric conditions, i.e. to measure the electron content in the region of the "ray" and to observe short term fluctuations of amplitude and phase of the received signal to be able to detect scatter and diffraction influences. Based on climatological knowledge one may schedule the observations for expected optimum conditions. This may be important since ionospheric irregularities can produce phase fluctuations which are one or two orders of magnitudes stronger than the phase fluctuations of the measuring system.

## 6. CLIMATOLOGY OF IONOSPHERIC IRREGULARITIES

Recently results of some climatological studies of ionospheric irregularities became available. The following characteristics have been observed for TIDs:

- [1] the occurrence of TIDs is a regular phenomenon, since they can be observed continuously in any direction of the sky (Kelder and Spoelstra, 1987; Soicher, 1988; Van Velthoven, 1990);
- [2] at solar maximum the number of occurrences maximizes in winter and minimizes at equinox; while at solar minimum the number of occurrences maximizes in summer and minimizes at equinox according to Soicher (1988). Van Velthoven (1990) found, however, that at solar minimum the number of occurrences during winter and summer were similar;

- [3] at solar maximum the total number of occurrence exceeds those at solar minimum in winter but is less than those at the solar minimum in summer and at equinox (Soicher, 1988). However, this was not confirmed by Van Velthoven (1990): he found that at solar maximum the total number of occurrences exceeds that at solar minimum in all cases;
- [4] the time of most frequent occurrence of TIDs as a function of season is the same at both solar epochs except during equinox (Soicher, 1988). Van Velthoven (1990) showed that this is probably not the case: the most frequent occurrence showed a shift to hours around sunrise at solar minimum;
- [5] the phase of the diurnal variation where TIDs occur most frequently is the same for both solar epochs (Soicher, 1988);
- [6] the magnitude of TIDs is normally larger at solar maximum than at solar minimum in all seasons (Kelder and Spoelstra, 1987; Soicher, 1988; Van Velthoven, 1990);
- [7] the time rate of change of TIDs is larger at solar maximum than at solar minimum in all seasons (Soicher, 1988);
- [8] the maximum of TIDs is larger in winter than in summer (Van Velthoven, 1990).

The study of Soicher (1988) was based on Faraday rotation measurements at Haifa, Israel, during a number of months in 1980 to 1984. The results of Kelder and Spoelstra (1987) are based on about 700 observations with the WSRT and of differential Doppler measurements of satellites of the Navy Navigation Satellite System, NNSS, made in the winter months of 1982 and 1983. The study of Van Velthoven (1990) is based on more than 5500 WSRT observations during different periods in the years 1980 - 1988. Discrepancies between the available climatologies may be due to unequal and insufficient time coverage of the data. Based on a continuous series of radio astronomical observations with the WSRT since 1970 an extensive climatological study is currently undertaken (Spoelstra, in preparation). Van Velthoven (1990) found that his results were similar to those obtained by Munro (1958), Titheridge (1968), Evans (1983) and Waldock and Jones (1986). He noted also some discrepancies: Evans (1983) found an overall occurrence of TIDs in summer which was relative to the other seasons larger than Van Velthoven (1990) found. The discrepancies between these results imply that such a more complete climatological study is needed. In particular any geographic dependence might be important as well as the sensitivity of the results for instrumental biases (Van Velthoven, 1990).

As had been indicated by Kelder and Spoelstra (1987) and Van Velthoven (1990) the TID-climatology contains information about mechanisms which play a role in the excitation of these irregularities (such as atmospheric tides), or which proposed mechanisms are not sufficiently supported by the data (such as the solar terminator and orographic excitation). However, so far a critical energy budget evaluation of different excitation mechanisms for ionospheric irregularities does not exist yet.

A climatology for TIDs will be different from a climatology for irregularities causing scintillation. This is partly due to the fact that scintillation events are more strongly related with geomagnetic events which are known to be related with activity on the Sun.

## 7. RECONSTRUCTION TECHNIQUES

In practically every method to correct for ionospheric influences a model is used. The most simple and general model used describes the ionosphere as a time independent spherically symmetric shell with either an infinitesimal thickness or a parabolic density distribution. If the thickness is infinitesimal the vertical TEC is represented by a two- or three-dimensional polynomial in angular coordinates over a subarea of this shell. The height corresponds to the

average altitudinal position of electron density profile peaks, which is often taken as 350 km. A parabolic density profile is taken with a peak altitude of also about 350 km.

Reconstruction techniques may be used to improve the structural knowledge of the ionosphere. The parabolic density profile assumption is of course a first step in this direction. More sophisticated models are e.g. the ones discussed by Brown et al.(1991) (see Section 5). By using measured ionospheric parameters, sunspot numbers and other experimental values these models can be used to determine the desired ionospheric quantity along the line of sight. This type of reconstruction method does not use the measured data to determine the electron density distribution except to tune an already assumed a priori algorithm for this distribution.

Recently ionospheric tomography has generated interest because of its ability to reconstruct the ionospheric density distribution with higher dimensionality than the measured ionospheric data, i.e. differential Doppler data. The data are measured between a low orbit beacon satellite and one or more fixed receivers in a well-known configuration with respect to the projected orbital path of the satellite.

The following receiver configurations are currently used:

- [1] A series of receivers located along the projected orbital path of the satellite (e.g. Austen et al., 1988; Andreeva et al., 1990; Raymund et al., 1990; Na, 1991; Raymund, 1992; Walker et al., 1992).
- [2] A series of receivers located perpendicular to the projected orbital path of the satellite (Kunitsyn and Tereshchenko, 1990, 1991).
- [3] A single receiver (Terekhov, 1991).

These different methods may be used in the calibration to reconstruct the satellite response using the reconstructed ionospheric electron density distribution. In this application it is important that the reconstructed satellite response corresponds with the data within the required tolerances. If this is achieved the geodetic parameters can be determined with the required accuracy.

The preliminary results of the tomographic method are very promising. The present state-of-the-art indicates that a number of algorithms have to be developed, since not every observing site is run with a configuration ideal for this method. Also the reconstruction algorithms which are currently available for use in combination of the NNSS satellites have to be made applicable for use with other satellite systems since the NNSS will be phased out within a few years. And finally this method might be extended for the use with different measuring techniques, such as interferometry.

## 8. CONCLUDING REMARKS

Ionospheric refraction may degrade geodetic measurements done at frequencies below a few GHz. The main problem is the variation of the magneto-ionic properties of the ionosphere at various spatial and temporal scales. One may alleviate the refraction effects by measurements at two widely spaced frequencies, but also then one should note that the propagation path and refraction errors are different for each of the frequencies used.

At present the knowledge of the dynamic behaviour of the ionosphere is far from complete. Open questions are related to e.g. dynamical models of the ionosphere, climatological knowledge of ionospheric irregularities, knowledge of the two- or three-dimensional electron density distribution, excitation of ionospheric irregularities. Not all these questions are equally relevant for the improvement of geodetic parameters. Geodetic

measurements may on the other hand provide aeronomics research with very valuable data. For multi-disciplinary reasons it is, therefore, desirable to pursue research on various aspects of ionospheric irregularities and reconstruction techniques. Improved knowledge of the propagation medium results in calibration improvement and a better understanding of our limitations.

## REFERENCES

- Andreeva, E.S., Galinov, A.V., Kunitsyn, V.E., Mel'nichenko, Yu.A., Tereshchenko, E.E., Filimonov, M.A., Chernyakov, S.M. (1990) *JETP Letters* **52**, 145
- Austen, J.R., Franke, S.J., Liu, C.H. (1988) *Radio Science* **23**, 299
- Beer, T. (1978) *Planet. Space. Science* **26**, 185
- Bertin, F., Testud, J., Kersley, L. (1975) *Planet. Space Sci.* **23**, 493
- Bertin, F., Testud, J., Kersley, L., Rees, P.R. (1978) *J.atmos.terr.Phys.* **40**, 1161
- Brown, L.D., Daniell, R.E., Fox, M.W., Klobuchar, J.A., Doherty, P.H. (1991) *Radio Science* **26**, 1007
- Evans, J.V. (1977) *Rev.Geophys.Space Phys.* **15**, 325
- Evans, J.V. (1983) *Radio Science* **18**, 435
- Gavrilov, N.M., Kal'chenko, B.V., Kashcheyev, B.L., Shved, G.M. (1981) *Izvestiya, Atmospheric and Oceanic Physics* **17**, 499
- Giraud, A., Petit, M. (1978) "Ionospheric techniques and phenomena", Reidel, Dordrecht
- Kelder, H., Spoelstra, T.A.Th. (1987) *J.atmos.terr.Phys.* **49**, 7
- Kunitsyn, V.E., Tereshchenko, E.D. (1990) Polar Geophysical Institute, USSR Academy of Sciences, preprint 90-01-69
- Kunitsyn, V.E., Tereshchenko, E.D. (1991) "Ionospheric Tomography" (in Russian), Nauka Publ.
- Munro, G.H. (1958) *Aust.J.Phys.* **11**, 11
- Na, H.R-L. (1991) Ph.D.Thesis, University of Illinois
- Raymund, T.D., Austen, J.R., Franke, S.J., Liu, C.H., Klobuchar, J.A., Stalker, J. (1990) *Radio Science* **27**, 771
- Raymund, T.D. (1992) Proc.of the 49th AGARD EPP symposium, 14-1
- Soicher, H. (1988) *Radio Science* **23**, 283
- Spoelstra, T.A.Th. (1983) *Astron.Astrophys.*, **120**, 313.
- Spoelstra, T.A.Th. (1987) *Publ.Astr.Ops.Beograd* No.35, 213
- Terekhov, A.I. (1991) preprint
- Titheridge, J.E. (1968) *J.Geophys.Res.* **73**, 243
- Van Velthoven, P.F.J. (1990) Ph.D.Thesis Eindhoven University of Technology
- Waldock, J.A., Jones, T.R. (1986) *J.Atmos.terr.Phys.* **48**, 245
- Walker, I.K., Pryse, S.E., Russell, C.D., Rice, D.L., Kersley, L. (1992) Proc.of the 49th AGARD EPP symposium, 15-1

# CLIMATOLOGY OF PHASE ERRORS DUE TO IONOSPHERIC ACOUSTIC-GRAVITY WAVES OBSERVED BY THE WESTERBORK RADIO SYNTHESIS TELESCOPE

P.F.J. VAN VELTHOVEN  
Centre de Recherche en Physique de l'Environnement  
4 Av. de Neptune, 94107 Saint Maur, France

**ABSTRACT.** At frequencies of 100 MHz to 1 GHz the phase variation of the signal at time scales of several minutes to an hour is largely due to ionospheric irregularities associated with propagating acoustic-gravity waves, so-called medium scale travelling ionospheric disturbances (MSTIDs). A climatological study of these irregularities has been performed using observations of calibrated intense point sources made with the Westerbork Synthesis Radio Telescope (WSRT) between 1980 and 1988. Daily, seasonal, interannual and solar-cycle variations have been studied, as well as variations with the line-of-sight. The magnitude and occurrence of MSTIDs show a large maximum at noon, a smaller maximum around midnight and minima around sunrise and sunset, during all seasons except summer when there is a large decrease in wave activity. Wave activity was largest in the winter-spring months of 1982-1984, i.e. slightly after the 1980 solar-cycle maximum. The dominant period of the waves shows variations related to the background wind in the ionosphere. This is shown by comparing different lines-of-sight.

## 1. OBSERVATIONAL TECHNIQUE AND DATA ANALYSIS

The Westerbork Synthesis Radio Telescope, WSRT, ( $6.6^{\circ}$  E,  $52.9^{\circ}$  N) is an east-west array of 14 radio telescopes with a maximum baseline length of 2.7 km. For calibration purposes the WSRT frequently observes cosmic radio sources which are point sources for the frequencies and beamwidths used. The observed fields are dominated by one single point source with a known position and intensity. Since the wavefront of emission from these objects is basically flat, these observations can be used for the climatological study of medium scale travelling ionospheric disturbances (MSTIDs). On the one hand such a climatology indicates when good radio propagation conditions are likely to occur. On the other hand it gives us a climatology of the associated acoustic-gravity waves and thereby a means to investigate the possible sources of these waves.

In order to facilitate the statistics we have arranged the observations, having durations of 1-12 h, into half hour periods. To reduce effects caused by the motion of the line-of-sight, observations for which the velocity of the line-of-sight at 350 km altitude was greater than 50 m/s, were rejected. A total number of 5508 half hour observations, made between 1980 and 1988 at observational wavelengths of 49 and 92 cm, has now been analysed. Of these only data in half hour intervals during which coherent wave patterns were observed along most baselines and for which the assumption of scaling with baseline length was satisfied with an accuracy of at least 50% (signal-to-noise ratio, SNR,  $>1$ ) were used in the climatological analysis.

Results for part of the present dataset (Jan-Mar 1982 and Dec 1982-Mar 1983) have already been presented by Kelder and Spoelstra (1987) and Spoelstra and Kelder (1984). The extended database has enabled the investigation of seasonal and interannual trends in MSTID related quantities and the dependence of these quantities on the direction of the line-of-sight. A detailed discussion of the trends found in the extended dataset can be found in Van Velthoven (1990). Here a brief summary of results will be presented.

## 2. THE OCCURRENCE AND THE AMPLITUDE OF THE MSTIDs

Figure 1 presents the daily variation in the frequency of occurrence of MSTIDs for eight periods of observation with a large amount of data. For the winter-spring periods (Jan-Mar 1982, Dec 1982-Mar 1983, Dec 1983-Mar 1984, Nov 1987-Feb 1988) there is a large maximum around noon and a secondary maximum at night. Such a daily variation has also been reported by others. The maximum at noon was larger in the years with high solar activity (Jan-Mar 1982, Dec 1982-Mar 1983, Dec 1983-Mar 1984) than for Nov 1987-Feb 1988 when solar activity was low. Later in the year (Feb-May 1985, Apr-Jun 1980) the time of the maximum seems to shift towards earlier in the morning and the overall frequency of occurrence is smaller. For the summer periods Jul-Aug 1985 and Jun-Aug 1986 the daytime maximum is absent, but there is still a maximum at night.

The amplitude of the MSTIDs showed qualitatively the same behaviour. This can be expected since the MSTIDs with the largest amplitudes are most easily observed. Note that the daytime variation of the amplitude and occurrence of MSTIDs in winter cannot be explained solely by the increased number of tracers (electrons). The daytime peak in the amplitude and the occurrence is considerably narrower and less pronounced than the daytime peak in  $N_m F_2$  (Van Velthoven, 1991).

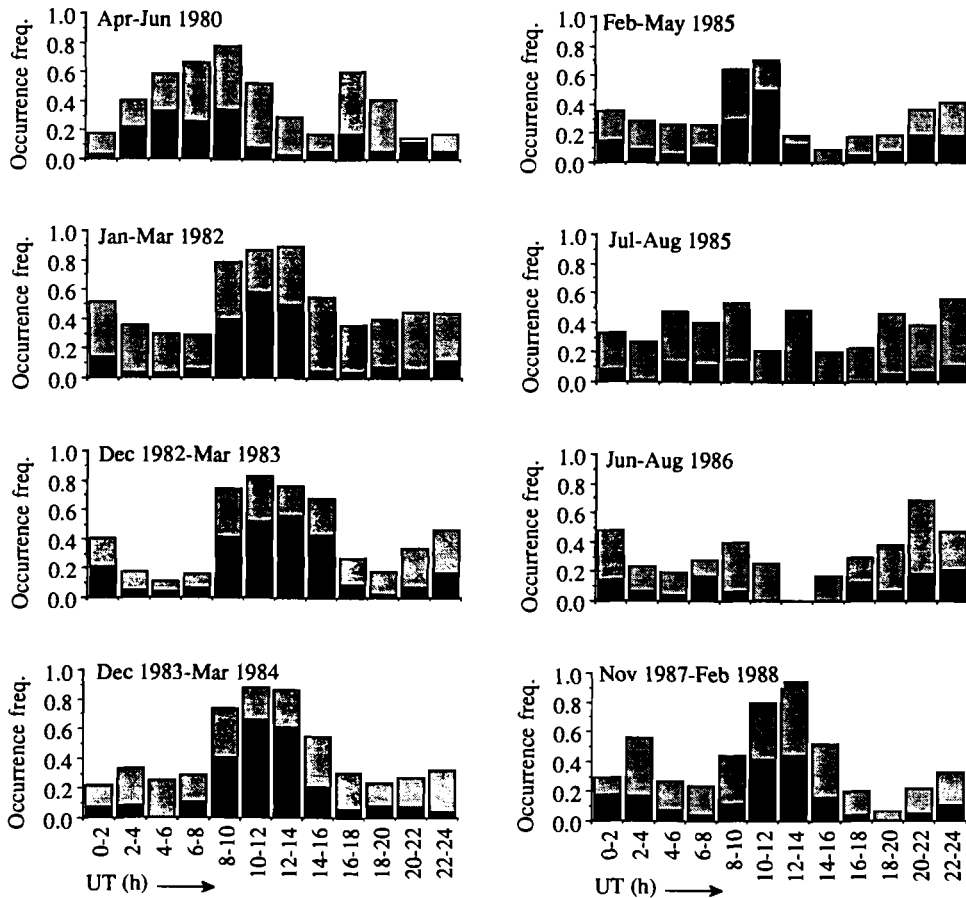


Figure 1. Frequencies of occurrence versus universal time for eight periods of observation. Black: MSTIDs with  $\text{SNR} > 4$ ; grey:  $1 < \text{SNR} < 4$ .

Figure 2 shows the monthly mean values that we observed over the years. The largest amplitudes were found between 1982 and the beginning of 1984, somewhat later than the solar cycle maximum (1980-1981). It is well known that the electron density in the ionosphere shows large variations in the course of a solar cycle, which are partly about 2 years out of phase with respect to the sunspot number cycle. No evidence for possible recurrence of trends from one solar rotation interval to another has been found.

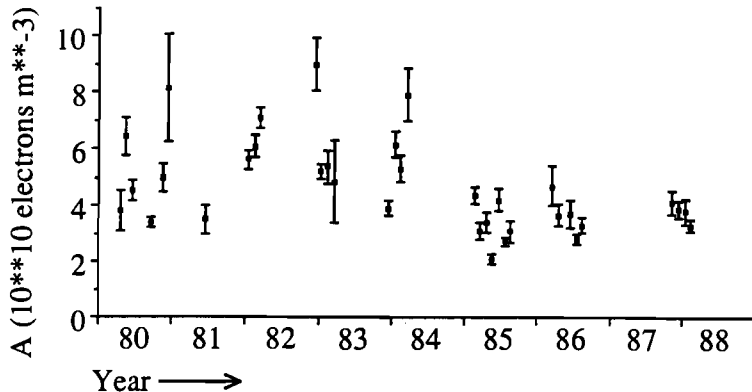


Figure 2. Mean monthly amplitude, A, of MSTIDs (in  $10^{10}$  electrons/m<sup>3</sup>) for all available months in the database.

### 3. THE APPARENT PERIOD OF THE MSTIDs

The daily variation in the apparent period of MSTIDs is shown in Figure 3a. The daily variation of the Brunt-Väisälä period, which is no more than about 2 min, cannot explain the variation in Figure 4a. Note that many of the apparent periods are well below the Brunt-Väisälä period (12-16 min). The daily variation may be caused by either Doppler shifting or filtering (critical coupling and reflection) of the gravity wave spectrum by the neutral background wind. At thermospheric heights this wind rotates 360° clockwise in 24 h. It is equatorward at night and poleward at noon.

Doppler shifting by the background wind explains the observed variation in the apparent period if one also assumes that gravity waves propagate equatorward on the average. The assumption of equatorward propagation is corroborated by some experimental evidence.

Critical coupling would remove those waves from the spectrum whose phase velocity is smaller than the component of the neutral wind in the direction of the phase velocity, and therefore it reduces the average period (waves with the same horizontal wavelength but larger periods have smaller phase velocities and are more easily filtered). On the other hand waves with phase velocities antiparallel to the neutral wind may encounter a reflection level and this happens first with waves with small periods (fixed horizontal wavelength), so reflection increases the average period. Waves with phase velocities perpendicular to the neutral wind can propagate freely. Thus, filtering can, in combination with the assumption of average equatorward propagation, explain the observed daily variation in the apparent period as well as Doppler shifting.

The above reasoning may be tested by considering different lines-of-sight. A radio interferometer is most sensitive to observe waves with a horizontal component of the phase velocity that is parallel to the horizontal component of the line-of-sight from the observer towards the radio source. So with an eastward (westward) line-of-sight one will most likely observe waves with a phase velocity with an eastward (westward) component of the phase velocity. Taken into account the rotating neutral wind one expects to observe smaller periods with westward lines-of-sight than with eastward lines-of-sight in the morning and smaller periods with eastward lines-of-sight than with westward lines-of-sight in the afternoon. In Figures 3b-c we present the daily variation in the apparent period for observations with the

line-of-sight in the quadrant around east resp. west. The results agree with the hypothesis of the effect of the neutral wind we just sketched briefly. For eastward lines-of-sight the morning maximum is largest while for westward lines-of-sight the afternoon maximum is largest. We must note, however, that on the basis of our data no choice can be made in favour of either the Doppler shifting or the filtering hypothesis.

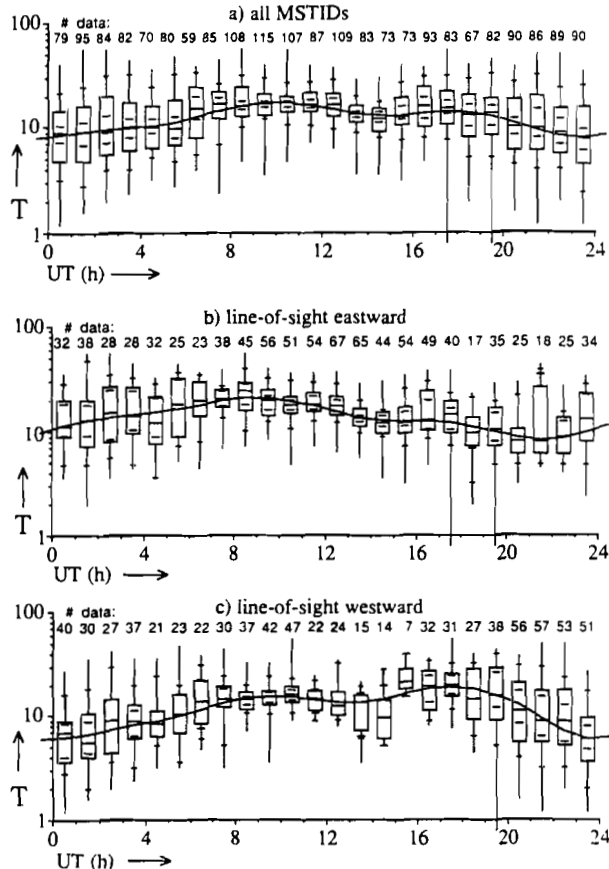


Figure 3. Daily variation of the apparent period,  $T$ , of MSTIDs (in min) by means of boxplots for a) all observations, b) all observations with eastward lines-of-sight, c) all observations with westward lines-of-sight. The solid lines give the fitted sum of a constant background and 24-h, 12-h and 8-h harmonics to the hourly medians.

## ACKNOWLEDGEMENTS

The Westerbork Synthesis Radio Telescope is operated by the Netherlands Foundation for Research in Astronomy with financial support from the Netherlands Organization for Scientific Research (NWO). P.F.J. van Velthoven has partly been supported by the Netherlands Organization for Scientific Research (NWO).

## REFERENCES

- Kelder, H., Spoelstra, T.A.Th. (1987) J.Atmos.Terr.Phys. 49, 7  
 Spoelstra, T.A.T., Kelder, H. (1984) Radio Sci. 19, 779  
 Van Velthoven, P.F.J. (1990) Ph.D. thesis, Eindhoven University of Technology

## THE PHYSICAL COMPOSITION OF THE OSCILLATION SPECTRUM OF TOTAL ELECTRON CONTENT IN THE IONOSPHERE

E.L. AFRAIMOVICH, O.N. BOITMAN, V.N. ZVEZDIN, N.P. MINKO,  
S.V. FRIDMAN  
SibIZMIR,  
Irkutsk 33, P.O. Box 4026, 664033 Russia

**ABSTRACT.** On the basis of complex measurements, made in Irkutsk, of Faraday rotation, angles of arrival and of the UHF signal amplitude from the geostationary ETS-2 satellite, a classification of the components of the total electron content (TEC) spectrum according to their origin is carried out. The following physical components of the spectrum in the range of periods from a few minutes to several days have been revealed:

- 1) Diurnal variations caused by the Earth's rotation.
- 2) Travelling ionospheric disturbances (TID) produced by acoustic-gravity and internal gravity waves. The range of 10-30 min periods is characteristic for this component, and a similarity of the TEC spectra, angles of arrival and of the signal amplitude is observed. The phase velocity estimated by comparing the spectra of these values is hundreds of meters per second and depends on the frequency.
- 3) A component which seems to be associated with short-period oscillations of the solar UV radiation. This component has a period of 10-30 min and can persist during several days. Unlike the TID's, this component does virtually not manifest itself in the angle-of-arrival variations.
- 4) A component associated with magnetic Pc5 and Pc6 pulsations has a period larger than or about 10 min and takes effect in periods of high geomagnetic activity only in TEC variations.
- 5) Frozen-in irregularities drifting together with the background plasma. Their period is less than 10 min. For this component, the ratio of spectra of angles of arrival to TEC and of the amplitude to TEC is proportional, respectively, to the frequency and to the frequency squared. The phase velocity of these disturbances does not depend on the frequency.

The above classification of the components of the TEC oscillation spectrum may be useful when interpreting results of distortion estimations of transionospheric signals in navigation systems and in radio astronomical interferometers with different baselines as well as for methods to correct for them.



# EVALUATION OF TOTAL ELECTRON CONTENT FROM SIGNALS OF POLAR ORBITING SATELLITES

P.F.J. VAN VELTHOVEN

Centre de Recherche en Physique de l'Environnement  
4 Av. de Neptune, 94107 Saint Maur, France

**ABSTRACT.** The total electron content (TEC) along the line-of-sight between a ground-based receiver and a transmitter on board of a polar orbiting satellite can be evaluated from the differential Doppler shift between the signals at two different frequencies. For NSSS-satellite signals the initial differential Doppler shift is not known: it has to be evaluated in a fitting procedure together with the parameters that describe the spatial dependence of TEC. Several evaluation schemes have been tested using observations from three sites located on an east-west line in France at mutual distances of 109 and 285 km. It is found that in practice all schemes introduce large errors in the evaluation of the TEC coefficients. This is due to our ignorance of the initial differential Doppler phase and the collinearity of the functions that are fitted.

## 1. MEASUREMENT TECHNIQUE

The differential Doppler technique uses the fact that the phase shift of radio signals due to ionospheric refraction is inversely proportional to their frequency. The phases  $\phi_1$  and  $\phi_2$  of two signals at frequencies  $m_1 f$  and  $m_2 f$  (multiples of the basic frequency  $f$ ) are measured simultaneously. The weighted phase difference  $\Delta\phi = \phi_1/m_1 - \phi_2/m_2$  only depends upon its initial value and the slant total electron content  $S$  along the path from satellite to receiver:  $\Delta\phi(t) = \Delta\phi(0) + C.S$ . It does not depend upon the geometrical distance between the satellite and the receiver and it is not affected by tropospheric refraction.  $C$  is an instrumental constant.

Several schemes for the evaluation of the vertical total electron content  $V$  from the differential Doppler phases, recorded at times  $t_j$  during a satellite pass, were suggested by Leitinger and Putz (1978). If we make the assumptions that the vertical total electron content  $V$  only depends on latitude  $\beta$ , and that the zenith angle  $Z_j$  of the line-of-sight from the satellite to the receiver in the ionosphere is constant at a particular instant  $j$ , the following two generalized evaluation schemes can be proposed:

$$\Delta\phi(t_j) = \Delta\phi(0) + C \frac{1}{\cos(Z_j)} \left[ \sum_{n=0}^N \frac{V^{(n)}(\beta_j - \beta_o)^n}{n!} + \varepsilon_j \right] \quad (1)$$

$$\Delta\phi(t_j) = \Delta\phi(0) + C \left[ \frac{1}{\cos(Z_j)} \sum_{n=0}^N \frac{V^{(n)}(\beta_j - \beta_o)^n}{n!} + \varepsilon_j \right] \quad (2)$$

Here the  $\varepsilon_j$  are the errors which will be minimalized. The  $V^{(n)}$  are the unknown coefficients in the expansion of the vertical TEC in powers of the difference between the latitude of the

subionospheric point of the line-of-sight at instant  $j$ ,  $\beta_j$ , and the latitude of the observer,  $\beta_0$ .  $C$  is a constant. The number of terms in the series,  $N$ , has to be chosen. For a mean ionosphere height of 350 km the zenith angle  $Z_j$  varies from 0 to about  $71^\circ$  for a satellite passing from local zenith to the horizon. Hence the inverse of its cosine can vary from 1 to about 3. Note that the "mean" ionosphere height at which  $Z_j$  and  $\beta_j$  are evaluated also has to be chosen.

The two evaluation schemes only differ in the way the errors are supposed to affect the differential Doppler phase. A least squares procedure is used in each case to minimize their sum and thereby to evaluate the unknown  $\Delta\phi(0)$  and the  $N+1$  unknown TEC coefficients  $V^{(n)}$ . More sophisticated evaluation schemes taking into account the longitudinal dependence of the TEC and the variation of the zenith angle of the line-of-sight in the ionosphere are given in Van Velthoven (1990).

## 2. OBSERVATIONS

From 10 to 30 November 1987 during a joint Dutch-French campaign the differential Doppler shift measurements of satellites of the Navy Navigation Satellite System (NNSS) have been done. The NNSS-satellites have orbits that are approximately north-south, and the duration of a pass is less than 20 minutes. During such a time-interval the vertical total electron content is not liable to change much, unless the observation coincides with sunrise or sunset. Therefore, it should in principle be possible to determine the latitudinal variation of vertical total electron content at a fixed time and longitude from the differential Doppler phase recorded by a receiver during a satellite pass.

During the campaign three receivers were located in France at approximately the same latitude: at Tours ( $47^\circ$  N,  $1^\circ$  E), Nançay ( $47^\circ$  N,  $2^\circ$  E) and Besançon ( $47^\circ$  N,  $6^\circ$  E). Their longitudinal distances were 109 km (Tours-Nançay) and 285 km (Nançay-Besançon). For a mean ionosphere height of about 350 km these distances correspond to distances of about 75 km and 195 km in the ionosphere. Thus three, almost parallel, latitudinal profiles of TEC were observed. During the campaign 109 satellite passes were recorded at at least two of the stations. The latitudinal TEC profile for the passes was initially evaluated using the two schemes given above. Firstly the mean ionosphere height was chosen at 350 km and the series were truncated after  $N=1$ .

In figure 1 the values obtained for the vertical TEC at  $47^\circ$  N for the stations are compared.  $47^\circ$  N differs from the latitudes of the stations by less than  $0.4^\circ$ , so the calculated values of TEC are about equal to the values of TEC at the points of closest approach of the satellite. Values for two stations differ less than 10 % in most cases, although there are some points for which the difference is considerably larger. Such large differences cannot be explained as being due to longitudinal gradients in the TEC, since except during the time intervals of about an hour around sunset and sunrise, such large longitudinal gradients in TEC do not occur. The deviating points in figure 1 do not refer systematically to the same universal time. Neither can an explanation be provided by the approximation of the ionosphere by a spherical shell of vanishing thickness, since errors due to this approximation can be estimated to amount to no more than about 10 % (Van Velthoven, 1990). If TEC values at another latitude are compared similar differences are found. The errors in the evaluated TECs might have the following causes:

- the way in which the errors are chosen in the evaluation scheme may introduce errors in the TEC coefficients evaluated by a least squares method.
- the value for the mean ionosphere height used in the evaluation scheme ( $h_{ion}=350$  km) may differ from the actual value.
- the order of the polynomial that describes the latitudinal behaviour of TEC,  $N$ , may not have been chosen optimally.

Figure 2 shows that the difference between TEC-values obtained with the help of evaluation scheme 1 and scheme 2 are negligible. We conclude that the obtained results for the TEC are relatively insensitive to the way the errors are chosen in an evaluation scheme.

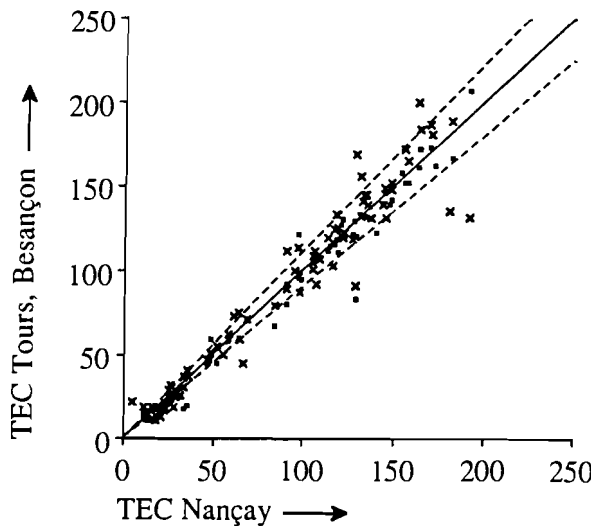


Figure 1. Comparison of the total electron content (TEC) values at 47° N, found from differential Doppler shift observations at Tours (crosses) and Besançon (squares), with those found from observations at Nançay. Evaluation scheme 1 was used with  $N=1$ . The solid line indicates equal values and the dashed lines 10 % deviation between two stations. Units are  $10^{15}$  electrons  $m^{-2}$ .

Calculations show that the differences, introduced by changing the assumed mean ionosphere height, for example from 350 to 400 km, amount to less than 10 % in most cases. The obtained results for the TEC are thus quite insensitive to changes of the mean ionosphere height. However, when we compare results, obtained by representing the latitudinal behaviour by a polynomial of first resp. third order, large differences are found (Figure 3).

### 3. DISCUSSION

Above we showed that the particular choice of functions fitted to the data is the main cause of the errors in the evaluated TECs. The problem can not be resolved by choosing a polynomial of higher order. If we examine the TEC evaluation schemes (1-2), it is clear that determination of both the phase constant  $\Delta\phi(0)$  and an arbitrary latitudinal TEC profile, which can be represented by an infinite power series in the latitude, is impossible, because the cosine can also be represented by a power series in the latitude. The functions used in the least squares fit are collinear. Accurate values of TEC can still be obtained if the coefficients  $V^{(n)}$  tend to zero sufficiently fast with increasing  $n$ . In the mid-latitude domain, characterized by a strong decrease in the total electron content, from its large value in the equatorial region to its small value at high latitudes, this is not the case. TIDs, which are considered to be noise in the TEC evaluation procedure, will further deteriorate the results.

The collinearity can only be removed by combining observations from stations located at approximately the same longitude but different latitudes. Leitinger et al. (1978) have given evaluation schemes for such two station configurations.

### ACKNOWLEDGMENTS

This research was supported by the Netherlands Organisation for Scientific Research.

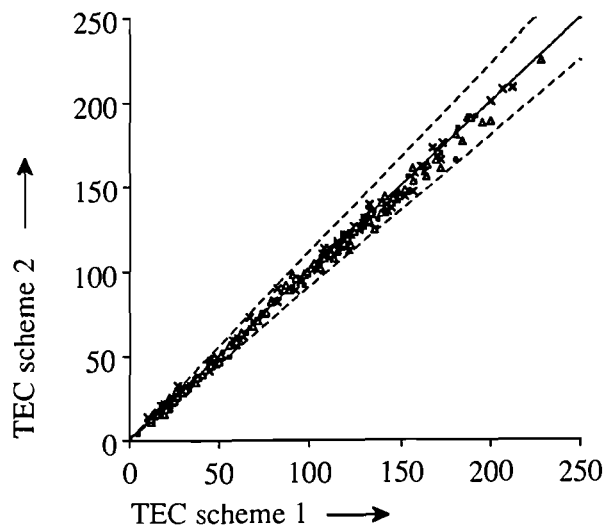


Figure 2. Comparison of TEC values at  $47^\circ$  N evaluated using scheme 1 resp. 2. A mean ionosphere height  $h_{\text{ion}} = 350$  km was assumed and  $N$  was chosen 1 (linear latitudinal dependence). Crosses indicate the TEC from differential Doppler shift observations at Tours, squares that from observations at Nançay, and triangles that from observations at Besançon.

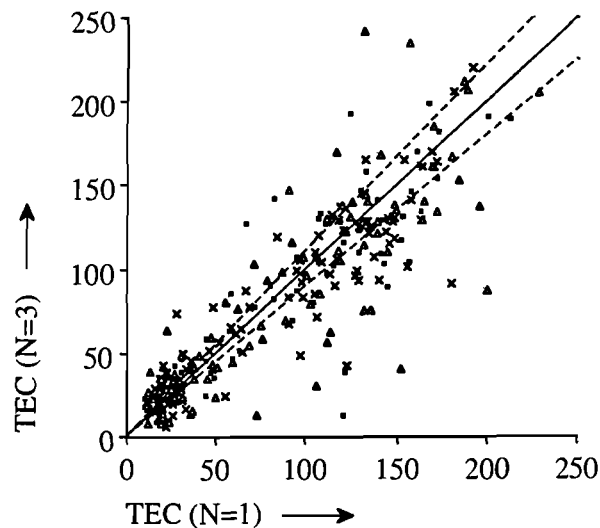


Figure 3. Same as Figure 2, except that all values were evaluated with the same scheme (1) but with different  $N$ : along the vertical axis with  $N=3$ , along the horizontal axis with  $N=1$ .

## REFERENCES

- Van Velthoven, P.F.J. (1990) Ph.D. thesis, Eindhoven University of Technology.
- Van Velthoven, P.F.J., Mercier C., Kelder H.(1990) J.Atmos. Terr.Phys. 48, 245.
- Leitinger, R., Putz, E. (1978), Technical Report of the Institute of Meteorology and Geophysics of the University of Graz.

## MODELLING OF THE IONOSPHERE OVER NORTH AND SOUTH CHINA FOR A SUNSPOT CYCLE

HUANG TIANXI, HE JIN, LIU XUANMOU

Department of Space Physics,

Wuhan University, China

**ABSTRACT.** Ionospheric data observed at four stations in South China for a sunspot cycle from 1964 to 1976 have been used to draw up the ionospheric behaviour pattern and to examine the similarity and diversity of the ionosphere over South China compared with the ionospheric features observed at five stations in North China. Results show that the ionospheric over North China belongs to a typical mid-latitude one, similar to other longitude sectors like Japan and Middle Asia, however the ionosphere over the South China has its own characteristics and there is some distinction between both sides of the crest zone of the ionospheric equatorial anomaly, i.e. 25°N latitude line in East Asia.

# THE REFRACTION OF ELECTROMAGNETIC WAVES FOR A MAGNETOPLASMA SLAB

Y. YAN

Xidian University, P.O. Box 273,  
710071 Xi'an, China

**ABSTRACT.** The refraction of electromagnetic waves in the ionosphere is investigated. The model is the S-polarized electromagnetic wave propagation for a homogeneous, collisional, magnetoplasma slab. This is due to the fact that the signals in geodesy cross the ionosphere and that their accuracy is essentially limited by refraction effects. The expressions for the transmission of a wave incident on the ionosphere in the presence of a uniform static magnetic field are derived. The modulating wave crossing the ionosphere is also simulated with the Monte Carlo method.

## 1. INTRODUCTION

The characteristics of the electromagnetic wave propagation for a magnetoplasma slab have been of theoretical and practical interest for the past several decades. During these past studies both deterministic periodic and random functions have been used as mathematical models for plasma diagnostic, reentrancy communication, signal interrupt and distortion. Since the natural ionosphere is a magneto-ionic medium, we model the ionosphere by a ranged magnetoplasma slab. The frequency characteristics of the refraction of electromagnetic wave propagation for a homogeneous, collisional, magnetoplasma slab are investigated.

In problems of refraction of electromagnetic waves in a magnetoplasma, its dielectric characteristics are anisotropic. Previous work in the area of wave refraction in a magnetoplasma includes the reflection and transmission of wave propagation for unrange and semi-unrange magnetoplasma. In this paper, we model magnetoplasma by a cryogenic, homogeneous and stationary magnetic field, and ignore the effect of space chromatic dispersion, so that the equations can be linearized.

## 2. PROBLEM FORMULATION

For the physical model considered in this paper, it is assumed that the plasma under consideration satisfies the following assumptions: The background is free-space and the effect of space chromatic dispersion and the movement of the ions can be ignored. The direction cosines of the applied magnetic field  $B$  and wave vector of the incident wave are  $(-1, -m, -k)$  and  $(\sin a, 0, \cos a)$ , respectively. On the basis of these assumptions, the equation of electron motion in the plasma can then be written as

$$e\vec{E} + e\vec{V} \times \vec{B} = m\vec{dV}/dt + mu\vec{V} \quad (1)$$

where  $e$  is the electron charge,  $m$  the electron mass,  $u$  the collision frequency and  $\bar{V}$  the electron velocity. Let us express the electric polarization  $P$  in the electron density  $N$ :

$$\partial \bar{P} / \partial t = N \bar{e} \bar{r} \quad (2)$$

where  $\bar{r}$  is the average displacement of an electron.

Maxwell's equations can be written as:

$$\nabla \times \bar{E} = -\partial \bar{B} / \partial t \quad (3)$$

$$\nabla \times \bar{H} = \partial \bar{D} / \partial t + \bar{J} \quad (4)$$

where  $E$  is the electric field intensity,  $D$  the electric flux density, and  $J$  the conduction current density.

From Fresnel's law and equations (1) - (4), the waves in the plasma can be described. Considering the boundary conditions, the transmission coefficients can be given as (with a vertical applied magnetic field)

$$t_{II} = \frac{1}{A} \left( \frac{(1 + A_1)Q_1 - (1 + A_2)}{w_{11}} - \frac{(1 - A_1)Q_2 - (1 - A_2)}{w_{22}} \right) \quad (5)$$

$$t_{\perp} = \frac{\cos a}{A} \left( \frac{(1 + A_1)P_1 - (1 + A_2)}{w_{11}} - \frac{(1 - A_1)P_2 - (1 - A_2)}{w_{22}} \right) \quad (6)$$

and (horizontal applied magnetic field)

$$t = \frac{4n_2 \exp(-ik_0 n_2 d) \exp(ik_0 d)}{(n_2 + 1)^2 - (1 - n_2)^2 \exp(-2ik_0 n_2 d)} \quad (7)$$

where,  $k_0$  is the propagation constant,  $d$  is the thickness of the plasma and the index of refraction  $n_2$  can be obtained from the equation of chromatic dispersion.

$A = \exp(-ik_0 d \cos a)$ ,  $A_1 = 1 / \exp(-ik_0 d n_3)$ ,  $A_2 = 1 / \exp(-ik_0 d n_4)$ ,  $n_3, n_4$  are the indices of refraction which correspond with a downward travelling wave.  $Q_1, Q_2, P_1, P_2, W_{11}$  and  $W_{22}$  are the solutions of matrix equation.

### 3. MONTE CARLO METHOD

In this section, we calculate the refraction of an electromagnetic wave crossing a magnetoplasma. For the ionosphere we consider a magnetic field, and discuss the propagation of a modulating wave through the ionosphere.

On the basis of forward scattering the complex amplitude  $U$  satisfies the equation

$$U - 2i \langle k(z) \rangle \frac{\partial U}{\partial z} - \langle k^2(z) \rangle \frac{(\Delta Ne / \langle Ne \rangle)(w_p^2 / w^2)}{(1 - w_p^2 / w^2)} U = 0 \quad (8)$$

where  $\langle k(z) \rangle$  is the statistical mean of the propagation constant,  $w_p$  is the plasma frequency and  $w$  is the angular frequency of signal. Consider a modulating wave

$$s(t) = \operatorname{Re}(m(t) \exp(iw_0 t)) \quad (9)$$

where  $m(t)$  is the modulating waveform,  $w_0$  is the angular frequency of the carrier wave. If the envelope waveform is a delta wave

$$m(t) = \begin{cases} 1 - \frac{|t|}{T}, & |t| \leq T \\ 0, & |t| > T \end{cases} \quad (10)$$

$T$  is the pulse duration of the delta wave, we have simulated the refraction wave with the Monte Carlo method. The result is shown in figure 1. It can be seen that the influence of the ionosphere on the signal cross is of more significance.

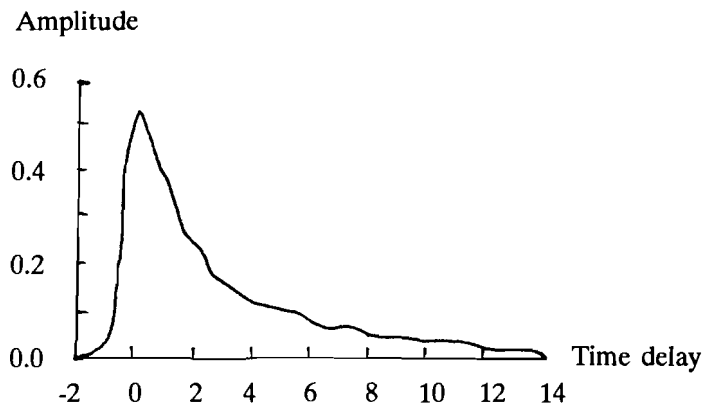


Figure 1. Envelope waveform of statistical processing.

## ACKNOWLEDGMENTS

This research was partially supported by a grant from X. Song.

## REFERENCES

- Chang, H. et al (1986), *IEEE Trans. Microwave Techniques MTT-34*, p. 32
- Lee, J.J. (1979), *IEEE Trans. Antennas Propag. Ap-27*, p. 880
- Singh, Y.P. et al (1983), *Acta Physica Hungarica*, p. 101

# DEVIATION OF RAY TRAJECTORIES IN REFRACTIVE MEDIA UNDER THE INFLUENCE OF RANDOM INHOMOGENEITIES

S.M. GOLYNSKI, V.D. GUSEV  
 Physics Faculty, Moscow State University,  
 119899 Moscow GSP, Russia

**ABSTRACT.** We define most probable paths of rays in stratified media with random isotropic inhomogeneities by means of the diffusion markovian approximation. The model of a parabolic layer with constant diffusion coefficient is considered. A discussion is given on the deviations of the most probable exit angle and the horizontal displacement of the exit point upon the upper boundary of the layer in question as compared with the corresponding parameters of the undisturbed trajectory described by Snell's law.

## 1. INTRODUCTION

The most probable (m.p.) path of a random diffusion process defines the trajectory of the process m.p. realizations by analogy of the m.p. meaning of a random variable which defines the maximum of a probability distribution. There is much literature on the problem of calculating the m.p. paths for an m-dimensional continuous markovian process  $x(t) = \{x^\mu(t)\}$  ( $\mu = 0, 1, \dots, m-1; t \geq 0$ ) [1 - 4]. In these papers the probability of the process  $x(t)$  transition from an initial state  $x_i = x(t_i)$  to a final state  $x_f = x(t_f)$  ( $t_f > t_i$ ) is represented in the form of the path integral along all possible trajectories

$$P \left\{ x_f, \frac{t_f}{x_i}, t_i \right\} dx_f = \int \int D\{x(t)\} \exp [-S(\{x(t)\})], \quad (1)$$

$$S(\{x(t)\}) = \int_{t_i}^{t_f} L[x(t), \dot{x}(t)] dt, \quad (2)$$

where  $D\{x(t)\}$  is the invariant measure providing the corresponding normalization of the transition probability;  $S(\{x(t)\})$  is the action functional, which extremum describes the m.p. trajectory of the process.

The transition probability (1) is the Green function of the nonlinear Fokker-Planck equation (FPE) for the probability density  $P(x, t)$  (summation over repeated indices is always applied)

$$\frac{\partial}{\partial t} P(x, t) = - \frac{\partial}{\partial x^\mu} [C^\mu(x) P(x, t)] + \frac{1}{2} \frac{\partial}{\partial x^\mu} \frac{\partial}{\partial x^\nu} [C^{\mu\nu}(x) P(x, t)] \quad (3)$$

The FPE convention  $C^\mu(x)$  and local dispersion  $C^{\mu\nu}(x)$  coefficients define the integrand of the action functional (2), which is usually named the Onsager-Machlup lagrangian (OML)

$$L(x, \dot{x}) = \frac{1}{2} C_{\mu\nu} (\dot{x}^\mu - \alpha^\mu)(\dot{x}^\nu - \alpha^\nu) + \frac{1}{2} \sqrt{C} \frac{\partial}{\partial x^\mu} \left( \frac{\alpha^\mu}{\sqrt{C}} \right) + \frac{1}{8} R \quad (4)$$

where  $C_{\mu\nu}$  are the components of the matrix reversed to the matrix of the FPE dispersion coefficient;  $C = \|C_{\mu\nu}\|$ ;  $R$  is the scalar curvature [5];

$$\alpha^\mu = C^\mu - \frac{1}{2} \sqrt{C} \frac{\partial}{\partial x^\nu} \left( \frac{C^{\mu\nu}}{\sqrt{C}} \right); \quad \dot{x}^\mu = \frac{dx^\mu}{dt}$$

The OML is invariant with respect to arbitrary nonlinear coordinate transformations. Thus the m.p. path of the process does not depend on the choice of the variables.

We make use of the results [1 - 4] for the definition of the ray m.p. path in the case of oblique wave propagation in randomly stratified magneto-ionic media.

## 2. LAGRANGIAN FOR THE RAY MOST PROBABLE PATH

Ray statistics in randomly stratified media can be described by means of the diffusion markovian approximation under specific conditions [6]. If scattering inhomogeneities are isotropic the corresponding FPE has the form

$$\frac{\partial P(\theta, \gamma, \sigma)}{\partial \sigma} = \frac{1}{n} \frac{dn}{dz} \frac{\partial}{\partial \theta} \{ \sin \theta P \} - \frac{D}{n^2} \frac{\partial}{\partial \theta} \{ \operatorname{ctg} \theta P \} + \frac{D}{n^2} \frac{\partial^2 P}{\partial \theta^2} + \frac{D}{n^2 \sin^2 \theta} \frac{\partial^2 P}{\partial \varphi^2} \quad (5)$$

Here  $P(\theta, \varphi, \sigma)$  is the probability density that, after having propagated over a distance  $\sigma$ , the ray has the direction defined by the polar and azimuthal angles  $\theta$  and  $\varphi$ ;  $\theta_0$  and  $\varphi_0$  are the initial angles of incidence;  $n = n(z)$  is the regular part of the refractive index of the medium;  $D$  is the diffusion coefficient of the ray ( $D = \sqrt{\pi} \langle n_1^2 \rangle / a$  when the correlation function of scattering inhomogeneities is gaussian);  $\langle n_1^2 \rangle$  is the variance of the fluctuations of the refractive index and  $a$  is the typical scale of the inhomogeneities of the medium.

In our problem the distance along the ray trajectory  $\sigma$  plays the role of an independent variable analogue to  $t$  in (3). Substituting the FPE (5) coefficients into (4) and taking into account  $R = -4D/n^2$  for the case considered we obtain the OML

$$L(\theta_p, \dot{\theta}_p, \varphi_p, \dot{\varphi}_p) = \frac{n^2}{4D} \left[ \dot{\theta}_p + \frac{1}{n} \frac{dn}{dz} \sin \theta_p \right]^2 - \frac{1}{n} \frac{dn}{dz} \cos \theta_p + \frac{n^2 \sin^2 \theta_p}{4D} (\dot{\varphi}_p)^2 - \frac{D}{2n^2} \quad (6)$$

Where  $\theta_p(\sigma)$  and  $\varphi_p(\sigma)$  are the m.p. values of the polar and azimuth angles by which the m.p. path of rays is defined.

The Lagrange-Euler equations corresponding to (6) have the following form ( $d\delta = dz \cos \theta_p$ )

$$\ddot{\theta}_p - \operatorname{tg} \theta_p (\dot{\theta}_p')^2 + \left( \frac{2n'}{n} - \frac{D'}{D} \right) \dot{\theta}_p' + \left( \frac{n'}{n} - \frac{D'n'}{Dn} \right) \operatorname{tg} \theta_p = \frac{2Dn'}{n^3} \frac{\sin \theta_p}{\cos^2 \theta_p}, \quad (7)$$

$$\ddot{\varphi}_p + \left[ (2 \operatorname{ctg} \theta_p - \operatorname{tg} \theta_p) \dot{\varphi}_p' + \left( \frac{2n'}{n} - \frac{D'}{D} \right) \right] \dot{\varphi}_p' = 0, \quad (8)$$

where the prime denotes the differentiation with respect to  $z$ .

We make (7) and (8) complete by adding the initial conditions on the lower boundary of the scattering layer (the conditions for  $\theta_p'$  and  $\varphi_p'$  are imposed according to definition of the m.p. path of the infinitely small transition [7])

$$\theta_p(z=0) = \theta_0, \quad \theta_p'(z=0) = -\frac{n}{n'} \operatorname{tg} \theta_p, \quad \varphi_p'(z=0) = \varphi_0, \quad \varphi_p'(z=0) = 0. \quad (9)$$

Taking into account (9) we obtain the solution of (8), viz.  $\varphi(z) = \varphi_0$ , which is obvious as the result of the problem symmetry.

To investigate the law of reflection in the scattering stratified medium let us use a new variable  $y = n \sin \theta_p$  and in accordance with (7) and (9) investigate the equation

$$y'' - \left( \frac{D'}{D} \right) y' = \left( \frac{2Dn'}{n^2} \right) \frac{y}{\sqrt{n^2 - y^2}}, \quad y(z=0) = \sin \theta_0, \quad y'(z=0) = 0 \quad (10)$$

In the medium without scattering ( $D=0$ ) the solution of (10) leads to classical Snell law, which defines the ray unperturbed trajectory

$$n \sin \theta_p = \sin \theta_0. \quad (11)$$

In [8,9] the equation (10) was used to determine the m.p. paths of rays for the case of wave reflection from the refractive random layer. In this report we consider the case when waves pass through the layer without reflection.

### 3. THE INTEGRAL LAW OF REFRACTION

To solve (10) we make use of the perturbation method by expanding the function  $y = y(z)$  in successive powers of the small dimensionless parameter  $\gamma \sim \langle n_f^2 \rangle$

$$y(z) = s_0 \{ 1 + \gamma f_1(z) + \gamma^2 f_2(z) + \dots \},$$

where  $s_0 = \sin \theta_0$ .

For simplicity we consider here a model of the medium with  $D_0 = \text{Const}$ . Then according to (10) we have to first approximation

$$f_1(z) = \frac{2D_0}{s_0^2} \int_0^L \left[ \frac{\sqrt{n^2 - s_0^2}}{n} - c_0 \right] dz. \quad (12)$$

Here  $L$  is the width of the layer and  $c_0 = \cos \theta_0$ . In this approximation the integral law of refraction has the form

$$n \sin \theta_p \sim \sin \theta_0 \{ 1 + f_1(z) \} \quad (13)$$

As an example we consider the model of the parabolic layer

$$n^2 = 1 - 2\beta^2 \left( \frac{z}{z_m} \right) + \beta^2 \left( \frac{z}{z_m} \right)^2,$$

where  $\beta = f/f_c$ ;  $f$  is the frequency of the incident wave;  $f_c$  is the critical frequency of the layer and  $z_m$  is the half-width of the layer. The condition of transmission through the layer without reflection is defined by the inequality  $\beta < c_0$ . For this model the integral (12) can be solved analytically. For example, if  $L = 2z_m$ , we obtain for the ray m.p. exit angle

$$\sin \theta_p \sim \sin \theta_0 + \frac{4Dz_m}{s_0} \left\{ \beta^{-1} \left[ \frac{n_m^2 - s_0^2}{n_m} F(\mu, t) - n_m E(\mu, t) + \frac{\beta}{c_0} \right] - c_0 \right\},$$

$$n_m^2 = 1 - \beta^2, \quad \mu = \arcsin \left( \frac{\beta}{c_0} \right), \quad t = \frac{s_0}{n_m},$$

$F(\mu, t)$  and  $E(\mu, t)$  are the elliptic integrals of the first and the second order. So the integral law of reflection makes it possible to calculate deviations of the m.p. polar angle from the angle defined by (11). Bearing in mind (13) the horizontal displacement of the ray m.p. trajectory compared with the undisturbed one, can be determined by the formula (10):

$$x = \int_0^L \left[ \frac{y}{\sqrt{n^2 - y^2}} \right] dz \quad (14)$$

Analyzing (12) and (14) we conclude that the scattering in the direction  $\nabla n$  is less than in the opposite one. But in general we can have different cases ( $\theta_p > \theta_0$ , or  $\theta_p < \theta_0$ , i.e. the displacement can be in both directions), which depends on the relation between  $\theta_0$  and  $\beta$ . As usual we define the area of validity of (13) by the inequality  $|f_2| \ll |f_1|$ , which leads to the condition  $2Dz_m \ll c_0$ . It means that our results are not valid in the case of small incident angles.

The more detailed discussion about the deviations of the m.p. paths of rays from the undisturbed ones for different models of the medium and different relations between parameters is given in our report.

#### 4. CONCLUSION

It was shown that in the presence of random inhomogeneities in refractive magneto-ionic media as the ionosphere the ray m.p. trajectories have small deviations from the undisturbed ones. It seems reasonable to take them into account in high precision geodetic measurements by means of satellites.

#### REFERENCES

- Graham, R. (1977), *Z. Physik* **B26**, 281
- Dekker, H. (1981), *Phys. Rev.* **A24**, 3182
- Grabert, H., Graham, R., Green, M.S. (1980), *Phys. Rev.* **A21**, 2136
- Langouche, F., Roekaerts, D., Tirapegue, E. (1982), Functional integration and semiclassical expansion, D. Reidel Publishing Co., Dordrecht-Boston-London
- Weinberg, S. (1972), Gravitation and cosmology, Wiley, New York
- Golynski, S.M., Kampen van, N.G. (1984), *Phys. Lett.* **102A**, 220
- Dekker, H. (1980), *Phys. Lett.* **80A**, 99
- Golynski, S.M., Gusev, V.D. (1982), *Geomagnetizm i aeronomiya* **22**, 960
- Golynski, S.M., Gusev, V.D. (1984), *Geomagnetizm i aeronomiya* **24**, 52
- Ginzburg, V.L. (1961), Propagation of electromagnetic waves in plasma, Gordon & Breach, New York

## **5. GPS AND OTHER SATELLITE SYSTEMS**



## THE EFFECT OF THE IONOSPHERE AND TROPOSPHERE ON SATELLITE POSITIONING SYSTEMS

R.B. LANGLEY

Geodetic Research Laboratory, Department of Surveying Engineering,  
University of New Brunswick, Fredericton, N.B. E3B 5A3, Canada  
Voice: (506) 453-5142 Fax: (506) 453-4943 E-mail: lang@unb.ca

**ABSTRACT.** The range and range-rate measurements obtained from satellite positioning systems are biased by the refraction of the earth's atmosphere. For radiometric measurements, the effect is twofold. Radio waves emitted by satellites must first traverse the ionosphere where the refractive index differs from unity by an amount that is proportional to electron density and inversely proportional to the square of the carrier wave frequency. At the 1575.42 MHz frequency of the L1 signal emitted by the satellites of the Navstar Global Positioning System (GPS), for example, the measured range of a vertically propagating signal can be biased by the ionosphere by up to 30 metres or so. The non-ionized part of the earth's atmosphere also takes its toll on radio signals. The refractive index of the non-ionized atmosphere (primarily the troposphere but to a much lesser extent also the stratosphere) is governed by the density of the dry gases and water molecules therein. Below about 30 GHz, the non-ionized atmosphere is non-dispersive and so its effect on radio waves is independent of their frequency. Vertically propagating radio signals experience a propagation delay of roughly 2.3 metres. Systems using visible light waves, such as satellite laser ranging, are immune from ionospheric effects but have to contend with a dispersive troposphere. The density of electrons, atoms, and molecules in the atmosphere is both spatially and temporally variable. This variation makes the modelling of biases experienced by trans-atmospheric electromagnetic signals a challenging exercise. In this paper, I will review the attempts being made to understand and model the effects of the atmosphere on the signals of satellite positioning systems including GPS, GLONASS, the Navy Navigation Satellite System (also known as Navsat and Transit), Tsikada, Argos, COSPAS-SARSAT, and satellite laser ranging.



# THE GPS TECHNIQUE AND IONOSPHERIC RESEARCH IN THE GGRI

L. BÁNYAI, K. KOVÁCS

Geodetic and Geophysical Research Institute (GGRI),  
of the Hungarian Academy of Sciences (HAS),  
H-9401 Sopron, Csatkai u. 6-8, P.O. Box 5, Hungary

**ABSTRACT.** The principles of the ionospheric investigations by the traditional vertical sounding and by the satellite navigation systems are summarized. Estimating the accuracies of the DOPPLER and GPS navigation systems the P-code "ROGUE" type GPS receivers proved to be a very useful devices from ionospheric point of view. Based on the ionosonde measurements the vertical electron density can be monitored only up to the most dense layer (F2). Because the most variable regions are below the F2 layer, the simultaneous ionosonde and GPS observations can be used to estimate the electron density in the whole ionosphere.

## 1. INTRODUCTION

The application of the navigation satellite systems namely the DOPPLER NNSS and the GPS NAVSTAR is one of the areas where the geodetic and the geophysical investigations can complete each other.

The GGRI of the HAS, where each of the mentioned disciplines are present, makes such a useful cooperation possible. The investigations were started ten years ago based on the CMA-751 DOPPLER receiver, which was used for geodetic and ionospheric investigations in different international campaigns. Single station software for the determination of the electron content was also developed (Bencze et al 1986).

The recent developments in the Geophysical Observatory Nagycenk, where the installation of the KEL Aerospace IPS-42 IONOSONDE was started in 1991, as well as the presence of the GPS technique assure further possibilities.

## 2. IONOSPHERIC INVESTIGATIONS BY VERTICAL SOUNDING

The ionized part of the atmosphere which can be considered as a spherical shell around the Earth is called as ionosphere. The density of the free electrons is measured in electron/cm<sup>3</sup> or el m<sup>-3</sup> units. The vertical distribution of the electron density is shown in Figure 1 referring to the minimum and maximum of the sunspot cycle, where the different regions (D, E, F1, F2) are also indicated.

Beside the sunspot cycle, the electron concentration depends on many other factors, e.g. geographic and geomagnetic latitude and longitude, on local time (hour angle of the Sun) and seasons as well as on the solar and geomagnetic activity.

The most variable part is the so-called "subpeak" ionosphere below the F2 layer. The most intensive variations are related to periods of geomagnetic storms generated by solar flares.

The other changes in the F region are connected with anomalous diurnal and seasonal variations.

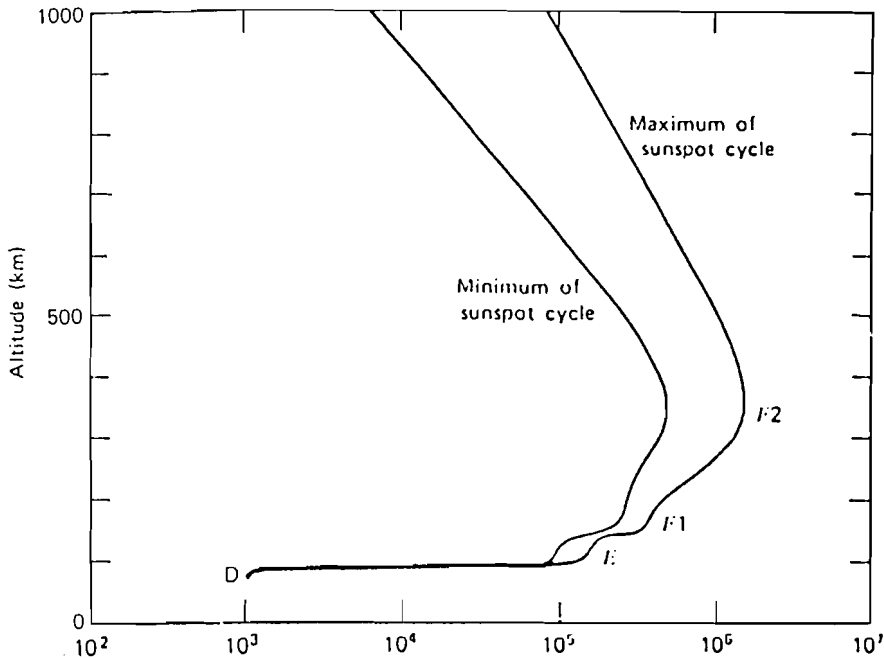


Figure 1. Vertical distribution of the electron density ( $\text{el cm}^{-3}$ )

The traditional vertical sounding is based on the reflectivity of the ionosphere depending on the frequency of the transmitted radio waves. If the travel time ( $dt$ ) of the vertical pulse (transmitted-reflected-received) can be measured, then the virtual height of the reflecting layer can be computed directly and the height can be estimated as

$$h' = c * dt/2 \quad \text{and} \quad h = \int \frac{v}{c} dh' = \int n dh'$$

where  $n$  is a refractivity index,  $c$  and  $v$  are the velocities of light and electromagnetic propagation respectively.

The reflection occurs where the refractive index is zero e.g. the transmitted frequency  $\omega$  equals the local plasma frequency. The plasma frequency being proportional to the  $N_e$  concentration of free electrons the functions  $N_e(h')$  and  $n(h', \omega)$  may be estimated. Since signals at those frequencies for which reflection by the most dense layer does not occur, travel through the ionosphere, this technique can be used only up to the F2 layer.

### 3. IONOSPHERIC INVESTIGATIONS BY SATELLITE NAVIGATION SYSTEMS

The geometry of the investigations with spherical earth and ionosphere approximations is given in Figure 2. The  $r_R$  and  $r_P$  distances referring to the ionospheric point can be found for different elevation angles in Table 1.

Disregarding the signal path bending and the horizontal gradient of the refractive index  $n$  the electromagnetically measured distance between the satellite and the receiver is biased by the ionospheric range error:

$$\Delta R = \int_0^s (n - 1) ds \approx \frac{1}{\cos E} \int_0^h (n_v - 1) dh$$

According to Hartman and Leitinger (1984) and introducing

$$\int_0^s N_e ds = I \text{ and } \int_0^h N_{ev} dh = I_v$$

as notation for the total and vertical electron content ( $\text{el m}^{-2}$ ), the components of  $\Delta R$  may be estimated.

Based on the so-called geometry-free linear combination (L4) the code and phase measurements may be written as

$$R_1 - R_2 = \Delta R_{i1} - \Delta R_{i2}$$

$$\Phi_1 - \Phi_2 + \Phi_{o1} - \Phi_{o2} = -(\Delta R_{o1} - \Delta R_{o2})$$

where all the systematic errors, except the ionospheric effects are already eliminated on the zero-difference level (Beutler et al., 1989). Taking the second order term of the refractive index (Hartman and Leitinger, 1984) and eliminating the phase ambiguities by the subtraction of epochs  $m$  and  $n$ , the total electron content can be estimated from satellite measurements as

$$I_n = C(R_{1n} - R_{2n})$$

$$\Delta I_{mn} = -C[(\Phi_{1m} - \Phi_{1n}) - (\Phi_{2m} - \Phi_{2n})]$$

where  $C = \frac{f_1^2 * f_2^2}{f_1^2 - f_2^2} * 40.3^{-1}$  is a constant value.

Based on these equations and the precision estimates of different receiver types, the accuracy of the total electron content and its change are estimated in Table 2.

TABLE 1

$$\begin{aligned} R_{\text{earth}} &\approx 6371 \quad h_{\text{mean}} \approx 400 \\ H_{\text{min.}} &\approx 100 \quad h_{\text{max.}} \approx 1000 \text{ km} \end{aligned}$$

E (deg.)	$r_R$ (km)	$r_p$ (km)
15	1073	1711
30	603	1116
45	366	717
60	215	432
75	101	207
89	7	13

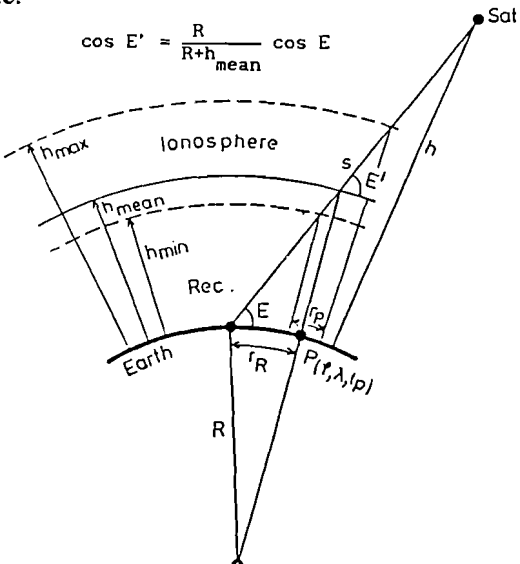


Figure 2. Spherical geometry of the ionospheric investigations

TABLE 2

Comparison of different receiver performance for ionospheric investigation (not the vertical electron contents  $\sigma_{\text{lv}}$  are estimated !)

Receiver types	$\sigma_{\text{P1}}$	$\sigma_{\text{P2}}$	$\sigma_{\Phi 1}$	$\sigma_{\Phi 2}$	$\sigma_{\text{In}} [\text{el m}^{-2}]$	$\sigma_{\Delta \text{Imn}} [\text{el m}^{-2}]$
DOPPLER	--	--	15 cm	15 cm	--	$1.9 \cdot 10^{14}$
Squaring GPS P-code GPS	-- 30 cm	-- 30 cm	2 mm 2 mm	9 mm 3 mm	-- $4.0 \cdot 10^{16}$	$1.2 \cdot 10^{15}$ $4.9 \cdot 10^{14}$
P-code ROGUE* Non-code ROGUE*	9 mm 6 cm	12 mm 20 cm	0.4 mm 0.3 mm	0.6 mm 10 mm	$1.4 \cdot 10^{15}$ $2.0 \cdot 10^{16}$	$9.7 \cdot 10^{13}$ $1.3 \cdot 10^{15}$

\*  $\sigma_p$  is system noise for  $T = 5$  min and  $\sigma_\phi$  is a system noise for  $T = 1$  sec

#### 4. CONCLUSIONS

According to Table 2 the P-code "ROGUE" type GPS receivers are preferable for ionospheric investigations.

The vertical electron content can be computed only up to the F2 layer from the ionosonde measurements. Fortunately this is the most variable region, therefore from the simultaneous observations the distribution over F2 can also be investigated, which depend on the proper separation of the ionosonde and GPS stations as well as on the satellite configuration.

In the future, based on the proposed IONOSONDE - GPS experiment, we would like to develop a "quasi real-time model" which on the one hand could improve the measurements of the C/A code geodetic and navigation receivers in the few hundred kilometre neighbourhood of the Geophysical Observatory Nagycenk and on the other hand can be used to estimate the electron density in the whole ionosphere.

#### REFERENCES

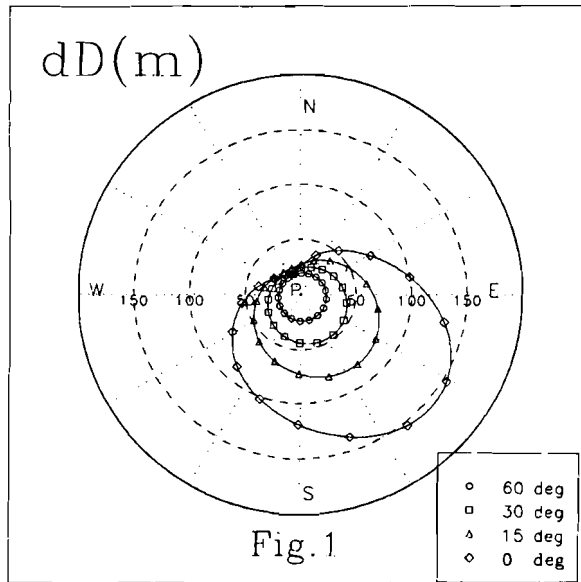
- Bencze, P., Verö, J., Bányai, L. (1986) Spacereasearch Activity in the Geodetic and Geophysical Research Institute of the HAS between 1980-1985 (In Hungarian). *Hungarian Spacereasearch 1981-1985*, p.1-13
- Beutler, G., Gurtner, W., Rothacher, M., Wild, U., Frei, E. (1989) Relative Static Positioning with the Global Positioning System: Basic technical considerations. *Global Positioning System: An Overview*. Eds.: Y. Bock and N. Leppard. *Springer-Verlag*
- Hartman, G.K., Leitinger, R. (1984) Range Errors Due To Ionospheric and Tropospheric Effects for Signal Frequencies Above 100 Mhz. *Bull. Geod.*, **58**, p. 109-136

## REFRACTION OF TRANSIONOSPHERIC L BAND SIGNALS

V.V. VODJANNIKOV, O.G. GONTAREV, B.V. TROITSKY  
Institute of the Ionosphere Academy of Sciences,  
480086 Alma-Ata, 68 Kazakhstan

**ABSTRACT.** For use with satellite systems "GPS" and "GLONASS" a ray-tracing method of superprecise calculation of ionospheric group delay and refraction of L band radiowaves has been developed.

Results of trial calculations obtained for an analytical ionospheric model, which corresponds to the IRI model, for equinox conditions and mean solar activity level (noon value of  $f_0F2$  at the equator is equal to 12 MHz) are presented in Fig. 1 and Fig. 2. Fig. 1 gives the azimuth variations of the difference ( $dD$  [m]) between group radiowave path at the frequency  $f = 1.2$  GHz and optical path in the dependence on elevation, and Fig. 2 gives the dependence of refraction angle ( $\theta$ ) on the azimuth. Point P is a station on the ground at the latitude 45° N, LT=6<sup>h</sup> 00<sup>min</sup>.



From the figure we can see that  $dD$  and  $\theta$  variations are real quantities and have azimuth asymmetry for small elevations. Delay quantity due to refraction is small (0.5 nanoseconds for  $f = 1.2$  GHz), therefore calculations of ionospheric delay using the integral over straight ray have an error 0.1 %, if the refraction has not been taken into account.

## REFRACTION

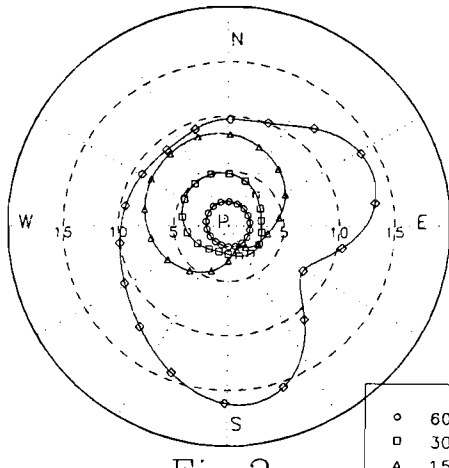


Fig. 2

## A THREE DIMENSIONAL REPRESENTATION OF TROPOSPHERIC REFRACTIVITY WITH APPLICATION TO GPS

JEAN-GUY LECLERC, ABDELLAH EL ABDI EL ALAOUI

Département des sciences géodésiques et de télédétection,

Pavillon Casault, local 1343, Université Laval,

Sainte-Foy (Québec), Canada G1K 7P4 (418)656-7116

Fax: (418)656-7411

**ABSTRACT.** The tropospheric correction for satellite distance measurements is computed from Saastamoinen's analytical solution and from a numerical integration of the refractivity integral. Kriging is used to interpolate the refractivity in space along the propagation path. Numerical results show that Saastamoinen's solution gives smaller tropospheric corrections whose magnitude can be up to 1 meter for large zenith distances. In some cases, the effect of horizontal variations of meteorological parameters on the tropospheric correction to satellite distance measurements can be large and it is concluded that surface meteorological parameters should be used within a radius of 400 km around the station for accurate tropospheric corrections.

Case Studies 1, 2 and 3 are used to evaluate internal consistency of both methods under homogeneous conditions (no horizontal variation of meteorological parameters). Case studies 4, 5 and 6 used the same relative humidity as in study cases 1, 2 and 3 but include horizontal variations of meteorological parameters.

Some preliminary results are shown in tables 1 to 6 and from a more elaborate study it is concluded that surface meteorological data should be used when earth-satellite distances are observed at large zenith distances. The horizontal variation of meteorological parameters can be very important in the presence of warm front or slow moving cold front.

TABLE 1  
Dry atmosphere (relative humidity  $U = 0\%$ ,  $T_s = 19^\circ\text{C}$ ): Case 1

Zenith distance $\beta$ (deg)	Numerical integration $\Delta S$ (m) (1)	Saasta $\Delta S$ (m) (2)	Differences (m) (1) - (2)
0	2.29	2.28	0.01
10	2.41	2.31	0.10
20	2.64	2.42	0.22
30	2.97	2.63	0.34
40	3.40	2.97	0.43
50	4.04	3.54	0.50
60	5.17	4.54	0.63
70	7.38	6.59	0.79
80	11.65	12.60	-0.95

TABLE 2  
Wet atmosphere (relative humidity  $U = 50\%$ ,  $T_s = 19^\circ\text{C}$ ): Case 2

Zenith distance $\beta$ (deg)	Numerical integration $\Delta S$ (m) (1)	Saasta $\Delta S$ (m) (2)	Differences (m) (1) - (2)
0	2.38	2.36	0.02
10	2.50	2.40	0.10
20	2.75	2.51	0.24
30	3.09	2.73	0.36
40	3.55	3.08	0.47
50	4.28	3.67	0.61
60	5.42	4.71	0.71
70	7.61	6.84	0.77
80	12.19	13.07	-0.88

**TABLE 3**  
 Saturated atmosphere (relative humidity  $U = 100\%$ ,  $T_s = 19^\circ\text{C}$ ): Case 3

Zenith distance $\beta$ (deg)	Numerical integration $\Delta S$ (m) (1)	Saasta $\Delta S$ (m) (2)	Differences (m) (1) - (2)
0	2.47	2.45	0.02
10	2.60	2.48	0.12
20	2.86	2.60	0.26
30	3.22	2.82	0.40
40	3.70	3.19	0.51
50	4.43	3.80	0.63
60	5.67	4.88	0.79
70	8.14	7.09	1.05
80	12.45	13.53	-1.08

**TABLE 4**  
 Horizontal variation of meteorological parameters  
 (relative humidity  $U = 0\%$ ,  $T_s = 8^\circ\text{C} - 22^\circ\text{C}$ )

Zenith distance $\beta$ (deg)	Numerical integration $\Delta S$ (m) (1)	Saasta $\Delta S$ (m) (2)	Differences (m) (1) - (2)
0	2.34	2.28	0.06
10	2.46	2.31	0.15
20	2.70	2.42	0.28
30	3.03	2.63	0.40
40	3.46	2.97	0.49
50	4.12	3.54	0.58
60	5.26	4.54	0.72
70	7.38	6.59	0.79
80	11.77	12.60	-0.83

TABLE 5  
Horizontal variation of meteorological parameters (relative humidity U = 50%)

Zenith distance $\beta$ (deg)	Numerical integration $\Delta S$ (m) (1)	Saasta $\Delta S$ (m) (2)	differences (m) (1) - (2)
0	2.43	2.36	0.07
10	2.56	2.40	0.16
20	2.81	2.51	0.30
30	3.15	2.73	0.42
40	3.62	3.08	0.54
50	4.31	3.67	0.64
60	5.51	4.71	0.81
70	7.81	6.84	0.97
80	12.41	13.07	-0.63

TABLE 6  
Horizontal variation of meteorological parameters (relative humidity U = 100%)

Zenith distance $\beta$ (deg)	Numerical integration $\Delta S$ (m) (1)	Saasta $\Delta S$ (m) (2)	Differences (m) (1) - (2)
0	2.52	2.45	0.07
10	2.65	2.48	0.17
20	2.91	2.60	0.31
30	3.28	2.82	0.46
40	3.77	3.19	0.58
50	4.50	3.80	0.70
60	5.76	4.88	0.88
70	8.24	7.09	1.15
80	12.70	13.53	-0.83

## **RESPONSE OF THE IONOSPHERE TO A VERY STRONG MAGNETIC STORM OF APRIL 9-11, 1990 AND ESTIMATING THE ERROR OF A GPS-TYPE NAVIGATION SYSTEM**

**E.L. AFRAIMOVICH, YU.I. VAKULIN, N.M. MINKO**  
SibIZMIR, P.O. Box 4026  
Irkutsk, 664033, Russia

**ABSTRACT.** On the basis of complex measurements of Faraday rotation, angles of arrival and amplitude of the HF signal from the geostationary satellite ETS-2 obtained at Irkutsk, an analysis is made of the ionospheric response during a very strong magnetic storm of April 9-11, 1990. The storm parameters are: onset 0845 UT April 9; and 2100 UT April 11; duration 61 h.. The maximum amplitudes according to data from the magnetic observatory at Irkutsk are: H-component - 312 nT, D - 284 nT, and Z - 216 nT. The most active period of the storm covered 0700 to 2000 UT on April 10.

A typical feature of activity in this period was that only 6 hours after the end of the storm a new large storm of 91-h duration was produced.

A major effect of the magnetic storm manifested itself in a change of global ionospheric parameters, foF2 and total electron content (TEC). On April 10 the diurnal variation of TEC exceeded its daily mean variation by a factor of 1.5, with an increase and decrease, respectively, of its maximum and minimum values. On April 11 the TEC decreased so that its daytime value was at the level of the nighttime TEC value for undisturbed geomagnetic conditions. The critical frequency of the F2 layer varied in a similar way.

This paper presents also data, deduced from complex TEC measurements, on the large- and medium-scale disturbance dynamics caused by the magnetic storm development.

By analyzing the structure and dynamics of an ionospheric disturbance during the magnetic storm, we have obtained estimates of the error of the GPS-type navigation system (NAVSTAR) and of radio astronomical interferometers with different values of baselines and their orientation.



## WET PATH DELAY EFFECTS ON PRECISE GPS HEIGHT DETERMINATION

A H DODSON & P J SHARDLOW

University of Nottingham, University Park  
Nottingham NG7 2RD, England

G ELGERED & P O J JARLEMARK

Chalmers University of Technology  
Onsala Space Observatory  
S-43900 ONSALA, Sweden

**ABSTRACT.** Considerable interest has been generated recently in the use of GPS for precise height measurement with a particular emphasis on tide gauge measurements for absolute sea level determination. A major error source in these measurements is the tropospheric wet path delay.

This paper describes a dedicated GPS campaign to be undertaken in Sweden which will use Water Vapour Radiometer (WVR) and radiosonde data as well as stochastic modelling techniques to evaluate the methods of correcting for the wet path delay. A comparison of the three approaches will be undertaken.

Measurements will be taken in four different seasons in an attempt to quantify the secular variations in a temperate coastal climate. The first observations were carried out in February 1992, and the preliminary results of the campaign are presented.

### 1. INTRODUCTION

This paper describes a collaborative project aimed at improving the heighting accuracy obtainable from GPS, by better quantification of tropospheric wet path delay errors. Recent interest in the use of GPS for vertical positioning, for example in studying sea-level changes, may be limited by the wet path delay error. Simulation studies have shown that water vapour radiometry data should significantly improve GPS measurements (Hurst, 1987) but this has not yet been clearly demonstrated using real data. Additionally, the use of a stochastic model which corrects for the tropospheric delay has proved promising, but such models rely on constraints determined through a knowledge of the variations expected. Neither approach has really been tested in the temperate European climate, and this project aims to do just that.

Four seasonal field observation campaigns, employing a Fiducial GPS network approach, will be undertaken, with Water Vapour Radiometer (WVR), radiosonde and GPS data being analysed. The first campaign was undertaken in February 1992, and the preliminary results of those observations are presented here. Further observations in the Spring, Summer and Autumn will follow. The aim of the project will be to compare the vertical positioning accuracies of GPS using WVR data directly, and using stochastic models where the parameters can be based upon WVR and radiosonde measurements.

### 2. FIELDWORK

The Winter field campaign consisted of making GPS observations at four fiducial sites as illustrated in Figure 2.1. The fiducials were chosen to encompass the area of interest. The CIGNET<sup>1</sup> stations Tromsø and Wettzell are occupied by Rogue receivers, whilst Metsahovi at

<sup>1</sup> Cooperative International GPS NETwork; continuously tracking stations which have accurate coordinates determined by either VLBI, SLR or Mobile VLBI.

present is occupied by an Ashtech receiver (although a Rogue receiver was being installed at the time of the first campaign). Buddon, although a fiducial point, does not have a continuously tracking receiver. The station was included however because it provided strength in the East/West direction in the network.

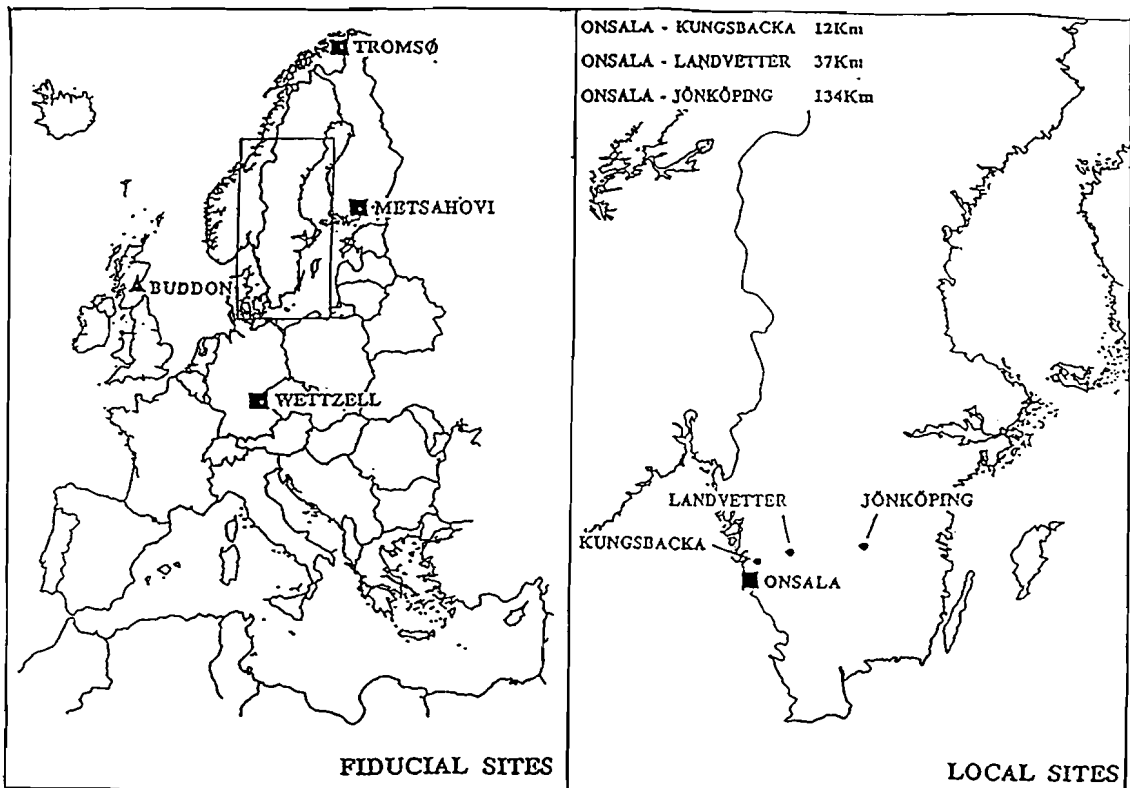


Figure 2.1     Location of Fiducial and Local Sites.

The local network was observed simultaneously and includes Onsala (a CIGNET station), Landvetter, Jönköping and Kungsbacka. The latter being used only to aid integer fixing. The CIGNET Rogue receiver was used at Onsala and TRIMBLE 4000 SST P-code receivers were used at the remaining sites. A backup receiver, a Mini-rogue, was used for 2-days after an Antenna failure at Landvetter on the 12th of February.

The GPS observation schedule spanned 8 hours from 0830 - 1630 UT (Figure 2.2) from the 10 - 14 February. The lengthy observation span was used to provide a data set with variations in the troposphere and to facilitate the process of orbit improvement using the fiducial technique. The monumentation and meteorological data collected at each of the local sites is summarised in Table 2.1.

WVR data were collected throughout the GPS observation session. A previously used WVR data acquisition procedure (Elgered et al., 1990) had been slightly modified for the GPS campaign. The WVR completes one data acquisition cycle every 13 minutes, it consists of 1 clockwise azimuth scan at a 30° elevation, starting in the north followed by 4 elevation scans from horizon to horizon over the zenith. The goal is to make a coarse map of the wet delay over the sky for the period of the GPS observations. The procedure is illustrated in Figure 2.3.

Table 2.1 Local Network Observation Schedule.

SITE	Kungsbacka	Göteborg/ Landvetter Airport	Jönköping / Axamo Airport	Onsala Space Observatory
Observations	GPS	GPS	GPS	GPS
Purpose	Integer Fixing	Local Network	Local Network	Local Network
Atmospheric Correction Data		Surface Met Radiosonde (12-hourly)	Surface Met	Surface Met WVR
Monumentation	Roof-top Site	Pillar with a 5/8" thread	Bolt in Bedrock	CIGNET Pillar

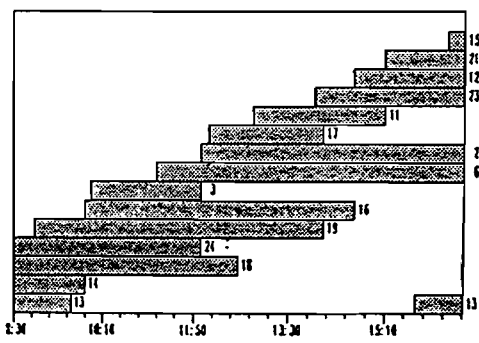


Figure 2.2 Satellite Availability Plot

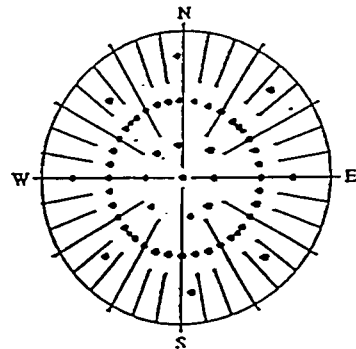


Figure 2.3 Polar Plot of WVR Data Acquisition

### 3. PRELIMINARY RESULTS

The first campaign was planned for February in order to acquire GPS data during cold, dry and stable weather conditions, example WVR data for this is illustrated in Figure 3.1. However, significant variations in the atmospheric water vapour also occurred during the observation period. On the morning of the 13th of February a cold front passed over the WVR site, resulting in rain. By the time the GPS observations had started (08.30 UT), the rain had ceased. Figure 3.1b shows the rapid decrease in the wet delay as the cooler, drier air takes over with the passage of the front.

An ionospherically free (L1/L2) solution was obtained for four consecutive days for the baseline Landvetter to Jönköping (107km) using different meteorological models. Ambiguity free solutions were obtained using a broadcast ephemeris. Day to day baseline vector repeatabilities were used as a measure of precision of the results (Figure 3.2).

The eastings and length component were found to be the worst. This is not too surprising since the baseline has an east-west orientation whilst the satellites orbit in a north-south direction. Orbit improvement using the fiducial technique should improve these repeatabilities, leaving the height component as the least well determined. Figure 3.2 demonstrates that the choice of meteorological model can improve the repeatability of the baseline vector components and in particular, height.

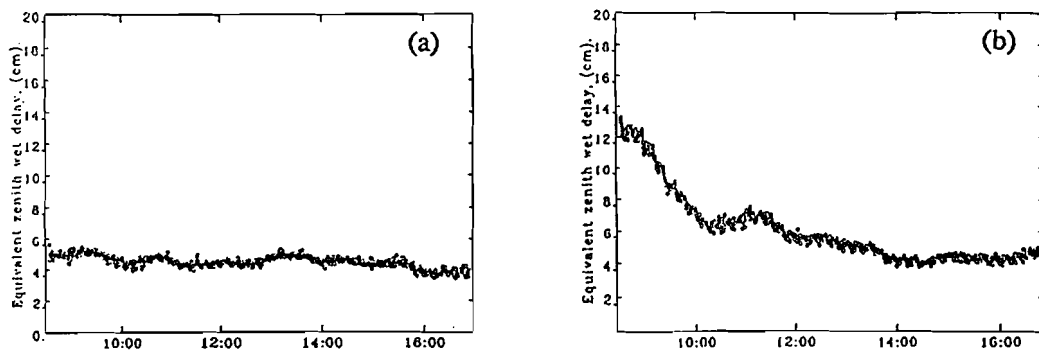


Figure 3.1 Preliminary results of the equivalent zenith wet path delay for:  
 (a) 11 February 1992 and (b) 13 February 1992

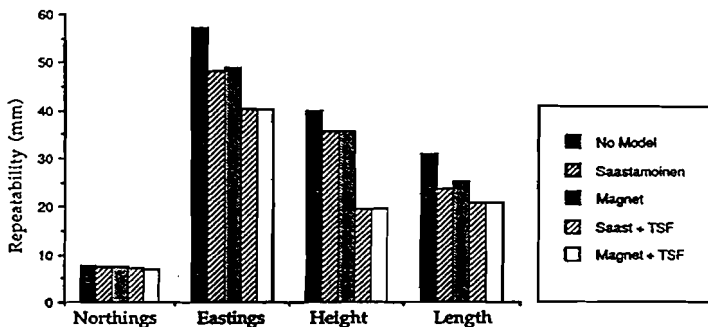


Figure 3.2 Day to day repeatabilities of an Ambiguity Free Solution for the baseline vectors Landvetter to Jönköping using different meteorological modelling techniques.

#### 4. CONCLUSIONS

A few preliminary results have been presented which do suggest that the vertical component can be improved through the correct modelling of the troposphere. The remaining error sources are attributed to the wet path delay, and it is hoped that the use of the WVR data and stochastic modelling will account for these.

#### ACKNOWLEDGEMENTS

The project is supported by the EC-SCIENCE programme.

We would like to thank Tommy Carlsson, Lisa Hubbard, Peter Clarke and Kenneth Jaldehag for their help with the GPS data acquisition and for the field support at the GPS sites mentioned in Table 2.1.

#### REFERENCES

- Elgered, G., Johansson, J.M., Rönnäng, B.O. (1990) Characterizing Atmospheric Water Vapour fluctuations using Microwave Radiometry. Research Report No 165. Dept of Radio and Space Science with Onsala Space Observatory, Chalmers University of Technology.  
 Hurst, K.J. (1987) The measurement of vertical crustal motion, Ph.D. Thesis, Columbia Univ.

## **6. SATELLITE LASER RANGING**



## ATMOSPHERIC REFRACTION AND SATELLITE LASER RANGING

PETER L. BENDER\*

Joint Institute for Laboratory Astrophysics, University of Colorado and  
National Institute of Standards and Technology, Boulder, CO 80309, USA

### ABSTRACT

The current purely instrumental measurement inaccuracy for satellite laser ranging normal points from a number of stations is believed to be 1 cm or less. If proposed instrumental improvements were made soon, the instrumental inaccuracy for upgraded stations could be reduced to 2 or 3 mm by 1995 for at least STARLETTE and LAGEOS type satellites. The challenge for atmospheric refraction studies is to achieve similar accuracy. The present estimated uncertainty for calculating the extra optical path length due to the atmosphere is roughly 2 to 5 mm at an elevation angle  $E$  of 45° and 7 to 15 mm at 20°.

One important atmospheric limitation is uncertainty in the size of horizontal gradients in the density. Such gradients cause range correction errors for slant paths which depend on azimuth and vary as ( $\csc E \cdot \cot E$ ). A partial correction for gradients may be possible based on gridded meteorological data versus height every 12 hours. This is because a substantial part of the correction comes from gradients at altitudes comparable with the scale height, which are expected to extend over considerable areas and be fairly stable in time. Also, fitting of the range data during each satellite pass may help to determine the integrated effect of gradients at all altitudes.

Another limitation which may occur only rarely at most sites is deviations from the hydrostatic equilibrium assumption used in calculating the range corrections from surface pressure measurements. Little is known about the size and frequency of such deviations, except for some rough estimates of effects at mountain sites. The uncertainty in the range correction due to ray bending also may be significant. Inaccuracy in the local barometric pressure measurement and in the atmospheric water vapor correction appear to be correctable problems for typical elevation angle cutoffs of about 20°.

Dual wavelength satellite range measurements with streak camera detectors appear capable of giving very valuable overall information on horizontal gradients and on possible deviations from hydrostatic equilibrium. If such measurements show that the approach of correcting for horizontal gradients based on 12 hour meteorological data works fairly well, or that fitting two gradient parameters to the range data during each pass works, and if significant deviations from hydrostatic equilibrium are indeed rare at most laser ranging sites, then substantial improvements in the atmospheric correction accuracy appear likely. Such improvements may be particularly important in providing highly accurate radial station coordinates for studies of global sea level changes, vertical crustal movements, and motion of the geocenter.

## 1. INTRODUCTION

The single shot range jitter for a number of the present satellite laser ranging stations is 1 cm or less. With a measurement repetition rate of 10 pulses/second for many of these stations, the statistical uncertainty for a two-minute range "normal point" formed from the data is well under 1 mm. Thus the precision of the range measurements often is not a significant limitation.

The real limitation to the instrumental measurement accuracy comes from systematic errors in measuring the round trip travel time. Microchannel plate photomultipliers followed by discriminators usually are used to measure the time delay between the transmission of the outgoing laser pulse and the arrival of the retroreflected pulse. Since similar light levels and the same photodetectors and electronics can be used for creating timing pulses from the outgoing and return light pulses, many types of errors are reduced. Calibrations are made based on ranging to extend targets at known distances or to internal targets within the ranging system. The calibrated range normal points are used to fit an improved theoretical range curve during a given pass, which might last 30 min for the LAGEOS satellite. Fluctuations in the normal point residuals from the theoretical curve are substantially larger than the expected statistical fluctuations, indicating some of the limitations of the ranging systems. However, collocations of two systems near each other are necessary in order to detect constant offsets in the ranges or variations in the range differences from pass to pass or over periods of days or weeks. This kind of test indicates an accuracy of 1 cm or better for a number of ranging systems at present.

For the future, some improvements can be made by using shorter laser pulses and improved photodetectors and discriminators. However, the most promising approach is the use of a streak camera for measuring the travel time, as discussed later in connection with dual wavelength laser range measurements. It seems clear that the instrumental accuracy can be improved to 1 mm or better with this method. This expected improvement provides strong motivation for developing more accurate atmospheric range correction methods in the near future.

Assuming that 1 mm or better instrumental range measurement accuracy will be achieved, the one other significant limitation on the usefulness of the range accuracy improvement besides the atmospheric correction uncertainty is connected with the geometrical distribution of the retroreflectors on the satellite. With each of the fused silica retroreflectors on STARLETTE or LAGEOS having essentially the same distance of its apex from the center-of-mass of the satellite, the distances measured from the Earth to different retroreflectors will be different [Degnan 1985]. The retroreflector closest to the observing station will give the biggest single contribution to the signal, but several "rings" of retroreflectors around the closest one will contribute substantially. Thus the expected laser pulse shape distortion from this effect will have to be modeled carefully in order to obtain the highest accuracy. Very careful pre-launch laser range measurements have been made to the LAGEOS II satellite in the laboratory under a wide range of observing conditions in order to characterize such geometrical effects.

Further studies of the accuracy of corrections for geometrical effects may reduce the uncertainties, but such effects may turn out to limit the overall range measurement accuracy, independent of the atmospheric correction uncertainty, to 2 or 3 mm through the 1990's. For the future, other approaches are possible. For example, with a

sufficiently short laser pulse length, the return pulse from the closest retroreflector could be resolved from the pulse contributions of the other retroreflectors. However, the simplest approach for future satellites may be to change the geometry of the retroreflector locations. In view of the possibility of accurately modeling the geometrical effects, we will assume that the accuracy goal for atmospheric range corrections should be to approach the 1 mm level as closely as possible.

The largest contribution to the atmospheric correction uncertainty for elevation angles  $E$  of roughly  $45^\circ$  or less is likely to be from horizontal gradients in the atmospheric density. For this reason, we will concentrate on describing the effects of such gradients and their possible size in this paper. Some other limitations on the atmospheric corrections will be discussed briefly, and estimates of the range of uncertainty in the overall atmospheric correction accuracy will be given.

## 2. HORIZONTAL GRADIENTS IN DENSITY: THEORY

Neglecting the curvature of the Earth and the curvature of the ray path, the atmospheric range correction is given by the following expression

$$S(E, \phi) = \int_0^\infty 10^{-6} N(x, z, \phi) d\ell . \quad (1)$$

Here  $N = 10^6(n - 1)$  is the group refractivity,  $\ell$  is the distance from the ranging station along the slant path, and the coordinates  $x$ ,  $z$ , and  $\phi$  of points along the path are the horizontal distance from the ranging station, the height difference, and the azimuth. In the simple case where  $N$  depends only on  $z$ ,  $d\ell = dz \cdot \csc E$ , and

$$S(E) = S(90^\circ) \cdot \csc E . \quad (2)$$

This case is often referred to as the spherically symmetric case.

Assume next that the refractivity depends only on the atmospheric density but that horizontal gradients in the density are present. For a particular azimuth, if the refractivity at each height can be modeled adequately by a linear gradient,

$$N(x, z) = N(o, z)[1 + \alpha(z) \cdot x] ,$$

then

$$S(E) = S(90^\circ) \cdot \csc E + 10^{-6} \csc E \cdot \cot E \int_0^\infty z \cdot \alpha(z) \cdot N(o, z) dz . \quad (3)$$

This can also be written as follows:

$$S(E) = S(90^\circ) \cdot \csc E \{1 + \cot E \langle z \cdot \alpha(z) \rangle\} , \quad (4)$$

where

$$\langle z \cdot \alpha(z) \rangle = \left\{ \int_0^\infty z \cdot \alpha(z) \cdot N(o, z) dz \right\} / \left\{ \int_0^\infty N(o, z) dz \right\} . \quad (5)$$

Here  $\alpha(z)$  is the fractional gradient in the refractivity, and  $\langle z \cdot \alpha(z) \rangle$  is the average of  $\alpha(z)$  weighted by the height above the ranging station.

The reason that  $\langle z \cdot \alpha(z) \rangle$  occurs in Eq. (4) is that the fractional difference in refractivity between a point on the slant path at height  $z$  and the corresponding point above the ranging station for a given value of  $\alpha$  is proportional to the horizontal distance  $z \cdot \cot E$  at which the slant path reaches that altitude. The difference of  $S(E)$  from  $S(90^\circ) \cdot \csc E$  is the horizontal gradient part of the atmospheric range correction.

It also is instructive to consider the case where there is no variation in temperature or density scale height  $H(x)$  with altitude, but where the temperature varies with position to the east of the ranging station in such a way that  $H(x)$  decreases linearly with distance to the east:

$$H(x) = H(o) \cdot (1 - \beta x). \quad (6)$$

Then

$$N(o, z) = N(o, o) \exp \{-z/H(o)\} \quad (7)$$

and

$$N(x, z) = N(x, o) \exp \{-z/[H(o) \cdot (1 - \beta x)]\}. \quad (8)$$

Expanding the exponential to first order in  $\beta$ :

$$N(x, z) \cong N(x, o)[1 - \beta xz/H(o)] \exp\{-z/H(o)\}. \quad (9)$$

To keep the surface pressure constant requires that

$$\int_0^\infty N(x, z) dz = H(o) \cdot (1 - \beta x) \cdot N(x, o) \quad (10)$$

be independent of  $x$ , or

$$N(x, o) = N(o, o)/(1 - \beta x). \quad (11)$$

Thus, to first order in  $\beta$ :

$$N(x, z) \cong N(o, o)[1 + \beta x - \beta xz/H(o)] \exp\{-z/H(o)\}, \quad (12)$$

$$\alpha(z) = \beta[1 - z/H(o)]. \quad (13)$$

This means that the fractional density gradient will be positive at heights less than one scale height because of the reduced scale height to the east of the ranging station, but negative above one scale height. Integrating, we find

$$\langle z \cdot \alpha(z) \rangle = \beta H(o) - 2\beta H(o). \quad (14)$$

Thus the decrease in density to the east above one scale height has twice as much effect as the increase at lower heights because of the weighting of  $\alpha(z)$  by the height  $z$ , and

$$S(E) = S(90^\circ) \cdot \csc E \{1 - \beta \cdot H(o) \cdot \cot E\}. \quad (15)$$

### 3. ESTIMATED SIZE OF HORIZONTAL DENSITY GRADIENTS

Before proceeding, it is useful to review some of the general properties of the atmosphere, as discussed e.g. by Webb [1984]. The lowest part of the atmosphere,

the surface layer, extends up to heights of 30 m or so. Conditions in this layer are highly variable, but have little effect on the horizontal gradient correction because the gradient is weighted by the height. The next layer is the atmospheric boundary layer, which typically has a depth of between a few hundred meters and 2 km or so. And above this is the free atmosphere.

The boundary layer can be very shallow under stable conditions (clear night over land, or warm air over cooler water, with light wind). However, when the boundary layer becomes convective, there is strong vertical mixing throughout the depth of the layer, which typically is about 1 km. Thermal upcurrents usually rise through the layer, fed by an irregular net of polygonal warmer cells near the surface layer. There generally is some temperature rise at the top of the convective boundary layer, so that some heat is also fed downward into this layer from the stably stratified overlying free atmosphere.

The horizontal air flow in the boundary layer meets substantial resistance from an effective eddy viscosity [Horton 1979], which under convective conditions is related to the thermal upcurrents. However, this resistance is overcome at higher altitudes, and the flow pattern becomes geostrophic in the free atmosphere. For this reason, the temperature in the free atmosphere is influenced much less by local surface conditions such as ground cover and albedo than for the surface and boundary layers. Because of this, the horizontal temperature gradient in the free atmosphere is expected to be fairly stable over periods of 12 to 24 hours in good weather. As Webb says [1984], the airmass properties "depend on the trajectory the air has followed over the past few days," and "the air trajectory itself is determined by the large-scale synoptic flow, as seen on the daily weather chart."

The first published analysis of radiosonde data to investigate the magnitude of the horizontal gradient correction was done by Gardner [1976]. He made use of data from nearly simultaneous radiosonde launches at 8 sites near Washington, D.C. during January and February, 1970. In his initial paper, the data analyzed consisted of 17 sets of 3 nearly simultaneous launches at sites located approximately 100 to 150 km from each other. Linear horizontal refractivity gradients in the N-S and E-W directions were fit to the data, and horizontal gradient range corrections were calculated. The sizes of the resulting mean and standard deviation were  $-0.07$  and  $1.16$  cm for  $E = 20^\circ$  and  $-0.01$  and  $2.87$  cm for  $E = 10^\circ$ . The standard deviation for  $E = 10^\circ$  would imply a value of  $0.71$  cm for  $E = 20^\circ$  if the gradient correction varied as  $\csc E \cdot \cot E$ . The rms effects of assumed random errors in the radiosonde measurements were found to be  $0.33$  and  $0.72$  cm for  $E = 20^\circ$  and  $10^\circ$ , but it is not stated whether possible constant biases for different radiosondes were included.

Other studies based on the same radiosonde data set were reported by Gardner and Hendrickson [1976] and Gardner et al. [1978]. For these studies either 6-coefficient (group A) or 4-coefficient (group C) refractivity variation models at each height were fit to nearly simultaneous radiosonde data from all 8 sites or from 7 sites, respectively. The mean differences of the range corrections from the spherically symmetric model were negligible. The standard deviations for  $E = 20^\circ$  and  $10^\circ$  respectively were  $0.51$  and  $1.96$  cm for group A (21 data sets) and  $0.29$  and  $1.90$  cm for group C (10 other data sets) [Gardner and Hendrickson 1976]. The means for group A were  $0.65$  and  $2.4$  cm at an azimuth of  $0^\circ$  from north for  $E = 20^\circ$  and  $10^\circ$  [Gardner et al. 1978].

The above results of Gardner and Hendrickson [1976] and Gardner et al. [1978] indicate a remarkably constant horizontal gradient effect during the period covered by

the data. It is suggested in these articles that the average gradient is due to the normal latitudinal decrease in temperature from south to north. However, direct integration using the U.S. Supplemental Standard Atmospheres for January at 45° N and 30° N gives a horizontal gradient effect of only 0.11 cm at  $E = 20^\circ$ . Thus more local effects such as the typical atmospheric conditions along the east coast of the U.S. in winter or particular weather patterns during the period of the data are more likely to be responsible.

Another evaluation of the effects of large scale horizontal gradients was made in connection with lunar laser ranging observations at the McDonald Observatory on Mt. Locke, near Fort Davis, Texas. Special radiosonde launches were made at Mt. Locke during three periods of 2 weeks each. The launch times were 0 hr, 6 hr, 12 hr, and 18 hr UT. The 0 hr and 12 hr times agreed approximately with the radiosonde launch times at the El Paso (TX), Midland (TX), and Albuquerque (NM) airports. The baselines from McDonald to El Paso and Midland were 260 and 220 km long, and those from El Paso to Albuquerque and Midland were 350 and 390 km long. The McDonald observations at 6 hr and 18 hr were obtained in case they were needed for evaluating diurnal atmospheric profile variations.

The results for the horizontal gradient effect for slant paths from McDonald toward El Paso and Midland were reported briefly in an AGU abstract [Bender and Kirkpatrick 1972]. The horizontal gradient effect was reported to be 0.2 to 0.5 cm for 20° elevation angle. This was based on linear interpolation of the radiosonde results, using only the values at elevations above the 2085 m height of McDonald. The smaller gradient effect compared with the results of Gardner and his colleagues may be partly due to the mountaintop location of McDonald and the longer baselines. For consistency, only data above the McDonald height was used for the baselines from El Paso to Albuquerque and Midland also. The gradient effect was even smaller for these still longer baselines.

The horizontal gradient results for both the Washington, D.C. area and the McDonald Observatory area are based on radiosonde observations at points separated by roughly 100 to 400 km. Dunn et al. [1982] have emphasized the possible importance of horizontal gradients with wavelengths comparable with or shorter than 100 km, which would have been largely missed for the data sets discussed above. In order to obtain some idea of the size of shorter wavelength gradients, they analyzed nearly simultaneous radiosonde data from White Sands, NM. The launch site separations were roughly 10 to 15 km in the N-S direction and 15 to 25 km in the E-W direction. Detailed results for the temperature differences between radiosondes for one typical launch time are shown in the report. The horizontal drifts in the radiosondes during the observations were substantial, but the radiosonde separations did not vary by large percentages. A common feature in the temperature variation was seen between 4 and 5 km height for all 6 of the radiosondes.

The observed temperature differences shown for the typical launch time were large enough to give serious range correction errors, and could not be explained by the quoted uncertainty of about 0.7 K in the radiosonde measurements. However, because of several factors, including the variations in radiosonde separations and the somewhat limited maximum altitude for the data, only the surface values for the radiosonde results were used in the final analysis. A constant lapse rate was chosen for each launch site and launch time to give a temperature profile which approached the temperature

value for a standard atmosphere at 11 km altitude. The typical horizontal gradient effect for 33 sets of launches was roughly 2 cm at  $E = 20^\circ$ .

The question raised by Dunn et al. about short wavelength horizontal gradients possibly giving larger errors than the longer wavelength gradients which the other studies were sensitive to is still an open issue. Resolving this question deserves the highest priority in studies of atmospheric refraction corrections for laser ranging. On the other hand, from the characteristics of the data set for 10:30 on Nov. 2 which are shown by Dunn et al. in Figs. 3-8, it does not appear likely that such data can provide the desired answers. One problem is that the apparent gradients do not decrease substantially above 2 or 3 km height, as would be expected above the boundary layer. In addition, the radiosondes labeled NW, W, and SW show no evidence for gradients above 3 km height to the temperature measurement accuracy, but there are large differences with respect to the one labeled N and the pair labeled S and L. The latter pair agree well with each other up to the 6 km height where L has its last measurement point. Whether temperature measurement biases for some of the radiosondes might have been larger than normally expected, or whether substantial sensitivity to systematic cloud cover differences was present, are possible concerns. As stressed by the authors, the main message from the study is that better data on the effect of short wavelength horizontal gradients is strongly needed. Such gradients might include, for example, the effects of heat islands around major cities.

#### 4. OVERALL UNCERTAINTY IN ATMOSPHERIC LASER RANGE CORRECTIONS

Probably the second largest source of uncertainty in atmospheric refraction corrections to satellite laser range measurements comes from possible deviations from hydrostatic equilibrium. Such deviations are expected to be small for synoptic scale motions – i.e. over distances of thousands of kilometers. However, large vertical accelerations certainly can be experienced in aircraft, even in clear weather. The question is to what extent vertical air motions caused by either orographic or thermal effects can cause the surface pressure measurements to deviate from the hydrostatic values.

An initial study of deviations from hydrostatic equilibrium for observation sites in mountainous areas has been carried out by Hauser [1989]. He concluded that the expected range correction error is less than 1 cm most of the time for  $E = 20^\circ$ . However, it was not possible in that study to provide quantitative information on how frequently an error of a specified size might occur under conditions which were suitable for laser ranging. Also, no studies are available of what might occur in nonmountainous areas. In the absence of other information, we assume here that the range correction uncertainty due to deviations from hydrostatic equilibrium is somewhere between 0 and 3 mm at the zenith, and varies as  $\csc E$ .

A third source of atmospheric correction error is inaccurate measurement of the surface pressure. If the present measurement accuracy is 0.4 millibar, the corresponding range error is 2.8 mm at  $E = 20^\circ$ . This is expected to be reduced to below 1 mm by future improvement of the pressure measurement accuracy to 0.1 millibar.

For atmospheric water vapor, various methods appear to be capable of reducing the zenith range correction uncertainty for microwaves to about 5 mm. In view of the

much smaller effect of water vapor on the atmospheric index of refraction for light, the corresponding range correction error for  $E = 20^\circ$  is only about 0.2 mm. In two-color laser range measurements the sensitivity to water vapor is higher, but would still give only about 0.5 mm range correction uncertainty.

The last range correction error source which usually is considered is bending of the light ray path. An estimate of the error at  $E = 20^\circ$  can be obtained by extrapolation from the sensitivity parameters at  $E = 5$ , 10, and  $15^\circ$  for the CfA-2.2 mapping function, as described by Davis et al. [1985]. The sensitivity parameters give the sensitivity of the range correction to various parameters used in the atmospheric model, such as the surface temperature, the lapse rate, and the tropopause height. As crude estimates under conditions when good meteorological data is available, we take 2 mm for the ray bending contribution to the range uncertainty for  $E = 20^\circ$  and 0.3 mm for  $E = 45^\circ$ .

We now want to provide some rough estimates of error budgets for the atmospheric range correction. The most difficult question is what to assume for the uncertainty due to horizontal gradients. An uncertainty of 6 mm at  $E = 20^\circ$  is roughly consistent with the results of Gardner [1976], Gardner and Hendrickson [1976], and Gardner et al. [1978]. For Case I, which is intended to be somewhat pessimistic, we take twice this value, or 12 mm. However, from the paper of Dunn et al. [1982], this certainly is not an upper limit. For Case II we take 6 mm. For an optimistic case, where meteorological data is found to be useful in estimating the size of the horizontal gradient correction, we take an uncertainty of 3 mm.

The estimated error budgets for the three cases are given in Table 1. The effect of deviations from hydrostatic equilibrium are taken to be 3, 1, and 0.5 mm at the zenith, respectively, for these cases. The surface pressure measurement accuracy is 0.4 millibars for Case I and 0.1 millibars for the other two cases. We use 2 mm for the uncertainty due to ray bending at  $E = 20^\circ$  in all three cases, and 0.5 mm for the water vapor contribution at this elevation angle.

**Table 1**  
Error budgets in mm for atmospheric range corrections at different elevation angles

Error source	Case I		Case II		Case III	
	45°	20°	45°	20°	45°	20°
Horizontal gradient	2.1	12	1.1	6	0.5	3
Hydrostatic assumption	4.2	8.8	1.4	2.9	0.7	1.5
Pressure measurement	1.4	2.9	0.3	0.7	0.3	0.7
Ray bending	0.2	2	0.2	2	0.2	2
Water vapor	0.2	0.5	0.2	0.5	0.2	0.5
Root sum square error	5	15	2	7	1	4

There are two methods which may become available in the near future for checking on the above estimates of the laser range correction accuracy. If a range measurement accuracy of 2 to 3 mm becomes available soon, then fitting the range residuals as a function of elevation angle and azimuth probably will make it possible to separate at least some of the range correction errors from other model errors. The present normal point residual level of roughly 3 cm for 3 day arcs fit to global data for LAGEOS is not understood, and presumably would make it necessary to work with single pass residuals in investigating range correction errors.

An even more attractive possibility is to use dual wavelength laser distance measurements to test the accuracy of atmospheric range corrections, as well as to provide corrected distance measurements. This approach was discussed earlier by Degnan [1985] and by Abshire and Gardner [1985], and more extensive information is contained in the proceedings of the bi-annual International Workshops on Laser Ranging Instrumentation. Review articles concerning work on this topic under the NASA Crustal Dynamics Project are currently being prepared by J. J. Degnan and by T. K. Varghese.

The basic idea is to use a commercially available linear streak tube to provide much higher time resolution than is available with microchannel-plate photomultipliers. The timing resolution of such streak tubes is 1 or 2 picoseconds. If lasers are used which have pulse widths narrow enough to resolve the returns from different retroreflectors, then the difference in travel times for two transmitted laser wavelengths derived from the same laser pulse will determine the atmospheric refraction delay difference. The achievable accuracy appears to be sufficient to provide a strong test of the accuracy of atmospheric refraction corrections.

\*Quantum Physics Division, National Institute of Standards and Technology

## REFERENCES

- Abshire, J. B., and Gardner, C. S. (1985) IEEE Trans. Geosci. Remote Sens., **GE-23**, 414-425.  
Bender, P. L., and Kirkpatrick, A. W. (1972) Eos Trans. AGU, **53**, 347.  
Davis, J. L., Herring, T. A., Shapiro, I. I., Rogers, A. E. E., and Elgered, G. (1985) Radio Sci., **20**, 1593-1607.  
Degnan, J. J. (1985) IEEE Trans. Geosci. Remote Sens., **GE-23**, 398-413.  
Dunn, P. J., Pearce, W. A., and Johnson, T. S. (1982) Final Report: Studies of Atmospheric Refraction Effects on Laser Data (EG&G, Riverdale, MD).  
Gardner, C. S. (1976) Radio Sci., **11**, 1037-1044.  
Gardner, C. S. and Hendrickson, B. E. (1976) Correction of Laser Ranging Data for the Effects of Horizontal Refractivity Gradients (Radio Res. Lab., Univ. of Illinois, Pub. No. 478).  
Gardner, C. S., Rowlett, J. R., and Hendrickson, B. E. (1978) Appl. Opt., **17**, 3143-3145.  
Hauser, J. P. (1989) J. Geophys. Res., **94**, 10,182-10,186.  
Horton, J. R. (1979) An Introduction to Dynamic Meteorology (Academic Press, New York, Second Ed.).  
Webb, E. K. (1984) in Geodetic Refraction, ed. F. K. Brunner (Springer-Verlag, Berlin), 85-141.



## **7. GEODETIC IMAGING, REMOTE SENSING, INSTRUMENTATION**



# DEVELOPMENT OF A PORTABLE DUAL FREQUENCY MICROWAVE WATER VAPOR RADIOMETER FOR GEODETIC APPLICATIONS

Bürki, B.<sup>1</sup>, M. Cocard<sup>1</sup>, A. Geiger<sup>1</sup>, R. Gyger<sup>2</sup>, H.-G. Kahle<sup>1</sup>

1 Institute of Geodesy and Photogrammetry, Federal Institute of Technology ETH  
CH-8093 Zurich, Switzerland

2 CAPTEC Consulting, Microwave, Components and Systems Corp. CH - 3012 Berne, Switzerland

**ABSTRACT.** Radio-astronomical measurements and applications in satellite geodesy such as Very Long Baseline Interferometry (VLBI) and Global Positioning System (GPS) require accurate determination of the path delay along the propagation path. While the path delay due to dry air is quite stable and can be well calibrated by surface meteorological measurements, the effect due to water vapor and liquid water within the troposphere is highly varying in time as well as in space. This tropospheric path delay can be obtained by means of a dual frequency ground based water vapor radiometer (WVR) operating at 23.8 and 31.5 GHz. The path delay may be deduced from passive measurements of the brightness temperature(s) as emitted by the troposphere. The equipment as described in this paper is transportable and can be operated on a normal tripod. The WVR construction in connection with an electronic steering unit and a Laptop PC enables to track automatically the actually measured GPS Satellites or other space targets.

## 1. INTRODUCTION

One of the fundamental limitations in GPS is the systematic extension of the propagation path due to the tropospheric path delay which affects mainly the height component. At microwave frequencies, the path delays is caused primarily by the columnar water vapor content thus introducing biases in phase measurements. While the effect due to dry air is quite stable and can be calibrated by surface meteorological measurements, the effect due to water vapor and liquid water in the troposphere is highly varying. Therefore it can not be modelled adequately by surface measurements only.

The amount of water vapor in the troposphere is related to the thermal emission of the 22.235 GHz spectral line. The brightness temperature of both frequencies responds to water vapor as well as to liquid water. While the 23.8 GHz frequency is influenced more by the water vapor, the 31.5 GHz frequency depends more on the liquid. The two chosen frequencies for the water vapor radiometer (WVR) minimize the effect of liquid water. Therefore they are nearly independent on meteorological profiles. After Wu (1979) the path delay  $P_D$  error can be denoted as the integrated columnar water vapor content along the propagation path s:

$$P_D = k \int_0^{\infty} \frac{\rho(s)}{T(s)} ds \quad (1)$$

with:  $k = \text{const.} = 1,723 \cdot 10^{-3} [\text{K}/(\text{g}/\text{m}^3)]$ ,  $\rho(s) = \text{water vapor density } [\text{g}/\text{m}^3]$  and  $T(s) = \text{temperature along the propagation path } [\text{K}]$ .

## 2. THEORY

The main task of a microwave radiometer is to measure the thermal radiation emitted by the atmosphere in the direction of the antenna. This radiation is related to an equivalent black-body temperature or brightness temperature  $T_B(f)$  at frequency  $f$ . In microwave range observations within the atmosphere various simplifying assumptions must be introduced: (1) The atmosphere is in local equilibrium, (2) The Planck's black-body radiation formula is replaced by the Rayleigh-Jeans approximation, (3) scattering is neglected, (4) the background radiation is assumed to be 2.7 K and independent on frequencies. (5) Furthermore it is assumed that the atmosphere is spherically stratified and symmetric.

### 2.1 Brightness Temperature

With these assumptions, the brightness temperature is related to the emission and absorption of the medium, i.e. mainly due to water vapor and other atmospheric constituents, by the radiative transfer equation (Westwater, 1978):

$$T_B(f) = T_{back} e^{-\tau(f, \infty)} + \int_0^\infty T(s) \alpha(f, s) e^{-\tau(f, s)} ds \quad (2)$$

where:  $T_B(f)$ : brightness temperature [K],  $T_{back}$ : background radiation [K],  $\tau(0, \infty)$ : optical depth;  $f$ : frequency [GHz],  $T(s)$ : absolute temperature [K],  $\alpha$ : absorption coefficient [1/km], depending on  $f$ ,  $T(s)$ ,  $\rho(s)$ , atmospheric pressure  $P$  and spectral parameters;  $\alpha = \alpha_v + \alpha_l + \alpha_o$  with  $v$  denoting the water vapor,  $l$  the liquid water and  $o$  the oxygen contribution.

### 2.2 Linearized Brightness Temperature

For small  $\tau$  the exponential factor  $e^{-\tau}$  can be approximated by  $(1-\tau)$  and the radiative transfer equation (2) can be linearized

$$\begin{aligned} T_B'(f) &= T_{back} (1 - \int_0^\infty \alpha ds) + \int_0^\infty T \alpha ds \\ T_B'(f) &= T_{back} + \int_0^\infty (T - T_{back}) \alpha ds \end{aligned} \quad (3)$$

where  $T_B'$  is the linearized brightness temperature. Its relation to the measured brightness temperature  $T_B$  is as follows:

$$T_B' = T_{back} - (T_{eff} - T_{back}) \ln \left( 1 - \frac{T_B - T_{back}}{T_{eff} - T_{back}} \right) \quad (4)$$

Following the mathematical description as given in Wu (1979) it is possible to write the path delay as a linear combination of the linearized brightness temperatures  $T'_{B,1}$  and  $T'_{B,2}$ ,

where the subindices 1 and 2 denote the two observation frequencies 23.8 and 31.5 GHz:

$$P_{D,R} = a_0 + a_1 T'_{B,1} + a_2 T'_{B,2} \quad (5)$$

The constants  $a_0$ ,  $a_1$  and  $a_2$  are the *inversion coefficients*.

### 2.3 Determination of the Inversion Coefficients

In principle the inversion coefficients depend on the meteorological conditions at a particular location. In order to have more detailed knowledge of possible variations and their impact on to the path delay pattern has been investigated in Switzerland. Therefore a one-year meteorological radiosonde data set from Payerne, performed by the Swiss Meteorological Service, was used to compute the inversion coefficients. The summarized result from this simulation analysis (c.f. table 1) indicates that the error for the path delay determination using sonde measurements is in the order of some 2 to 4 mm (depending on whether seasonal variati

INVERSION COEFFICIENTS AND RESIDUAL ERORS IN ZENITH PATH DELAY CORRECTIONS AS DERIVED FROM RADIOSONDE DATA				
Season	$a_0$ [cm]	$a_1$ [cm/K]	$a_2$ [cm/K]	error [cm]
Winter	-0.717	0.545	-0.311	0.23
Spring	-0.707	0.539	-0.307	0.35
Summer	-0.669	0.510	-0.291	0.37
Fall	-0.691	0.526	-0.300	0.39
<b>Year (mean)</b>	<b>-0.696</b>	<b>0.530</b>	<b>-0.302</b>	<b>0.47</b>

Table 1: Inversion coefficients and residual errors in path delay computation in zenith as obtained from radiosonde data performed by the Swiss Meteorological Service.

### 3. HARDWARE INSTRUMENTATION

The main goal of the project was to develop a TRANSPORTABLE radiometric system for field applications which is able to match the envisaged measurement accurarcy. In order to permit an easy transportation, the system was subdivided into four main parts (c.f. fig. 1):

1. The 23.8 / 31.5 GHz radiometer with mount and tripod,
2. meteorological data acquisition system,
3. PC and control electronics.
4. Calibration box for hot- and cold loads (not visible in fig. 1)

The WVR is suspended in a mount which enables the tracking of GPS satellites in time and space. A meteorological data acquisition system measures ground temperature, pressure and relative Humidity. This data can either be stored or transmitted directly to the connected PC.

The computation of the satellite ephemerides as well as the steering of the entire system is performed by a Laptop Computer and a control unit containing power supplies, an interface selector and the motor control circuits. Since it is possible to track the satellites the path delay pattern as a function of the satellite distribution can directly be measured.



*Fig. 1: Transportable Microwave Water Vapor Radiometer (WVR) measuring system of the Institute of Geodesy and Photogrammetry at ETH Zurich in operating position.*

#### 4. FIELD APPLICATIONS

Extended measurements have been carried out in 1990 and 1991 in the framework of an ERS-1 - Project dealing with precise relative vertical position measurements called Compass II. It is organised under the leadership of the Space Radar Group of the Rutherford Appleton Laboratory in Didcot, Chilton, U.K. The main task of this project is to determine the vertical range to the ERS-1 satellite over selected land stations during the overpass of the satellite using specially designed radar transponders. These transponders perform a high precision altimeter delay calibration technique which can be compared with SLR-measurements. Since the radar transponders work in the microwave range, the obtained range measurements are affected by the tropospheric path delay.

Therefore several WVR's as well as dedicated sonde equipments have been used in order to perform direct measurements of the columnar water vapor content and thus the path delay at the transponder locations. The selected stations are located in the Zillertal (Tirol,Austria) and in Revine-Lago in Northern Italy. Presently one WVR equipment of ETH is working at Zimbabwe while another WVR from JPL is working at Lions Head in Alaska. Recent results of the transponder measurements revealed a very high resolution of about  $\pm 2$  mm. With the corrections due to the tropospheric columnar water vapor content as determined by the WVR and sonde equipments, the resulting accuracy is estimated to be in the order of 1 to 3 cm.

## 5. CONCLUSIONS

From the geodetic point of view many tasks remain where an improved knowledge of the tropospheric path delay is of high interest, such as ongoing or future satellite missions (ERS-1, ERS-2, Topex/Poseidon) or VLBI and GPS in general. Hereby the use of transportable WVR systems is urgently needed.

## 6. REFERENCES

- Liebe, H.: "An updated model for millimeter wave propagation in moist air", *Radio Science*, Vol. 20, No. 5, pp. 1069-1089, 1985.
- Wu, S.: "Optimum Frequencies of a passive Microwave Radiometer for Tropospheric Path Length Correction.", *IEEE Trans. Ant. and Prop.*, Vol. AP 27, No. 2, 1979.
- Westwater, E.: "The accuracy of water vapor and cloud liquid determination by dual frequency ground-based microwave radiometry.", *Radio Science*, Vol. 13, No. 4, pp. 677-685, 1978.



## THE "TIR"-PROJECT - TRANSIONOSPHERIC RADIO PROBING WITH SATELLITE SIGNALS

E.L. AFRAIMOVICH, V.N. ZVEZDIN, N.P. MINKO, A.I. TEREKHOV,  
S.V. FRIDMAN  
SibIZMIR, Irkutsk 33, P.O. Box 4026,  
664033, Russia

**ABSTRACT.** The objective of the competitive "TIR"-Project funded by the Siberian Division of the USSR Academy of Sciences (1988-1991), was to develop a package of hardware-software and models which are thought to provide a qualitative break through in investigations of the ionosphere as a physical medium and as a radio wave propagation channel on the basis of transitionospheric sounding using satellite signals.

Within the "TIR"-Project, SibIZMIR constructed three instruments which were used to conduct a series of simultaneous measurements during the period November 1989 - December 1990. The data obtained (the overall amount of ~200 MB), referenced to exact time, are stored on magnetic tape and diskettes, with the purpose of a subsequent digital processing on a computer of the type of PDP-11 and IBM-compatible personal computers.

1) The TIR radio interferometer is designed for simultaneous measurement of the main parameters of the radio signal from geostationary satellite ETS-2 at 136 MHz (polarization, angles of arrival, Doppler frequency shift, and amplitude - with a time resolution of 30 s; amplitude and phase scintillations and fast depolarization at spaced-antenna reception with 0.2 s resolution).

2) The hardware-software system is intended for investigating, at spaced-antenna reception, of scintillations of the satellite radio signal with circular polar orbit (Polar Bear-4) at 137 MHz as well as of small- and medium-scale irregularities causing these scintillations.

3) The hardware-software system is designed for studying the medium- and large-scale (100-2000 km) ionospheric structure on the basis of Doppler measurements of signals from navigation "Transit" satellites at 150 and 400 MHz using a standard receiver of this system and a personal computer.

We have been using the experimental data obtained within the "TIR"-Project, in conjunction with data of routine measurements of ionospheric conditions, the Earth's magnetic field and of solar activity made at the SibIZMIR observatories near Irkutsk, in comprehensive studies of the transitionospheric propagation of radio waves, including estimating errors of navigation systems and radio astronomical interferometers; and when investigating the structure, dynamics, interaction and transformation of ionospheric irregularities simultaneously in a wide range of scales (from 100 m to 1000 km).

For a more effective data processing and interpretation, within the "TIR"-Project we have developed new algorithms based on state-of-the-art ideas of computer tomography and on methods of spectral, correlation and fractal analyses.

An important component of the project involves the development of geophysical models of the ionospheric inhomogeneous structure, without which it is impossible to achieve an adequate data interpretation and to develop effective methods to predict and correct distortions of transitionospheric signals.

Results of an investigation of refraction effects during the transitionospheric propagation under quiet and magnetically disturbed conditions, and also relevant prediction and correction methods obtained as part of the "TIR"-Project, are presented in separate papers.

The purpose of this paper is also to call researchers' attention to the data obtained by these authors, for possible cooperation at the stage of problem formulation or a cooperative secondary processing and interpretation of the data.

## LIMITATIONS IN DATA QUALITY IMPOSED BY THE IONOSPHERE

YANG YI-PEI

Beijing Astronomical Observatory, Academia Sinica,  
Beijing 100080, China

T.A.TH. SPOELSTRA

Netherlands Foundation for Research in Astronomy,  
Postbus 2, 7990 AA Dwingeloo, The Netherlands

**ABSTRACT.** The aim of the correction methods to improve the data affected by ionospheric refraction is to reduce the ionospheric influences to such a low level that the accuracy of the data is only limited by the instrument used to detect the radio signals of interest. We estimate the tolerances that are required and can be expected for different measurement techniques.

Fundamental limitations relate the inhomogeneities in the magneto-ionic characteristics of the medium and too simple models and algorithms.

### 1. INTRODUCTION

Geodetic observations need to be calibrated to provide meaningful results. Calibration means comparison with an a known reference, which ultimately determines the accuracy. In the calibration process one has to take into account several constraints, such as characteristics of the measuring instrument, characteristics of the calibrator, logistic constraints. In this paper we restrict ourselves to calibration of ionospheric refraction, so that after calibration the quality of the data is limited by other sources.

### 2. REFRACTION PROBLEM IN THE CALIBRATION

We define dynamic range as the ratio between the maximum value of the parameter of interest and the maximum of its error and tolerance as the maximum acceptable spread in position errors allowed to reach the desired dynamic range. The tolerances one derives for the corrected data (and from those also for the correction parameters) depend strongly on the distribution of the remaining errors as a function of spatial coordinate, time and frequency used. In the calibration we are mainly concerned with the error map which involves also propagation errors, and which can be considered as a component of the sky-brightness-distribution times the beam reception pattern, convolved with an unknown complex function (Spoelstra, 1992). For the present problems this function implies the determination of the propagation errors. Tolerances for calibration are properly reached when the unknown complex error function is made smaller than the noise by calibration of the data.

The delay in a plasma is proportional to inverse frequency squared as is approximately expressed by:

$$t(\text{n sec}) = 134 v^{-2} \int N ds = 134 v^{-2} N_{\text{tot}} \quad (1)$$

where  $\nu$  is the frequency (Hz),  $N$  is the electron density ( $m^{-3}$ ),  $s$  is the pathlength (m) and  $N_{tot}$  is the total electron content along the ray path ( $m^{-2}$ ). For a required dynamic range of 1 mm on 1000 km or 90 dB at a frequency of 1 GHz  $N_{tot}$  should be known with an accuracy of  $6 \times 10^{13} m^{-2}$  or typically better than 0.1%. This accuracy cannot be achieved with the available techniques. It is realistic to assume that neither actual ionospheric data nor models provide an accuracy for the electron content along the line of sight better than typically about 10 - 15%.

The accuracy of sky coordinates is limited by the accuracy of the reference frames. A major problem concerns the systematic offsets between radio and optical reference frames which are independent of the catalogue used and which may be due to structure in the source. The current accuracy of available source positions is  $(0.^{\circ}01/\nu)$ , where the frequency is  $\nu$  in GHz.

TABLE 1  
Achievable Dynamic Range (in dB) [frequency  $\nu$  in GHz]

technique	range		geodetic baseline	
	single frequency	dual frequency	single frequency	dual frequency
altimetry	51 + 20 log $\nu$			
Faraday rotation	60 + 20 log $\nu$			
diff. Doppler	64 + 20 log $\nu$		64 + 20 log $\nu$	
GPS	66 + 20 log $\nu$	76 + 20 log $\nu$	78 + 20 log $\nu$	88 + 20 log $\nu$
VLBI			73 + 10 log $\nu$	~ 72

### 3. COMPARISON WITH MEASUREMENTS

In general it is very difficult to determine the ionospheric electron content with an accuracy of better than 15%. Taking this into account we may evaluate the following techniques (see also Table 1):

#### 3.1. Satellite Altimetry

Satellite altimetry utilizes a microwave radar altimeter to measure the nadir distance between an orbiting satellite and the earth's surface. The achieved accuracy is 2 - 10 cm (Callahan, 1984). With one frequency it is difficult to remove the first order of the propagation delay effect caused by ionized medium. Variations of total electron content, TEC, will directly affect the precise measurements. TEC variations can be  $6 - 40 \times 10^{16} m^{-2}$  in daytime, giving a range error of 1.3 - 8.0 cm at 13.7 GHz. Irregularities in the ionospheric electron content (spatial scales of a few hundred km) will cause errors of 0.1 - 4 cm. Dual frequency measurements (5 GHz and 14 GHz) may give errors of < 2 cm. A second limitation is due to the regularity of the surface: the more regular surface provides a better reflection and thus higher accuracy. It is also essential to know the precise satellite's orbit, particularly the radial component, since any error will directly affect the accuracy of the geoid determination.

#### 3.2. Faraday rotation

The Faraday rotation technique utilizing polarization of radio signals transmitted by quasi-geostationary satellites may also be used for geodetic purposes. A typical achievable

accuracy is  $\approx 3 \times 10^{16} \text{ m}^2$  because of the Faraday cycle ambiguity since in general only single frequency measurements are possible.

### 3.3. Differential Doppler

The US Navy Navigation Satellite System, NNSS, has been used for differential Doppler studies over the past two decades. The accuracies obtainable vary according to the length of time over which measurements were taken and on the computational techniques employed. Single-point positioning can not be achieved to better than about  $0.4/\nu^2 \text{ m}$ . Residual order effects restrict the achievable accuracy for vertical incidence typically by  $(0.4/\nu^3 + 0.2/\nu^4) \text{ m}$ , where the frequency is in GHz (Hartmann and Leitinger, 1984). The accuracy of the individual measurements is typically  $0.005/\nu^2 \text{ m}$  which implies that the quality of the results is largely limited by ionospheric effects. In particular, large errors may exist in the transformation between the slant electron content to the vertical content. In addition ionospheric irregularities will affect the accuracy.

### 3.4. VLBI

The VLBI technique employs radio telescopes to measure the delay difference in arrival time of a radio signal at two (distantly) separated stations. The signal is generated by any suitable extra-galactic radio source. It is possible to derive the three dimensional baseline between the stations with approximately centimetre accuracy. By dual frequency observations the first order of ionospheric effects can adequately be removed.

A limitation in VLBI is of course the limited accuracy of the source positions. This implies that the absolute positional accuracy cannot be better than  $\sim 5 \text{ cm}$ . Another important problem is that the physical states of the atmosphere above each interferometer element are not correlated with each other. In general it is assumed that the refraction error is the arithmetic mean of the contributions above each of the interferometer elements. This may imply a residual error source. A typical rms-spread in the results based on ionospheric data and dual frequency calibration is 0.23 nsec per day (Brouwer, 1985). With dual frequency techniques an accuracy level of 0.1 nsec is feasible which is equivalent with a relative positional accuracy for a baseline of 1000 km of 70 cm or a dynamic range of 72 dB. Using Faraday rotation measurements mapped to the VLBI observing direction a simple mapping algorithm gives results of lower quality than if solar and geomagnetic effects are included. The correlation between dual frequency and Faraday rotation calibration is weak (Scheid, 1985) indicating that the ionosphere has not been adequately modelled in the mapping function applied to Faraday rotation data at the required level for processing VLBI data.

### 3.5. GPS

The Global Positioning System NAVSTAR is primarily designed to provide high accuracy instantaneous three-dimensional positioning capability. Although the instantaneous positioning capability is less accurate than the NNSS system can provide (albeit from about 3 days observations), GPS can obtain relative position accuracies of the order of 1 cm by using interferometric techniques (Dodson, 1986). The achievable rms scatter of the range residuals for a single satellite from dual frequency P-code data is  $\approx 0.5 \text{ nsec}$  (or  $\approx 1.5 \times 10^{16} \text{ electrons m}^{-2}$ ) (e.g.: Lanyi and Both, 1988). Then the achievable tolerance for geodetic baseline  $L$  (km) is  $\Delta L \text{ (m)} \approx 0.15 L / (20000\sqrt{n})$  where  $n$  is the number of satellites used. Or for  $L = 1000 \text{ km}$  and  $n = 4$ ,  $\Delta L \approx 3.8 \text{ mm}$ .

Brunner and Gu (1991) proposed an improved model to calculate dual frequency corrections for ionospheric effects. In this model the ionospheric effects are calculated along the ray rather than along a geometric straight line. The higher order errors arising from the series expansion of the refractive index, the geomagnetic field effect and the bending effects of the ray paths are accounted in the model, that may reduce the range error to mm order in some extreme cases (less than 3 cm as a mean estimate).

Multipath effects may cause typical delay errors with magnitude of 3 nsec or 90 cm (Bishop et al., 1985). The correction method may be a combination of antenna design and siting, data processing, day-to-day correlation and fitting of data to simultaneous 'phase advance' measurements.

#### 4. DISCUSSION

Currently available models and formulas are based on the assumption that the ionosphere is uniform and homogeneous. Reality is much different and may be difficult to take into account to meet the requirement of higher accuracy for geodetic positioning. In practice the error considerations must of course be specialized for the measuring system used and for the actual situation. The limited accuracy of the models and algorithms (higher order of ionospheric effects, dispersion, ray bending, etc., are generally not sufficiently included) may reduce the accuracy by typically several cm (Hartmann and Leitinger, 1984).

Short term ionospheric variations complicate the calibration and imply a significant reduction of the achievable accuracy. They imply often range errors of a several mm. Single frequency observations can at times easily become useless for precise geodetic positioning under conditions of intense ionospheric activity. In radio astronomy, "self-calibration" methods have proved to be a successful tool to remove these rapidly varying effects. This technique may also be used in geodesy.

To schedule observations one may try to make a careful choice of ionospheric conditions. Climatological knowledge of ionospheric irregularities is useful since they can produce phase fluctuations which are one or two orders of magnitudes larger than the phase fluctuations of the measuring system. Another problem is the determination of ionospheric effects along the line of sight. In particular at large zenith angles no simple geometry can be assumed and due to the frequency dependence of the ray path errors of several percent may be introduced easily.

If ionospheric effects have a stochastic character long integration times may improve the achievable accuracy. However, if one integrates too long - and this depends of course on the conditions of the moment - systematic variations in the ionosphere may deteriorate the quality of the results. Improved climatological knowledge may be useful to improve estimates for achievable quality of the results.

#### 5. REFERENCES

- Bishop, G.J., Klobuchar, J.A., Doherty, P.H. (1985) *Radio Science* **20**, 388.
- Brouwer, F.J.J. (1985) Ph.D.Thesis, Delft University of Technology.
- Brunner, F.K., Gu, M. (1991) *Manuscripta Geodetica* **16**, 205.
- Callahan, P.S. (1984) *Marine Geodesy* **8**, p.249.
- Dodson, A.H. (1986) *Int.J.Remote Sensing* **7**, 515.
- Hartmann, G.K., Leitinger, R. (1984) *Bull.Géodesique* **58**, 109.
- Lanyi, G.E., Both, T. (1988) *Radio Science* **23**, 483.
- Scheid, J.A. (1985) *TDA Progress Report* 42-82, 11.
- Spoelstra, T.A.Th. (1992) this volume.

# MONITORING TOTAL IONOSPHERIC ELECTRON CONTENT AND IONOSPHERIC IRREGULARITIES WITH GPS

LAMBERT WANNINGER

Institut für Erdmessung (IfE), Universität Hannover  
Nienburger Str. 6, 3000 Hannover, F.R.G.

**ABSTRACT.** Dual-frequency code and carrier phase GPS measurements offer an excellent opportunity to monitor total ionospheric electron content (TEC) and ionospheric irregularities. This paper will discuss observation biases and errors. It will be shown that differential equipment group delays of the satellite and receiver hardware are the most significant biases. Their accurate determination depends on the ionospheric conditions. The ability to monitor irregularities is not affected by these biases.

## 1. IONOSPHERIC OBSERVABLES

The ionosphere is defined as that part of the atmosphere where sufficient ionization can exist to affect the propagation of radio waves. The most important effects on GPS signals are the retardation, or group delay, on the modulation carried on the radio wave, and the advance of the carrier phase. The degree of both effects depends on the physical properties of the ionosphere and the frequency of the penetrating electromagnetic wave – the higher its frequency the less the effect. The group delay of a signal propagated through the ionosphere is directly proportional, at least to first order, to total ionospheric electron content (TEC) along the signal path. First order effects of the phase advance correspond to those of the group delay except for their sign (e.g. Klobuchar, 1985). Higher order effects do not exceed 0.5 % of TEC at GPS frequencies, but they are usually much smaller. Therefore, TEC can be estimated from measurements of the two L-band GPS signals.

The ionospheric electron content is integrated along the signal path up to the GPS satellite altitude of 20,000 km. TEC from GPS includes the plasmaspheric electron content above an altitude of some 2000 km. Its contribution to the total electron content amounts to about 10–50 % mainly depending on the time of day and the world region (Soicher, 1977; Davies, 1990). Other TEC measuring systems (Faraday rotation measurements to geostationary satellites, or dual-frequency Doppler measurements to NNSS Transit satellites) or ionospheric models (Bent model, IRI) do not take the plasmaspheric electron content into account.

TEC is calculated from GPS code observations by

$$TEC_P = S * (P_2 - P_1) \quad [el/m^2] \quad (1)$$

$$S = \frac{1}{40.3} * \frac{f_1^2 * f_2^2}{f_1^2 - f_2^2} = 9.52 * 10^{16} \quad [el/m^3] \quad (2)$$

with the GPS frequencies  $f_1 = 1575.42$  MHz and  $f_2 = 1227.60$  MHz,  $S$  being a factor to convert differences of dual-frequency GPS P-code measurements  $P_1, P_2$  [m] to  $TEC$  [ $el/m^2$ ].

TEC can also be determined from dual frequency phase measurements except for the unknown numbers of whole cycles, the carrier phase ambiguities  $N$ , by

$$TEC_\phi = -S * ((\phi_2 + N_2) * \lambda_2 - (\phi_1 + N_1) * \lambda_1) \quad (3)$$

with subscripts identifying the signals  $L_1$  and  $L_2$ ,  $\phi$  [cycles] being the measured carrier phases,  $\lambda$  [m] the carrier wavelength, and  $S$  is defined in equation (2). Phase measurements are only suitable for determination of TEC if the unknown carrier phase ambiguities can be estimated.

Another way to use the ionospheric information of dual frequency phase measurements is to eliminate the ambiguities by forming time differences. If no cycle slip occurs between two measurement epochs  $t_1$  and  $t_2$ , the time difference is free of any unknowns:

$$\Delta TEC_\phi(\Delta t_{12}) = -S * ((\phi_2(t_2) - \phi_2(t_1)) * \lambda_2 - (\phi_1(t_2) - \phi_1(t_1)) * \lambda_1) \quad (4)$$

The resolution of GPS carrier phase measurements is so high that this rate of TEC observable gives an excellent means to observe ionospheric irregularities.  $\Delta TEC_\phi$  depends very much on the GPS satellite orbits for two reasons. On the one hand the elevation angle of the signal incidence direction changes with up to 0.5 deg/min. The smaller the elevation angle the longer is the signal path through the ionosphere and the larger is the measured TEC. Thus, the primary effect which is observed is the change of the elevation angle. However, periodic effects caused by irregularities can be detected quite easily, as long as their period is considerably smaller than the length of an orbit arc as seen from one station (2–7 hours, 1000–2000 km in ionospheric altitude). Moreover, the point of interception of a GPS signal with the area of ionospheric irregularities (in an altitude of e.g. 400 km) moves due to the satellite orbit with a velocity of 50 to 450 m/s. Taking into account that a typical GPS receiver has a maximum output rate of 1 Hz, an irregularity has to have an extension of at least some hundred meters to be observable. Smaller structures can be detected but not observed in detail. In this paper rate of TEC over a time difference of 1 min is discussed because it can be obtained as a by-product of geodetic GPS measurements.

## 2. BIASES AND ERRORS

In order to estimate the electron content of the ionosphere differences of dual-frequency measurements are formed. All those biases and errors which are the same for both frequencies cancel out: clock biases of the satellites and of the receiver, clock dithering due to Selective Availability (SA), and tropospheric refraction. The remaining biases and errors are differential equipment group delays, multipath, phase center offsets, phase center variations and imaging effects.

## *2.1 Differential equipment group delays*

The P-codes transmitted from GPS satellites at the two frequencies show a synchronization bias due to different hardware paths inside the transmitter. Similar effects are also known for the receiver hardware.

The requirements on the GPS satellites demand that the satellite differential equipment group delays shall not exceed 15 ns ( $43 \times 10^{16} \text{ el/m}^2$ ) and random variations shall not exceed 3 ns ( $9 \times 10^{16} \text{ el/m}^2$ ,  $2\sigma$ ) (Rockwell, 1984). Actual differential delays were determined in prelaunch factory tests. These values do not exceed 3 ns ( $9 \times 10^{16} \text{ el/m}^2$ ) for Block I satellites (Dahlke et al., 1988; Coco et al., 1991). Prelaunch testing values are also included in the satellite broadcast message (Rockwell, 1984). They have been broadcast for all satellites since the fall of 1990. Maximum values are about  $12 \times 10^{16} \text{ el/m}^2$ . But these values do not agree with those in the literature, nor with values estimated as combined satellite and receiver differential delays at Institut für Erdmessung (IfE) from GPS P-code measurements.

Satellite and receiver differential delays can only be separated from each other if additional ionospheric information is introduced: Coster and Gaposchkin (1989) separated these delays by using an ionospheric model, and thus they introduced errors due to inaccuracies of the model.

From GPS observations alone an estimation of combined satellite and receiver differential delays can be performed as shown by Lanyi and Roth (1988) and Dahlke et al. (1988). They used  $TEC_P$  measurements from a mid-latitude nighttime observation period to estimate the coefficients of a two-dimensional low-order polynomial model of the vertical TEC and the combined satellite and receiver differential delays in a least-squares process.

The same approach can be used for  $TEC_\phi$  data (Wild et al., 1989). Here, one unknown is estimated for each satellite consisting of the carrier phase ambiguities plus satellite and receiver differential equipment phase delays. One additional unknown has to be introduced for each cycle slip. But accurate results are only achievable if (almost) all cycle slips have been removed beforehand. The advantage of using  $TEC_\phi$ -data lies in the ability to use observations of hybrid receivers, which do not measure the P-code on  $L_2$  but obtain the phase on  $L_2$  by squaring the signal.

Four important assumptions are made in this estimation method: TEC is constant in a rotating reference frame, TEC and vertical TEC (VTEC) are related by an obliquity factor which is a function of the elevation angle only, satellite and receiver differential delays are constant over several hours and the electron distribution of the ionosphere shows small horizontal gradients in order to fit to a simple model.

Therefore, best results can be achieved in a mid-latitude nighttime observation period. Results are poorest in equatorial daytime observation periods with their large TEC gradients. The main problem is the separation of the receiver differential delay from average VTEC. Both unknowns are highly correlated due to the limited geometry of GPS-TEC-measurements. Measurements at low elevation angles reduce this correlation but introduce the problems of increased multipath (can be effectively reduced by carrier smoothed code) and of much poorer results in mapping TEC to VTEC. The contribution of the satellite differential delays to the combined delays is estimated with much higher accuracy. Here, a dense coverage of the sky with satellite paths is of importance. Mid-latitude and high-latitude sites experience a poorer coverage than equatorial sites because of the Block II satellite orbital inclination of just 55 deg.

If satellite and receiver delays or combined delays are known, GPS- $TEC_P$ -observations can immediately be corrected. But this requires that the delays are fairly constant between two calibrations. Differential equipment group delays are known to be very sensitive to temperature changes. The receiver must be calibrated at the temperature of its later use. Geodetic GPS-receivers are usually not built to keep a constant differential equipment delay. Periodic effects or drifts do not affect positioning accuracy, as long as they are identical for all channels. Experiences with Ashtech P-code receivers (beta version) show that day-to-day variations of up to 3 ns ( $9 \times 10^{16} el/m^2$ ) occur. Variations of the TI 4100 are much smaller if the receiver is temperature controlled.

Coco et al. (1991) reported that no significant variations of differential delays of Block I satellites could be found over a time span of five weeks, nor over a time span of 2 years. No experiences with variations of differential delays of Block II satellites have been reported in the literature.

If the variations of the differential delays are too big or as long as they are not calibrated, combined delays must be determined from existing GPS observations together with a simple ionospheric model. This approach succeeds in areas and time periods of very small horizontal gradients (mid-latitude, nighttime) with an accuracy of about  $2 \times 10^{16} el/m^2$ . But in areas and time periods of large gradients (e.g. equatorial anomaly, daytime) the accuracy degrades considerably.

## 2.2 Multipath

Multipath errors occur if the received signal is composed of the direct line of sight signal and one or more constituents which have propagated along paths of different length. Different propagation paths result from either reflection at the satellite or in the surroundings of the receiving antenna. Multipath effects are not identical for signals of different frequencies. Thus, they do not cancel out forming an ionospheric observables. The effect of multipath on code measurements is 2 orders of magnitude larger than its effect on carrier phase measurements (Bishop et al., 1985).

Satellite multipath can hardly be proven nor estimated from actual GPS measurements (Young et al., 1985). Its effect is expected to be considerably smaller than maximum receiver multipath.

Experiments at IfE showed that the effect of receiver multipath on ionospheric observables can reach up to 10 ns (code) or 0.1 ns (phase) in a highly reflective environment. It appears in cyclic variations with periods from 1 min to more than 1 h due to changing geometry between satellite, reflector and antenna. Especially the short periodic multipath effects influence the rate of TEC observable with biases of up to 0.1 ns/min. Multipath effects can be minimized by selection of an appropriate antenna (reduced low-angle response), careful attention to antenna siting and the use of absorbing material in the vicinity of the antenna. Effects on  $TEC_P$  observations can substantially be reduced by combining code and carrier observations.

## 2.3 Phase center offsets and imaging

The physical center of a GPS antenna does not generally coincide with the point at which the signal is received. The point to which the radio measurements are referred, the phase center, is the apparent electrical center of the antenna. The phase centers of the two GPS frequencies are independent of each other and will coincide only by chance. Moreover, the apparent phase center position will be a function of the signal

TABLE 1.  
Biases and errors of ionospheric GPS observables

Observable	$TEC_P$	$TEC_\phi$	$\Delta TEC_\phi(\Delta t = 1 \text{ min})$
Units	$10^{16} \text{ el/m}^2$	$10^{16} \text{ el/m}^2$	$10^{16} \text{ el}/(\text{m}^2 * \text{min})$
Range	1 – 500	1 – 500	0 – 7
Differential equipment group delays			
– of satellites	0 – 12 (- 43)		
– of receiver	0 – 20 (- ??)		
– combined determination from observations (including carrier phase ambiguities of $TEC_\phi$ )	2 – 15	2 – 15	
Multipath	0 – 30	0 – 0.3	0 – 0.3
Phase center offsets		0 – 0.5	0.00
Random Observation Errors ( $1\sigma$ )	1.5 – 15	0.02 – 0.05	0.03 – 0.07

incidence direction due to a non-spherical phase pattern of the antenna. The antenna phase patterns of the two frequencies are independent of each other.

Phase center locations for copies of a single model of antenna tend to be consistent. They can be determined in laboratory experiments and then be used to correct the ionospheric observable. Schupler and Clark (1991) determined phase center offsets and phase center variations for 5 standard GPS antennas, according to which  $L_1/L_2$  offsets can reach 0 – 5 cm ( $0.0 – 0.5 \times 10^{16} \text{ el/m}^2$ ). The full bias propagates to the ionospheric observable when the  $L_1/L_2$  offset direction coincide with the signal incidence direction. Rate of TEC will almost not be affected because the  $L_1/L_2$  offset changes slowly with time due to the slow changes in satellite geometry.

Antenna imaging is caused by conducting material in the vicinity of the antenna. An antenna 'image' in the conductor interferes with the phase pattern of the antenna (Tranquilla, 1986). It causes environmentally-induced phase center variations. This effect diminishes with increasing distance between antenna and conducting body. Antenna imaging has to be avoided by careful attention to antenna siting.

#### 2.4 Random observation errors

Observation errors are due to the limitations of the receiver's electronics and are of a random character. They can effectively be reduced by averaging. Depending on the quality of the receiver a single P-code measurement can be performed with an observational error ( $1\sigma$ ) of 0.1 – 1 m and a carrier phase measurement with 1 – 3 mm. These errors propagate to the ionospheric observables with  $1.5 – 15 \times 10^{16} \text{ el/m}^2$  and  $0.02 – 0.05 \times 10^{16} \text{ el/m}^2$  respectively. The rate of TEC observable has then a random observation error of  $0.03 – 0.07 \times 10^{16} \text{ el/m}^2$  per time unit. The accuracy of codeless (cross-correlating) receivers is degraded at low elevation angles.

#### 2.5 Summary

Biases and errors of ionospheric GPS observables are summarized in Table 1. Differential equipment group delays are of systematic character. If they are not corrected, they can easily lead to misinterpretation of TEC data, especially when TEC is small. The accuracy of a combined determination from observations depends very much on the ionospheric conditions. Multipath effects and random observation errors of code

measurements can be reduced to a neglectable level by smoothing with the carrier phases. Multipath is the only error source of importance of the rate of TEC observable. It must be avoided by careful attention to antenna site selection.

### 3. CONCLUSIONS

The accuracy of GPS-TEC-observations is primarily limited by differential equipment group delays originated in the satellite and receiver hardware. An estimation of the combination of these biases can be performed from GPS observations. But the accuracy of this determination depends on the present conditions of the ionosphere. Therefore, it would be very advantageous to use predetermined calibration values of these biases. This requires receivers with a very much stable differential delay. It requires as well the observation of the satellite differential delays and their publication. GPS rate of TEC observations offer en excellent means to monitor ionospheric irregularities. Here, the effect of biases and errors are usually very small.

ACKNOWLEDGEMENT. This work was supported by the Deutsche Forschungsgemeinschaft under grant SE 313/12.

### REFERENCES

- Bishop, G.J., Klobuchar, J.A., Doherty, P.H. (1985). Multipath effects on the determination of absolute ionospheric time delay from GPS signals. *Radio Science*, **20**, 388-396
- Coco, D.S. (1991). GPS - Satellites of opportunity for ionospheric monitoring. *GPS World*, **2**, No.9, 47-50
- Coco, D.S., Coker, C., Dahlke, S.R., Lynch, J.R. (1991). Variability of GPS satellite differential group delay biases. *IEEE Transactions on Aero. Elec. Sys.*, **27**, 931-938
- Coster, A.J., Gaposchkin, E.M. (1989). Use of GPS pseudo-range and phase data for measurement of ionospheric and tropospheric refraction. *Proc. ION-GPS '89*, Colorado Springs
- Dahlke, S.R., Coco, D.S., Coker, C.E. (1988). Effect of GPS system biases on differential group delay measurements. ARL-TP-88-17, The University of Texas, Austin
- Davies, K. (1990). *Ionospheric Radio*. Peter Peregrinus Ltd., London
- Georgiadou, Y., Kleusberg, A. (1988). On carrier signal multipath effects in relative GPS positioning. *Manuscripta Geodaetica*, **13**, 172-179
- Klobuchar, J.A. (1985). Ionospheric time delay effects on earth-space propagation. In *Handbook of Geophysics and the Space Environment*, ed. A.S. Jursa, U.S. Air Force
- Lanyi, G.E., Roth, T. (1988). A comparison of mapped and measured total electron content using GPS and beacon satellite observations. *Radio Science*, **23**, 483-492
- Rockwell (1984). NAVSTAR GPS space segment / navigation user interfaces ICD-GPS-200, Rockwell Int. Space System Group
- Sochier, H. (1977). Plasmaspheric signal time-delay effects in satellite navigation systems. In *AGARD CP 209*
- Schupler, B.R., Clark, T.A. (1991). How different antennas affect the GPS observable. *GPS World*, **2**, No.10, 32-36
- Tranquilla, J.M. (1986). Multipath and imaging problems in GPS receiver antennas. *Proc. 4<sup>th</sup> Int. Geod. Symp. Sat. Pos.*, Austin
- Young, L.E., Neilan, R.E., Bletzacker, F.R. (1985). GPS satellite multipath: an experimental investigation. *Proc. 1<sup>st</sup> Int. Symp. Pos. GPS*, Rockville
- Wild, U., Beutler, G., Gurtner, W., Rothacher, M. (1989). Estimating the ionosphere using one or more dual frequency GPS receivers. *Proc. 5<sup>th</sup> Int. Geod. Sym. Sat. Pos.*, Las Cruses

# WATER VAPOR RADIOMETER FOR CHINESE VLBI AND GPS GEODESY

XU PEIYUAN

Institute of Electron Physics,  
Shanghai University of Science and Technology,  
Shanghai 201800, China

**ABSTRACT.** The water vapor radiometer (WVR) developed for meteorologic observation will be used to determine the wet path delay (WPD). Main characteristics of this WVR are described. This WVR may be suitable for high-accuracy VLBI and GPS Geodesy.

## 1. INTRODUCTION

In recent years several space geodesy projects and several VLBI and GPS networks have been established or are under development in China. To determine the WPD of space geodetic signals a proposal for developing the WVR had been considered in the early eighties. But when the parameter estimation method had been successfully used in the reduction of the space geodetic data, it was doubted whether the expensive WVR's are actually needed for high-accuracy VLBI and GPS. The development of WVR has been delayed for several years in the Chinese space geodesy community.

Such a parameter estimation can only accurately account for the temporal changes of the zenith delay, but is not effective for the spatial variations. A special experiment with five WVR's has shown that there are strong spatial WPD variations (Rocken, C. et al. 1991). When the Chinese space geodesy community reconsidered the WVR as one of the approaches for determining the WPD, they had no WVR in their hands.

Fortunately, the plan for developing WVR got strong support from the Chinese meteorological community. A new generation WVR has been operational in the Mesoscale Meteorological Experiment since 1988 and has shown its high accuracy, good stability and reliability (XU, P. et al. 1989). The second WVR was completed at last May and has been used in a weather modification experiment. Since 1991 the Radio Astronomical Openning Laboratory of the Academia Sinica has supported our research on the WPD with these WVR's. The research work has just begun. We introduce this Chinese WVR in the next section and give some discussion in the third section.

## 2. CHINESE NEW GENERATION WVR

The 20.60 GHz and 31.65 GHz radiometers are incorporated into one dual frequency WVR. The outline and the block diagram are shown in Figure 1, 2 and 3 respectively. The radiometer is of the Dicke type with digital demodulation. The 90° offset paraboloid antenna system not only has low sidelobes and high beam efficiency, but also simplifies the antenna mounting, decreases the antenna elevation rotating room and driven load, and provides high mechanical stability. The receiver box is controlled at  $30 \pm 0.5^\circ\text{C}$  and furthermore the ferrite

switch and the reference load are assembled in a small constant temperature ( $40 \pm 0.1$  °C) enclosure for each channel. So this WVR has very good thermal stability. The digital demodulation simplifies the analogue electronics and provides the precision, flexibility and reliability. This WVR is equipped with detectors for surface temperature (T), pressure (P) and humidity (e). Using the observed brightness temperature and surface values T, P and e, the IBM PC/AT can provide the WPD and transmit it to the VLBI and GPS data reduction system.

TABLE 1.  
WVR characteristics

Parameter	Specifications
Operating frequencies	20.60 and 31.65 GHz
Beamwidth	2.5 deg
Sidelobes	- 27 dB
Beam efficiency	90%
Pointing range	elevation 0 -- 270 deg azimuth 0 -- 360 deg
Scanning velocity	2 deg/sec
Pointing accuracy	elevation 0.1 deg azimuth 0.5 deg
Integration time	software selectable
Sensitivity	0.2 K (1 sec integration time)
Reference load	313 ± 0.1 K waveguide terminal
Calibration means	solid state noise diode, hot and cold microwave absorbers, tipping curve
Calibration accuracy	0.5 K
Observation, data preprocess	real time programmed, unattended

### 3. DISCUSSION

Before using the meteorological WVR to measure the WPD, it is necessary to review the meteorological observations and make a numerical experiment to estimate the possible achievable accuracy of the retrieved WPD. The numerical experiment (Zhao, Y. et al. 1990) with five years radiosonde data of the Shanghai Meteorological Observatory shows that the rms error of the WPD may be less than 4 mm. The precipitable water vapor measurement had been carried out with both the WVR and radiosonde (Zhao, C. et al. 1990 and 1991) by the Chinese Academy of Meteorological Science at Beijing. The rms difference of the precipitable water vapor between the WVR and the radiosonde is 0.3 (7%) in winter and 2.6 mm (6.4%) in summer. This measurement accuracy is comparable to that of the five WVR's mentioned above (Rocken, C. et al. 1991). These results are encouraging. We may conclude that the new generation Chinese WVR is suitable to determine the WPD for high-accuracy space geodesy.

## REFERENCES

- Rocken, C., Johnson J.M. et al. (1991), *IEEE Trans. Geosci. Remote Sensing* **29**, 3  
 Xu Peiyuan, Jin Peiyu et al. (1989) in *Proc. of URSI/IAU Sym. on Radio Astronomical Seeing*,  
 eds. J.E. Baldwin and Wang Shouguan, International Academic Publishers, Beijing, p. 87  
 Zhao Conglong, Cai Huaqing et al. (1991), *Quarterly Journal of Applied Meteorology* **2**, 200  
 Zhao Conglong, Xu Peiyuan et al. (1990), *Chinese Science Bulletin* **35**, 1807  
 Zhao Yinlong, Xu Peiyuan et al. (1990), *Journal of Shanghai University of Science and  
 Technology* **13**, 67

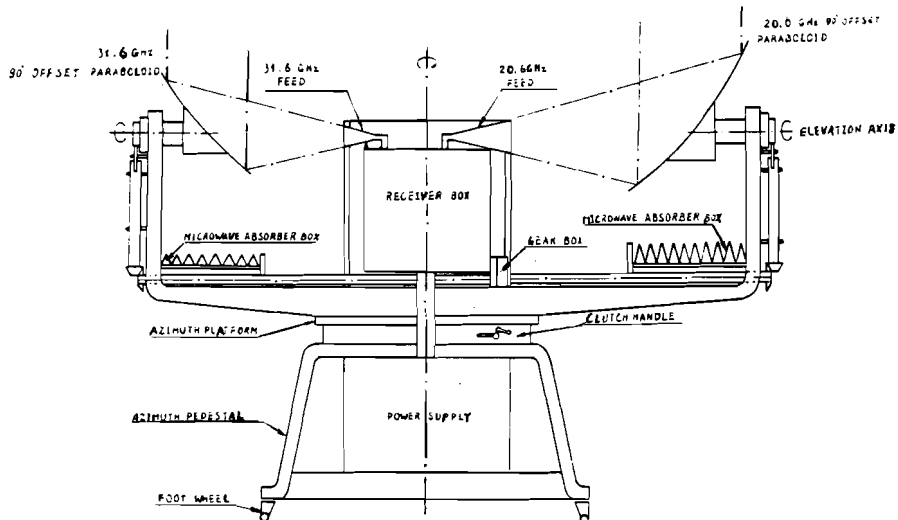


Figure 1. An outline of the Chinese WVR

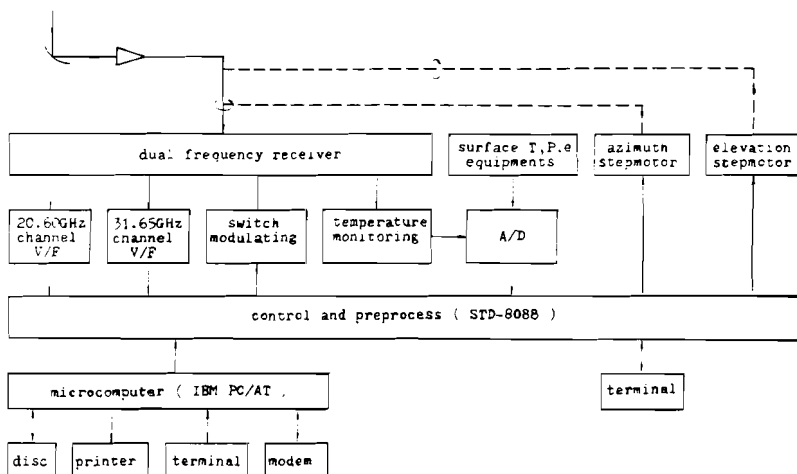


Figure 2. A block diagram of the Chinese WVR

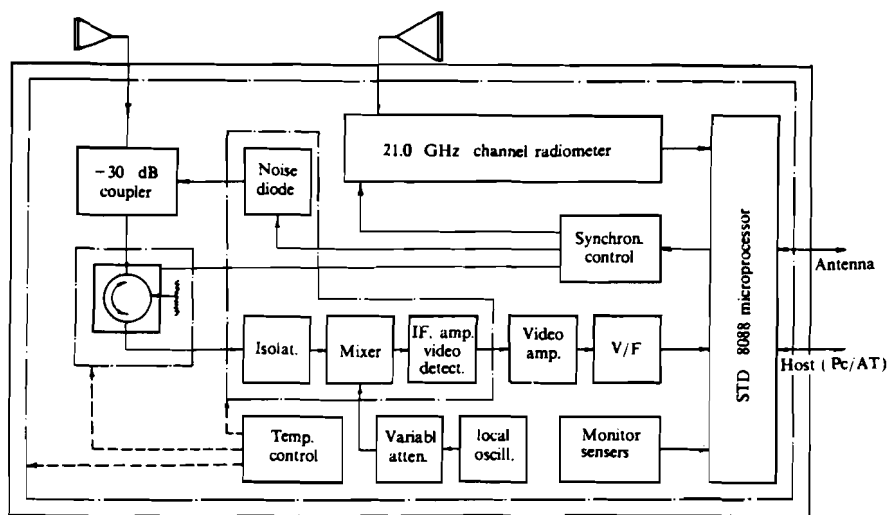


Figure 3. A block diagram of the Chinese WVR receiver

# IONOSPHERIC CORRECTIONS FOR RADAR ALTIMETRY AND GEODETIC POSITIONING TECHNIQUES

N. JAKOWSKI, H.-D. BETTAC, A. JUNGSTAND

Satellite Ground Station Neustrelitz

Kalkhorstweg, D-2080 Neustrelitz, FRG

**ABSTRACT.** Ionospheric refraction effects and corresponding propagation errors in satellite altimetry and geodetic positioning are estimated on the basis of long-term Total Electron Content (TEC) observations carried out in Neustrelitz and Havana at different longitude and latitude sectors. Since the accuracy of geodetic space techniques is limited in particular during ionospheric perturbations, the use of averaged storm pattern for correction and prediction purposes is discussed.

The use of ionospheric data for correction in geodetic space technique involves a suitable data transformation to the moving line of sight between transmitter and the receiver. This problem is discussed in relation to the ionospheric correction of altimeter radar data.

## 1. INTRODUCTION

Characteristic parameters of electromagnetic waves traversing the Earth's ionosphere are generally changed after leaving the ionosphere. Precise measuring and tracking systems using transitionospheric radio waves therefore have to take care for ionospheric corrections. This is done at different ways: 1. elimination of the first order ionospheric errors by difference methods using two frequencies (e.g. NNSS, GPS, PRARE), 2. calculation of the ionospheric errors on the basis of empirical models, 3. real time observation of the near-by ionosphere by separate techniques and calculation of the resulting errors.

Due to the complex spatial and temporal behaviour of the ionosphere all these methods are limited to a certain degree. This paper will contribute to points 2 and 3. In section 3. we discuss the use of experimental TEC data for the estimation of ionosphere induced range errors in active measuring systems. In section 4. the problem is discussed how altimeter radar data should be corrected by means of simultaneous beacon observations onboard the same satellite.

## 2. GENERAL CONSIDERATIONS

In order to discuss the following chapters in a more effective way the basic relations and assumptions are shortly outlined. At radio wave frequencies  $f$ , lying well above the plasma frequency  $f_p$  ( $\approx 10$  MHz), the refractive index of the ionosphere is approximated by  $n^2 = 1 - f_p^2 / f^2$ , where  $f_p$  is related to the electron density by  $N_e = 1.24 \times 10^{-2} f_p^2$  in S.I. units.

At frequencies above 100 MHz the refractive index can be written in the form

$$n = 1 - K / f^2 N_e, \quad \text{where } K = 40.28 \text{ in S.I. units.}$$

Thus transitionospheric radio waves suffer ionosphere induced delays for the phase  $\Phi$  and the travel time  $t$  according to  $\Phi_D = -\frac{2\pi}{c} \frac{K}{f} \int^R N_e ds$  and  $t_D = \frac{1}{c} \frac{K}{f^2} \int^R N_e ds$ , respectively.

The ionospheric range error  $\Delta R_I$  is then given by  $\Delta R_I = \frac{K}{f^2} \int_0^R N_e ds$  or, introducing the total

$$N_T = \int_0^R N_e ds \quad \text{by} \quad \Delta R_I = \frac{K}{f^2} N_T$$

Ray path bending and other second order effects can be ignored at higher frequencies since these errors fall with order 3 and higher in  $1/f$ . Following Hartmann and Leitinger (1984) a worst case estimation of residual ionospheric errors for vertical incidence provide an total error of about 2 cm at 2 GHz. From numerical ray tracing of radio waves at frequencies between 40 and 300 MHz emitted by geostationary satellites the ray path bending follows about  $\Delta s \sim N_T^2/f^4$  for Neustrelitz. At GPS-and higher frequencies this error is extrapolated to be less than 1 cm.

Typical ionospheric range errors for operating systems are summarized in table 1.

TABLE 1.

SYSTEM	frequencies (GHz)	$K/f^2$ ( $m^3$ )	$\Delta R_I$ (m) ( $N_T = 5 \times 10^{17} m^{-2}$ )	$t_D$ (ns)
GPS	$L_2=1.227$	$2.675 \times 10^{-17}$	13.38	44.6
	$L_1=1.575$	$1.624 \times 10^{-17}$	8.12	27.1
PRARE ERS-1	$f_S = 2.248$	$0.797 \times 10^{-17}$	3.99	13.3
	$f_X = 8.489$	$0.056 \times 10^{-17}$	0.28	0.9
ALT	$f_{ku}=13.8$	$0.021 \times 10^{-17}$	0.11	0.4

### 3. CORRECTIONS USING EMPIRICAL TEC DATA

Ionospheric refraction depends on a variety of ionospheric parameters reflecting a big variability with day-time, season, solar and geomagnetic activity. The regular or large scale variations may be well reflected within an empirical model for a fixed station where the data are taken from. Problems arise when ionospheric perturbations or irregularities at various spatial and temporal scales shall be included or predictions for geographically and geomagnetically different locations have to be derived. Fig. 1 presents fitted day-time total electron content data obtained by means of the Faraday rotation technique (Bettac and Wiener, 1975) using the VHF beacons of various geostationary satellites received in Havana ( $23.1^\circ N$ ,  $82.5^\circ W$ ) and Neustrelitz ( $53.3^\circ N$ ,  $13.1^\circ E$ ). Both the seasonal variation as well as the dependence from the level of solar activity given by the 10.7 cm radio flux index F10.7 are well documented. The fitted curve has been derived using 27 day averages of a two hour interval around local noon. In order to illustrate the ionospheric error for a single-frequency GPS user, the range error for vertical incidence is scaled inside Fig. 1 in relation to the TEC scale. According to the absolute r.m.s. errors in TEC of  $6 \times 10^{16} m^{-2}$  at both stations the corresponding L1 range error amounts to about 1 m. But this estimation is only valid in a 27 day average sense. The day-to-day variability of TEC is higher and may reach 30% with respect to monthly averages (Jakowski and Jungstand, 1986). Nevertheless a single station empirical model can be constructed which allows more accurate estimations at TEC as global ionospheric models.

Taking into account recent results concerning the mean behaviour of ionospheric storms in TEC (Jakowski et al., 1989), the long term r.m.s. error in describing the average behaviour of TEC can be reduced to a certain degree. This is due to a seasonal difference in the mean storm behaviour over about 4 consecutive days after the storm onset. The averaged storm pattern of the percentage deviation from the "normal" behaviour derived for the Havana station are shown in Fig. 2. Comparing the mean storm behaviour of summer and winter, particularly on storm days SD2 and SD3, the opposite behaviour of deviations in TEC and foF2 are evident, showing a negative phase in summer and a well documented positive phase in winter. The knowledge of this behaviour which is well documented also at the

European sector. (Jakowski et al., 1989), may be helpful to give more accurate predictions of ionospheric errors during geomagnetic perturbations.

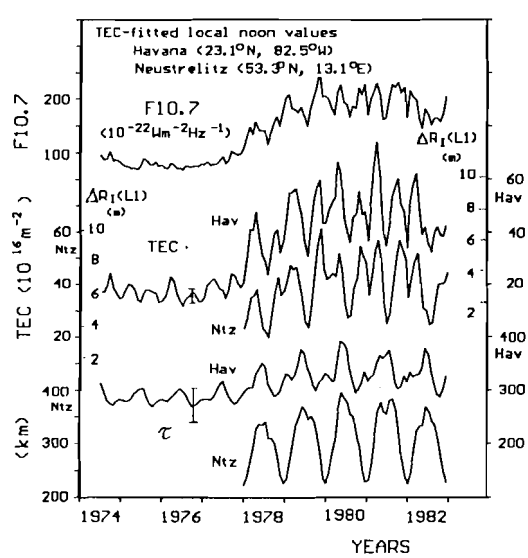


Figure 1. Best fitting functions of the vertical total electron content TEC and slab thickness  $\tau$  measured in Havana and in Neustrelitz around local noon. The data are related to the solar F10.7 cm radio flux.

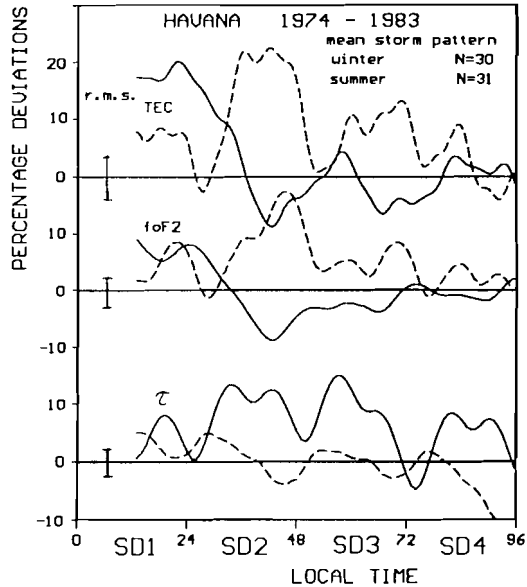


Figure 2. Local time variations of storm associated percentage deviations  $\Delta$ TEC,  $\Delta$ foF2 and  $\Delta\tau$  from control curves for winter and summer conditions derived from Faraday rotation observations in Havana.

#### 4. CORRECTION OF ALTIMETER RADAR DATA USING SIMULTANEOUS RADIO BEACON DATA ONBOARD THE SAME SATELLITE

According to table 1 altimeter radar measurements in the Ku-band have to take into account ionospheric range errors in the order of 1...2 decimeter. If a higher accuracy is required ionospheric corrections are necessary. Following the results discussed in the previous chapter, empirical models can be used to reduce the range error in general to less than 10 cm. A more accurate method are simultaneous observations of the ionosphere traversed by the altimeter radar. Such a combination of measuring systems has been planned for the ERS-1 mission, where the precise range and range rate equipment (PRARE) was planned to provide ionospheric correction data for the altimeter radar. Although PRARE could not be activated onboard ERS-1, future missions will have similar opportunities.

Let's assume an operative radio beacon system called PRARE onboard the altimeter radar satellite (Fig.3). In order to remove the ionospheric range errors some problems remain. Since the radio beacon link is directed to the receiving stations this ray path differs usually seriously from the vertical radar path. Thus the mapping of the measured slant TEC to the vertical TEC at the location of the altimeter measurement is of crucial importance. Although the shape of the electron density profile plays a certain role, in a first approximation the vertical content  $N_{TV}$  can be derived by the measured slant content  $N_{TS}$  by  $N_{TV} = N_{TS} / \sec \chi$  where  $\sec \chi$  is taken from a mean ionospheric height. Although the problem

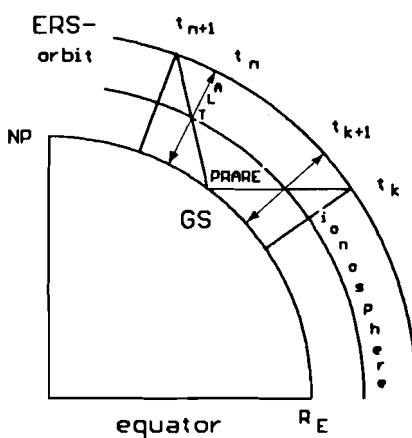


Figure 3. Illustration of the geometry of the vertical altimeter radar and a slant radio beacon (PRARE) onboard of an Earth Research satellite in the meridional plane

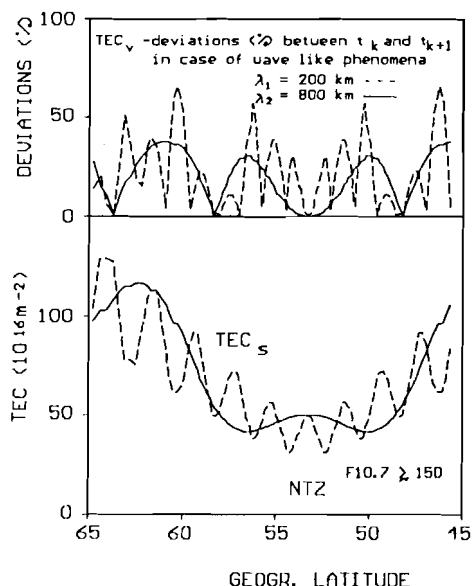


Figure 4. Relative errors in TEC determination when the time displacement between PRARE and altimeter radar observation is ignored.

of data reduction is much more comprehensive, in this paper we want to underline that the altimeter data should be corrected with PRARE data obtained at those times which minimize the difference between the location of the mapped vertical content and the altimeter subsatellite point. If this is ignored considerable errors may occur which are illustrated in Fig.4 for a wave-like variation of TEC assuming wavelength's of  $\lambda_1 = 200$  km and  $\lambda_2 = 800$  km (bottom). The percentage errors which arise when simultaneous data are taken instead of corresponding time-displaced data are shown in the upper part of Fig.4. Steep meridional gradients of the electron density induce considerable errors exceeding 50% in this example which results in an average error of about  $\pm 8$  cm in the altimeter data.

## 5. CONCLUSIONS

Long-term observations of TEC may help to develop empirical models of the ionosphere, well suited for corrections in geodetic and navigational space technique and radar altimetry. Comprehensive models of the ionosphere like the International Reference Ionosphere IRI (Bilitza, 1986) are mainly related to the lower ionosphere up to F2 layer heights. Since the "center of gravity" of the electron density profile lies above the F2 layer maximum height, such models should be updated by regional and global TEC-measurements for the correction of radio propagation errors. The development of regional TEC-models based f.i. upon radio beacon observations on NNSS, geostationary and GPS satellites should be valuable for the estimation of the ionospheric error sources in various operating measuring systems. Due to the high variability of the ionosphere the accuracy can be enlarged only by simultaneous observations of the ionospheric behaviour. In case of non-local observations, the data reduction to the point of measurement has to be done carefully, particularly in case of irregularities and wave-like phenomena, both characterized by steep gradients in TEC.

## REFERENCES

- Bettac, H.-D., Wiener, A. (1975) Nachrichtentechnik-Elektr. **25**, 452
- Hartmann, G.K., Leitinger, R. (1984) Bull. Geod. **58**, 109
- Bilitza, D. (1986) Radio Sci. **21**, 343
- Jakowski, N., Jungstand, A. (1986) Gerl. Beitr. Geophys. **95**, 213
- Jakowski, N., Putz, E., Spalla, P. (1990) Ann. Geophys. **8**, 343

## **8. MODELS, THEORY, CORRECTION TECHNIQUES**



## MODELING ATMOSPHERIC DELAYS IN THE ANALYSIS OF SPACE GEODETIC DATA

T. A. HERRING,  
Massachusetts Institute of Technology,  
77 Massachusetts Avenue,  
Cambridge, MA 02139, USA

**ABSTRACT.** We examine the rationale for some of the modern techniques for accounting for and modeling atmospheric delays, and we present new results and models for use in the analysis of space geodetic data. In particular, we review the separation of the atmospheric delay into hydrostatic and wet components, and we examine the elevation angle dependence of each of these components of the delay. We will show that a relatively simple function for the elevation angle dependence can predict the atmospheric delays at 5° elevation with a root mean square (RMS) error of <1 mm if the coefficients in the function are known, and with an RMS error of ~30 mm if the coefficients are determined from their correlation with location and surface temperature. Estimation of azimuthal asymmetry in the atmosphere from VLBI data indicates that these contributions are typically <100 mm at 5° elevation angle, but are at times highly significant.

### 1. INTRODUCTION

Errors in accounting for the effects of electromagnetic signals propagating through the Earth's atmosphere are considered to be one of the limiting error sources in modern space-based geodetic systems. Modern space-based geodetic systems operate in one of two distinct frequency bands, either the microwave band e.g., very long baseline interferometry (VLBI) and the global positioning system (GPS), or in the optical band e.g., satellite laser ranging (SLR). Within each of these bands the properties of the refractive index of the Earth's atmosphere are distinctly different. For microwave systems, the Earth's ionosphere is dispersive and its contribution to the propagation delay can be approximately removed using dual-frequency band measurements (we will not discuss ionospheric refraction further). The refractive index of the remaining constituents in the atmosphere are (effectively) non-dispersive. Microwaves are also able to efficiently excite the dipole component of the water vapor refractivity and therefore there is a large contribution to the refractive index from water vapor in the atmosphere. For optical systems, the ionosphere makes no significant contribution to the refractive index, nor does the dipole component of the water vapor refractivity. In addition, the neutral atmospheric constituents are dispersive in the optical band thus potentially allowing the use of multiple frequency measurements to calibrate the atmospheric delay.

The atmospheric delay contribution is given by

$$L_a = \int_{atm} ds n(s) - \int_{vac} ds \quad (1)$$

where  $L_a$  is the atmospheric delay correction, and  $n(s)$  is the (group) refractive index along the path followed by the ray. The first integral is along the path followed by the ray and the second integral along the vacuum path. The group refractivity for a packet of air is given by

$$N = (n-1) \times 10^6 = k_1 \frac{p_d}{T} Z_d^{-1} + k_2 \frac{p_w}{T} Z_w^{-1} + k_3 \frac{p_w}{T^2} Z_w^{-1} \quad (2)$$

where  $k_1$ ,  $k_2$  and  $k_3$  are experimentally determined values which for microwave frequencies are constant and, for optical frequencies, wavelength dependent (for optical frequencies,  $k_3$  is zero);  $p_d$  and  $p_w$  are the partial pressures of dry constituents and the water vapor in the packet;  $T$  is the absolute temperature of the packet; and  $Z_d^{-1}$  and  $Z_w^{-1}$  are the inverse compressibilities of the dry air and water vapor (see also *Owens* [1967] and references therein for a discussion of the theoretical basis for refractivity formulas). For microwaves the values of the constants from *Thayer* [1974] are  $k_1=77.604 \pm 0.014$  K mbar $^{-1}$ ,  $k_2=64.79 \pm 10$  K mbar $^{-1}$ , and  $k_3=377600 \pm 3000$  K $^2$  mbar $^{-1}$ , where for  $k_2$  and  $k_3$  the uncertainties represent the observational uncertainties in these coefficients (see *Davis et al.* [1985] and *Hill et al.* [1982] for discussion). *Owens* [1967] gives a complete expressions for the optical band. Because, in general,  $n(s)$  is not known along the ray path, models have been developed which allow approximate values of  $L_a$  to be computed from meteorological conditions and the elevation angle (and possibly azimuth) of electromagnetic signal.

Three of the major developments in modeling the Earth's atmospheric propagation delay were the developments of (1) the hydrostatic zenith delay formula by *Saastamoinen* [1972]; (2) the continued fraction, in sine of elevation angle, form of the elevation angle dependence (often called the mapping function) of the atmospheric delay by *Marini* [1972] and *Marini and Murray* [1973]; and (3) the azimuthal asymmetry model by *Gardner* [1977].

The Saastamoinen result showed that if the atmosphere were in hydrostatic equilibrium then the  $p/T$  term in the refractivity of moist air reduced to an integral of density which in the zenith direction would be directly proportional to total surface pressure if the gravity were independent of height. Saastamoinen also gave an expression for the effective value of gravity to be used to convert pressure to delay which depended only on latitude and height of the site above the ellipsoid (see also Appendices A of *Davis et al.* [1985] and *Baby et al.* [1988]). Taking advantage of the accurate representation of the hydrostatic zenith delay, the atmospheric delay can be written in the form

$$L_a(\varepsilon) = L_h^z m_h(\varepsilon) + L_w^z m_w(\varepsilon) \quad (3)$$

where  $L_h^z$  and  $L_w^z$  are the zenith values of the hydrostatic and wet delays,  $m_h(\varepsilon)$  and  $m_w(\varepsilon)$  are the mapping functions for the hydrostatic and wet components, and  $\varepsilon$  is the elevation angle of the vacuum path. The Saastamoinen expression for hydrostatic zenith delay is

$$L_h^z = 10^{-6} k_1 R_d g_m^{-1} P_s \quad (4)$$

where  $R_d$  is the specific gas constant for dry air defined using a molar mass for dry air of  $28.9644 \pm 0.0014 \text{ kg kmol}^{-1}$ ,  $P_s$  is total surface pressure, and  $g_m$  is the gravitational acceleration at the center of mass of the air column. The expression for  $g_m$  given by Saastamoinen is

$$g_m = 9.7840 (1 - 0.00266 \cos 2\phi - 0.00028 H) \text{ m s}^{-2} \quad (5)$$

where  $\phi$  is latitude and  $H$  is the ellipsoidal height in km. No one has successfully developed a sufficiently accurate expression for  $L_w^z$  based on surface meteorological conditions, and such an expression is likely not possible because of the highly variable mixing ratio of water vapor (see Baby *et al.*, [1988] for a recent expression). In general, surface metrological based models for  $L_w^z$  are able to determine  $L_w^z$  with a root mean square (RMS) error of between 20 to 30 mm depending on location and climate. Such errors are not acceptable for most microwave geodetic systems, and therefore  $L_w^z$  is usually estimated, along with geodetic parameters, in most data analysis schemes (see Herring *et al.* [1990] for discussion of applications of Kalman filtering to the estimation of  $L_w^z$ ). An alternative to modeling the wet delay is to infer it from sky brightness temperature measurements using an instrument such as a water vapor radiometer (WVR). These instruments have so far proved to be expensive, unreliable, and sensitive to radio noise interference and rain, and therefore have not had a major impact on geodetic measurement programs (see Elgered *et al.* [1991] for an extensive discussion of the largest geodetic data set analyzed using WVR data). We will not discuss these instruments further here.

The next major development in modeling the atmospheric delay was the demonstration by Marini and Murray that if the atmosphere were assumed to azimuthally symmetric then the mapping functions for the atmospheric delay were asymptotic in  $\sin(\epsilon)$  near zenith and in inverse  $\sin(\epsilon)$  near the horizontal, and that a continued fraction in  $\sin(\epsilon)$  satisfied both of these asymptotic limits. For a truncated form of continued fraction, the mapping function has the form

$$m(\epsilon) = \frac{1 + a/(1 + b/(1 + c))}{\sin \epsilon + \frac{a}{\sin \epsilon + \frac{b}{\sin \epsilon + c}}} \quad (6)$$

where  $a$ ,  $b$ , and  $c$  are coefficients which depend on integrals refractivity through the atmosphere. In particular, Marini and Murray [1973] show that

$$aL^z \approx \frac{10^{-6}}{r_o} \int dh hN + 10^{-12} \int dh N^2/2 \quad (7)$$

where  $r_o$  is the radius of the Earth, and  $h$  is the height above the site. The first integral is the main contributor, and we have written this integral assuming a non-dispersive refractive index. From this expression, it can be seen that the mapping function coefficients are determined not by surface values but by bulk atmospheric properties. (The integrals for the other coefficients are much more complicated and involve higher powers of  $N$ ,  $h$ , and their products.) We can also use this expression to partly justify the separation of atmospheric mapping functions into hydrostatic and wet components, at least for

relatively high elevation angles. The dominant integral in equation (7) is linear in the refractivity and therefore can be separated into two integrals, one for the hydrostatic term and one for the wet, and each of the integrals can be associated with the corresponding mapping functions. Although Marini and Murray showed the above continued fraction form was asymptotic when expressed in teRMS of the ray's arrival elevation angle, fitting the functional form of equation (7) with vacuum elevation angles to raytracing results through atmospheric profiles measured with rawinsondes shows that this form (with three coefficients) can be used to represent the elevation angle dependence of the atmospheric delay with an RMS error of <0.2 mm for elevation angles between 90° and 3°.

The next major development by *Gardner* [1977] was the study of the effects of azimuthal asymmetries in the atmosphere. In this work, the effects of linear gradients in temperature and pressure on the atmospheric delay were considered and a simple formula expressed in teRMS of these gradients and a mapping function dependent on  $1/[\sin(\epsilon)\tan(\epsilon)]$  was given. Although this work indicated that gradient effects could reach several centimeters at 20° elevation angle, there has never been a data set of sufficient quality available during a geodetic experiment for these formulas to be applied in the analysis of space geodetic data. However, given the ever increasing precision of geodetic measurements, and the trend, particularly in VLBI to make observation at ever decreasing elevation angles, these gradient effects must always be kept in mind.

In this paper, we will give simple expressions for the hydrostatic and wet mapping functions determined from raytracing through rawinsonde data, and we will present geodetic results obtained from the analysis of VLBI data using these new mapping functions and we will present estimates for corrections to the mapping functions and the estimates of azimuthal asymmetry also obtained from the analysis of the VLBI data.

#### ATMOSPHERIC DELAY MODELS

We have developed a new set of mapping functions based on the continued fraction form of equation (6). The mapping functions were developed by raytracing through atmospheres with temperature and water vapor profiles measured by rawinsondes launched from ten locations in the United States located near VLBI stations. The locations covered by these data were Westford, Massachusetts; Richmond, Florida; Ft. Davis, Texas; Pietown, New Mexico; Mojave and Vandenberg, California; and Fairbanks, Alaska. The raytracing was performed at sixteen elevation angles between 3° and 90°. (Larger numbers of elevation angles were tested, but the additional elevations did not significantly affect the results.) For each raytrace, the pressure was determined assuming hydrostatic equilibrium, and the path of the integration was determined from the total refractivity and its gradients at each point along the path. The delays along the path were accumulated separately for the part of the refractivity associated with the hydrostatic component of the refractivity, the residual wet component, and geometric contribution from the bending the ray. The first ray was in the zenith direction and these zenith delays were used to determine the hydrostatic and wet mapping functions. The geometric bending teRMS was added to the hydrostatic delay part. After each set of raytraces was performed, the coefficients in the mapping function were determined by a least squares fitting separately for the hydrostatic and wet components. The RMS fit of

the mapping to hydrostatic delay was consistently about 0.15 mm and to the wet delay typically less than 0.1 mm. The coefficients from each location were analyzed and the following mapping functions deduced which depend only on latitude (range used 27° to 65°), height of site (range used 0 to 1.6 km) and surface temperature.

$$m_h(\varepsilon) = \frac{1 + a_h/(1 + b_h/(1 + c_h))}{\sin \varepsilon + \frac{a_h}{\sin \varepsilon + \frac{b_h}{\sin \varepsilon + c_h}}} \quad (8)$$

where

$$a_h = [1.2320 + 0.0139 \cos \varphi - 0.0209 H_s + 0.00215 (T_s - 10)] \times 10^{-3},$$

$$b_h = [3.1612 - 0.1600 \cos \varphi - 0.0331 H_s + 0.00206 (T_s - 10)] \times 10^{-3},$$

$$c_h = [71.244 - 4.293 \cos \varphi - 0.149 H_s - 0.0021 (T_s - 10)] \times 10^{-3},$$

and  $\varphi$  is the latitude of the site,  $H_s$  is the height of the site in km, and  $T_s$  is the surface temperature in C. For the wet mapping function the expression is

$$m_w(\varepsilon) = \frac{1 + a_w/(1 + b_w/(1 + c_w))}{\sin \varepsilon + \frac{a_w}{\sin \varepsilon + \frac{b_w}{\sin \varepsilon + c_w}}} \quad (9)$$

where

$$a_w = [0.583 - 0.011 \cos \varphi - 0.052 H_s + 0.0014 (T_s - 10)] \times 10^{-3},$$

$$b_w = [1.402 - 0.102 \cos \varphi - 0.101 H_s + 0.0020 (T_s - 10)] \times 10^{-3},$$

$$c_w = [45.85 - 1.91 \cos \varphi - 1.29 H_s + 0.015 (T_s - 10)] \times 10^{-3}.$$

In Figure 1 these mapping functions, along with others, are compared with raytrace results from the worst of the sites studied: Fairbanks, Alaska. (This site is problematic because of the large temperature inversions which occur during the winter months).

The typical root-mean-square (RMS) differences between raytracing at 5° elevation angles and these empirical mapping functions is 30 mm for the hydrostatic delay and 10 mm for the wet delay. The effects of these differences on the estimates of station heights will depend on the nature of the observing schedule used, however, some rules-of-thumb can be established by analyzing a series of experiments using different mapping functions. One method for these analyses is to use the temperature dependence in the above mapping functions to determine a mapping function partial derivative with respect to surface temperature and to then estimate this surface-temperature-like quantity from the VLBI data themselves (along with stochastic variations in the wet delay). For recent VLBI experiments which include observations made with elevations angles as low as 5°, this type of analysis indicates that the sensitivity of the station height estimates varies between 0.5 and 1.5 mm per C. Combining this sensitivity with the changes in the mapping function at 5° elevation angle for changes in  $T_s$  (4.4 mm/C), yields that the RMS height variations expected from hydrostatic delay mapping function errors lies between 3 to 10 mm.

In addition to these azimuth independent atmospheric models, some azimuthal dependent variations should be expected but quantitative values for such parameters are

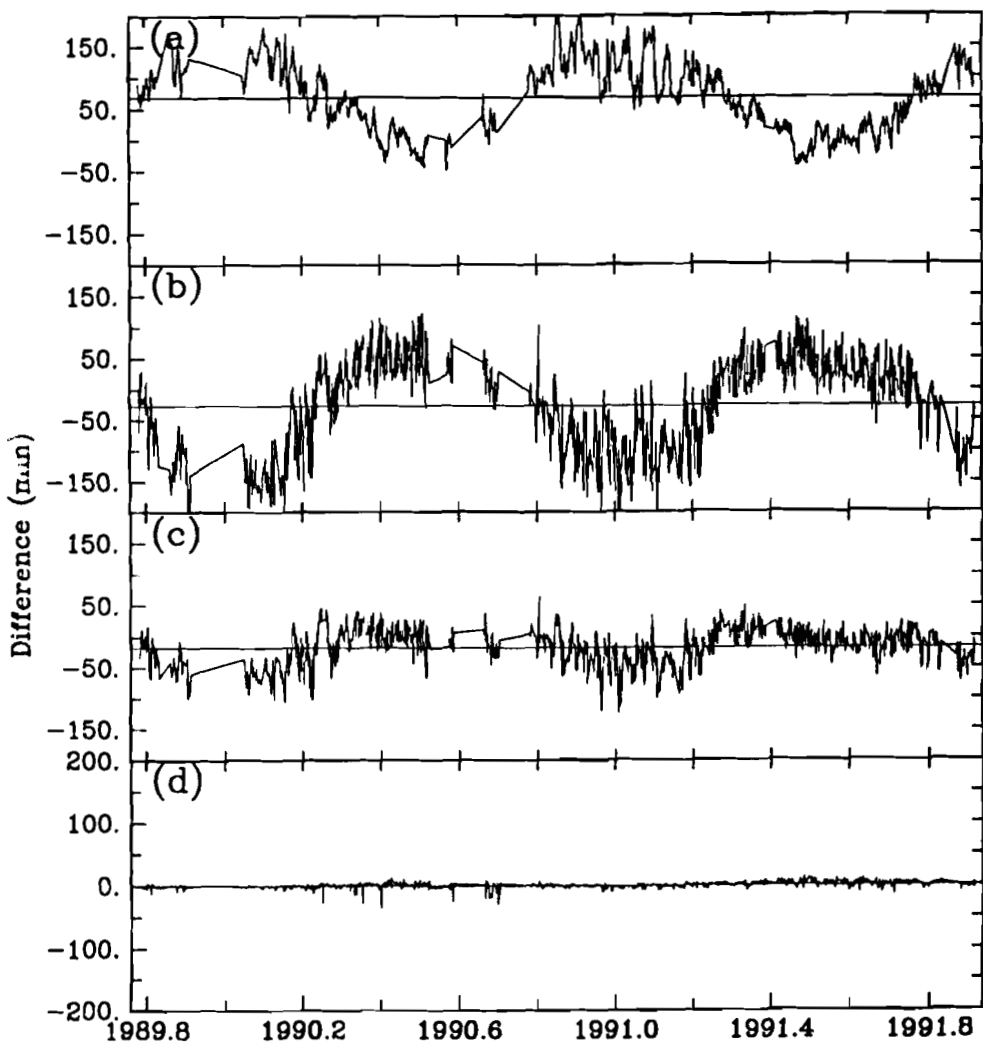


Figure 1. Differences between raytrace results at  $50^\circ$  elevation angle and the delay computed using various mappings for the Fairbanks, Alaska rawinsonde station: (a) difference from a constant mapping function computed from the expression for  $m_h(\varepsilon)$  with  $\varphi=0$ ,  $H_s = 0$  and  $T_s = 10$  C; (b) differences from a standard type analysis using a mapping function of the form of Davis *et al.* [1985] with a constant temperature gradient (-5.6 K/km) and constant height of tropopause (10 km) and surface values for temperature and pressure; (c) differences from the expression for  $m_h(\varepsilon)$  evaluated with the surface temperature; and (d) differences for the wet delay evaluated using the expression for  $m_w(\varepsilon)$ . In all cases, the zenith delays were computed by raytracing in the zenith direction. For each part of the figure, the mean and RMS differences are (a) 67 mm, RMS 56 mm, (b) -29 mm, RMS 74 mm, (c) -18 mm, RMS 30 mm, and (d) 0 mm, RMS 4 mm.

not normally available. One method that can be used to model azimuthal asymmetry is based on a "tilted" atmosphere assumption and can be approximately written as

$$L_{az} = NS \cos \alpha \ m_a(\varepsilon) + EW \sin \alpha \ m_a(\varepsilon) \quad (10)$$

where

$$m_a(\varepsilon) = 1/(\sin \varepsilon \tan \varepsilon + 0.0032)$$

and  $NS$  and  $EW$  are parameters representing the delays due to the azimuthal asymmetry,  $\alpha$  is the azimuth, and the numerical constant is an empirically determined value which matches this form of mapping function to a tilted atmosphere model for elevation angles ranging between  $90^\circ$  and  $5^\circ$ . Table 1 gives the mean and RMS scatter of the estimates of these gradients teRMS determined from the analysis of IRIS VLBI data from January 1989 to October 1991. The estimation of these gradients left the RMS scatter of the baseline lengths largely unchanged, and often improved it, but the  $\chi^2/f$  of the fits of the baseline lengths to linear rates of change were considerably improved. At those sites which make frequent low elevation angle observations, significant gradient effects appear to have been detected in this analysis indicating that more detailed analysis is warranted. For the Westford to Wettzell baseline with 187 determinations the RMS scatter of the baseline length estimates about the best-fit linear rate of change with and without gradients estimated was 8.3 and 9.2 mm with  $\chi^2/f$  of 2.8 and 3.8, respectively. If corrections to the mapping function are also estimated (simultaneously with the gradients), the RMS scatter is 9.2 mm with a  $\chi^2/f$  of 1.6. The improvements in the 90 day averages of the baseline length estimates are even greater: 4.7 mm, 4.1 mm, and 3.3 mm with  $\chi^2/f$  of 15.2, 10.7 and 3.0 for the standard analysis, gradients estimated, and gradients and mapping function corrections estimated, respectively.

#### ACKNOWLEDGMENTS

This work was supported by the National Aeronautics and Space Administration under grant NAG 5-538, by the National Oceanic and Atmospheric Administration under grant NA90AA-D-AC481, and by the Kerr-McGee Foundation. The views expressed herein are those of the author and do not necessarily reflect the views of NOAA or any of its subagencies.

#### REFERENCES

- Baby, H. B., P. Gole, and J. Lavergnat, A model for the tropospheric excess path length of radio waves from surface meteorological measurements., *Radio Science*, 23, 1023–1038, 1988.
- Chao, C. C., The troposphere calibration model for Mariner Mars 1971, *JPL Technical Report*, 32-1587, 61-76, 1974.
- Davis, J. L., T. A. Herring, I. I. Shapiro, A. E. E. Rogers, and G. Elgered, Geodesy by radio interferometry: Effects of atmospheric modeling errors on the estimates of baseline length, *Radio Science*, 20, 1593-1607, 1985.

TABLE 1.  
Estimates of gradients from the analysis of 2.8 years of IRIS VLBI data.

Site	Number*	NS gradient			EW gradient		
		Mean†, mm	RMS, mm	$\chi^2/f^{\ddagger}$	Mean†, mm	RMS, mm	$\chi^2/f^{\ddagger}$
Westford	188	-0.29	0.48	5.6	0.01	0.45	7.1
Richmond	163	0.29	0.84	0.7	-0.11	0.63	3.0
Mojave	158	0.09	0.48	1.5	0.01	0.54	1.5
Wettzell	189	-0.03	0.45	3.0	-0.15	0.42	1.9
Onsala	32	-0.17	0.36	5.0	0.00	0.36	3.0

\* Number of values used to compute the mean and root-mean-square scatters.

† Mean value of the gradient term. At 5° elevation angle, a mean value of 0.1 mm would introduce a delay change of 9.2 mm.

‡  $\chi^2$  per degree of freedom of the estimates based on the statistical uncertainty from the Kalman filter analysis.

- Elgered, G., J.L. Davis, T.A.Herring, and I.I. Shapiro, Geodesy by radio interferometry: Water vapor radiometry for the estimation of the wet delay, *J. Geophys. Res.*, 96, 65416556, 1991.
- Gardner, C. S., Correction of laser tracking data for the effects of horizontal refractivity gradients, *Appl. Opt.*, 16, 2427-2432, 1977.
- Saastamoinen, J., Atmospheric correction for the troposphere and stratosphere in radio ranging of satellites, in *The use of artificial satellites for geodesy*, *Geophys. Monogr. Ser.*, 15, eds. S. W. Henriksen *et al.*, 247-251, AGU, Washington, D.C., 1972.
- Herring, T. A., J. L. Davis, and I. I. Shapiro, Geodesy by radio interferometry: The application of Kalman filtering to the analysis of VLBI data, *J. Geophys. Res.*, 95, 12561-12581, 1990.
- Hill, R. J., R. S. Lawrence, and J. T. Priestly, Theoretical and calculational aspects of the radio refractive index of water vapor, *Radio Science*, 17, 1251-1257, 1982.
- Marini, J. W., and Murray, C. W., Correction of laser range tracking data for atmospheric refraction at elevations above 10 degrees, *NASA report X-591-73-351*, Goddard Space Flight Center, 1973.
- Marini, J. W., Correction of satellite tracking data for an arbitrary atmospheric profile, *Radio Science*, 7, 223-231, 1972.
- Owens, J. C., Optical refractive index of air: Dependence on pressure, temperature and composition, *Appl. Opt.*, 6, 51-58, 1967.
- Thayer, G. D., An improved equation of the radio refractive index of air, *Radio Science*, 9, 803-807, 1974.

# COMPARISON OF TOTAL ELECTRON CONTENT PREDICTED BY IRI WITH THE DATA OBSERVED IN CHINA

DAI KAILIANG

China Research Institute of Radiowave Propagation,  
P.O. Box 138-23, 453003, Xinxiang, Henan, P.R. China

MA JIANMING

Polar Research Institute of China,  
200129, Shanghai, P.R. China

**ABSTRACT.** Values of Total Electron Content calculated using the International Reference Ionosphere are compared with the data measured at Xinxiang based on Faraday Rotation measurements. It is found that the IRI gives fairly accurate values except during solar maximum. Making use of foF2 and M (3000)F2 predicted by the Asia Oceania Region F2 Layer Prediction method instead of using CCIR maps, the IRI gives more accurate TEC values. In winter and spring during solar maximum however, the IRI underestimates TEC obviously during daytime, which could be attributed to an inaccuracy in the topside electron density profile.

## 1. INTRODUCTION

Electron content and other integral parameters for the ionosphere from the ground to ceiling heights around 1000 km are important both for geophysical and for engineering applications, they impose propagation delay on radio signals traversing the ionosphere. Since actual measured values are not always available, one has to rely on models for many purposes. One of the global models is the International Reference Ionosphere (IRI). By integrating the electron concentration profiles given by IRI, one can get predicted total electron content.

A few papers have been published that deal with the comparison of the measured electron content with the IRI (e.g. McNamara and Wilkinson, 1983; McNamara, 1985; Bilitza, et al, 1988; Reinhart Leitinger, 1990; Dai Yue-qin, 1986; Wang Weiping, 1988). This paper compares the predicted total electron content, using the IRI-86, with the observed TEC measurements and is also concerned with the electron density profile of the IRI.

## 2. DATA

Measured data used in this study were obtained by means of Faraday rotation measurements at Xinxiang. The TEC values were obtained by using the Faraday factor for a height of 400 km and can be regarded to specify the total content up to a height of about 2000 km. The locations for the TEC measurement are as follows:

Xinxiang:	35.30°N	113.85°E
400 km sub-ionospheric point:	32.40°N	115.58°E
ETS-II:	00.00°N	130.00°E
Wuchang:	30.57°N	114.35°E

The electron content was obtained from the IRI-86 by means of numerical integration from 60 km to 1000 km using a step-size of 10 km. It could approximately be considered as identical with that from ground to an altitude of 2000 km, because electron contents from 1000 km to 2000 km hardly exceed 5% of TEC.

Here the predicted monthly median TEC values are compared with monthly median values of TEC observed at Xinxiang which imply a sub-ionospheric point about 200 km away from Wuchang. Comparisons are made for the time period from 1982 through 1989. By comparison of foF2 and M(3000)F2 predicted by using CCIR maps with data measured at eight ionospheric observatories in China, we found that the Asia Oceania Region F2 Layer Prediction method gives a better prediction in China (Dai Kailiang etc.). Therefore we made use of the AOR model in the calculation of the IRI electron content as well as the original CCIR model in the IRI.

In order to show the relationship between the behaviour of TEC and NmF2, we intended to display variations of foF2 both measured and predicted; but unfortunately, there is no ionosonde at the sub-ionospheric point, so foF2 measured at Wuchang, the nearest site from sub-ionospheric point, has been selected. Though Wuchang is over 200 km away, there should be some similarities between the behaviours of foF2 of the two sites.

Typical diurnal variations of TEC for both high solar activity (1989) and R12 not greater than 50 (1987) are given in Figure 1.

### 3. COMPARISON

Generally, the IRI gives the TEC with very good accuracy in summer both for Low Solar Activity (LSA) and High Solar Activity (HSA). Though calculated TEC values are usually greater than those measured during daytime, they are almost identical in summer during solar minimum.

In the other months for both LSA and HSA, however, discrepancies exist. When R12 is smaller than 130, the IRI overestimates the TEC greatly for daytime, which may not be attributed to the discrepancies of foF2 obtained by means of CCIR model and AOR model; while R12 is over 130, however, the IRI total electron content seems to be inert while the measured TEC rises abruptly at noon, greatly exceeding the IRI TEC. This may not be attributed to the discrepancies of foF2 either, because the relationship of calculated foF2 and measured ones remains the same.

Although some of the discrepancies may be due to errors in the prediction of foF2 to some extent, the major errors found may not be explained in this way. The discrepancies must therefore originate in the IRI profile layer shape. In particular, it is the topside profile which must be in error, for the topside contributes to roughly two-thirds of the TEC.

### 4. CONCLUSION

The IRI may be used to give useful values of TEC in China, but it yields systematic discrepancies which may be attributed to an incorrect topside electron density profile.

## REFERENCES

- Dai Kailiang, Luo Fageng, etc.(1991), *Proc. of the Fourth National Symposium on Radiowave Propagation*, p. 703
- Dai Yue-qin (1986), *Chinese Journal of Space Science* 6, n. 2, p. 143 - 146
- Ma Jianming, Shi Yizhong, Long Qili (1984) *Radiowave and Antenna* 2, p. 37-41
- Ma Jianming, Long Qili (1988) *Proc. of the International Beacon Satellite Symposium, Beijing*, p. 191 - 198
- McNamara, L.F., Wilkinson, P.J. (1983) *J.A.T.P.* 45, n. 2/3, p. 169 - 174
- McNamara, L.F. (1984) *Adv. Space Res.* 4, n. 1, p. 25 - 50
- Evans, J.V. (1969) *Proc. of the IEEE* 57, n. 4, p. 496 - 530
- Wang Weiping (1988) *Proc. of the International Symposium on Radiowave Propagation*, p. 173 - 176.

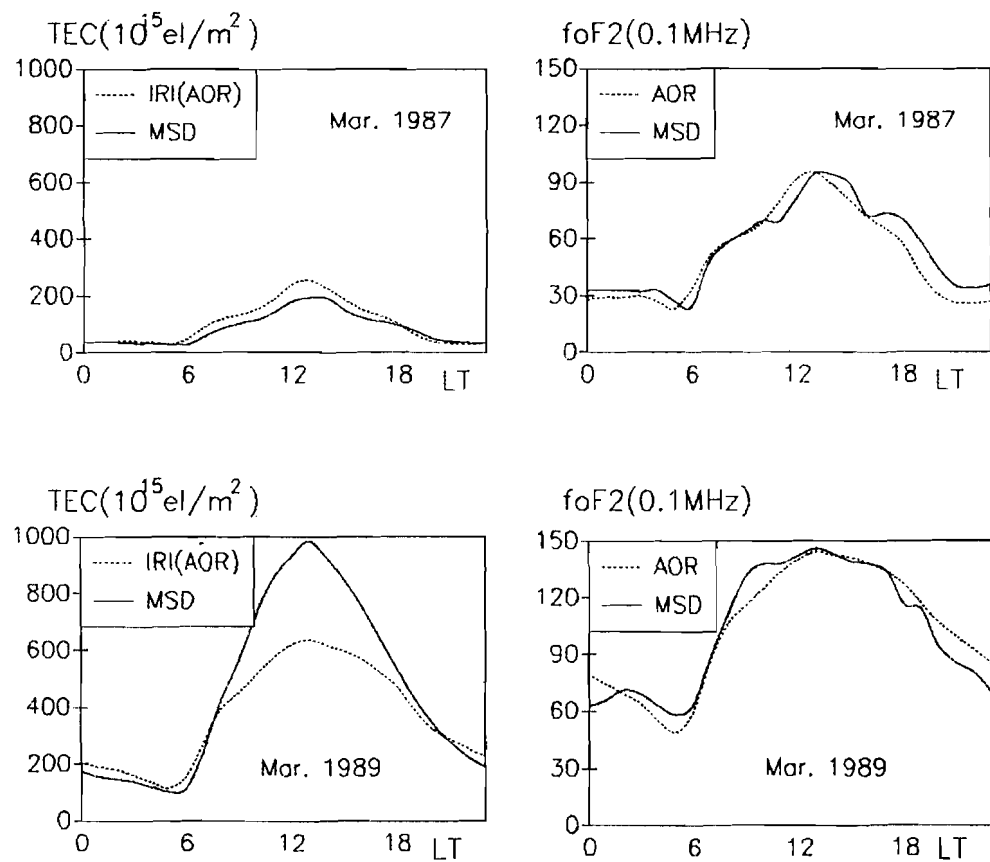


Figure 1: Diurnal variations of TEC and foF2

## A SIMULATION STUDY OF THE REFRACTION EFFECT

K. BECEK

School of Surveying, University of New South Wales,  
Sidney NSW 2033, Australia

**ABSTRACT.** The atmosphere, an optical environment of electromagnetic observations has an unstable and chaotic structure which is also seen in the refraction effect of electromagnetic wave propagation.

For over 300 years hundreds of models were created describing the influence of the refraction effect on the results of geodetic observations. So far no universal solution has been found which fulfils precision requirements of geodesy.

This paper describes the application of fractals as a tool for modelling the optical environment of electromagnetic observations.

The principles on the creation of such a "fractal system" of the atmosphere along the propagation path are described. Theoretical considerations are illustrated by results of the simulation study of the "fractal model" which are in agreement with known empirical results of refraction investigations.

# CORRECTION FOR IONOSPHERIC REFRACTION DISTORTIONS ON THE BASIS OF A TOMOGRAPHIC PROCESSING OF SIGNALS FROM NAVIGATION SATELLITES NNSS

A.I. TEREKHOV, M.YU. UDODOV  
SibIZMIR, Irkutsk 33, P.O. Box 4026,  
664033, Russia

**ABSTRACT.** In order to be able to adjust refraction corrections to angles of arrival caused by ionospheric effects, it is necessary to know the electron density distribution. It is impossible to predict the electron density distribution using regular models; therefore, current diagnostics of the inhomogeneous ionospheric structure is needed.

We demonstrate a possibility of reconstructing the electron density distribution via a processing of signals from navigation satellites using tomographic methods and models of travelling ionospheric disturbances (TID's). Examples are given of the reconstruction of TID parameters on the basis of experimental data obtained in the USSR (Irkutsk). Each time during the fly-over of one satellite of navigation systems NNSS one fan-shaped tomographic projection (Fig. 1) was recorded, which represented the time-dependence of the frequency Doppler shift.

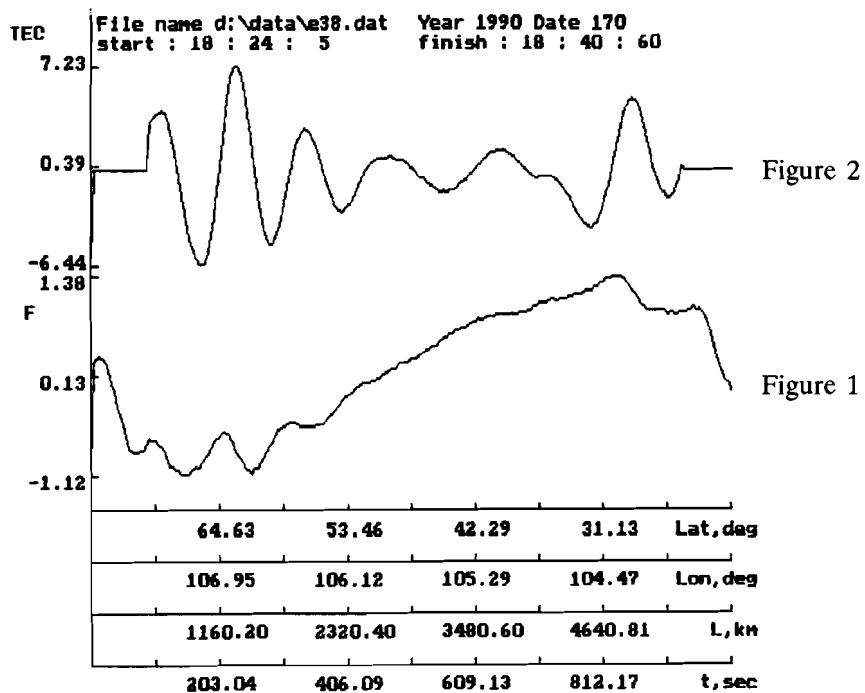


Figure 1 and Figure 2

These data were subsequently converted to the total electron content, from which the TID induced component was separated (Fig. 2). By applying the reconstruction algorithms, the electron density distribution shown in Fig. 3 was determined. By knowing the reconstructed TID parameters, one can calculate the desired refraction corrections using the formulas obtained before.

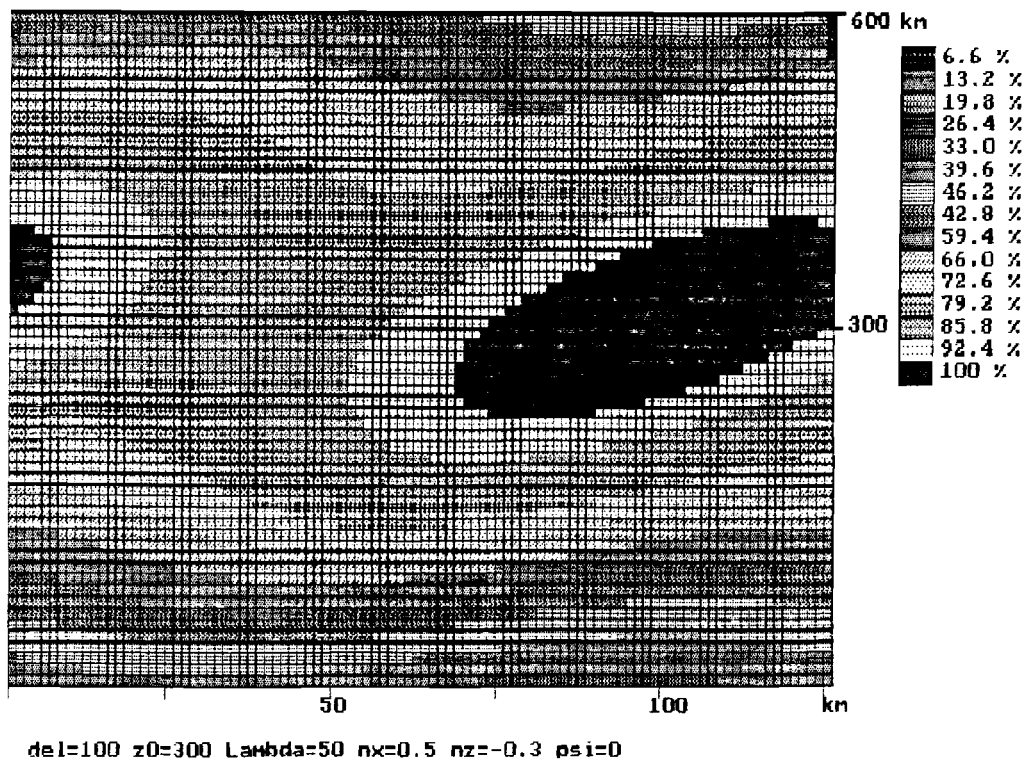


Figure 3

# COMPENSATION FOR IONOSPHERIC ERRORS IN GEODETIC MEASUREMENTS WITH THE HELP OF RADIOTOMOGRAPHY DATA

V.E. KUNITSYN

Physics Faculty, Moscow State University,  
119899 GSP Moscow, USSR.

**ABSTRACT.** We consider methods of satellite ionosphere radiotomography (RT) including ray RT and tomography of scattering inhomogeneities. Results of experiments and possibilities of the RT are discussed. Methods to compensate for ionospheric errors by means of RT data about global electron density distributions and the statistical structure of ionospheric inhomogeneities are suggested.

## 1. INTRODUCTION

The transatmospheric signals used in geodetic measurements are significantly influenced by the propagation media, i.e. by the ionosphere and the troposphere. In general this influence is unknown and leads to the loss of accuracy of geodetic systems. Information about the structure of the inhomogeneous medium allows us to compensate for transatmospheric signal distortions. So the problem of the reconstruction of the structure of the inhomogeneous medium is very important for geodetic applications.

We consider the theory and methods of satellite RT of the ionosphere. RT problems can be divided into deterministic problems and statistical ones. The deterministic problems can be subdivided into ray RT as well as diffraction RT. The method of phase-difference ray RT of global ionospheric structures is developed in [1, 2]. Using the data about the phase difference of navigation satellites, which can be measured by a set of receivers in the plane of a satellite trajectory, it is possible to reconstruct the 2D cross-section of the ionosphere. The diffraction RT methods permit us to reconstruct the 2D structure of isolated inhomogeneities [3]. A new approach connected with the statistical RT makes it possible to determine the distribution of the fluctuation intensity and the correlation function of the electron density fluctuations thanks to the measurements of the statistical characteristics of radiowaves [3, 4].

## 2. RAY RADIOTOMOGRAPHY

The ionosphere has a stratified regular structure with 3D irregularities. So it is necessary to have different remote sensing variants for various type of ionospheric structures. Solution methods for reconstruction problems of the electron density profile of the regularly stratified ionosphere are widely known. There were no methods to reconstruct the structure of ionospheric irregularities till recently. Different methods of satellite RT are elaborated: RT of the global structure of the ionosphere, diffractional RT of localized scattering irregularities and RT of the random ionosphere [1 - 4]. RT is a new geophysical tool which opens great

perspectives for the investigation of the ionosphere. We suggest the solution of the satellite RT problem for large-scale global ionospheric irregularities when diffractional effects may be neglected [1, 2]. The diffraction on small-scale irregularities may be smoothed by means of the corresponding filtering.

Nevertheless the direct use of a well-known scheme, in particular, the scheme of seismic tomography for ionospheric investigations, does not give good results. We suggest a method of phase-difference RT based on differential Doppler measurements using radiowaves from satellites [1]. The numerical simulation shows the suitability of global structure reconstruction by means of the phase-difference RT method. We used three receivers and obtained a resolution of the reconstruction of some dozens of kilometres. Usually for reaching of 5 - 10% of reconstruction accuracy 10 - 20 iterations were sufficient. It turns out that standard phase methods are not suitable to reconstruct complicated geophysical structures. The RT experiments for the reconstruction of the main ionospheric trough were carried out in spring and autumn 1990 - 91. Receivers were situated near Murmansk, Kem (Carelia) and Moscow. In most cases we observed the regular smooth cross-sections of the ionosphere. The ionospheric trough was observed at night and it had often a complicated structure with many additional extrema. An example of the reconstruction for 28 March 1990 at 02<sup>h</sup> 22<sup>m</sup> of the ionospheric trough in isolines in units 10<sup>6</sup> el/cm<sup>3</sup> is presented in Fig. 1.

### 3. APPLICATION OF RAY RT

Let us consider the ionospheric influence on geodetic data using the example of distance determination. It is known that due to the ionospheric effects we measure the group path  $G$  instead of the real distance  $L$

$$\begin{aligned} G &= \int \left[ 1 - \left( \frac{N}{N_m} \right) \left( \frac{f_c}{f} \right)^2 \right]^{-1/2} d\sigma \approx \\ &\approx L + \left( \frac{f_c}{f} \right)^2 \int \left( \frac{N}{2N_m} \right) d\sigma + \left( \frac{f_c}{f} \right)^4 \int \left( \frac{3N}{8N_m} \right) d\sigma + \dots \end{aligned}$$

Here  $N_m$  is the maximum value of the electron density  $N$ ;  $f_c$  is the critical frequency;  $f$  is the sounding frequency and integration over  $d\sigma$  is carried out along the ray between the transmitter and the receiver. Corrections connected with the expansion with respect to the reversed frequency decrease sufficiently fast but they can put together a significant value. For example, the first correction ( $\sim 1f^{-2}$ ) gives (10 - 20) km for satellites of the Transit type and 100 - 200 m for GPS.

If we use single frequency navigation data, it is necessary to use ionosphere models for removing errors. But the models of the ionosphere give an error ~20 - 30% in the midlatitude ionosphere and very bad results in the high-latitude ionosphere where the deviation can reach hundreds of percents and application of models is senseless. So it is reasonable to use RT data in such cases. The calculation of the first two corrections permits us to reduce the ionospheric influence in 10 - 20 times. The dual frequency correction enables us to remove the first term  $\sim \int N d\sigma$ , but the influence of the second term  $\sim \int N^2 d\sigma$  can also be significant. The deviation  $G$  be  $\sim (100 - 200)$  m (Transit) and (1 - 2) m (GPS). The residual effect, however, may be significant for some applications. The calculation of the second correction  $\sim \int N^2 d\sigma$  with the help of RT data makes it possible to decrease this remaining error in 10 - 50 times.

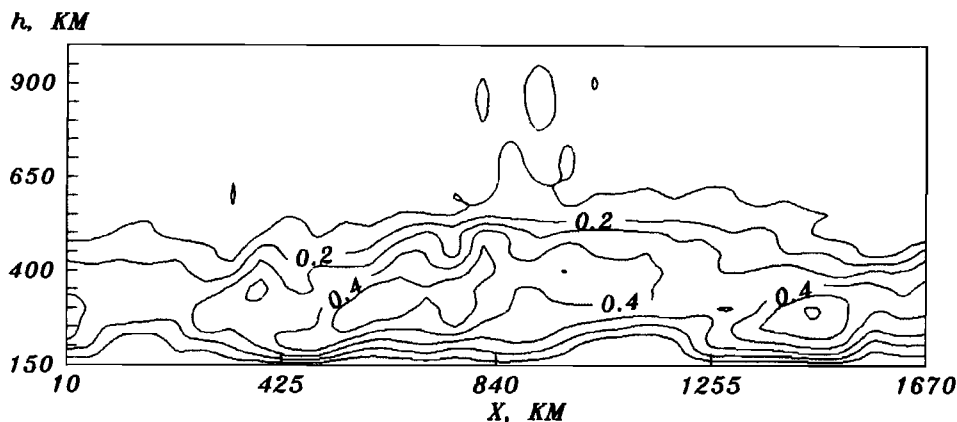


Fig. 1 h - the ionospheric height, X - the distance along Earth's surface

#### 4. RADIOTOMOGRAPHY OF SCATTERING IONOSPHERE IRREGULARITIES

The reconstruction problems concerning the structure of scattering irregularities are related to diffractional tomography problems. The satellite RT can be divided into deterministic and statistical problems. We obtain the solution of diffractional RT in the case of weak and strong scattering using the small-angle scattering data. This solution permits us to reconstruct the integral electron density and collision frequency along the radio propagation path. An experimental complex has been built for the reconstruction of the 2D structure of the inhomogeneities by using a beacon signal of metre-range wavelength on the board of a navigation satellite. We discuss the experimental results of the reconstruction of the 2D structure of isolated irregularities.

In the case of severely disturbed ionospheric layers it is necessary to use a statistical approach to RT. We derive an integral equation connecting the second coherence function of the field measured with the correlation function cross-section of scattering inhomogeneities. In the case of a statistically homogeneous medium it is possible to determine the height of a layer and a set of correlation function projections by means of one receiver, which registers the satellite probing radiation which passed through the layer under different angles. The 2D normalized spectrum of electron density fluctuations, as a function of polar angle  $\theta$  ( $-\pi/2 < \theta < \pi/2$ ) and spectral variable  $\kappa$  ( $0,1 < \kappa < 2,5 \text{ km}^{-1}$ ) were obtained experimentally [3, 4]. We developed the method in the case of arbitrary clusters of inhomogeneities. The method enables the reconstruction of the spatial intensity distribution, correlation coefficient's structure of electron density fluctuations.

#### 5. APPLICATION RT SCATTERING IONOSPHERE IRREGULARITIES

The statistical structure of the ionosphere influences the results of navigation measurements strongly. Physically it is connected with the fact that all irregularities situated in the Fresnel zone (which scale is about 200 - 300 m for navigation systems) give contribution to the phase and group path disturbances. So, if in the ionosphere there are strong disturbances with the scale of the order of tens of meters, this can influence the results significantly.

We shall estimate group path variations for a plane wave propagating through a layer of 3D irregularities. The solution of this problem within the Rytov approximation gives the mean square deviation,  $\sigma$ , of the group path  $G$  [5], as

$$\sigma_G^2 = (2\pi r_e)^2 \int d\zeta \int d^2 \mathbf{k} \left[ \frac{\partial}{\partial k} \left( \frac{1}{kn} \cos \left( \frac{\zeta \mathbf{k}^2}{2k} \right) \right) \right]^2 \hat{B}_N(\bar{\mathbf{k}}, \zeta)$$

Here  $\hat{B}_N(\bar{\mathbf{k}}, \zeta) = (2\pi)^{-3} \int B_N(\bar{\rho}, z, \zeta) \exp(i\bar{\mathbf{k}}\bar{\rho}) d^2 \rho dz$ ,  $B_N(\bar{\rho}, z, \zeta)$  – correlation function of the electron density fluctuations (it may depend slightly on the coordinate  $\zeta$  of the scattering layer),  $\lambda$  - wavelength,  $k = 2\pi/\lambda$  - wave number,  $n$  - refractive index of the background ionosphere, and  $r_e$  - classical electron radius.

The analysis of the variance of the group path fluctuations shows that for strong ionospheric disturbances  $\sigma_N \sim 10^{11} \text{ m}^3$  the variations of group paths can reach centimetres (GPS). It is clear, that sufficiently long time averaging of measurement results allows us to decrease this error significantly. But this is not always possible in practice. The algorithms for data processing have to depend on the spectrum of electron density fluctuations. The application of RT data to determine this spectrum permits us to evaluate the arising error correctly and to choose the corresponding algorithm for data processing, which reduces the error considerably.

## 6. CONCLUSION

The satellite RT methods described show the possibility to improve the navigation data. It is possible to reconstruct global cross-sections of the electron density and the statistical structure of ionospheric irregularities based on results of RT experiments. Such RT data make it possible to improve the accuracy of navigation systems considerably by taking into account contribution of the ionosphere more carefully.

## REFERENCES

- [1] Kunitsyn, V.E., Tereshchenko, E.D., Andreeva, E.S., et al. (1990), Preprint *Polar Geophysical Inst. 90-10-78*, p. 1 - 30
- [2] Andreeva, E.S., Kunitsyn, V.E., Galinov, A.V., et al. (1990), *Lett. Journal Exp. Theor. Phys.* **52** no. 3, p. 145 - 148
- [3] Kunitsyn, V.E., Tereshchenko, E.D. (1991), *Tomography of the Ionosphere*, Moscow, Nauka (In Russian)
- [4] Galinov, A.V., Kunitsyn, V.E., Tereshchenko, E.D. (1991), *Geomagnetism and Aeronomy*, **31** no. 3, p. 446 - 453
- [5] Kalinin, Yu.K., Kunitsyn, V.E. (1988), *Adv. Space Res.* **8** no. 4, p. 4

# THREE-DIMENSIONAL MODELLING OF ATMOSPHERIC PARAMETERS FOR AUTOMATIC PATH DELAY CORRECTIONS

MARC COCARD, VINCENT ECKERT, ALAIN GEIGER, BEAT BÜRKI

Institute of Geodesy and Photogrammetry,

Federal Institute of Technology ETH, CH-8093 Zürich, Switzerland

Tel: +41 1 377 3244, Fax: +41 1 371 2593

BRUNO NEININGER

Laboratories of Atmospheric Physics, LAPETH,

Federal Institute of Technology ETH, CH-8093 Zürich, Switzerland

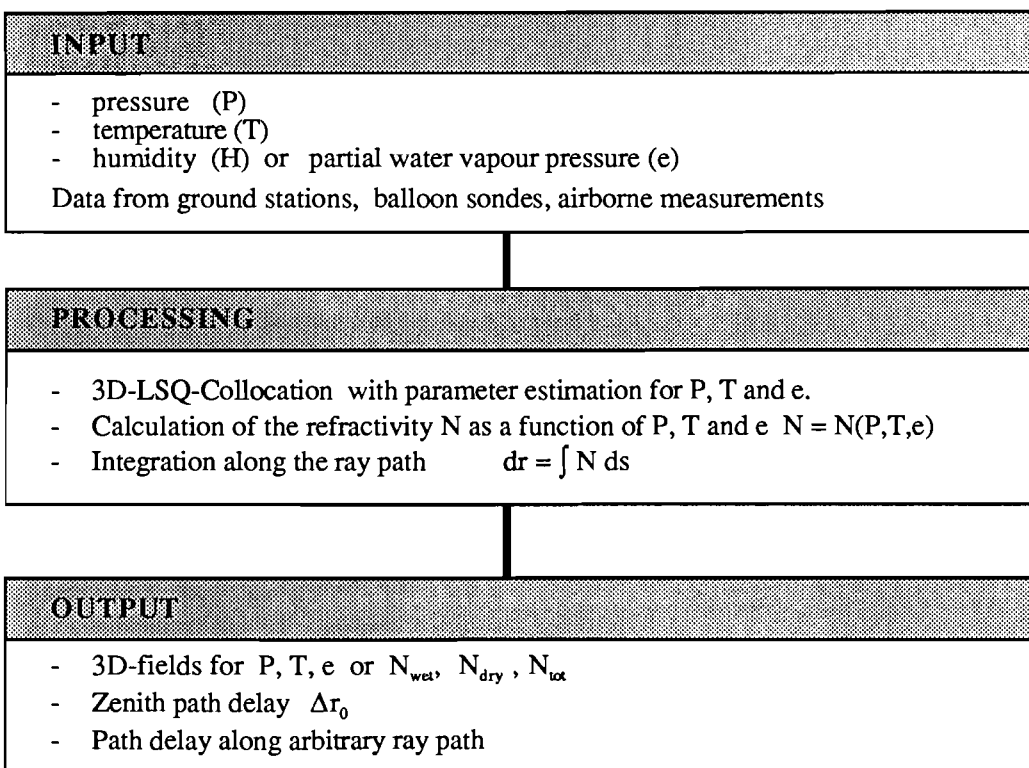
**ABSTRACT** One of the most limiting factors for precise height determination by GPS is the uncertainty in the atmospheric path delay correction. In this paper we present a correction model in which data from automatic meteorological stations are used to calculate a 3-d atmospheric model and to finally predict the actual path delays. Data from balloon sondes can be introduced as well. In Switzerland there exists an automatic meteorological station network (ANETZ) of about 64 stations operated by the Swiss Meteorological Service. The elevation of the stations ranges from 200 to 3500 m. From meteo data measured every 10-minutes a threedimensional field of refractivity given by pressure, temperature and humidity is calculated. The construction of the model is based on parameter estimation and collocational methods. The path delay is automatically calculated by summation of the effects of the refractivity along the GPS signal path.

## 1. INTRODUCTION

The most commonly used methods to take the tropospheric influence into account are :

- Standard corrections with standard meteo values. (Saastamoinen, Hopfield, Marini, etc).
- Standard corrections with measured meteo values. (Saastamoinen, Hopfield, Marini, etc).
- Direct measurements. (for example : measurements of the wet path delay by radiometry).
- Estimation of tropospheric biases directly from the GPS-measurements. (zenith path delay, random walk).
- 3-dimensional modelling of the refractivity.

In this paper a 3-dimensional approach for modelling the troposphere and evaluating path delays for correcting GPS-measurements is presented. The model approach can be summarized by the following scheme.



Tab. 1.: Model approach

For the 3D-LSQR-collocation the following simple deterministic models were chosen :

- Pressure : an exponential function of the height (2 parameters).
- Temperature : a linear function of the height (2 parameters).
- Water vapour: an exponential function of the height (2 parameters).

For the stochastical model the following covariance function has been implemented :

$$\phi_{ij} = \frac{\sigma}{1 + \alpha \left[ \left( \frac{\Delta X_{ij}}{A} \right)^2 + \left( \frac{\Delta Y_{ij}}{B} \right)^2 + \left( \frac{\Delta Z_{ij}}{C} \right)^2 \right] \text{Exp} \left( -\frac{Z_i + Z_j}{2D} \right)}$$

where  $a$ ,  $A$ ,  $B$ ,  $C$ ,  $D$ ,  $\sigma$  are parameters characterising the covariance functions for the P, T, e fields. The values are chosen according to the behaviour of the corresponding field and the distribution of the measurement sites. Note the increasing correlation length with height.

## 2. DATA

The performance of the program system has been tested with data provided by the Swiss Meteorological Services (SMA). The meteo data are recorded on about 64 automatic stations spread homogeneously over the area of Switzerland [SMA, 1985]. A variety of parameters are recorded once every 10 minutes. For our purposes, only the three parameters P, T, e are used. The balloon recordings, which are measured every 12 hours are also provided by the SMA. While the stations, as shown in figure 2 are regularly distributed with respect to the horizontal, the vertical distribution suffers from a lack of higher stations. The minimal elevation being 200 m and the maximal 3500 m (Jungfraujoch). However, the lengthening of the correlation distance of the parameter field has to be taken into consideration. This means higher stations will normally represent the meteo conditions at the same height level much more precisely than stations at lower elevation do. It is obvious, that balloon soundings play a key role in supporting the interpolation of the higher and the free atmosphere. Especially atmospheric layers above 3500 m are mainly modelled by the measurements from the balloon sonde. In case of missing balloon data, the upper troposphere will be modelled by the estimated functional model.

## 3. EXAMPLE OF A COLD FRONT PROGRESSION

The following example shall visualize the possibility of the method. We choose a progression of a cold front in April. The predicted temperature field shows clearly the structure of a front. Evaluating the measurements at different epochs (e.g. 15:00 and 21:00) results in a progression monitoring of the meteorological events. The front progresses, as in most cases, from west to east, marked by a drop of temperature of more than 10 deg Celsius within 6 hours.

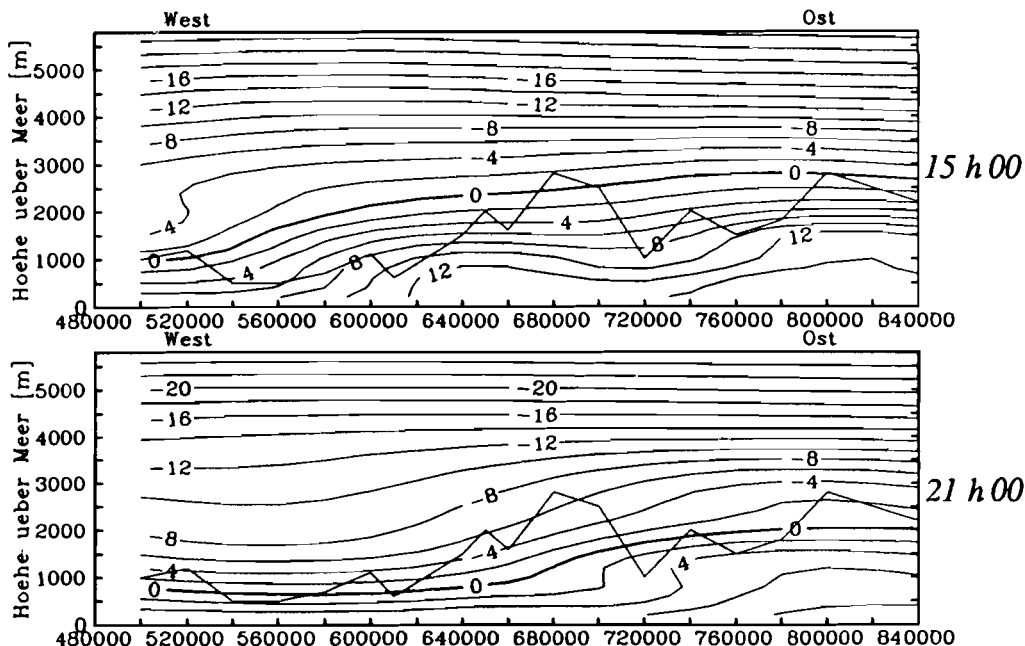


Fig. 1.: Evolution of a cold front. (Axes in meters, for clarity the topography has been overlaid).

Since the correction of path delays plays a significant role in surveys with considerable height differences between the stations, we considered stations at 1000 m height separation. The zenith path delay has been calculated over the whole region of Switzerland by three different methods :

Method A : Saastamoinen with standard ground values.

Method B : Saastamoinen with interpolated ground values.

Method C : Integration of the modelled 3D-field along the zenith path.

Type	Saastamoinen standard [mm]	Saastamoinen with interpolated ground values			3-dimensional Model		
		min [mm]	max [mm]	hor. grad. [mm/100km]	min [mm]	max [mm]	hor. grad. [mm/100km]
Wet	31	0	35	20	30	40	10
Dry	247	250	255	5	240	255	15
Total	278	250	285	20	270	285	15

Tab. 2.: Differences in the path delay for different models for a layer of 1000 m thickness.

Obviously the method A will generate constant values for the whole area . Method B takes the horizontal variation into account (a horizontal gradient appears), while method C represents a 3D-modelling with spacially correlated values. All the values are given in mm or in mm/100km for the gradient.

## ACKNOWLEDGMENT

All the meteorological data used for this work, have been provided by the Swiss Meteorological Office (Schweizerische Meteorologische Anstalt, SMA).

## REFERENCES

- ECKERT, V., M. COCARD, A. GEIGER, B. BÜRKI, B. NEININGER ( 1991): Three-Dimensional Modelling of Atmospheric Parameters for Automatic Path Delay Corrections. *IUGG, Wien.*
- GEIGER, A., M. COCARD (1992) : Collocational Methods in Atmospheric Ray Tracing. *Proc.: Refraction of Transatmospheric Signals in Geodesy, DenHaag.*
- MORITZ, H. (1980): Advanced Physical Geodesy. *Sammlung Wichmann Neue Folge Band 13, Wichmann Verlag Karlsruhe.*
- PULIAFITO, E., B. BÜRKI (1991): Tropospheric Path-Lenght Correction Using a Dual-Frequency Transportable Radiometer. In: *Proc. IGARSS'91, pp. 1337-1340, June 3-6, Helsinki.*
- SMA -diverse authors- (1985) : Charakteristiken der ANETZ-Daten. Beiträge zum ANETZ-Daten Kolloquium vom 17. April 1985, Zürich ,SMA.

# PATH LENGTH FLUCTUATIONS THROUGH THE EARTH TROPOSPHERE: TURBULENT MODEL AND DATA OF OBSERVATIONS

A.A. STOTSKII

Institute of Applied Astronomy,  
197042, St. Petersburg, Russia

The natural source of errors for the earth-based radio astronomical systems are the phase fluctuations arising when radio waves pass through the terrestrial troposphere.

As a universal characteristic of a tropospheric irregularity that determines various phase effects one can take the path length fluctuations in the direction of the zenith ( $l$ ). As the measure of these fluctuations it is convenient to use the structure functions: spatial  $D_l(\rho)$  and temporal  $D_l(\tau)$ .

Considering the tropospheric irregularity to be a result of air turbulence steering the structure functions which can be constructed on the basis of statistical turbulence theory (Tatarskii, 1964). Taking into account the different structure of the turbulence for small and large scales it is possible to construct the turbulence model of these structure functions for the complete space and time ranges.

There are three different domains which may be defined for the spatial structure function in such a way (Stotskii, 1972).

1) The small-scale domain ( $\rho < L_1$ ) where the turbulence is three-dimensional. Here the structure function is a power function with an exponent of 5/3. The outer scale of this domain  $L_1$  is of order of the thickness of the troposphere, i.e. several km.

2) When  $\rho > L_1$ , the turbulence is two-dimensional so that we have a power law with an exponent of 2/3. The outer scale  $L_2$  of two-dimensional turbulence is connected with the size of the largest tropospheric irregularities such as cyclones, i.e. several thousands of km.

3) For  $\rho > L_2$  there is the domain of saturation.

Thus the space structure function can be written as:

$$D_l(\rho) = \begin{cases} C_l^2 \rho^{5/3} & \rho < L_1 \\ C_L^2 \rho^{2/3} & L_1 < \rho < L_2 \\ C_s^2 & \rho > L_2 \end{cases} \quad (1)$$

In reality there were no breaks in structure functions at  $\rho = L_1$  and  $\rho = L_2$  of course. A smooth transition from "the law of 5/3" to "the law of 2/3" was calculated by Treuhhaft and Lanyi (1987).

The structure coefficients  $C_l$  and  $C_L$  in (1) are connected with the structure coefficient of air refractivity  $C_n$  and can be defined as:

$$C_l^2 = 2.91 \int_0^L C_n^2(h) dh, \quad C_L = \int_0^L C_n(h) dh \quad (2)$$

where  $h$  - altitude,  $L$  - total thickness of the troposphere.

Defining the values of  $L_1$  and  $L_2$  as abscissae for the intersections of the different branches of  $D_l(\rho)$  one can connect these outer scales with the structure coefficients:

$$L_2 = (C_s/C_L)^3, \quad (3)$$

$$L_1 = C_L^2/C_{l1}^2 = \left[ \int_0^L C_n(h) dh \right]^2 / 2.91 \int_0^L C_n^2(h) dh \quad (4)$$

From (4) we see that  $L_1$  depends on the  $C_n$  profile. For example:

homogeneous media:	$C_n(h) = \text{const}(h),$	$L_1 = 0.34 L$
linear function:	$C_n(h) \sim (L - h),$	$L_1 = 0.26 L$
exponential function:	$C_n(h) \sim \exp(-h/H),$	$L_1 = 0.69 H$
Fried's (1965) profile:	$C_n(h) \sim h^{-1/6} \exp(-h/H),$	$L_1 = 0.51 H$

In the last two profiles  $L \gg H$ .

The temporal structure function may be connected with the spatial one by using the principle of frozen turbulence:

$$D_l(\tau) = D_l(\rho/v), \quad (5)$$

where  $v$  is the average velocity of irregularities transference. Analysis of meteorological data (Stotskii, 1972) and special measurements (Stotskii and Stotskaya, 1991) give the magnitude of  $v \approx 10$  m/s. This value coincides with the typical velocity of air movement in synoptic processes.

Thus the temporal structure function has also three domains with the same exponents:

$$D_l(\tau) = \begin{cases} C_{l1}^2 \tau^{5/3} & \tau < T_1 \\ C_{l1}^2 \tau^{2/3} & T_1 < \tau < T_2 \\ C_s^2 & \tau > T_2 \end{cases} \quad (6)$$

The corresponding outer scales are:  $T_1 = L_1/v$  or several minutes and  $T_2 = L_2/v$  or several days. The structure coefficients  $C_{l1} = C_l v^{5/6}$  and  $C_{l1} = C_l v^{1/3}$ .

The final values of structure function parameters have been determined on the basis of experimental data.

The experimental meanings of spatial and temporal structure functions for different space and time intervals were obtained from results of radio astronomical observations and radiosonde measurements. Published results of different authors and original measurements were used. Obtained meanings are given in Tables 1 and 2.

Suitable values of the turbulent model parameters which give agreement with observations are:

$C_l = 1.7 \times 10^{-5} \text{ cm}^{1/6}$	$C_{l1} = 5.4 \times 10^{-3} \text{ cm} \cdot \text{s}^{-5/6}$
$C_L = 8 \times 10^{-3} \text{ cm}^{2/3}$	$C_{L1} = 8 \times 10^{-2} \text{ cm} \cdot \text{s}^{-1/3}$
$L_1 = 2.2 \text{ km}$	$T_1 = 220 \text{ s} = 3.7 \text{ min}$
$L_2 = 2400 \text{ km}$	$T_2 = 2.4 \times 10^5 \text{ s} = 2.8 \text{ days}$
$C_s = 5 \text{ cm}$	$v = 10 \text{ m/s}$

TABLE 1.  
Experimental meanings of spatial structure function  $D_l(\rho)$

$\rho$ (m)	$\sqrt{D}_l(\rho)$ (cm)	Instrument, location and altitude	Season	References
13	0.008	Horn-refl. Andover, USA, 274 m	May	Unger (1966)
100	0.04	BPR. Pulkovo, USSR, 70 m	During a year	Lipovka, Stotskii, (1972)
145	0.044	RATAN-600, Zelenchukskaya, USSR, 1000 m	February	Stotskii, Stotskaya (1991)
370	0.18	Int. MRAO, Cambridge, GB	Summer	Hinder (1970)
570	0.25		Summer	
750	0.22		During a year	
1120	0.33		Summer	
200	0.09	Int. NRAO. Green Bank, USA, 800 m	January	Basart et al. (1970)
300	0.06		April	
1800	0.12		April	
1900	0.12		January	
2100	0.15		Jan. Apr. June	
11300	0.50	(800-1180 m)	Jan. April	
2400	0.46	Int. NRAO, Green Bank, USA, 800 m	March - August	Baars (1967)
1000	0.048	VLA NRAO, Socorro, USA, 2124 m	During a year	Armstrong, Sramek (1982)
10000	0.23			
35200	1.5	Int. NRAO, Green Bank, USA, 800 m	September	Miley et al. (1967)
$3.5 \times 10^3$	2.8	Radiosonde.	February,	
$4.3 \times 10^5$	3.3	Albuquerque,	August	Waters (1967)
$5.2 \times 10^5$	2.5	Tucson,		
$2.1 \times 10^6$	3.6	El Paso,		
$2.3 \times 10^6$	4.5	Hantington,		
$2.6 \times 10^6$	4.1	USA.		

TABLE 2.  
Experimental meanings of temporal structure function  $D_l(\tau)$ .

$\tau$	$\sqrt{D}_l(\tau)$ (cm)	Instrument, location and altitude	Season	References
1.28 s	0.0055	RATAN-600,	February	Stotskii, Stotskaya (1991)
2.56 s	0.010	Zelenchukskaya, USSR, 1000 m.		
5.12 s	0.018			
6 h	2.3	Radiosonde,	July, December	Stotskii, Stotskaya (1992)
12 h	3.1	St. Petersburg, USSR, 50 m.		
24 h	3.6			
48 h	4.1			
96 h	5.1			
12 h	3.0	Radiosonde,	February, August	Waters (1967)
24 h	2.8	Albuquerque,		
48 h	4.1	Tucson,		
96 h	3.8	El Paso,		
1 year	5.4	Hantington.		
2 years	4.6			
3 years	6.3	USA.		

The model results with these parameters and experimental data are shown in Figure 1.

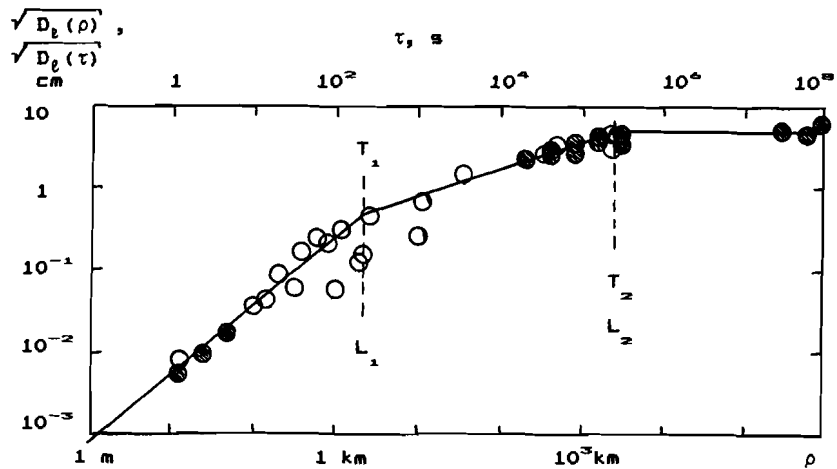


Figure 1. Turbulent model of path length fluctuations through the troposphere (zenith direction). Experimental data:  $\circ$  - for spatial structure function,  $\bullet$  - for temporal structure function.

The represented values of the parameters differ slightly from earlier estimations (Stotskii, 1973), when there were less experimental data.

The turbulence model can be used to construct characteristics of other fluctuation of the terrestrial troposphere such as a mean transfer function:

$$A(s) = \exp[-D_t(\lambda s) 2\pi^2/\lambda^2], \quad (7)$$

and a mean coherence interval:

$$K(\tau) = \exp[-D_t(\tau) 2\pi^2/\lambda^2], \quad (8)$$

where  $\lambda$  is wavelength.

## REFERENCES

- Armstrong, J.W., Sramek, R.A. (1982), *Radio Science* **17**, n. 6, p. 1579  
 Baars, J.W.M. (1967), *IEEE Trans. AP-15*, n. 4, p. 582  
 Basart, J.P., Miley, G.K., Clark, B.G. (1970), *IEEE Trans. AP-18*, n. 3, p. 375  
 Fried, D.L. (1965), *J. Opt. Soc. Am.* **55**, n. 11, p. 1427  
 Hinder, R.A. (1970), *Nature* **225**, Feb. 14, p. 614  
 Lipovka, N.M., Stotskii, A.A. (1972), *Izvestiya GAO AN SSSR* **188**, p. 238  
 Miley, G.K., Webster, W.J., Fullmer, J.W. (1967), *Astrophysical Letters* **6**, p. 17  
 Stotskii, A.A. (1972), *Radio Ing. and Electron. (USSR)* **17**, p. 1827  
 Stotskii, A.A. (1973), *Radiophys. and Quant. Electron. (USSR)* **16**, p. 620  
 Stotskii, A.A., Stotskaya, I.M. (1991), Preprint No. 34, Inst. Appl. Astr. Leningrad, Astr. Astroph. Trans. (In press)  
 Stotskii, A.A., Stotskaya, I.M. (1992), Inst. of Appl. Astron. Scientific Memor.  
 Tatarskii, V.I. (1964), *Wave Propagation in a Turbulent Medium*, McGraw-Hill, N.Y.  
 Treuhaft, R.N., Lanyi, G.E. (1987), *Radio Science* **22**, n. 2, p. 251  
 Unger, J.H.W. (1966), *BSTJ* **45**, n. 9, p. 1439  
 Waters, J.W. (1967), NRAO Scientific Memor. No. 8, Sept. 148

# A NEW METHOD TO PREDICT TROPOSPHERIC RANGE ERROR

W.J. HAN, Y.J. ZHENG

Beijing Astronomical Observatory, Chinese Academy of Sciences,  
Beijing 100080, China

X.D. WU, W.L. ZHANG

China Research Institute of Radiowave Propagation, Xixiang,  
Henan 453003, China

**ABSTRACT.** Based on the quasi-measured values of tropospheric refraction, the relation between  $\tau$  and  $\Delta R$  as expressed in eq. (3) is proved, and according to the stable feature of refractivity at 9 km above sea level, a simplified method to predict tropospheric range error is analysed. Some new parameters for linear regression analysis of tropospheric range error are given also.

## 1. INTRODUCTION

The studies of tropospheric refraction aim at obtaining an accurate atmospheric model and simplified expressions for computing the refraction errors. Until the end of the 1970's it was concluded that: Linear regression analysis between surface refractivity and refraction error is quoted (Bean 1964). The tropospheric model is divided into dry and wet terms (Hopfield 1969), and the last one can be accurately measured by using a water vapor radiometer (Decker et al. 1978; Westwater 1978). To avoid the computational difficulties at low elevation angles, the refraction error can be taken as the product of that at vertical incidence and a so-called mapping function which is an empirical expression containing an initial elevation angle (Marini 1972).

In the 1980's many people still try to find an empirical formula for computing the refraction errors (Hogg et al. 1981; Davis et al. 1985; Asknes et al. 1987). In this paper, a simplified method for predicting the range error is provided without using the historical meteorological data and some new parameters for linear regression analysis of the range error are given.

## 2. THEORETICAL ANALYSIS

The exponential model of the troposphere is well known (Bean 1964; CCIR 1986). The refractivity  $N$  is the function of height  $h$  (km) above the earth surface:

$$N(h) = (n - 1) \times 10^6 = N_s \exp(-\Gamma h) \quad (1)$$

where  $n$  is the refractive index,  $N_s$  is the surface refractivity, and  $\Gamma (km^{-1})$  is the reciprocal of scale height. When the initial elevation angle  $\theta_0$  is not too low, the range error  $\Delta R$  and the total bending  $\tau$  can be written as (Han 1964; Rowlandson et al., 1969):

$$\Delta R \approx \int N \times 10^{-6} ds$$

$$\tau = - \int_{n_s}^1 \cot \theta \frac{dn}{n} \approx \Gamma \cos \theta_0 \int N \times 10^{-6} ds \quad (2)$$

then we obtain,

$$\tau / (\Delta R \cos \theta_0) = \Gamma \approx const$$

Taking the characteristic points on the radiosonde profiles observed from six stations in China, a set of  $N$ -profiles consisting of stratified layers with a constant vertical gradient of refractivity in each one can be obtained. According to these profiles  $\Delta R$  and  $\tau$  are calculated exactly with various values in  $\theta_0$ . Some examples of calculated  $\Delta R$  and  $\tau$  are shown in table 1 (Based on the  $N$ -profiles observed in Beijing and Shanghai in July 1974, 07<sup>b</sup>).

It is obvious that the ratios of  $\tau$  to  $\Delta R \cos \theta_0$  calculated for various  $\theta_0$  are approximately constant and equal to  $\Gamma_0$  which may be regarded as a quasi-measured value. Therefore, eq. (3) is satisfied. If  $\Delta R$  and  $\tau$  are measurable, the model parameter  $\Gamma$  can be deduced.

From Han (1964) the following relations are obtained,

$$\Delta R \sim \begin{cases} N_s / \sqrt{\Gamma}, & (\theta_0 < 5^\circ) \\ N_s / \Gamma, & (\theta_0 \geq 5^\circ) \end{cases} \quad (4)$$

TABLE 1

Station	Beijing						Shanghai					
Date	1			15			1			15		
$N_s$	357			360			366			393		
$\theta_0$ (degree)	3	10	60	3	10	60	3	10	60	3	10	60
$\tau$ (mr)	5.51	1.96	.206	5.53	1.98	.208	5.62	2.02	.211	6.08	2.17	.277
$\Delta R$ (m)	40.2	14.8	3.06	41.7	15.4	3.19	41.4	14.9	3.07	43.3	15.6	3.21
$\Gamma_0$ (km <sup>-1</sup> )	.137	.135	.134	.133	.131	.130	.136	.137	.138	.141	.141	.141

### 3. SIMPLIFIED PREDICTION METHOD AND NEW PARAMETERS

If  $\theta_0$  is not too low the astronomical refraction formula is used because of its simplicity.

$$\tau = - \int_{n_s}^1 \cot \theta \frac{dn}{n} = N_s \cot \theta_0 \times 10^{-6} - O[(n-1)^2] \quad (5)$$

$$O[(n-1)^2] < \left( N_s \cot \theta_0 \times \frac{10^{-6}}{\sin^2 \theta_0} \right) \left( \frac{1}{r_0 \Gamma} - \frac{1}{2} N_s \times 10^{-6} \right) \quad (6)$$

where  $r_0$  is the radius of the earth. Using the measured value of  $N_s$ ,  $\tau$  can be obtained from eq. (5) if  $\Gamma$  is predictable.  $\Delta R$  is solved from eq. (3).

As we know that at 9 km above sea-level the value of refractivity is stable and is approximately equal to 105 (Bean 1964). Then the predicted value of  $\Gamma$  is obtained by

$$\begin{aligned} \Gamma_e &= \frac{1}{9-h_s} \ln \frac{N_s}{105} \\ \sigma &= \left( \sum_{i=1}^m \frac{(\Gamma_{oi} - \Gamma_{ei})^2}{m} \right)^{1/2} \end{aligned} \quad (7)$$

where  $\sigma$  is the standard deviation of prediction,  $h_s$  the height of station above sea-level in km.

To summarize, (3), (5) and (7) are expressions for a simple prediction of the tropospheric range error. Taking  $dN_s = \pm 1$ ,  $dN_g = \pm 5$ ,  $\Gamma = 0.138$ ,  $\bar{N}_s = 356$ ,  $\theta_0 = 10^\circ$ , the prediction error of  $\Delta R$  is less than about 8%.

From (4) the new parameters for linear regression analysis of  $\Delta R$  are provided to be  $Q = N_s / \sqrt{\Gamma}$  for  $\theta_0 < 5^\circ$  and  $T = N_s / \Gamma$  for  $\theta_0 \geq 5^\circ$ . Using the calculated data of  $\Delta R$  in Beijing and taking  $Q$ ,  $T$ ,  $N_s$  as regression variable, the linear regression analysis is carried out. The calculated results of correlation coefficients  $r(Q)$ ,  $r(T)$  and  $r(N_s)$  for various  $\theta_0$  are shown in table 2. Obviously,  $r(Q)$ ,  $r(T)$  are larger than  $r(N_s)$ . To use the new parameters the improvement in prediction of  $\Delta R$  is distinct.

TABLE 2

$\theta_0$ (degree)	$r(N_s)$	$r(Q)$	$r(T)$
3	0.7786	0.9498	
10	0.6447		0.9963
60	0.6039		0.9988

## REFERENCES

- Aske, J., et al. (1987), *Radio Sci.* 22, p. 379  
 Bean, B.R. (1964), in *Advances in radio research*, Ed. by J.A. Saxton, 1, p. 53  
 CCIR (1986), in *Recommendations and reports of CCIR* 5, p. 107 - 108  
 Davis, J.L., et al. (1985), *Radio Sci.* 20, p. 1593  
 Decker, M.T., et al. (1978), *J. Appl. Meteorol.* 17, p. 1787  
 Han, W.J. (1964), Tropospheric refraction and radar location, Internal report, Institute of Electronics, Academia Sinica, (in Chinese)  
 Hogg, D.C., et al. (1981), *Astron. Astrophys.* 95, p. 304  
 Hopfield, J.W. (1972), *J. Geophys. Res.* 74, p. 4487  
 Marini, J.W. (1972), *Radio Sci.* 7, p. 223  
 Rowlandson, L., et al. (1969), *Radio Sci.* 4, p. 927  
 Westwater, E.R. (1978), *Radio Sc.* 13, p. 667



# IONOSPHERIC CORRECTIONS FOR THE LAND BASED ALTIMETRY CAMPAIGN

R. LEITINGER

Institut für Meteorologie und Geophysik, Universität Graz,  
Halbärthgasse 1, A-8010 Graz, Austria

P. PESEC

I. f. Weltraumforschung, ÖAW, Lustbühelstr. 46, A-8042 Graz

**ABSTRACT.** In collaboration with RAL and the Dept. of Surveying, Newcastle upon Tyne, UK, and the ETH-Zürich the first part of COMPASS II was conducted during October 1991. The ERS-1 altimeter was used for height transfer over land: transponder were positioned at Ginzling (Tyrol, Austria) and Revine (Italy) to mimic altimeter return signals for the ERS-1 altimeter. An array of instruments was used to observe the state of the ionosphere around the useful ERS-1 passes ranging from Differential Doppler measurements on the signals of NNSS (formerly TRANSIT), via the European ionosonde network to dual frequency GPS observations. In addition, both sites were equipped with WVR from ETH-Zürich.

The ionospheric corrections were based on ‘now cast’ modelling of the ionospheric electron content in latitude and longitude. The range of the residual propagation errors is estimated by checking the plausibility bandwidth of the models.

The modelling method is demonstrated. Ionospheric height corrections are compared with height residuals computed from GPS measured heights minus altimeter measurements corrected for tropospheric effects (determined via WVR).

## 1. INTRODUCTION

The first order height error  $\delta h$  is proportional to the electron content of the ionosphere between satellite (antenna phase center) (S) and ground transponder (phase center) (T). Since pulse travel time through the ionosphere is longer than the free space pulse travel time the ‘measured’ height is true height plus  $\delta h$  with

$$\delta h = \frac{A}{2} \left( \frac{1}{f_1^2} + \frac{1}{f_2^2} \right) \int_{h_T}^{h_S} N dh = \frac{A}{2} \left( \frac{1}{f_1^2} + \frac{1}{f_2^2} \right) N_\perp \quad (1)$$

The constant  $A = 80.6$  for S.I. units.  $f_1$ : uplink frequency,  $f_2$ : downlink frequency,  $N$ : electron density in the ionosphere,  $dh$ : height element,  $h_T$ : height of transponder,  $h_S$ : height of satellite,  $N_\perp$ : electron content between  $h_T$  and  $h_S$ . The formula does not account for pulse delay in the transponder. Using the ERS-1 altimeter frequency ( $f_1 = f_2 = 13.9$  GHz) we have  $\delta h = 0.04N_\perp$  cm if  $N_\perp$  is measured in units of  $10^{15}\text{m}^{-2}$ .

For a (slightly) tilted ray path we have to replace  $\int N dh$  by  $\int N ds$ ,  $ds = dh/\cos\chi(h)$  being the ray path element,  $\chi$  the zenith angle along the ray path. Extracting a mean value for  $1/\cos\chi$  out of the integral leads to a projection from vertical to slant. A good estimate at least for small zenith angles is to take  $1/\cos\chi(h_i)$  instead of the true mean,  $h_i$  being a suitable ‘mean ionospheric height’. A good recommendation would be  $h_i = h_m + 50$  km ( $h_m$ : height of the maximum of electron density) but for most purposes and especially in the case

of small zenith angles a fixed mean ionospheric height  $h_i = 400$  km is good enough.

The application of ionospheric corrections to ERS-1 altimeter transponder measurements is the specific task of this paper. After a short introduction to the transponder experiment COMPASS II and an inventory of the available data, the evaluation procedure is described. Results will be available and discussed during the presentation.

## 2. THE CAMPAIGN COMPASS II (PHASE I)

### 2.1 Background

COMPASS II was proposed by R.J. Powell (Rutherford Appleton Lab.), phase I was conducted in collaboration with P. Cross (University Newcastle upon Tyne) and local agencies in Italy (Istituto per lo Studio della Dinamica delle Grandi Masse), Switzerland (ETH Zürich), and Austria (Institute for Space Research).

The basic idea is to use altimeter transponders which have been designed and built for ESA for use in the ERS-1 calibration procedures for the determination of the vertical distance between ERS-1 and selected sites. During phase I two transponders were deployed at Revine (Italy) and Ginzling (Austria) along the foot-print track of the 'Venice orbit' of ERS-1 (Fig.1).

Vertical distance measurements can be used in 3 different ways:

- Determination of terrestrial heights, provided the satellite orbit is accurately known;
- Determination of the satellite height and along-track, provided the position of the ground station is known in a well defined system and the transponder measurements are linked to a time frame (e.g. by GPS);
- Height transfer between stations, provided the shape of the orbit remains stable during the overpass (Fig.2).

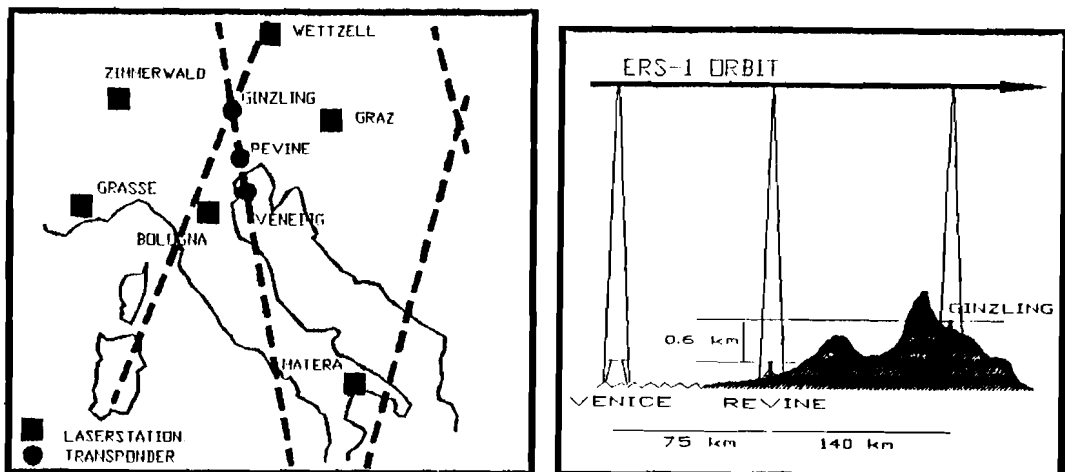


Figure 1: Transponder stations tied to the Laser-network (ITRF91) and ERS-1 tracks.

Figure 2: Geographical design of the COMPASS II phase I experiment.

Since the accuracy of the transponder measurements was expected in the cm-level a great deal of work was concentrated on monitoring disturbing effects of the same order of magnitude, mainly, tropospheric and ionospheric corrections. Water-vapour radiometers were deployed at both sites by ETH-Zürich. In addition, Ashtech and TI-4100 dual frequency GPS receivers were operated at Revine and Ginzling, supplemented by a MX-1502 Doppler receiver at Ginzling. Graz took over the responsibility to estimate the ionospheric corrections.

## 2.2. Available Data-Sets

5 passes of ERS-1 could be observed by transponders in Revine and Ginzling simultaneously. For this time a sample of 2 passes has been selected: day 302 21 UT and day 305 21 UT.

The preprocessing of the observed raw data involves the following steps:

- Extraction of 4.6 sec Doppler-counts for both 400 MHZ and 150 MHz frequencies together with the directions to the respective satellites at the respective epochs;
  - Extraction of 15 sec L1/L2 P-code and phase measurements (partly CA-code and L2 squared) together with the directions to the respective satellites at the respective epochs.
- Part of this work has been completed.

The data span for interpolation of the electron content to the actual observation time (nominal 21:00 UT) was set to 4 hours centered at 21:00 UT. Within this time span 4 NNSS passes were collected at Ginzling with the following C.A. epochs:

NNSS 23 at 19:46, NNSS 27 at 21:29, NNSS 29 at 21:54, NNSS 27 at 23:16.

GPS data are available at Ginzling and Revine for SV 2, SV 6, and SV 16 at elevations of higher than 50°. In addition, for checking the interpolation model further data are at disposal: NNNS data from Graz (Austria), Lindau/Harz, Neustrelitz (FRG), Brussels (Belgium); GPS data collected during the GPS campaign EUREF-EAST in FRG, Switzerland, Austria, Finland, Poland, CSFR, Hungary, and Russia. A selection of particular observation sites is shown in Figure 3, the satellite scenario at Ginzling is shown in Figure 4.

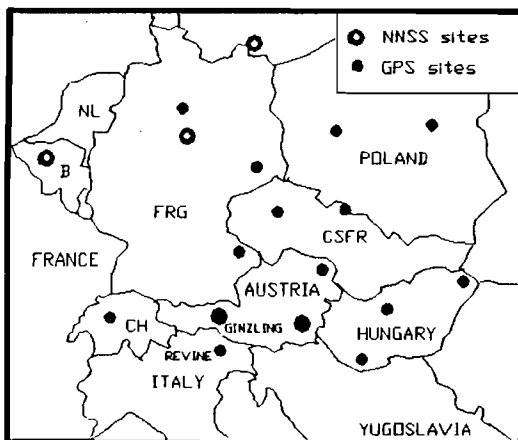


Figure 3: Distribution of GPS and NNSS sites which observed during the selected ERS-1 overpasses.

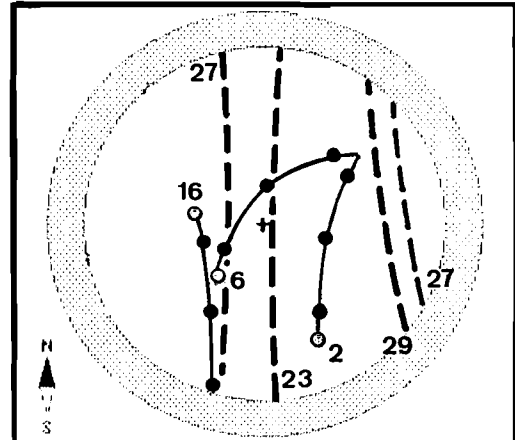


Figure 4: Distribution of GPS and NNSS satellites observed at Ginzling during the selected window 19 UT - 23 UT, day 302, 1991.

## 3. EVALUATION PROCEDURE

Since the electron content is not a directly measured quantity it is necessary to transfer data observed at an other location and at an other time. The observations are made by means of propagation effects on NNSS and GPS signals and we have to solve three problems: (1) adjust for local time differences, (2) adjust for spatial differences, (3) adjust for height differences. (1) and (2) need suitable interpolation or extrapolation procedures, (3) needs electron content differences calculated from electron density models.

In the following we describe a step by step procedure making use of Differential Doppler observations on the signals of NNSS satellites as the primary source for electron content data.

1. Find the electron content for the latitude of the transponder station from the NNSS passes closest in time before and after the ERS-1 pass of interest.
2. Adjust for time and longitude differences by interpolating between the data from the two NNSS passes.
3. Check the interpolation by means of a regional model of electron content.
4. Check the transfer in longitude by means of additional NNSS observations from other receiving stations if available.
5. Estimate the electron content between the NNSS and ERS-1 heights by means of an electron density model (updated with measured data if possible) but apply a correction only if the correction exceeds the error estimate for the electron content from NNSS observations.
6. Try a 'nowcasting' procedure using all available data to construct an electron content model for the vicinity (in space and time) of the ERS-1 pass of interest.
7. Estimate the accuracy of the resulting electron content for the link to ERS-1.

#### 4. CONCLUSION

The ionospheric correction for the ERS-1 altimetry can be estimated with very good accuracy provided that sufficient information is available about the spatial and temporal structure of ionospheric electron content. Because of the short time interval between the experiments and the deadline for submission of this summary no detailed results could be included but such will be given during the presentation of the paper. From the Diff. Doppler observations evaluated so far we estimate typical  $\delta h$  to range between 20 and 30 cm for the morning ERS-1 passes and between 3 and 10 cm for the evening passes.

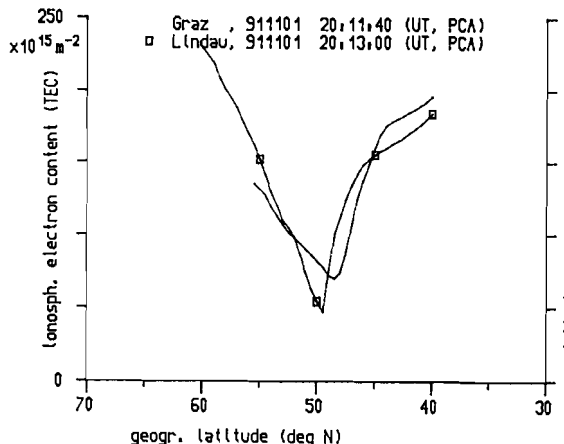


Figure 5. Example for  $\delta h$  estimate from NNSS Diff. Doppler observations. Ionosph. electron content (TEC) in units of  $10^{15} \text{ m}^{-2}$  (left hand scale) and corresponding  $\delta h$  for the ERS-1 altimeter frequency in cm (right hand scale) vs. geogr. latitude in  $^{\circ}\text{N}$ . Two stations evaluation (Leitinger et al., 1975), receiving stations Graz and Lindau/Harz. The difference in TEC between the two traces is typical for the vicinity of small scale structures (narrow trough due to geomagnetic storm effect).  $\delta h$  value from the Graz trace for  $47^{\circ}\text{N}$ ,  $10.5^{\circ}\text{E}$ : 5.0 cm.

#### REFERENCES

- Cross, P.A. (1991) *Minutes of the COMPASS II Planning Meeting at the ETH-Zürich, 7.5.1991*
- Leitinger, R., Schmidt, G., Tauriainen, A. (1975) *J. Geophys.* **41**, 201
- Leitinger, R., Hartmann, G.K. (1977) *Kleinheubacher Ber.* **20**, 267
- Powell, R.J., Birks, A.R. (1991) Paper on ground based transponders presented at XX. IUGG General Assembly, Session U13, Vienna
- Powell, R.J. (1992) *Interim Report at ESTEC, Noordwijk, 22.1.1992*

# COLLOCATIONAL METHODS IN ATMOSPHERIC RAY TRACING

ALAIN GEIGER and MARC COCARD

Institute of Geodesy and Photogrammetry, ETH-Zürich

CH-8093 Zürich, Switzerland

Tel: 1 377 32 44 Fax: 1 371 25 93

**ABSTRACT** The atmospheric path delay is one of the systematic effects which limits the obtainable accuracy of measurements in space geodesy as well as in terrestrial geodesy by a considerable amount. For the modeling of the path delay different models of numerical, physical and empirical type have been used. In this paper a method is presented where the refractivity field is developed into series by interpolating methods such as collocation. This approach results in an explicit representation of the N-field. The differential equations of the geodesic can then be directly solved by introducing the explicit representation of the field into an numerical integration algorithm. Solving the differential equations leads to path delays wherein also bending effects are considered.

## 1. INTRODUCTION

Working on geodetic methods, especially on GPS-, but also on conventional measurements, leaded our group at the ETH Zürich towards the investigation into systematic errors. One of the major parts being the tropospheric effects. For this purposes hardware such as water-vapor-radiometers (Puliafito and Bürki, 1991) as well as 3D-modeling algorithms are being developed (Eckert et al., 1991). A further development is to integrate ray tracing into our 3D-models. The problem of tropospheric refraction is well known. It is to calculate the geometrical corrections (angle and length) for a certain point to point measurement and for a given refractivity field. One possibility of getting the true ray path is by integrating the differential ray equation. This method is pursued in this approach. However, a main obstacle in applying well known integration procedures arises from lack of knowledge of the refractivity field. In many applications the field is interpolated on gridded values around an approximated ray path. The exact integration can then be done by interpolating the gridded values on the actual ray path. To bypass this cumbersome procedure, an explicit formula is given representing the derivative of the refractivity field at any point in dependency of the given meteomeasurements. This, in a certain sense analytical, representation is achieved by the use of collocational methods, where the needed values are directly connected to the measurements through the corresponding covariance functions. This method of representing any field values coincides exactly with the method used in (Eckert et al., 1991) for interpolating different meteorological parameters. The basic ideas of combining numerical integration and collocational methods are presented in the following chapters.

## 2. GEODESICS IN REFRACTIVE MEDIUM

The starting point of the following developments is Fermat's principle. It states, that the ray path will follow a curve such that the lighttime (of ray) between two points A and B will be minimized. This formulation in general doesn't correspond to the request of minimal path length. (The line element has to be adjusted in case of refractive medium).

We have

$$c \cdot t = c \int_A^B dt = c \int_A^B \frac{ds}{v} = \int_A^B n ds = \min$$

c	=	speed of light in vacuo
v	=	actual velocity of light
n	=	refractive index
ds	=	line element along ray path

Since we are considering a ray path in space we use a 3-dimensional parametrization of the curve by its arc length s.

$\dot{x}^i$	=	$\frac{dx^i}{ds}$
$x^j$	=	coordinates
$g_{ij}$	=	metric-tensor of the space under consideration

Our minimizing problem can be solved by the variational calculus. Another solving method has been developped in Geiger (1988) where coordinate transformations have been used. The variation of the 'lighttime' eikonal is solved by the well known Euler-Lagrange-Differential equations (see e.g. Klingbeil, 1966) resulting in the differential equations of the ray path in a refractive medium:

$$g_{ih} \ddot{x}^k + \Gamma_{i,kl} \dot{x}^k \dot{x}^l = \mu_i - \mu_k \dot{x}^k \dot{x}_i$$

$\Gamma_{i,kl}$  = Christoffel's symbols

$\mu$  =  $\ln(n)$

The right hand side term governed by the gradient of  $\ln(n)$  gives the effect of the refractive index. Obviously this term will disappear in a homogeneous medium.

### 3. SOLUTION OF THE DIFFERENTIAL EQUATION AND RAY TRACING

Multiplying the path differential equations by the inverse metric tensor  $g^{ij}$  and isolating the second derivatives results in a system of 6 first order differential equations:

$$\begin{aligned}\dot{x}^j &= v^j \\ \dot{v}^j &= f^j(x, v)\end{aligned}$$

Note, that in our case the vector function  $f$  doesn't depend explicitly upon the free parameter  $s$ . This non-linear system of differential equations can be solved numerically.

For the completeness of the problem we have to define some boundary conditions. If we

consider the boundary value formulation we may fix eg. the coordinates of the starting and the ending points of the ray path. In the case of the initial value problem we assume eg. the coordinates of the starting point and the starting ray velocity vector fixed.

Integrating the initial value problem represents in principle one of the main topic in ray tracing through an inhomogeneous continuous medium. Reflections and refractions on discontinuities, the second topic of ray tracing will not be treated here (see e.g. Stavroudis, 1972).

A considerable simplification is obtained if we restrict ourselves to the Euclidean space (which is far general enough for our purposes). In this case the metric tensor becomes unity. Further more we consider the refractive index to be close to 1. This may be true to great extend since

$$n = 1 + N \cdot 10^{-6} = 1 + \epsilon N$$

and  $N \sim 250$ : the refractivity for microwaves in air. Thus  $\nabla \mu = \nabla \ln(n) = \epsilon \nabla N$

#### 4. MODELLING THE REFRACTIVITY FIELD BY COLLOCATION

In most cases the refractivity field  $N(x)$  is not known. We seek some stations (on ground or surroundings) where the different meteoparameters are known by measurements. A common way to construct the  $N$ -field from these measurements consists in numerical interpolation resulting in a gridded dataset, which again has to be differentiated numerically in order to get the needed gradient of the field. This method, however, gives the requested values on discrete grid points only. The consequence is, that in the numerical integration a second interpolation will have to be carried out. A solution which directly delivers analytical functions whose gradient can be used as forcefunctions is obtained by parameter estimation. A characteristic function is fitted to the given measurements. The characteristic function can also be represented by a series of base functions.

In a certain sense all the above methods are combined in the collocation algorithm. We estimate a model of the  $N$ -field from the measurement and, at the same time, we estimate a signal which is determined through the chosen covariance function and the measurements. The interpolated signals turnout to be linear combinations of the measured values. For detailed description we refer to Moritz (1980). We consider measurements  $m$  which will be approximated by a linearized model with parameters  $p$ , a signal  $s$  and a certain noise  $w$ .

Thus we have  $m = Ap + s + w$ . Using the least square condition on  $s$  and  $w$  we end up with the equations for the parameters, noise and signal respectively. The interesting point is, that from this results a value  $m'$  at any location  $x$  can be predicted.

$$m'(x) = A'p + s' = A'p + C_{ss} k$$

where  $k = D^{-1}(m - Ap)$  and  $D = C_{ww} + C_{ss} C_{sw}$  is the noise covariance matrix (normally a diagonal matrix). While  $C_{ss}$  is the full signal covariance matrix.

$C_{ss}$  is the full covariance matrix (vector) of predicted signal depending upon the locations of the measurements and upon the location of prediction.  $k$  and  $p$  can be calculated once the measurements are given. Unfortunately we don't need the value  $m'(x)$  itself but its gradient. This can be achieved quite easily by differentiating the interpolation formula:

$$\nabla m'(x) = \nabla A'p + \nabla C_{ss} k$$

Note that  $p$  and  $k$  don't depend on the location of interpolation  $x$ .  
For refractivity we assume the standard model with two parameters

$$N_{\text{mod}} = N_0 e^{-\frac{z}{H}}$$

and the gradient

$$\mathbf{h}(\mathbf{x}; \mathbf{p}) = \nabla N_{\text{mod}} = -\frac{1}{H} N_{\text{mod}} \mathbf{e}_3$$

$N_0$  = refractivity at reference height ( $z = 0$ )  
 $H$  = scale height ( $\approx 8000$  m)

For the signal covariance we chose a function depending only on the distance  $R$  between the interpolation point  $\mathbf{x}$  and the measurements at  $\mathbf{y}$ . Then the gradient of the covariance matrix becomes

$$\mathbf{G} = \nabla C_{s's} \triangleq C_{ij} = \left. \frac{\partial \phi}{\partial R} \right|_{x,y} \frac{x_i - y_{ij}}{R_j}$$

$$\begin{aligned} 1 &\leq i \leq 3 \\ 1 &\leq j \leq \text{number of data points} \end{aligned}$$

Finally we get for the interpolated gradient of refractivity

$$\mathbf{u} = \nabla N = \mathbf{h} + \mathbf{G} \mathbf{k}$$

## 5. SUMMARY OF THE PROPOSED METHOD AND CONCLUSIONS

The method can be summarized by only two steps:

- 1) Use collocation to calculate from given measurements of  $N$  or  $p$ ,  $T$ ,  $e$ 
  - a) the  $\mathbf{k}$ -vector
  - b) estimate the model parameters  $\mathbf{p}$
- 2) Integrate the system of differential equations with appropriate initial values.

$$\dot{\mathbf{x}} = \mathbf{v}$$

$$\dot{\mathbf{v}} = (\mathbf{E} - \mathbf{v}\mathbf{v}^T)(\mathbf{h}(\mathbf{x}; \mathbf{p}) + \mathbf{G}(\mathbf{x}) \mathbf{k})$$

where  $\mathbf{h}(\mathbf{x}; \mathbf{p})$  and  $\mathbf{G}(\mathbf{x})$  are the gradient of the model  $N$ -field and the gradient of the signal covariance respectively. They do not depend on  $\mathbf{v}$  but on  $\mathbf{x}$ . While depending on the used integration method step 2) may be repeated,  $\mathbf{p}$  and  $\mathbf{k}$  remain fixed.

It has been shown that for a given meteorological data set it is possible to construct a consistent model of the  $N$ -field which can be introduced into the integration procedure. The use of the collocation in the sense of development at base function series and the direct derivation, allows, to form an analytical 'forcefunction' in the differential equation. All rays passing through the modeled space can be integrated with the same function. No calculations of intermediate grids etc. are needed, this may be a more flexible and versatile algorithm.

## REFERENCES

- ECKERT, V., M. COCARD, A. GEIGER, B. BÜRKI, B. NEININGER ( 1991): Three-Dimensional Modelling of Atmospheric Parameters for Automatic Path Delay Corrections. *IUGG, Wien.*
- GEIGER, A. (1988): Der Lichtstrahl in differentialgeometrischer Formulierung. *Bericht 140. Institut für Geodäsie & Photogrammetrie, ETH-Zürich.*
- HENRICI, P. (1964): Elements of Numerical Analysis. *John Wiley & Sons. Inc., New York.*
- KLINGBEIL, E. (1966): Tensorrechnung für Ingenieure. *Hochschultaschenbücher B.I., Band 197/197a.*
- MORITZ, H. (1980): Advanced Physical Geodesy. *Sammlung Wichmann Neue Folge Band 13, Wichmann Verlag Karlsruhe.*
- PULIAFITO, E., B. BÜRKI (1991): Tropospheric Path-Lenght Correction Using a Dual-Frequency Transportable Radiometer. In: *Proc. IGARSS'91, pp. 1337-1340, June 3-6, Helsinki.*
- STAVROUDIS, O.N. (1972): The Optics of Rays, Wavefronts, and Caustics. *Pure and Applied Physics. Vol. 38., Academic Press, New York.*

## TRANS-IONOSPHERIC PROPAGATION PREDICTION OF SHORT WAVE RADIO PROPAGATION ON THE WUHAN-ROME PATH

HUANG TIANXI, LIU XUANMOU, ZHANG WENPING  
Department of Space Physics,  
Wuhan University, China

**ABSTRACT.** Some characteristics of long and very long distance trans-ionospheric propagation of short wave radio links are studied in this paper. First, the EMI-81 model, the three-dimensional equinoctial model of electron density and effective electron collision in the ionosphere, is analyzed and revised. Prediction results of electron concentration profiles for three ionosondes, Manzhouli, Beijing and Guangzhou, during the period of March 1978 using the revised EMI-81 model are compared with that using the IRI-79 model as well as that using LSP transformation. The ionospheric duct is introduced from Maxwell equations and some parameters of long distance short wave radio propagation are given. The prediction method by means of the adiabatic approximation is incorporated in computer programmes which form a solid foundation for an expert system predicting the HF long distance propagation conditions. As an application of this method, the Eurasia propagation paths such as Wuhan-Rome, or Wuhan-Paris, or Wuhan-London, or Wuhan-Berlin, are studied and the diurnal variations of maximum limiting frequency for different propagation ducts are examined when the sunspot number  $R = 124$  and 10. It is suggested that our technique is also applicable for prediction of the telecommunication circumstances between Eurasia and America or between Eurasia and the Antarctica.

## AUTHOR INDEX

- Afraimovich, E.L. .... 81, 109, 135  
Akhundov, T.A. .... 37, 63  
Alaoui, A. El A. El .... 105  
Alexeev, V.N. .... 63  
Bányai, L. .... 99  
Baykov, G.B. .... 63  
Becek, K. .... 168  
Bender, P.L. .... 117  
Bettac, H.-D. .... 151  
Boitman, O.N. .... 81  
Brunner, F.K. .... 3  
Bürki, B. .... 129, 175  
Cocard, M. .... 129, 175, 191  
Dai Kailiang .... 165  
Davis, J.L. .... 25  
De Munck, J.C. .... 29  
Dodson, A.H. .... 111  
Eckert, V. .... 175  
Elgered, G. .... 13, 25, 111  
Eubanks, T.M. .... 55  
Fridman, S.V. .... 81, 135  
Geiger, A. .... 129, 175, 191  
Golynski, S.M. .... 91  
Gontarev, O.G. .... 103  
Gusev, V.D. .... 91  
Gyger, R. .... 129  
Han, W.J. .... 183  
He Jin .... 87  
Herring, T.A. .... 157  
Huang, J.Y. .... 33  
Huang Tianxi .... 87, 196  
Jakowski, N. .... 151  
Jarlmark, P.O.J. .... 111  
Jungstand, A. .... 151  
Kahle, H.-G. .... 129  
Kaniuth, K. .... 21  
Kovács, K. .... 99  
Kunitsyn, V.E. .... 171  
Langley, R.B. .... 97  
Leclerc, J.G. .... 105  
Leitinger, R. .... 187  
Liu Xuanmou .... 87, 196  
Ma Jianming .... 165  
Matsakis, D.N. .... 55  
Minko, N.M. .... 109  
Minko, N.P. .... 81, 135  
Niell, A.E. .... 25  
Pesec, P. .... 187  
Rius, A. .... 59  
Sardón, E. .... 59  
Schuh, H. .... 65  
Shapiro, I.I. .... 25  
Shardlow, P.J. .... 111  
Spoelstra, T.A.Th. .... 69, 137  
Stotskii, A.A. .... 37, 63, 179  
Terekhov, A.I. .... 135, 169  
Tremel, H. .... 21  
Treuhäft, R.N. .... 45  
Troitsky, B.V. .... 103  
Udodov, M. Yu. .... 169  
Vakulin, Yu.I. .... 109  
Van Velthoven, P.F.J. .... 77, 83  
Vodjannikov, V.V. .... 103  
Wang, Y.P. .... 33  
Wanninger, L. .... 141  
Wu, X.D. .... 183  
Yan, Y. .... 88  
Yang Yi-Pei .... 137  
Xu Peiyuan .... 147  
Zarraoa, N. .... 59  
Zhang, W.L. .... 183  
Zhang Wenping .... 196  
Zheng, Y.J. .... 183  
Zvezdin, V.N. .... 81, 135

